PACIFIC EARTHQUAKE ENGINEERING
RESEARCH CENTER

Earthquake Engineering for Resilient Communities:

2011 PEER Internship Program Research Report Collection

Heidi Faison, Editor
Stephen A. Mahin, Editor
Pacific Earthquake Engineering Research Center

PEER 2011/10
DECEMBER 2011

Disclaimer

The opinions, findings, and conclusions or recommendations expressed in this publication are those of the author(s) and do not necessarily reflect the views of the study sponsor(s) or the Pacific Earthquake Engineering Research Center.

Earthquake Engineering for Resilient Communities:

2011 PEER Internship Program Research Report Collection

Heidi Faison, Editor
Stephen A. Mahin, Editor
Pacific Earthquake Engineering Research Center

PEER Report No. 2011-10
Pacific Earthquake Engineering Research Center
College of Engineering
University of California, Berkeley

December 2011

CONTENTS

INTRODUCTION

Recent earthquakes in the United States and around the world have repeatedly shown that earthquake resilience is essential to building and sustaining urban communities. Earthquake resilience will play an increasingly important role in the professions associated with earthquake hazard mitigation, thus there is a need to educate the next generation of these professionals. To address this need, the Pacific Earthquake Engineering Research Center (PEER) coordinates a summer internship program for undergraduate students that focuses on the theme of earthquake-resilient communities. With funding from the National Science Foundation (NSF), eleven interns from a variety of backgrounds and universities participated in the 2011 program.

Achieving earthquake-resilient communities is a challenge that requires the interaction of many disciplines from engineering to public policy. To show the importance of multidisciplinary cooperation and collaboration, PEER assigns participating undergraduate interns with a project in one of the following disciplines: structural engineering, geotechnical engineering, urban planning, or public policy. The interns are then assigned faculty and graduate student mentors who help them complete a unique research project at one of the three partnering research sites: University of California Davis, University of Washington, and University of California Berkeley. During the summer of 2011, the interns at University of California Berkeley completed projects in collaboration with both the San Francisco Planning and Urban Research Association (SPUR) and University of California, San Diego.

The participating students (listed in alphabetical order with their home university) were:

- Gulzat Atymtayeva, University of Evansville
- David Deutsch, University of Southern California
- Amanjot Dhaliwal, University of California, San Diego
- Christopher Kissick, California State University, Chico
- Christopher Krage, University of California, Davis
- Zhi Liu, California Polytechnic State University, San Luis Obispo
- Andrew Makdisi, University of California, Davis

- Jason Naanos, California State University, Northridge
- John Pham, University of California: San Diego
- Douglas Spitzer, University Of Illinois at Urbana-Champaign
- Sarah Welsh-Huggins, Lafayette College

Many faculty, graduate student and earthquake professional mentors made this program a success for the interns, and PEER extends its sincere thanks to the participating mentors listed below:

- Sarah Karlinsky, SPUR
- Laura Dwelley-Samant, SPUR
- Mary Comerio, UC Berkeley
- Peter May, University of Washington
- Ashley Jochim, University of Washington
- Charles Roeder, University of Washington
- Dawn Lehman, University of Washington
- Arni Kristinn Gunnarsson, University of Washington
- Kenneth O'Neill, University of Washington
- Jay Lund, UC Davis
- Ross Boulanger, UC Davis
- Jason DeJong, UC Davis
- Jack Montgomery, UC Davis
- Brian Martinez, UC Davis
- Brina Mortensen, UC Davis
- Matt Schoettler, UC San Diego/UC Berkeley
- Jose Restrepo, UC San Diego

During the ten-week summer research experience, each intern conducted a research project while also regularly engaging with the full intern cohort during weekly web-meetings to discuss and learn how each of their projects related to earthquake resiliency. Students learned how to conduct independent research and how to participate effectively as a member of a research team. Supplemental activities, including a two-day orientation program with multiple skill-building workshops and participation in a research poster session at the 2011 PEER Annual Meeting, were conducted to broaden the intern experience and inspire them to make future contributions to the field of earthquake engineering and related research.

As a final research deliverable, each intern was required to prepare a final research report. This PEER report, “Earthquake Engineering for Resilient Communities: 2011 PEER Internship

Program Research Report Collection" is a compilation of the final research papers written by the 2011 interns. These reports follow this Introduction. A list of the institutions, projects, interns, and mentors is listed below:

University of California, Berkeley, and SPUR Projects

- "Assessing and Mapping Earthquake Damage in Christchurch, New Zealand" was completed by intern David Deutsch under the supervision of the following mentors: Professor Jose Restrepo and Dr. Matt Schoettler (University of California, San Diego) Note: Deutsch conducted his research at UC Berkeley with a two week site visit to Christchurch, New Zealand, funded under National Science Foundation RAPID award CMMI-1138358.
- "The Resilient City: Achieving Shelter-in-Place in San Francisco" was completed by intern Amanjot (Amy) Dhaliwal under the supervision of the following mentors: Sarah Karlinsky (SPUR), Professor Mary Comerio (UC Berkeley), and Laura Dwelley-Samant (consultant).
- "The Resilient City: San Francisco Shelter-in-Place Analysis" was completed by intern John Pham under the supervision of the following mentors: Sarah Karlinsky (SPUR), Professor Mary Comerio (UC Berkeley), and Laura Dwelley-Samant (consultant).

University of California, Davis

- "Overburden Correction Factor and the Effect of Fines Content on the Limiting Compression Curve of Intermediate Soils" was completed by intern Christopher Kissick under the supervision of the following mentors: Professors Ross Boulanger and Jason Dejong, and Ian Maki.
- "How Well Are Fines and Plasticity Represented in Liquefaction Triggering Curves?" was completed by intern Christopher Krage under the supervision of the following mentors: Professor Ross Boulanger and Jack Montgomery.
- "Micbrobial Induced Calcite Precipitation in Partially Saturated Soils' was completed by intern Andrew Makdisi under the supervision of the following mentors: Professor Jason Dejong and Brian Martinez.

- “The Effect of Microbially Induced Calcite Precipitation on the Liquefaction Resistance of Sand” was completed by intern Douglas Spitzer under the supervision of the following mentors: Professor Jason Dejong and Brina Mortensen.

University of Washington

- “High-volume SCM Concrete in Composite Construction” was completed by intern Gulzat Atymtayeva under the supervision of the following mentors: Professors Charles Roeder and Dawn Lehman, and Arni Gunnarsson.
- “CFT Bridge Pier Connections” was completed by intern Zhi Long Liu under the supervision of the following mentors: Professors Charles Roeder and Dawn Lehman, and Kenneth O’Neil (University of Washington).
- “Earthquake Resiliency: Managing Waste Water Sector Vulnerabilities through Green Infrastructure and Related Policies” was completed by intern Jason Naanos under the supervision of the following mentors: Professor Peter May and Ashley Jochim.
- “Disaster Resilience of Maritime Ports” was completed by intern Sarah Welsh-Huggins under the supervision of the following mentors: Professor Peter May and Ashley Jochim.

Funding for the 2011 PEER Internship Program is provided by the National Science Foundation under Grant No. EEC-1063138, as a part of NSF’s Research Experiences for Undergraduate (REU) Program. Any opinions, findings and conclusions or recommendations expressed in this material are those of the author(s) and do not necessarily reflect the views of the National Science Foundation (NSF) or the Pacific Earthquake Engineering Research Center (PEER). For more information about the 2011 PEER Internship Program, visit: http://peer.berkeley.edu/education/summer_internship_program2011.

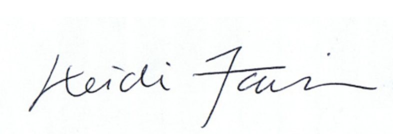

Heidi Faison
Outreach Director, PEER
PEER REU Coordinator

Stephen A. Mahin
Director, PEER
PEER REU Principal Investigator (PI)

1 Assessing and Mapping Earthquake Damage in Christchurch, New Zealand

DAVID DEUTSCH

ABSTRACT

A magnitude 6.3 earthquake caused massive damage in Christchurch, New Zealand on February 22, 2011. This report contains an assessment of the damage to a 9-story precast concrete hotel and a 5-story precast concrete parking garage resulting from these earthquakes, as well as background on this earthquake and two others that occurred near Christchurch. To generate this assessment, data was collected during a site visit to each building. Collected data included photographs of visible damage and acceleration data from earthquake events and ambient vibrations for both structures. A description of the damage documentation process, resulting crack maps, and processed acceleration data are included in this report.

1.1 INTRODUCTION

This report contains data on the structural performance of two precast concrete buildings and observations on the resiliency of the community in Christchurch, New Zealand. The buildings evaluated were a 5-story parking garage near the suburb of Papanui, shown in Figure 1.1, and a 9-story hotel in Christchurch's Central Business District (CBD), shown in Figure 1.2. Both of the buildings were designed using modern practices and standards; the parking garage was constructed in 2007 and the hotel was constructed in 2006, both under the New Zealand Standards 1170.5: 2004 loading standard. The structural damage data was collected to assess the adequacy of modern building standards for performance during large earthquakes and to provide a benchmark for analytical models to compare damage patterns. This data is valuable to the United States and New Zealand because it demonstrates the performance of design practices that are in use today. The resiliency of the Christchurch community was assessed through exploration of the city, interaction with residents, and interviews with business owners and engineers. Conclusions drawn in this report are overall impressions of the state of the recovery process, not a comprehensive investigation.

Figure 1.1 5-story parking garage hotel.

Figure 1.2 9-story hotel.

1.2 BACKGROUND

The initial earthquake to cause damage to Christchurch occurred on 4 September 2010. After the magnitude 7.1 September earthquake, referred to as the Darfield Earthquake, there was an ongoing series of aftershocks that included the magnitude 6.3 22 February 2011 earthquake known as the Christchurch Earthquake. Since the September 2010 earthquake there have been thousands of aftershocks in and around Christchurch including 23 earthquakes larger than magnitude 5.0[1]. This section will address the main earthquake and the two largest aforementioned aftershocks.

Figure 1.3 shows a map of Christchurch and the surrounding area of the South Island of New Zealand. The epicenter of the Darfield Earthquake is the pulse symbol on the far left of the map. The other pulse symbols are the epicenter locations of the 22 February 2011 earthquake and the 13 June3 2011 earthquake, from left to right respectively. Figure 1.4 shows a close-up view of the downtown Christchurch area, as well as some of the northern suburbs. The house shaped

[1] http://geonet.org.nz.

icons are New Zealand GeoNet[2] accelerometers that provided ground motion data for evaluation of the shaking in near the structures from these three events and comparison with the data collected on the expedition. The pin icons are the buildings that were investigated in this project. The northern pin icon is the 5-story parking garage, and the southern pin icon is the 9-story hotel. The sensor in the northwest corner is the Papanui High School (PPHS) sensor, located 4.8 km from the 9-story hotel and 2.0 km from the 5-story parking garage. The sensor that is due north of the 9-story hotel pin icon, 0.9 km from the 9-story hotel and 2.0 km from the 5-story parking garage is the Christchurch Resthaven (REHS) sensor. The sensor that is due south of the 9-story hotel pin icon is the QDR-0183 sensor. It was located in the basement of a tall office building in the CBD, 0.3 km from the 9-story hotel and 3.1 km from the 5-story parking garage, until November 2010. The most southeastern sensor, located in the bottom right corner of Figure 1.4 is the Christchurch Cathedral College (CCCC) sensor, located 1.2 km from the 9-story hotel and 4.0 km from the 5-story parking garage. The sensor due west of the 9-story hotel pin icon is the Christchurch Botanical Gardens (CBGS) sensor, 1.3 km from the 9-story hotel and 2.3 km from the 5-story parking garage, and the sensor located southwest form the 9-story hotel pin icon is the Christchurch Hospital (CHHC) sensor, situated 0.9 km from the 9-story hotel and 3.1 km from the 5 story parking garage. The shaded area outlines the boundaries CBD Red Zone, the area cordoned off by the Canterbury Earthquake Recovery Authority because of high collapse risk buildings, as of July 2011.

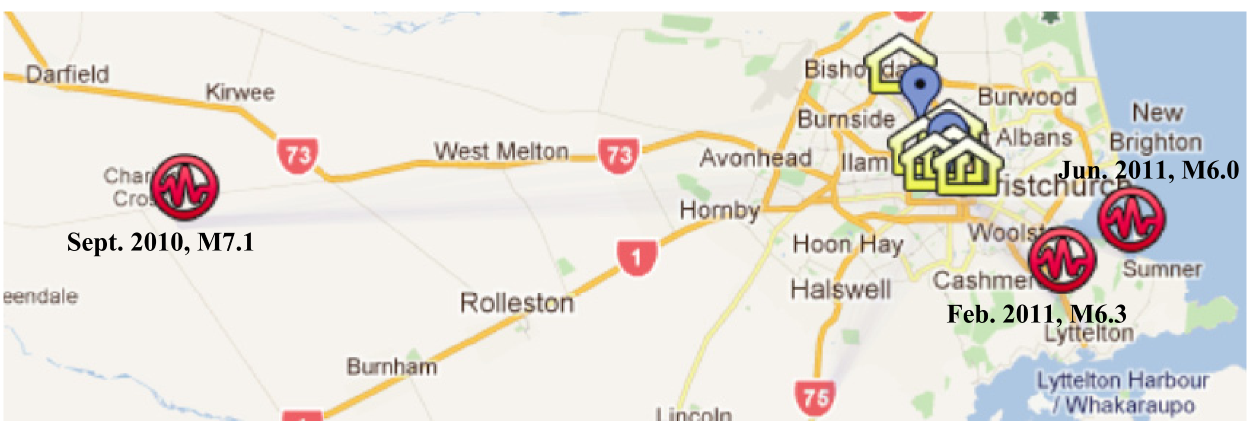

Figure 1.3 Map of the Christchurch region.

[2] http://geonet.org.nz.

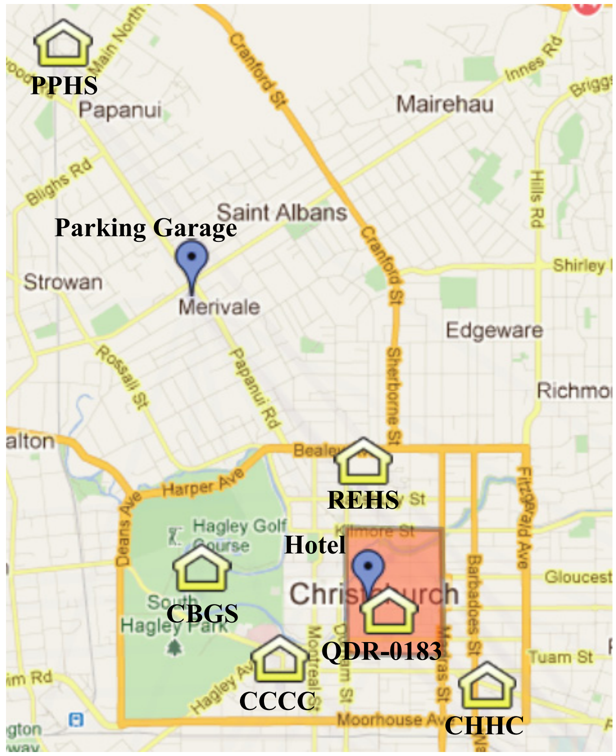

Figure 1.4 **Map of the Christchurch Central Business District and northern suburbs.**

1.2.1 The Darfield Earthquake

A magnitude 7.1 earthquake occurred on 4 September 2010 near Darfield at latitude -43° 33' 0.00" and longitude +172° 10' 48.00", 37 km outside of the Christchurch CBD at a depth of 10 km. This earthquake was the first in an ongoing series of tremors.

Despite having a significantly larger magnitude than the other two earthquakes reviewed herein, the Darfield earthquake was not the most damaging earthquake to hit Christchurch due to its epicentral distance. The significant distance between the epicenter and the city acted as a buffer, so the resulting damage was concentrated mostly in unreinforced masonry (URM) buildings that are known to have poor earthquake performance. Other buildings with constructed with modern standards experienced light and reparable damage.

Figures 1.5 and 1.6 contain information computed from GeoNet sensor data collected during the Darfield Earthquake. Figure 1.5 contains the North-South (solid lines) and East-West spectral ground acceleration data (dashed lines) as well as the targeted design spectra for the 9-story hotel with class D soil (deep or soft soils), which is representative of the soil conditions for the majority of the CBD and northern suburban area. Figure 1.6 is the spectral displacement calculated using the acceleration data from each sensor. Similar to Figure 1.5, Figure 1.6 depicts North-South spectral displacement with a solid line, and East-West spectral displacement with a dashed line. The maximum spectral acceleration obtained from the Darfield earthquake was 1.0 g at a period of approximately 0.6 sec, which exceeded the design acceleration at that period by 30%. A 0.6-sec period is a relatively short fundamental period associated with low- to mid-rise buildings. A large peak in spectral acceleration occurred at approximately 2.7 sec, a period associated with taller, flexible structures. The spectral acceleration peak reached 0.62 *g*, about three times the design acceleration at that period. Structures in the period range of 2.5 to 3.0 sec were subjected to large demands, as shown in Figure 1.6 where the peak spectral displacement exceeded 1.0 m. Figure 1.7 shows the vertical spectral acceleration of the Darfield earthquake, with a peak spectral acceleration of just over 1.0 g that is on the same order of magnitude as the peak vertical spectral acceleration computed from the June earthquake data, shown in Figure 1.11.

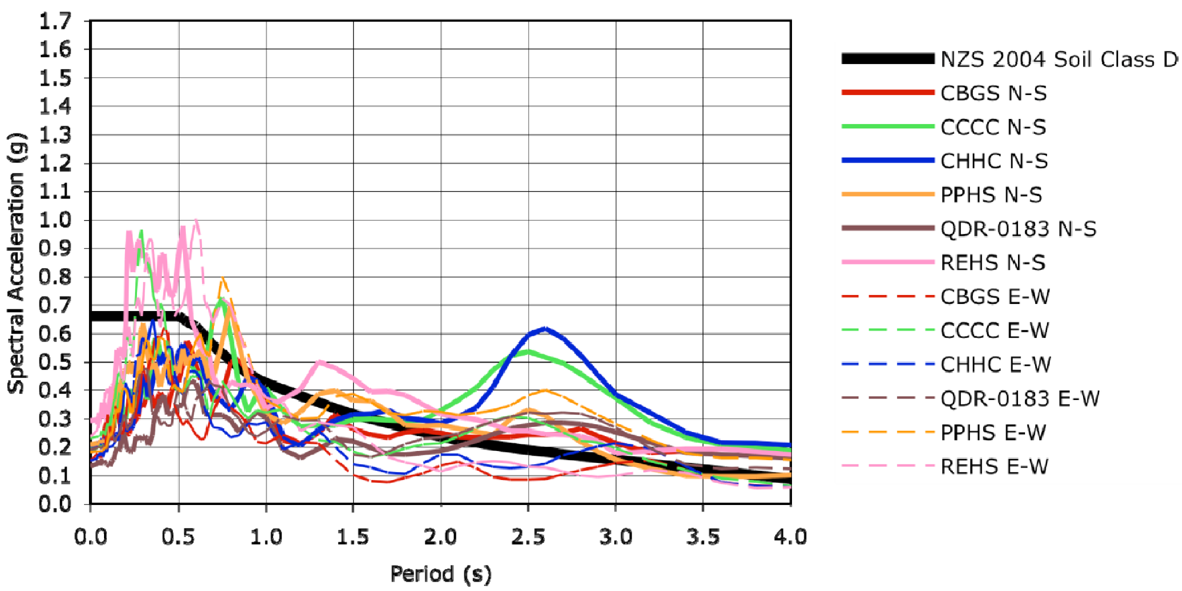

Figure 1.5 **Horizontal spectral acceleration, Darfield earthquake, 5% critical damping.**

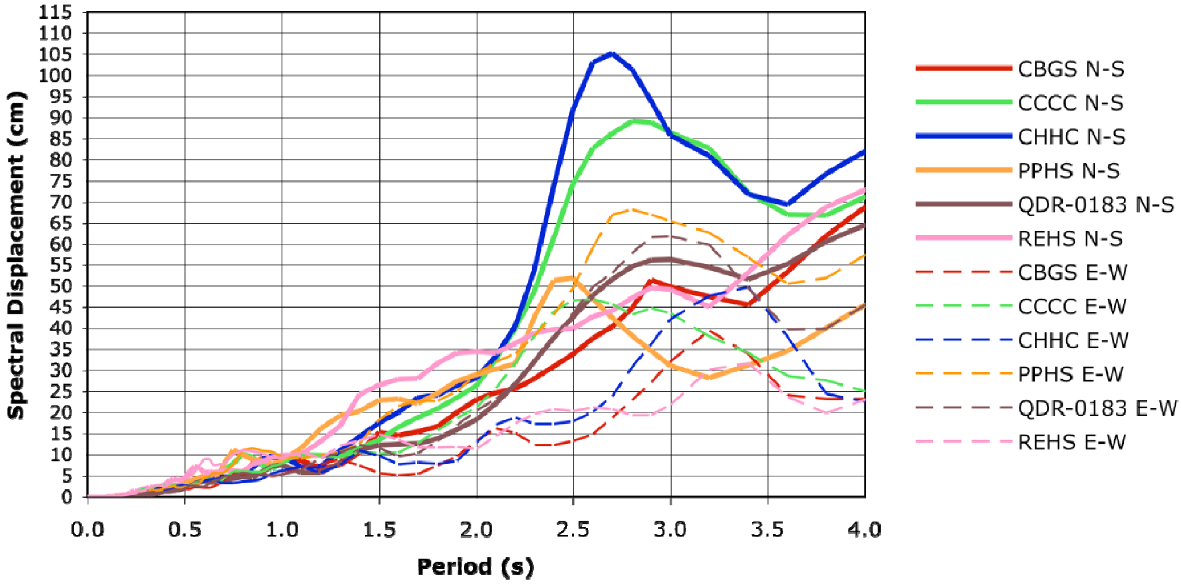

Figure 1.6 **Horizontal spectral displacement, Darfield earthquake, 5% critical damping.**

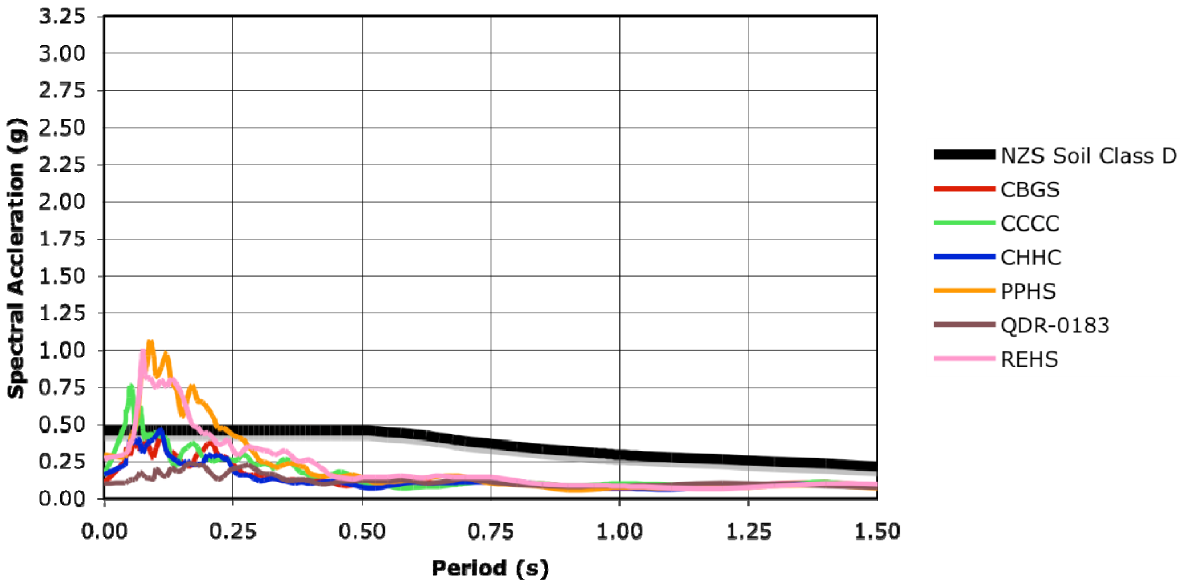

Figure 1.7 **Vertical spectral acceleration, Darfield earthquake, 5% critical damping.**

1.2.2 The Christchurch Earthquake

On 22 February 2011, a magnitude 6.3 aftershock of the Darfield earthquake occurred near Lyttelton at latitude -43° 34' 53.00" and longitude +172° 42' 7.00". The epicenter was 7.84 km outside of Christchurch and hypocentral distance was 5 km. This aftershock became known as the Christchurch earthquake and was the earthquake that caused the most damage to Christchurch.

The Christchurch earthquake was especially damaging to the city of Christchurch because of the proximity to the city, shallow depth, and strong vertical component of ground motion. Earthquake waves lose energy as they travel over distance, so the intensity of shaking decreases with increasing distance. The hypocenter depth and distance from the epicenter act as a buffer from strong shaking, but the city of Christchurch did not have an appreciable buffer from the Christchurch earthquake. The vertical peak ground acceleration recorded during the Christchurch earthquake was 0.69 g, with a peak spectral acceleration calculated to be 3.1 g in the 0.8 sec period range. These are extremely large vertical components when compared to the vertical spectral acceleration of the Darfield earthquake, shown in Figure 1.7, and the June earthquake shown in Figure 1.13. Design provisions for vertical forces in NZS 1170.5:2004, the building code used to design both of the buildings examined in this report, are specified to be 70% of the expected horizontal forces when using the equivalent static load method (structural ductility factor $\mu \geq 2.0$, flexible structures)[3].

The forces developed by the Christchurch earthquake would have been significantly beyond the required design strength for buildings in 0.05 to 0.18 sec vertical period range, even under the most modern provision of the building code. Figure 1.8 and Figure 1.9 show the horizontal spectral acceleration and displacement for the Christchurch earthquake respectively, with the North-South components indicated by a solid line and the East-West components indicated by a dashed line. The Christchurch earthquake greatly exceeded the NZS 1170.5:2004 seismic design spectra for Class D soils over almost the entire range of periods, and would have been a disastrous earthquake even without the unusually large vertical accelerations.

Another highly damaging consequence of the Christchurch earthquake was widespread liquefaction, which was most severe in the northeastern suburbs of Christchurch. Many neighborhoods were left without power or running water immediately after the earthquake,

[3] NZS 1170.5:2004 5.4 Vertical Design Actions

because utility lines and pipes were damaged as a result of the liquefaction. Some neighborhoods, like Bexley and Aranui near the eastern coastline, are still without sewer service as of July 2011 with chemical toilets serving certain areas.

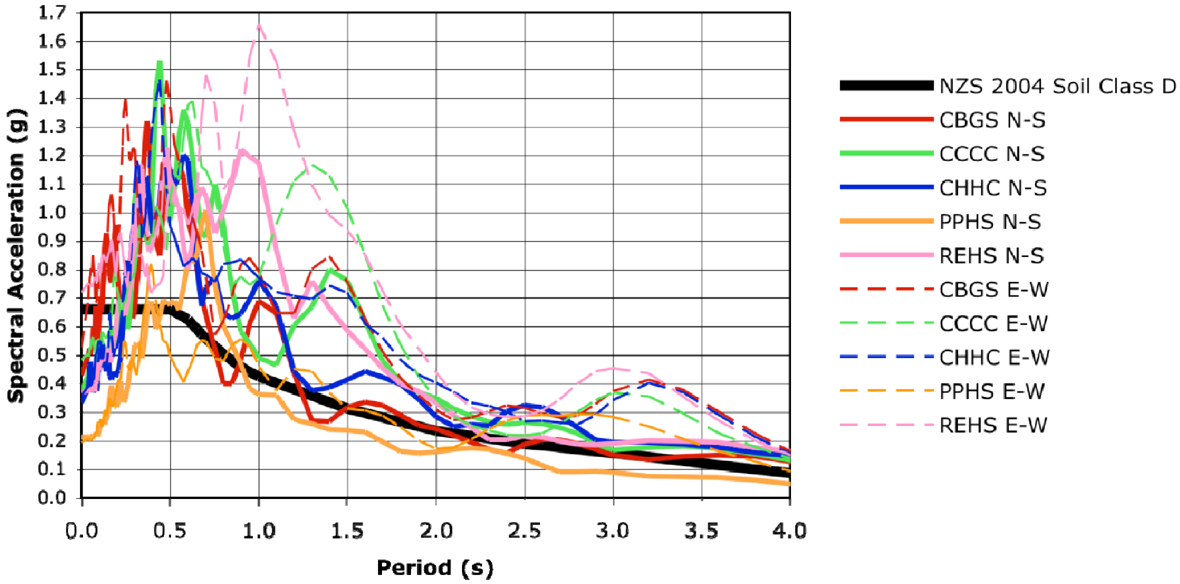

Figure 1.8 Horizontal spectral acceleration, Christchurch earthquake, 5% critical damping

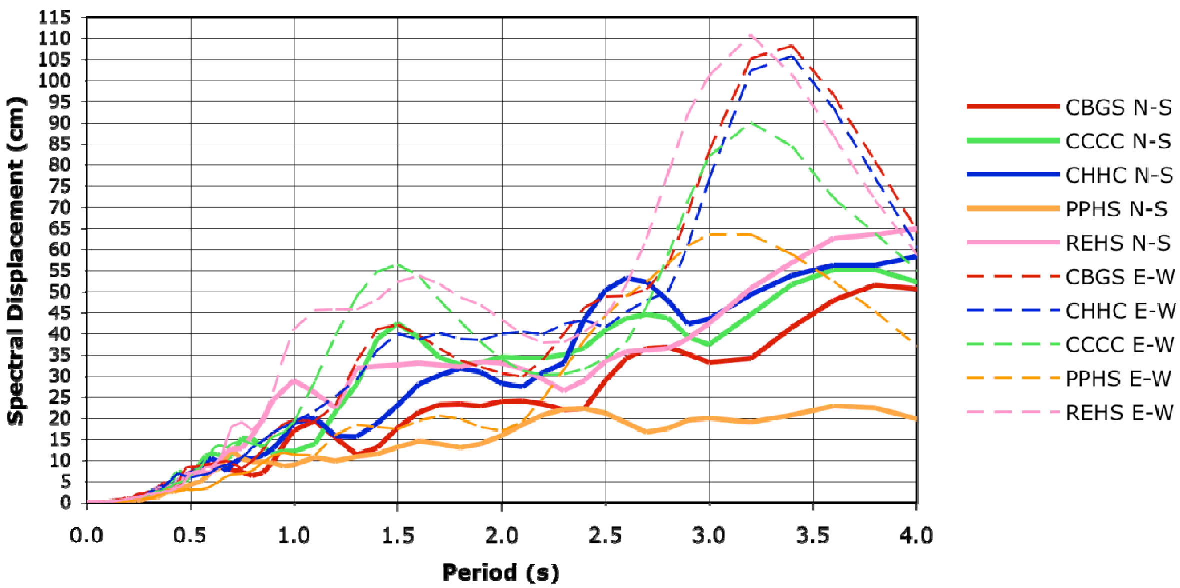

Figure 1.9 Horizontal spectral displacement, Christchurch earthquake, 5% critical damping.

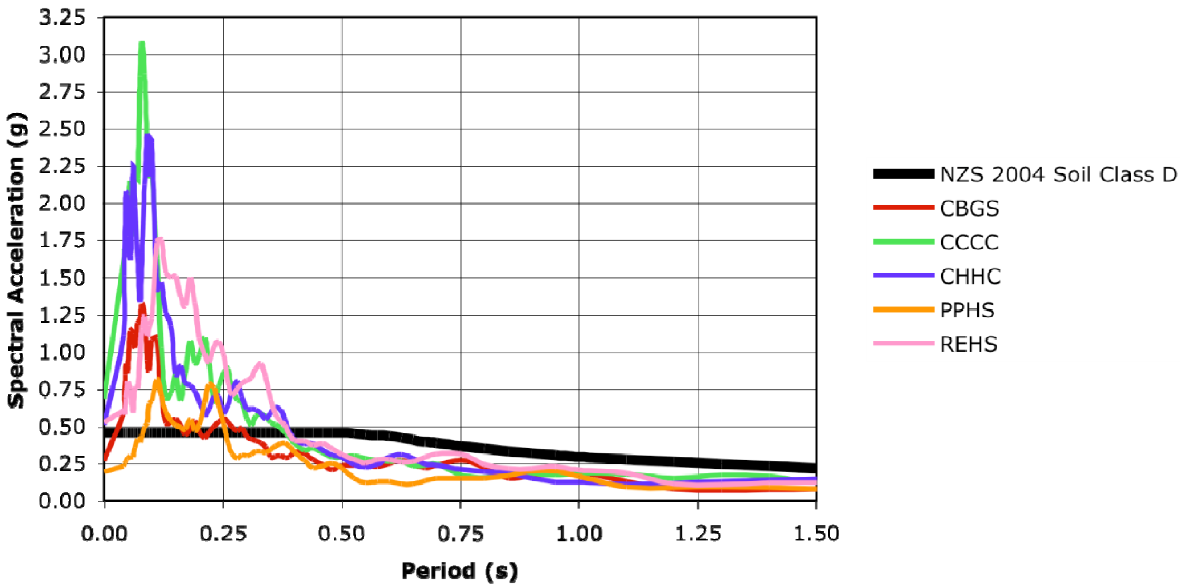

Figure 1.10 Vertical spectral acceleration, Christchurch earthquake, 5% critical damping.

Overall, the Christchurch earthquake caused more damage to Christchurch than any of the other earthquakes in the past year, including the magnitude 7.1 Darfield earthquake. The entire CBD, the commercial heart of the city, is closed to the public because of the collapse hazard of tall buildings and demolition efforts underway. The Christchurch earthquake also interrupted repairs that were in progress from the Darfield earthquake.

1.2.3 The June Earthquake

On 14 June 2011, a magnitude 6.0 aftershock of the Darfield earthquake occurred 9.35 km outside of Christchurch at longitude -43° 33' 50.00" and latitude +172° 44' 35.00", and 6 km below the surface of the earth.

The extent of damage caused by the June earthquake is difficult to evaluate, because the damage from the Christchurch earthquake had not yet been fully assessed when it occurred. Figure 1.11 illustrates the spectral accelerations computed from the June earthquake plotted with the NZS 1170.5:2004 design curve, with North-South accelerations indicated by a solid line and East-West accelerations indicated by a dashed line. The peak spectral acceleration of the June earthquake was less than 1.0 g, which was significantly smaller than the Christchurch earthquake peak spectral acceleration. The peak spectral displacement was 57 cm at a period of 1.7 sec, as shown in Figure 1.12, which is about half the peak spectral displacement during the Christchurch and Darfield earthquakes. The vertical spectral acceleration of the June earthquake, shown in Figure 1.13, is unremarkable when compared with the Christchurch earthquake. The June earthquake generated additional damage, and halted repairs that were in progress so that additional inspections could be conducted.

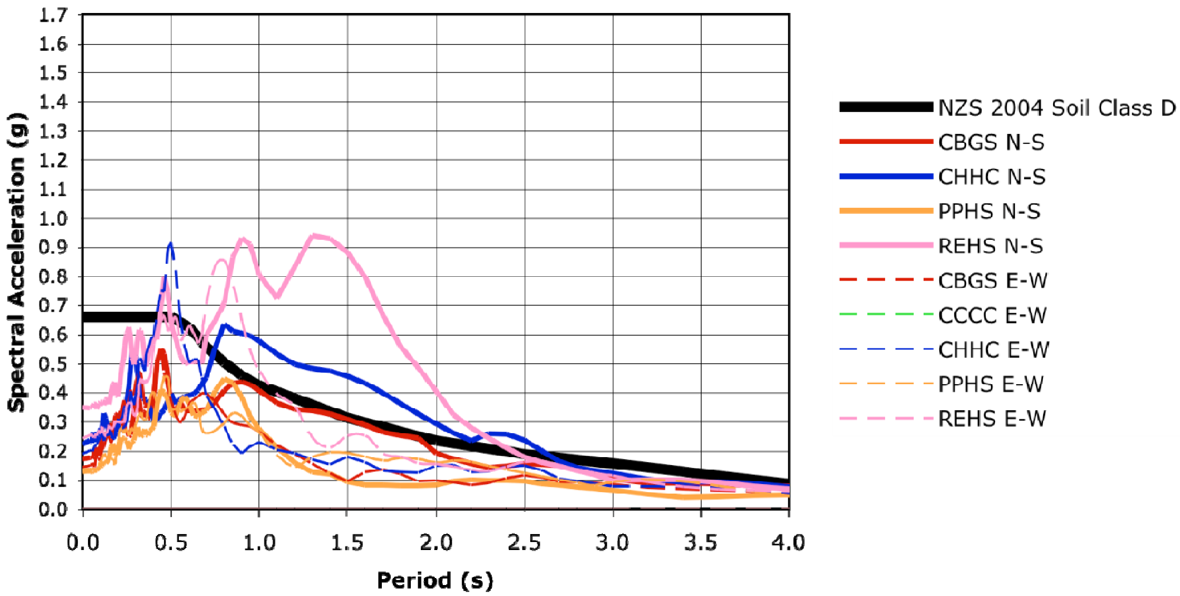

Figure 1.11 Horizontal spectral acceleration, June earthquake, 5% critical damping.

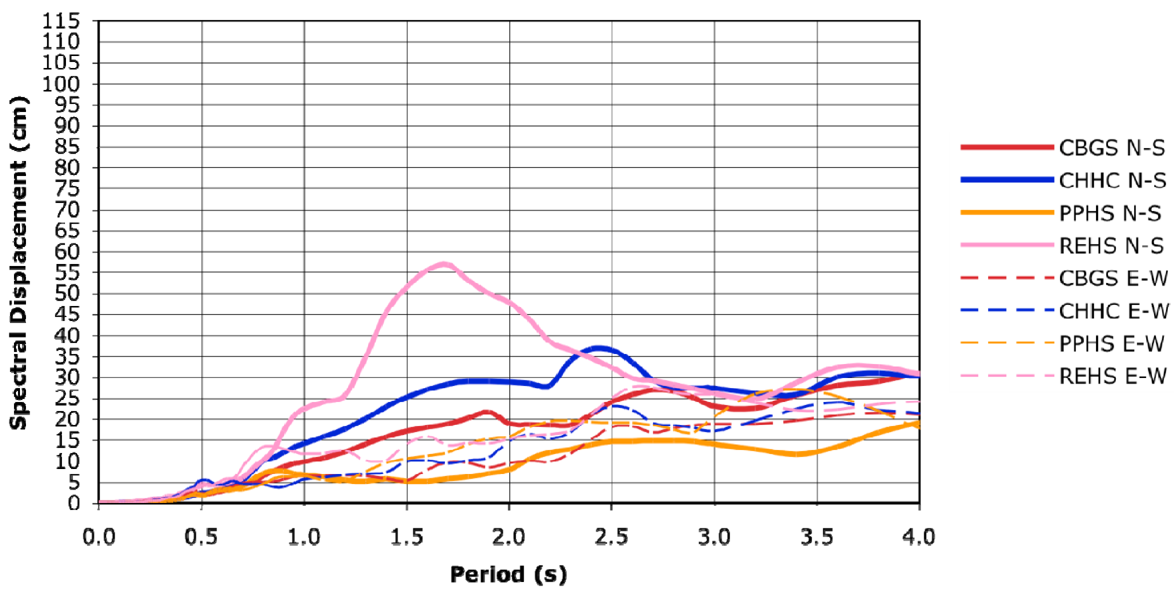

Figure 1.12 Horizontal spectral displacement, June earthquake, 5% critical damping

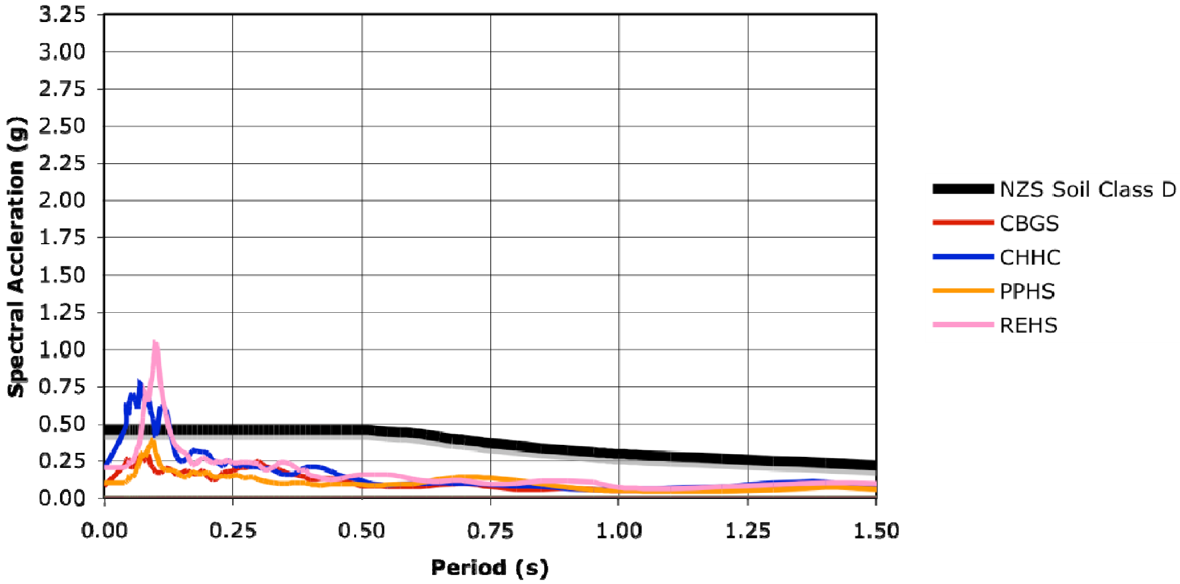

Figure 1.13 Vertical spectral displacement, June earthquake, 5% critical damping.

The greatest impact of the June earthquake was the blow to the confidence of the Christchurch community. An article in local Christchurch newspaper, *The Press,* polled Christchurch residents before and after the June earthquake about their opinions on the recovery process and their feelings of personal safety living in Christchurch, the results of which are summarized in Figure 1.14, which was taken from the Friday, July 22 edition. According to the poll, fewer people were content to stay in Christchurch. One percent of those polled intended to leave the city following the June earthquake, while 5% of people became unsure of their residency. There was also a 20% increase in the expectation of another large earthquake in the next year, and a 13% drop of confidence in the recovery process.

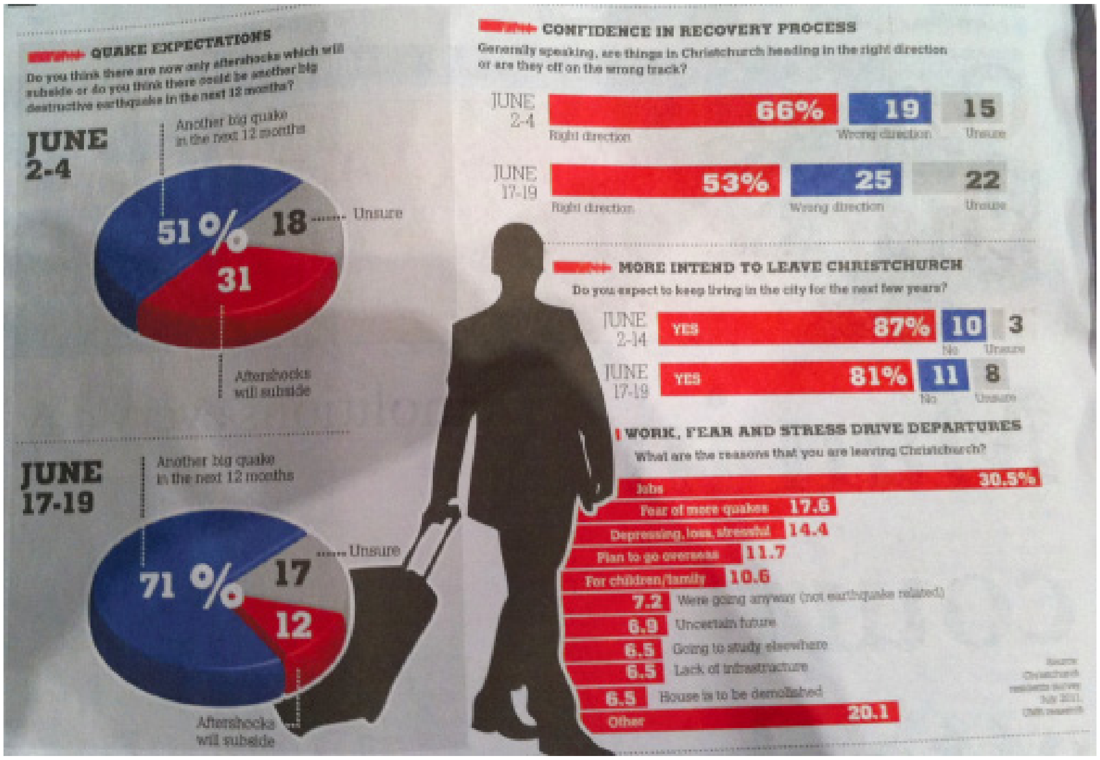

Figure 1.14 Poll of Christchurch residents after June earthquake.

1.3 METHODS

The primary objective of this investigation was to assess and map the damage in two precast concrete buildings in Christchurch: a 9-story hotel in the CBD and a 5-story parking garage in the suburb of Papanui. Earthquake response and ambient vibration responses of the buildings were recorded, as well as documentation of the structural damage. This section summarizes the methodology of data collection.

1.3.1 Damage Recording Methodology

Recording the structural damage to the 9-story hotel and the 5-story parking garage required careful attention to detail and optimal time management to coordinate the necessary activities in the two-week expedition. The damage recording system had three components: photographs, measurements and written descriptions. The photographs were taken in a specific order; the first was a picture of a structural plan view for that building, an example is shown in Figure 1.15, with a tape flag marker to indicate the location and orientation, followed by a context shot showing a wide view of the damage. The context shot is the picture A in Figure 1.16. Following the context shot, several close-up pictures (B, C, D and E) were taken with a scale included to document the dimensions and severity of the damage.

Figure 1.15 Damage location photograph

Figure 1.16 Context image and damage documentation.

Written descriptions were used to expedite the recording of crack patterns in beams and columns, and to note any unusual damage for reference. Narrow cracks in concrete, from hairline, here defined as less than 0.1 mm, to 0.3 mm, did not show up well in photographs. Furthermore, photographing each individual crack in a beam was very time consuming. Because there was a limited timeframe in which to collect data, a method for crack recording was used that allowed data to be recorded more quickly and in a manner that was easier to interpret than photographs. The data recorded consisted of the distance from the crack to a reference point, the width of the crack and any other characteristics of the crack, such as length of penetration into the face of the beam or column and angle of inclination. The photographs and written descriptions were used in concert to develop the crack maps discussed in Section 1.4.1 for both buildings.

1.3.2 Sensor Placement

In order to establish the dynamic properties of each of the buildings, accelerometer sensors were installed for two types of measurements: earthquake monitoring and ambient vibration monitoring. The earthquake monitoring sensors were installed in the 5-story parking garage for 3 days, and in the 9-story hotel for 7 weeks. In the 5-story parking structure, tri-axial earthquake monitoring sensors were installed at opposite ends of the ramp from the third story to the fourth story and the ramp from the third story to the second story at the base of columns. Additional tri-axial sensors were installed at the roof and basement levels in the southwest corner of the building. A total of 12 sensors were deployed for this monitoring. This array of sensors allowed for measurement of torsion of the building under earthquake loading.

In the 9-story hotel, tri-axial sensors were mounted in the basement at the northeast corner of the stairwell, on the floor of the third story, and on the roof. Three uni-axial accelerometers were also deployed. One was mounted on the opposite side of the building at the roof level, and two at the basement level oriented vertically. This sensor array made it possible to record the torsion and rocking of the foundation in response to ground motion.

For ambient vibration recording, two tri-axial accelerometers were installed temporarily at each level on opposite ends of the longitudinal span of the building for both the 9-story hotel and the 5-story parking garage. Each level was monitored individually. The accelerometers were put in place and data recorded for 20 minutes without any forced vibration of the building. After recording for 20 minutes, the sensors were moved to the next level of the building. Some of the earthquake monitoring sensors installed in both buildings were used as a reference to process the data. The ambient vibration data was processed to identify the fundamental periods of vibration of both buildings, as presented in Section 1.4.1.2 and Section 1.4.2.2.

1.4 RESULTS

This investigation resulted in two general categories of results: crack maps for damage assessment and tabulated values of fundamental periods and damping obtained from the damaged structures. Schmidt hammer rebound tests were conducted in both buildings to estimate the compressive strength of certain precast elements. Calibration tests were done on a small-scale bridge column test specimen and concrete cylinders taken at the time of casting the test specimen. These calibration tests were performed to assess the validity of the field Schmidt hammer tests, the results of which are summarized in Table 1.1. Calibration test results were not very accurate, and the actual compressive strength values fell outside the error margin in all trials of the calibration test. The results of the field Schmidt hammer tests have been included in the following sections to give a comparison of the relative compressive strengths of different elements, but should not be considered accurate in light of the calibration test results.

Table 1.1 Calibration testing of Schmidt Hammer

Component cast	Element	f'_c (ksi)	
		Schmidt hammer tests (Error)	Concrete cylinder strength[1]
Column	Column	4.3 (±0.8)	5.7
	Load stub	4.2 (±0.8)	
	Cylinder	2.5 (±0.7) [1,2]	
Footing	Footing	4.6 (±0.8) [3]	7.0
	Cylinder	4.4 (±0.8) [1]	

[1] Average of three cylinders.
[2] Moisture may have comprimised the rebound test results.
[3] Average of horizontal and vertical trials.

1.4.1 Nine-Story Hotel

The LFRS of the 9-story hotel consisted of a moment resisting frame system, consisting of precast beams and cast-in-place columns. The diaphragm consisted of 75 mm of topping poured over 75-mm-flat slabs. After the Christchurch earthquake the 9-story hotel was heavily damaged, with significant cracking in the longitudinal and transverse beams and in the slab between gridlines 2 and 3. Temporary shoring of the stairwell was installed for safety while the internal partitions were removed so that the severity of the damage could be assessed. This damage assessment was in progress when the June earthquake occurred, and had not yet been repaired. The June earthquake exacerbated the damage caused by the Christchurch earthquake by widening cracks and causing movement in partitions and cladding.

Table 1.2 contains the compiled Schmidt hammer test data for the 9-story hotel, separated by element and location. The precast beams all had a compressive strength of 7.5 ksi, plus or minus the margin of error. The cast-in-place columns had compressive strengths ranging from 5.5 to 7.3 ksi. The topping slabs in the 9-story hotel were measured at two levels. The average compressive strength values for the topping slabs were 5.6 and 6.5 ksi.

Table 1.2 Estimated concrete strengths, 9-Story hotel.

Element	Location	f'_c (ksi)	Error (ksi)
Beam	8th Floor (D4)	7.3	±1.0
	7th Floor (D4)	7.8	±1.0
	6th Floor (D4)	7.5	±1.0
	5th Floor (D4)	7.6	±1.0
	4th Floor (D4)	7.2	±1.0
	3rd Floor (D4)	6.8	±0.9
	2nd Floor (D4)	7.2	±1.0
	1st Floor (D4)	6.5	±0.9
Column	3rd Floor (A2)	7.3	±1.0
	3rd Floor (A4)	6.8	±0.9
	3rd Floor (G4)	7.0	±1.0
	Basement (A2)	5.5	±0.9
	Basement (B4)	6.5	±0.9
	Basement (E2)	6.1	±0.9
	Basement (E3)	5.6	±0.9
Topping Slab	3rd Floor (E2)	5.6	±0.9
	2nd Floor (E2)	6.5	±0.9

1.4.1.1 Crack Maps

The crack maps addressed in this section are the result of the compilation of photographed and documented damage, and are intended to show overall patterns in the earthquake damage.

Figures 1.17 and 1.19 are crack maps of the South and East elevations of the 9-story hotel respectively, and Figure 1.18 and Figure 1.20 are close up views. Figure 1.18 is an expanded view of level 4 and level 5 between gridlines A and B, and Figure 1.19 is an expanded view of level 4, level 5 and level 6 along gridline A. The grey color represents areas of exposed concrete. Solid black areas indicate spalling, and black lines indicate cracks. The more lightly colored areas are portions of the structure that were obscured by partitions at the time of investigation. When the crack's propagation into the beam could not be observed, a solid black circle marks the crack's location. All cracks and spalling indicated are documented in the same orientation and to the correct scale, with as much accuracy as was possible using high-resolution photography and detailed documentation.

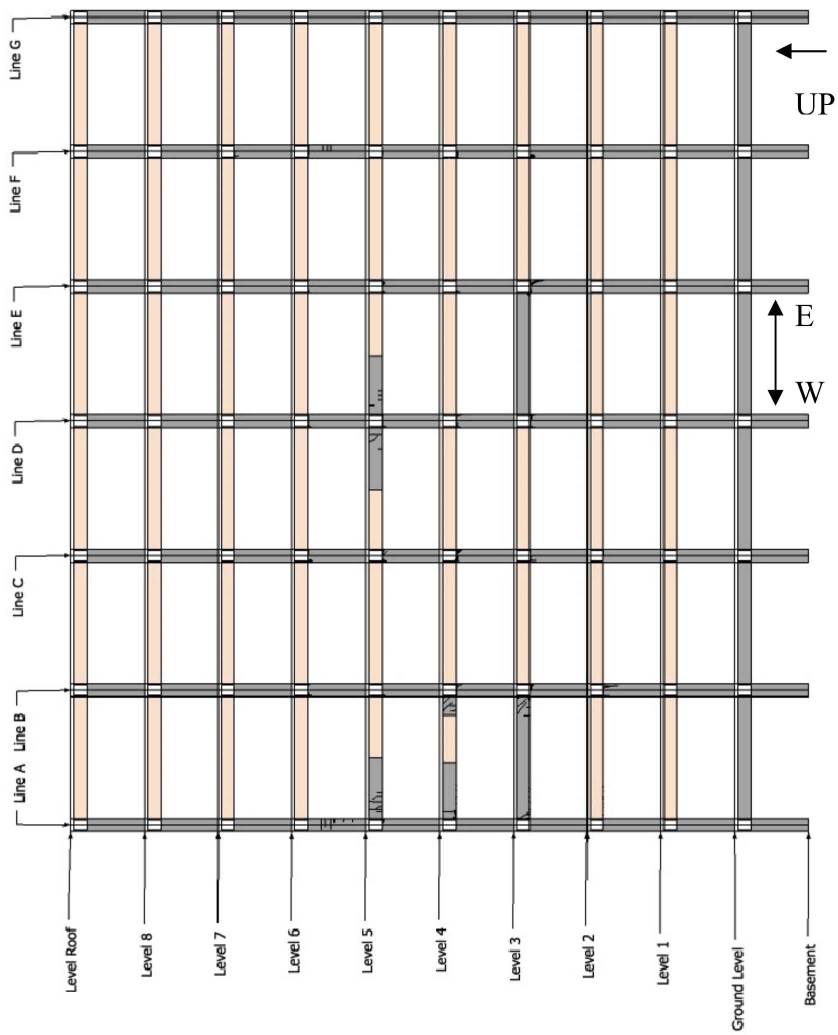

Figure 1.17 Nine-Story hotel line 2, South elevation.

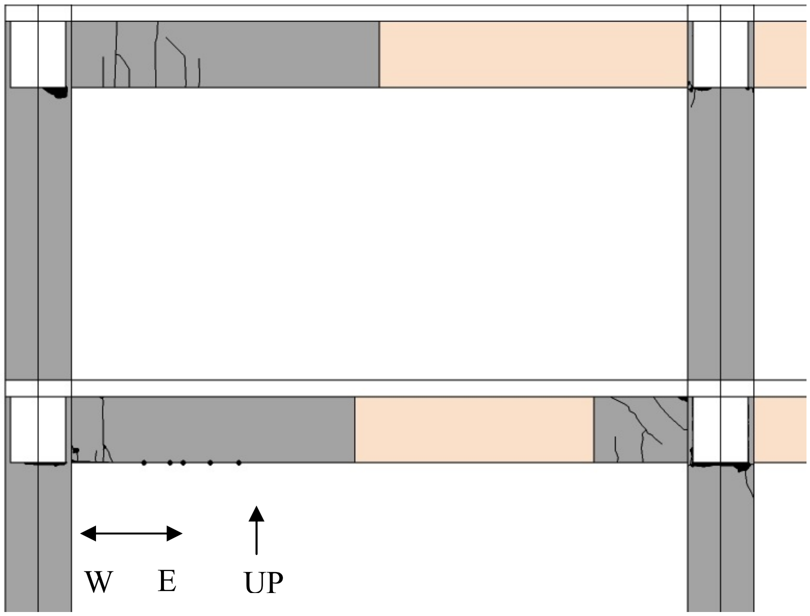

Figure 1.18 Nine-story hotel line 2, South elevation, levels 4, 5, beam AB.

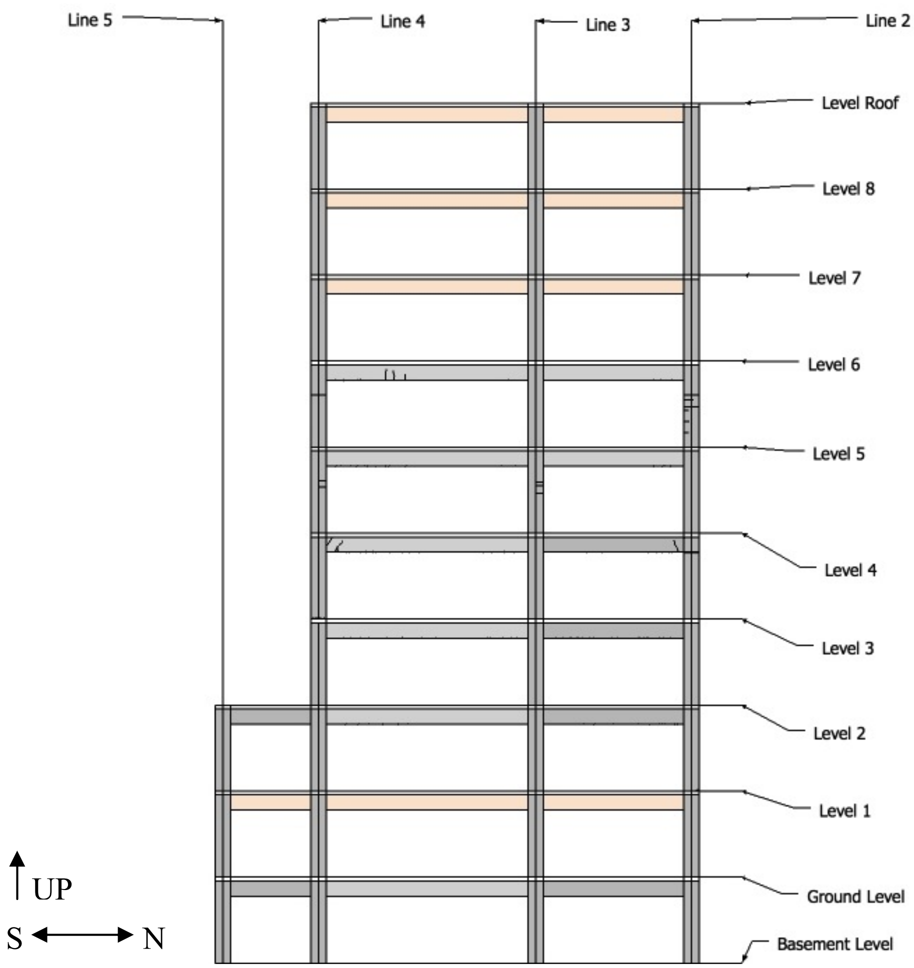

Figure 1.19 Nine-story hotel line A, East elevation.

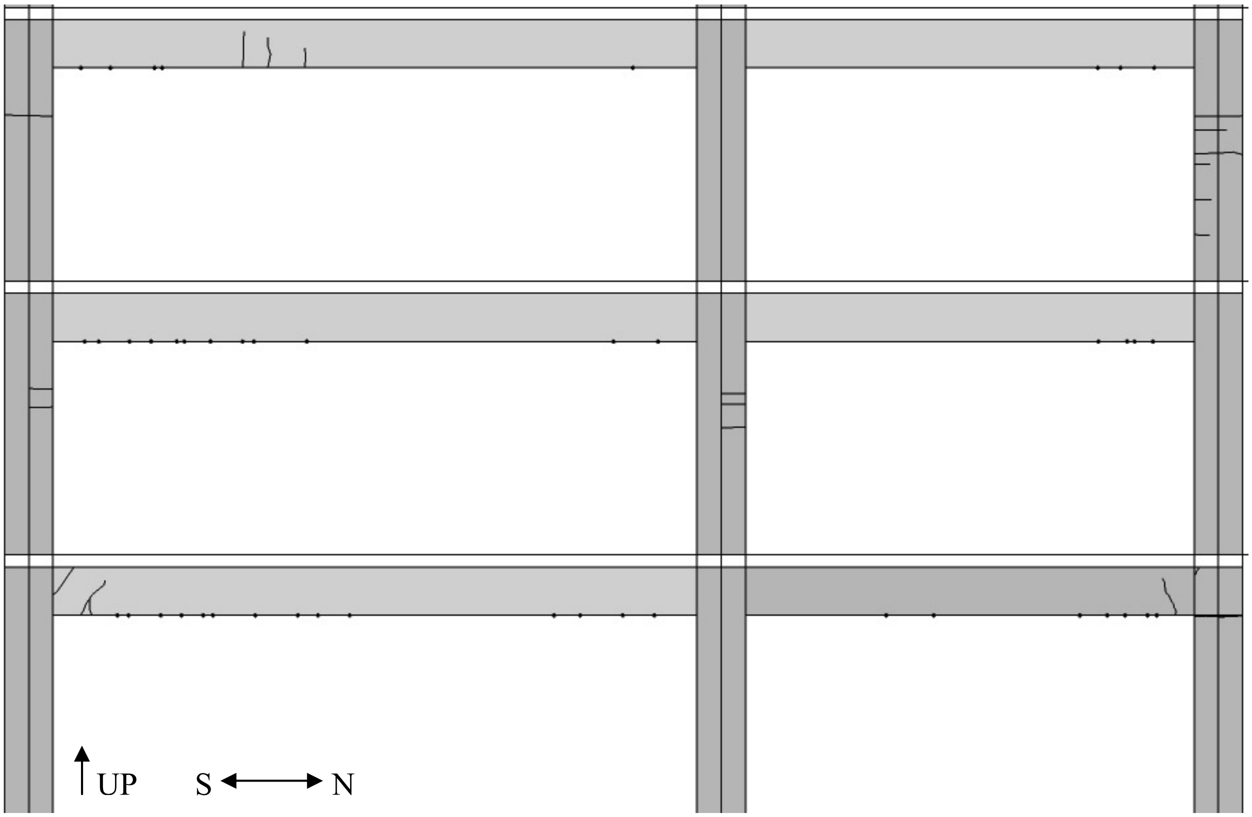

Figure 1.20 Nine-story hotel line A, East elevation, Levels 4, 5, and 6.

1.4.1.2 Fundamental Periods and Damping

The ambient vibration analysis results of the 9-story hotel are compiled in Table 1.3. The longest fundamental period was found to be 0.78 sec, with 2% damping. This damping value is lower than the 5% assumed by modern design codes, but is not a surprising value. Because ambient vibration analysis was used when calculating the damping values tabulated below, no hysteretic damping was measured.

Table 1.3 Fundamental periods and damping, 9-story hotel.

Direction (Mode)	Frequency (Hz)	Period (s)	Damping
Trans (1)	1.28	0.78	2%
Long (1)	1.32	0.76	2%
Torsion (1)	1.7	0.59	2%
Long (2)	4.1	0.24	1%
Trans(2)	4.2	0.24	2%
Torsion (2)	5.3	0.19	
Long (3)	6.6	0.15	
Trans (3)	7.1	0.14	

1.4.2 Five-Story Parking Garage

The LFRS of the 5-story parking garage consisted of vertical cantilevered structural walls. The diaphragm consisted of cast-in-place topping over precast hollowcore units. The 5-story parking garage was undamaged after the Darfield earthquake. After the June earthquake, four vertical cantilever walls were severely damaged enough at the ground level to warrant replacement, and one of the walls had wall-to-floor connection damage at the roof and fifth levels. The structure was under repair at the time of observation. The ground level panels of two of the vertical cantilever walls had been demolished for replacement and three more ground level panels had been replaced with cast-in-place wall elements.

Table 1.4 contains the compiled Schmidt hammer test data from the 5-story parking garage. Two Schmidt hammer tests were conducted at the 5-story parking garage, both on Wall 11 indicated in Figure 1.21. The first test was conducted on the corner wall, and the second test was conducted on the foundation beam supporting the wall. The wall was found to have a compressive strength of 7.6 ksi, and the foundation beam had a compressive strength of 6.8 ksi. These values are subject to the same uncertainty shown in the calibration tests in Table 1.1.

Table 1.4 Estimated concrete strengths, 5-Story parking garage.

Element	Location	f'_c (ksi)	Error (ksi)
Wall	North-West (Wall 11)	7.6	±1.0
Footing	North-West (Wall 11)	6.8	±0.9

1.4.2.1 Crack Maps

The crack maps in this section are also the compilation of damage photographs and documentation collected during the expedition. Figure 1.21 shows the west elevation of the 5-story parking garage, and Figure 1.22 shows an expanded view of Wall 17 at the ground level. Wall 11 and Wall 17 were the most significantly damaged walls that were observed on this expedition. Grey shading indicates areas of exposed concrete, and lighter shading indicates areas that were obscured from view. The white area on Wall 12 represents an area where the wall had been removed, and the shaded area on Wall 14 represents an area where the wall had already been replaced. Black lines represent cracks, and solid black areas represent spalling. The most significant damage to the west face, portrayed in Figure 1.22, occurred in the region around the openings in the wall.

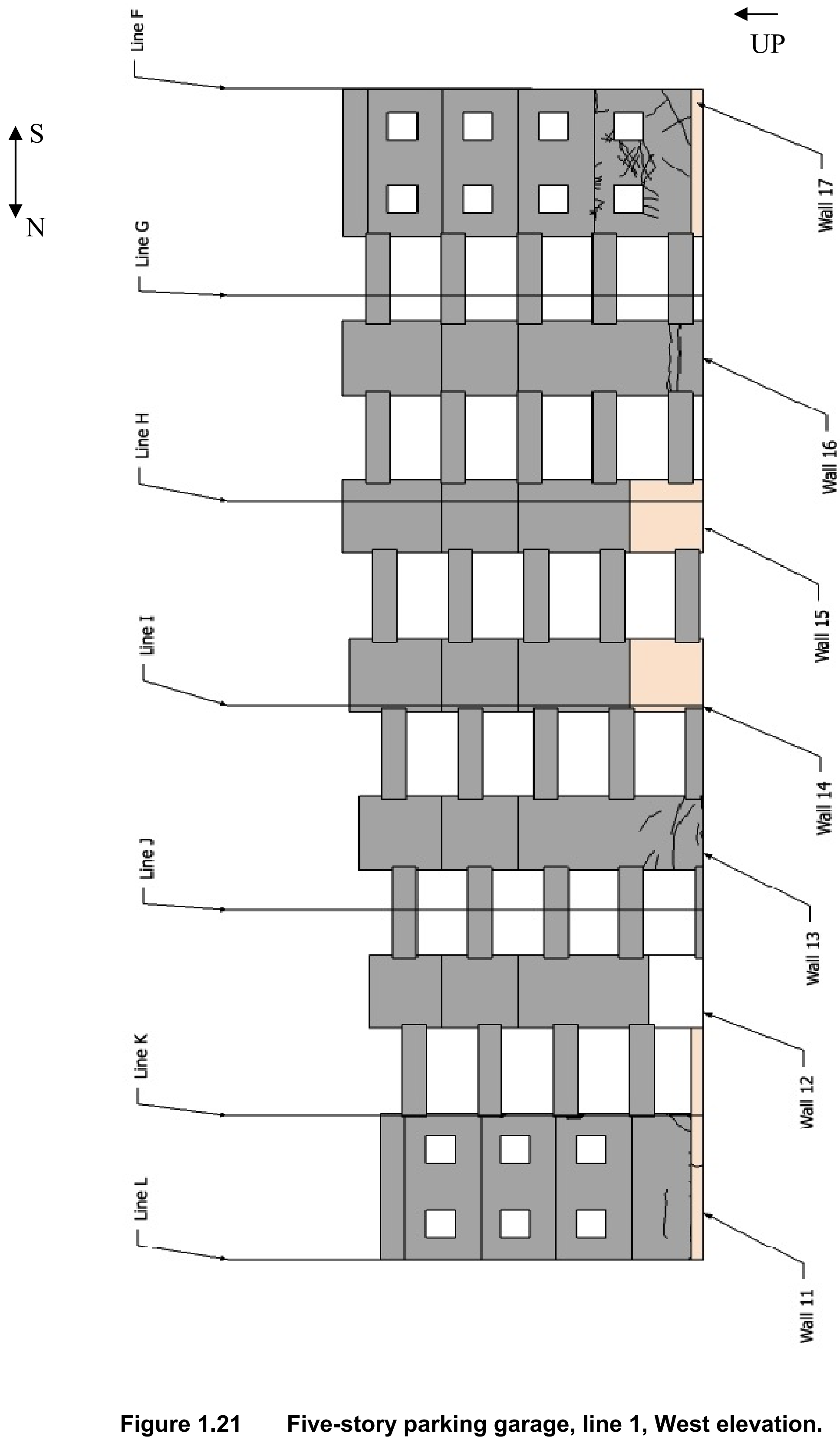

Figure 1.21 Five-story parking garage, line 1, West elevation.

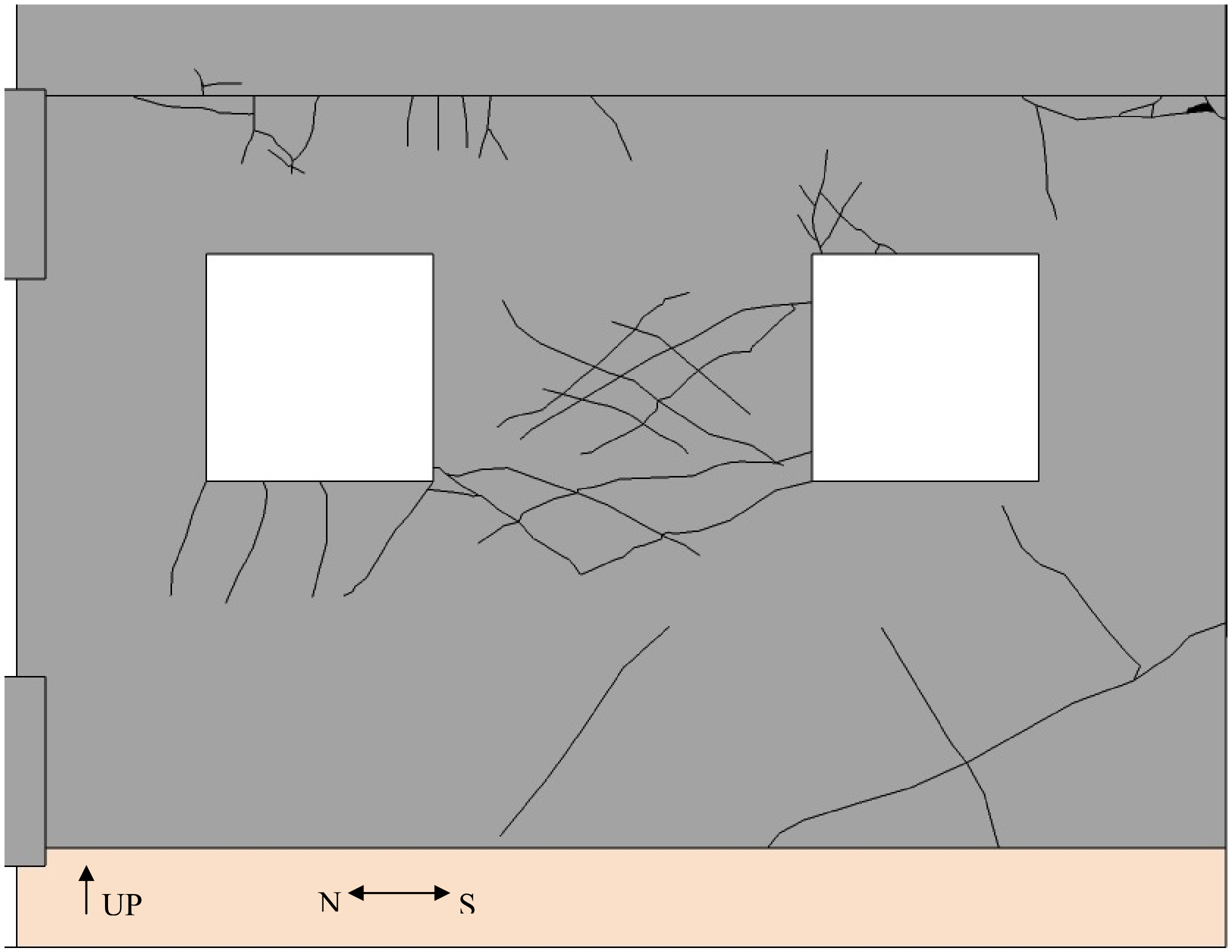

Figure 1.22 Five-story parking garage, line 1, West elevation, wall 17.

1.4.2.2 Fundamental Periods and Damping

The ambient vibration analysis of the 5-story parking garage is compiled in Table 1.5. The longest fundamental period was calculated to be 0.34 sec, with 3% critical damping. Because the damping values were calculated using ambient vibrations, hysteretic damping did not contribute to the damping value measured.

Table 1.5 Fundamental periods and damping, 5-story parking garage.

Direction (Mode)	Frequency (Hz)	Period (s)	Damping
Trans (1)	2.9	0.34	3%
Long (1)	3.2	0.31	2%
Torsion	4.5	0.22	
Trans (2)	9.1	0.11	
Long (2)	10	0.10	

1.5 CONCLUSIONS

The scope of this project was to collect perishable data on the damage to two precast concrete buildings, archive this data for future reference, and comment on the resiliency of the Christchurch community. As such, there are no detailed conclusions made about the structural damage since analysis of the performance was beyond the scope of this report. However, the buildings performed as intended, preserving life-safety during events beyond the design basis. Furthermore, they exhibited ductile deformation, and the sustained damage is repairable.

The crack maps developed to date are limited in content due to inaccessible regions in the structures. In the 5-story parking garage, the exterior above ground level was inaccessible, with the exception of Wall 17 as shown in Figure 1.21. The 9-story hotel had a similarly inaccessible exterior, with only the second level as an exception. On the interior, many areas of interest were obscured by partitions that were largely undamaged and thus had not been removed. It is presumed that the limited partition damage correlates to minor structural damage, but this was not investigated.

In the 9-story hotel, the crack maps indicate damage to the precast beam-column joints, beams, and columns. Beams and columns exhibited flexural cracking, while the joints developed limited spalling in the columns at the beam connection. There was only one instance of exposed longitudinal column reinforcement. Significant diaphragm cracking was isolated to the floor of levels 3 and 4 at the first joint between precast floor units. This 4 mm wide crack through the topping in the south end of the building between gridlines 2 and 3 along with beam cracking in both directions is evidence of beam elongation. At the foundation level of the hotel, there was no damage observed except cracking in retaining walls of the basement. Damage was concentrated on Levels 3, 4, and 5

In the 5-story parking garage, the crack map shows severe shear and flexural cracking in the vertical cantilever walls at each end of the structure, especially in the boundary area near window openings. Beams in the structure showed moderate flexural cracking, but the damage was difficult to date because it had not been documented between the successive earthquakes. The one-way slab on the ramped sections of the parking garage showed cracking between the two centrally located, transversely oriented shear walls. The damage was concentrated in the ground level panels of the vertical cantilever walls, with the exception of a wall-to-diaphragm connection failure that occurred at the top level of the parking structure in the northwestern corner.

The conclusions reached regarding the Christchurch community resiliency are based on observations made in Christchurch and are not meant to be a rigorous investigation. The impression after spending two weeks in and around the Christchurch area was that the resiliency of the community was strong, but was reduced by the continuing large earthquakes. The Central Business District, the downtown area containing the main commercial businesses in the city, was still closed to the public and demolition on several buildings at high risk of collapse had not yet begun six months after the Christchurch earthquake. Several suburbs were still without proper sewer service, and the residents of those areas were using chemical toilets. Many businesses were closed by their owners due to damage. Although all of these observed characteristics indicated poor resiliency in the Christchurch community, the current state of the city is most likely result of continued seismic activity and not poor resiliency. The 20% of Christchurch citizens who are estimated to have left the city may have been more inclined to return to their businesses and begin repairing their property if they were not afraid of another significant earthquake undoing all of their efforts. If not for large aftershocks continuing for several months after the most damaging earthquake, e.g. the magnitude 6.0 June earthquake that occurred five months after the devastating Christchurch earthquake, the city of Christchurch may have been able to recover more rapidly. Although 80% of the population is still committed to Christchurch a significant portion has been scared away, hopefully to return once the aftershocks become less frequent and intense.

ACKNOWLEDGMENTS

Dr. José Restrepo, of the University of California, San Diego, was the Principal Investigator (PI) for this project along with co-PI Dr. Robert Fleischman, of the University of Arizona. The investigation was a RAPID award funded by the National Science Foundation; Funding for the expedition to Christchurch was secured from the National Science Foundation under grant CMMI-1138358. Any opinions, findings, and conclusions or recommendations expressed are those of the author and do not necessarily reflect the views of the National Science Foundation.

Dr. Matt Schoettler, a post-doctoral researcher from the University of California, San Diego, was the mentor assigned by the PEER REU program that led the investigation and supervised the post-processing of the data gathered in New Zealand.

Dr. Robert Nigbor was a collaborator from the University of California at Los Angeles who participated in the expedition. Dr. Nigbor supervised the installation and monitoring of the ground motion data acquisition system, and was responsible for the ambient vibration data collection and processing. All information on the natural frequencies and damping of the buildings addressed in this report is credited to Dr. Nigbor.

Dr. Stefano Pampanin, of the University of Canterbury, and his graduate students were our New Zealand contacts and guides, and were critical to the success of our expedition. Dr. Pampanin facilitated our access to the Central Business District of Christchurch by interceding on our behalf with the Canterbury Earthquake Recovery Authority (CERA). His graduate students Sahin Tasligedik, Umut Akguzel, and Patricio Quintana Gallo assisted in damage documentation and data collection for both buildings. Their support and contribution is greatly appreciated.

REFERENCES

Filiatrault, A. [2002]. *Elements of Earthquake Engineering and Structural Dynamics*, 2nd ed. Montreal: Ecole Polytechnique de Montreal.

GeoNet, New Zealand [2011]. ftp://ftp.GeoNet.org.nz/strong/processed/Proc/ Strong Motion Processed Data. GNS Science and Earthquake Commission, NZ.

Sachdeva, S., Fri. Jul. 22, 2011. June quakes rattle confidence. A2. *The Press*, Christchurch.

Standards New Zealand [1992]. Code of practice for general structural design and design loadings for buildings, *NZS 4203:1992*, Wellington, New Zealand.

Standards New Zealand [2004]. Structural design actions, part 5: earthquake actions. *NZS 1170.5:2004*, Wellington, New Zealand.

2 The Resilient City: Achieving Shelter-in-Place in San Francisco

AMY DHALIWAL

ABSTRACT

In order for San Francisco to be considered a resilient city, 95% of residents need to be able to Shelter-in-Place. Shelter-in-Place means that after the event of an earthquake, residents should be able to stay in their homes instead of having to move to temporary shelters. Hence, creating a mapping scheme at a neighborhood scale which categorizes the amount and types of buildings in a neighborhood applicable to Shelter-in-Place is integral. The goal of this research effort has been to map the seismic vulnerability of buildings in San Francisco at a neighborhood scale to determine Shelter-in-Place capability, as well as to gain a better understanding of the people who live in the various neighborhoods of the city by creating and analyzing supplementary demographic documents for each neighborhood.

2.1 INTRODUCTION

The University of California, Berkeley Pacific Earthquake Engineering Research Center placed two interns, Amy Dhaliwal and John Pham, at the San Francisco Planning and Urban Research Association (SPUR) to get hands on experience in the field of planning. Mary Comerio, a professor at the University of California, Berkeley, and Sarah Karlinsky, Deputy Director at SPUR, served as mentors for interns. Furthermore, the interns were assigned to work on the same project entitled: San Francisco: The Resilient City. The report that follows is a summary of the work that completed by Amy Dhaliwal for the project.

The San Francisco Planning and Urban Research Association (SPUR) launched an effort to mitigate the current housing stock and provide policy recommendations for future housing construction in effort to make San Francisco a more resilient city. The goal of the Shelter-in-Place initiative is to prevent panic over temporary shelter after the event of an earthquake by aiming to have 95% of residents able to stay in their homes after an earthquake (see Figure 2.1). The Shelter-in-Place task force consists of many people, each working on a different piece of the same puzzle. There are two tasks covered in this report. First is the development of the mapping scheme that was created to help determine the number of units capable to Shelter-in-Place. Second is the analysis of the supplemental demographic documents, which were created to convey information that coincides with the maps created in task one. The information displayed through the maps and supplemental demographic documents is critical in helping the city plan for resiliency.

Figure 2.1 Homes destoryed by an earthquake in San Francisco.

2.1.1 Background

Natural disasters such as earthquakes, tsunamis, hurricanes, and tornadoes undoubtedly cause panic and fright within a community. Case studies of regions hit hard by natural disasters show that one major repercussion of a natural disaster is community loss. People who lose their homes in natural disasters are prone to moving out the region in search of another house somewhere else because they see no point in staying in a place where they no longer have a home. Also, people who have lost their homes to a natural disaster are frightful of rebuilding their home is the same location because they may feel that if a disaster can strike once, it is likely to happen again as well. This example especially holds true in the case of New Orleans after the disastrous Hurricane Katrina (see Figure 2.2). New Orleans saw a lot of population loss because thousands of people lost their homes and repair efforts would take too long to convince them to stay. Even today, six years later, traces of Hurricane Katrina are visible in New Orleans. Repair efforts have unsuccessful in restoring the housing stock to date as well as the spirits of the community. New Orleans is just one example of the numerous regions that have faced similar harsh repercussions for not being prepared to adequately handle post-disaster consequences. Thus, in order to deter community loss along with other post-disaster consequences, the San Francisco Planning + Urban Research Association (SPUR) has launched an initiative entitled "Shelter-in-Place" which aims at making San Francisco a more earthquake resilient and prepared city. Shelter-in-Place intends to keep people in their homes during and after the event of an earthquake instead of placing people in temporary shelters, which is something that is nearly impossible in city as compact as San Francisco, in order to preserve community and deter other unfortunate consequences brought about by natural disasters.

Figure 2.2 A home destroyed by Hurricane Katrina in New Orleans.

2.1.2 San Francisco Planning + Urban Research Association (SPUR)

The San Francisco Planning + Urban Research Association (SPUR), a think tank, promotes good, sustainable planning for San Francisco by education, advocacy, and research. SPUR tackles many different areas of planning, the following are some programs and initiatives lead by SPUR: community planning, disaster planning, economic development, regional planning, sustainable development, transportation, housing, climate adaptation, and the resilient city. The Shelter-in-Place initiative lead by SPUR ties into disaster planning and the resilient city programs by SPUR. SPUR launched the Shelter-in-Place initiative to inspire San Francisco to be become a resilient city. According to SPUR, a resilient city is one where 95% of residents can Shelter-in-Place and in order for San Francisco to be considered a resilient city, the current and planned housing stock must be mitigated to standards that allow residents to stay in their homes after an earthquake strikes. For this to be possible, there are many factors that need to be determined such as the engineering standards that will allow homes to be to provide shelter, the economic and social costs of Shelter-in-Place, and most importantly understanding how our current housing stock will perform, in regard to Shelter-in-Place, during the event of an earthquake. The Shelter-in-Place task force for task one tackled the obstacle of determining how the current housing stock will perform during an earthquake. The task force consisted of SPUR employees: Sarah Karlinsky, along with other residents involved in the city's disaster planning such as engineers: Chris Poland, David Bonowitz, David Friedman, consultants: Lauire Johnson, Laura Dwelley-Samant, Tom Tobin, Libby Seifel, Steve Murphy, inspectors: Debra Walker, Laurence Kornfield, professors: Mary Comerio, Jack Moehle, United States Geological Survey employees: David Schwartz, Kevin Knudsen, Tom Holzer, Jack Boatwright, city employees: Heidi Sieck, as well as PEER 2011 summer interns: Amy Dhaliwal and John Pham. While each member of the task force worked on a different portion of the same project, the interns, Amy and John, worked with various members of the task force to create a mapping scheme at the neighborhood scale to provide insight about the usability and resiliency levels of the current housing stock to help determine the units capable of allowing Shelter-in-Place. Also, supplemental demographic documents were created in addition to the maps to provide insight on the people who occupy the homes and to analyze the relationship between demographics such as age, income, and race with the usability and resilience of homes. The maps and supplement demographic documents created by the interns are beneficial to the other task force members because as each task force member writes up their piece for the SPUR resilient city report, they can glance over the maps and documents to get better understanding of the demographic and usability break down of the city.

2.1.3 City Action Plan for Seismic Safety

The City Action Plan for Seismic Safety (CAPSS) was a study that analyzed the earthquake vulnerability of all of San Francisco's privately owned buildings. The study broke down San Francisco into fourteen neighborhoods: Bayview, Central Waterfront, Downtown, Excelsior, Ingleside, Marina, Merced, Mission, North Beach, Pacific Heights, Richmond, Sunset, Twin Peaks, Western Addition. (The same breakdown of fourteen neighborhoods was used for the mapping scheme for seismic vulnerability.) Furthermore, results from the study are reliable to the citywide level due to the assumptions that were used; however the results are unreliable when aggregated to the neighborhood level. It is beneficial for the city, as well as the Shelter-in-Place task force, to have data on the earthquake vulnerability of buildings in San Francisco at a neighborhood scale so that it would be simple for the city, before the event of an earthquake, to match expected housing losses with likely demographic profiles and also get a better understanding of probable post-earthquake short-term and long-term shelter needs. As previously stated, setting up temporary shelters would be quite a feat in a city as compact as San Francisco. Hence, it is doubly importantly for the city to have access to data on seismic vulnerability and building usability post-earthquake at a neighborhood scale. Thus, since CAPSS study reported results accurate at a citywide scale but inaccurate at a neighborhood scale, it was important to use the CAPSS data but only after fine-tuning it by aggregated down to a neighborhood scale which was a major task on its own and will be discussed further under research methods.

2.2 RESEARCH GOALS

This research effort is aimed at making San Francisco a more resilient city. The entire Shelter-in-Place initiative was launched in the effort to make San Francisco more resilient, however mapping the usability of buildings after an earthquake and analyzing demographics of the city, two tasks tackled by the PEER Summer Interns, are specifically aimed disaster preparedness. The goal of mapping out the usability of buildings is to get a count of how many Shelter-in-Place units current exist in the city. The maps that contain usability information will be helpful in determining which buildings are sustainable as well as those that need extra work and retrofitting to be deemed usable after an earthquake. The goal of incorporating demographic information is to get an idea of the people who occupy the various buildings throughout the city. It will be interesting to see the relation between the buildings that will perform well during an earthquake, those with the highest usability and most Shelter-in-Place applicable, with the demographics of the people that occupy the building such as their age, income, race, along with other demographic characteristics. Also, it will be interesting to compare vice versa, the buildings with the lowest usability, least likely to be able to provide Shelter-in-Place, with the demographic characteristics of the people who live in those buildings. Thus, the research goals of this project are essentially aimed at disaster preparedness for San Francisco.

2.2.1 Resilient City: San Francisco

San Francisco is the heart of the Bay Area. The city has it all: culture, diversity, tradition, business, and entertainment, along with much more. However, there is a downside. The city of San Francisco is prone to earthquakes. Historically, San Francisco has endured many earthquakes. The 1906 earthquake devastated the city. It was a major earthquake that killed at least 3000 people and left the city in shackles. Another earthquake that is famously recalled hit the city in 1989 and is known as the 1989 Loma Prieta Earthquake. Luckily, the 1989 earthquake did not cause as much destruction as the one in 1906 because it was of a smaller magnitude, 6.9 as opposed to 7.9. However, even Loma Prieta caused a partial collapse of the Bay Bridge. San Francisco is due for another earthquake that could strike at any time. Thus, judging from previous natural disasters that have hit the region and the destruction they caused to the city, it is very important that resiliency be of utmost concern for San Francisco city planners. The Shelter-in-Place effort launched by SPUR is a big step in the right direction. The hope is that this effort by SPUR will ignite a trend to be followed by other organizations toward building a more resilient San Francisco.

2.2.2 Achieving Shelter-in-Place

San Francisco is a very small city when compared to other major cities of its caliber such as New York City, London, or Tokyo. San Francisco encompasses a land area of only about 46 square miles. However since the city is prone to natural disasters such as earthquakes, it is important to create an exclusive strategy for the city to prepare for and tackle an earthquake scenario. It is important to keep basic characteristics of a city in mind when designing a disaster preparedness strategy. A strategy that may work in a bigger city will probably be difficult to implement on a smaller scale. Hence, it is important that the size and compactness of San Francisco be taken into account when developing a strategy on how to manage a post-disaster situation. This is where Shelter-in-Place comes into play. Shelter-in-Place is a great strategy for a city as compact San Francisco because it does not involve bringing in temporary relief shelters. Temporary relief shelters require extra space that is not available in San Francisco. Hence, Shelter-in-Place is a great option for the city because it allows residents to stay in their homes while repair efforts take place. This will help prevent panic amongst the community because people will not have to scramble to find temporary shelter. Families will be able to stay together. Also, people will be more likely to stay in the city long term because they will still be able to be functional in their own home. Thus, Shelter-in-Place is the best strategy to implement in the effort to make San Francisco resilient since it is realistic and exclusive to the city.

2.2.3 Seismic Vulnerability

Understanding the seismic vulnerability of the housing stock in San Francisco is the first step towards reaching resiliency in the city. Without an accurate understanding about how the current housing stock will perform seismically makes it near impossible to mitigate it. Thus, the goal of this research effort and the Shelter-in-Place initiative has been to come up with a database that contains information on the seismic vulnerability of the current housing stock in San Francisco. The information from this database was mapped to make is visually easier to understand.

2.2.4 Demographic information

Not only is it important to understand the seismic vulnerability of the housing stock in San Francisco, it is equally as important to know who lives in the homes. Demographic information allows us to understand the age, income, race, the number of females versus males, the number of families, and the number of households, along a lot of other characteristics of the people living all over the city. Comparing the seismic vulnerability of homes to the people that occupy them gives a clear picture of where the repair and retrofit efforts need to be focused. Usually, the wealthy can afford to spend the money to seismically retrofit their own homes if their homes fall under the category of likely to be unusable after an earthquake. However, the middle and working class might not have to extra money or be able to spend it on seismically retrofitting their homes because they have other needs that take first priority. Thus, it is important to locate the people who are living in homes that are likely to incur severe damage from an earthquake and educate them on why they need seismic retrofitting. Also, once these people are located, they can be provided with assistance on how to go about getting their home seismically retrofitted. Furthermore, obtaining knowledge about the demographics of the city is helpful in making the city more resilient because it will help us create special assistance programs for people such as seniors and families with young children who will need more help than others after an earthquake. For example, even though a building may perform well seismically, meaning it does not collapse and residents can shelter inside it while repair efforts take place, the elevators will most likely be out which means the stairs will be the only option available to get in and out of the building for residents of buildings with multiple stories. Using the stairs will be difficult for seniors and families with young children, hence by locating where these people are who will need extra assistance after an earthquake is essential.

2.3 RESEARCH METHODOLOGIES

In order to complete the tasks of mapping out the housing stock in regard to seismic vulnerability and creating supplemental demographic documents, there were multiple research methodologies that were used. Software programs such as ArcGIS, Microsoft Excel, Microsoft PowerPoint, and Microsoft Word were used. Furthermore, there was a lot of different data from various sources that was also incorporated. Gathering all the relevant and necessary was quite a feat by itself along with finding data in the appropriate file forms was another mighty task. Various sources were able to assist in helping gather all the data that was needed to compile the maps and supplementary documents. Each of the research methodologies and how they helped shape the final results will be discussed in more detail below.

2.3.1 CAPSS HAZUS data

Data aggregated from the City Action Plan for Seismic Safety (CAPSS) was given as a starting point. The data was reliable only at the citywide scale because the CAPSS study was done at a citywide scale. A major task was cleaning up the data set. The data set was a for a magnitude 7.2 earthquake on the San Andreas Fault line. The database had the earthquake damage states as the following: Light Damage, Moderate Damage, Extensive Damage, and Complete Damage since this is how HAZUS, a nationally applicable standardized methodology that contains models for estimating potential losses from earthquakes, categorizes earthquake damage. However, since we were mapping the usability of the buildings post-earthquake, the damage states needed to be changed to usability states: Usable Light Damage, Usable Moderate Damage, Not Usable but Repairable, and Not Usable Not Repairable. Changing the damage states into usability states gives a better understanding about whether the building will be applicable to allow Shelter-in-Place. Furthermore, the CAPSS HAZUS data was in excel spreadsheet form with all the type of building by code along with their respective usability state. However, there was no data available on how many of each type of each building exists in each neighborhood. Hence, another sub-task became creating such a database, which was done by gathering city experts to help determine how many buildings pertaining to a specific building code exist in each neighborhood.

2.3.2 Meeting with City Experts

A meeting with city experts was held in order to determine how many buildings of a specific code exist in each neighborhood. The city experts were people on the SPUR task force along with other people who work or live in the city such as planners and structural engineers. There was a lot of preparation that went into the meeting with the experts. In order for the meeting to run smoothly and be a productive use of time, neighborhood worksheets were created to aid in determining the structural makeup of each neighborhood (Figure 2.3). At the meeting, the experts felt were told to simplify, if need be, and fill out the worksheets to the best of their ability. There was a lot of discussion on how to go about filling out the worksheets. The experts were finally able to come to a consensus and fill out about 6 of the 14 worksheets. Another meeting was then scheduled to complete the remaining 8 worksheets. The data that was collected from the experts was very helpful in determining the structural makeup of the neighborhoods because it clearly provided information on what type of buildings exist in each neighborhood.

Hence, when it came down to mapping the usability in each neighborhood it was important to know the structural breakdown of the buildings in each neighborhood because the seismic vulnerability varies from one building to another building based on the building's construction type. The meetings with the city experts helped create a necessary database that was extremely helping in mapping out the seismic vulnerability of buildings in each neighborhood.

Bayview

Neighborhoods: Bayview, Hunter's Point, Candlestick Point, Silver Terrace

Single family homes

______ Single family wood frame soft story pounding on one side (CAPSS custom)
______ Single family wood frame soft story pounding on both sides (CAPSS custom)
______ Single family wood frame soft story freestanding (CAPSS custom)
______Single family wood frame not soft story (CAPSS custom)
______Other:___________________________

Two units buildings

_____Duplex wood frame soft story (CAPSS custom)
_____Duplex wood frame not soft story (CAPSS custom)
_____Other:_____________________________

Three to Nine unit buildings

______Multifamily wood frame soft story (CAPSS custom)
______Multifamily wood frame not soft story (CAPSS custom)
______Concrete frame masonry infill walls mid rise low code
______Steel moment frame high rise high code
______Steel braced frame high rise medium code
______Steel frame masonry infill walls high rise low code
______Concrete shear wall high rise high code
______Concrete frame masonry infill walls low rise low code
______Concrete frame masonry infill walls mid rise medium code
______Reinforced masonry flexible diaphragm mid rise high code
______Reinforced masonry flexible diaphragm mid rise medium code
______Retrofitted URM (CAPSS custom)
______Other:___________________________
______Other:___________________________

Ten + unit buildings

______Multifamily wood frame soft story (CAPSS custom)
______ Multifamily wood frame not soft story (CAPSS custom)
______Concrete frame masonry infill walls mid rise low code
______Steel moment frame high rise high code
______Steel braced frame high rise medium code
______Steel frame masonry infill walls high rise low code
______Concrete shear wall high rise high code
______Concrete frame masonry infill walls low rise low code
______Concrete frame masonry infill walls mid rise medium code
______Reinforced masonry flexible diaphragm mid rise high code
______Reinforced masonry flexible diaphragm mid rise medium code
______Retrofitted URM (CAPSS custom)
______Other:___________________________
______Other:___________________________

Figure 2.3 Bayview District Neighborhood Worksheet

2.3.3 Microsoft Word

Microsoft Word was very helpful in getting a lot of documents together. For example, the neighborhood worksheets that were prepared for the meeting with the experts were created using Microsoft Word. Microsoft Word made it simple to create the fourteen neighborhood worksheets as well as the other supplementary documents.

2.3.4 ArcGIS

This was perhaps the most important software. ArcGIS is very powerful software that is commonly used to create maps. The software is not self-explanatory because it is very advanced and requires skill and practice. Employees from USGS and Seifel Consulting, who are also on the SPUR task force, were extremely helpful and served as GIS guides. ArcGIS was used to create usability maps and numerous other maps that convey demographic information. Furthermore, experimenting with the various abilities of ArcGIS helped the interns become better acquainted with the software. Moreover, when comparing the preliminary maps that were initially created to the final maps, progression, experience, and advancement with the ArcGIS software is evident. Figure 2.4 displays a map created with ArcGIS that shows the liquefaction and landslide zones in San Francisco. Figures 2.4, 2.5, 2.6, and 2.7 are examples of the preliminary maps that were created with ArcGIS.

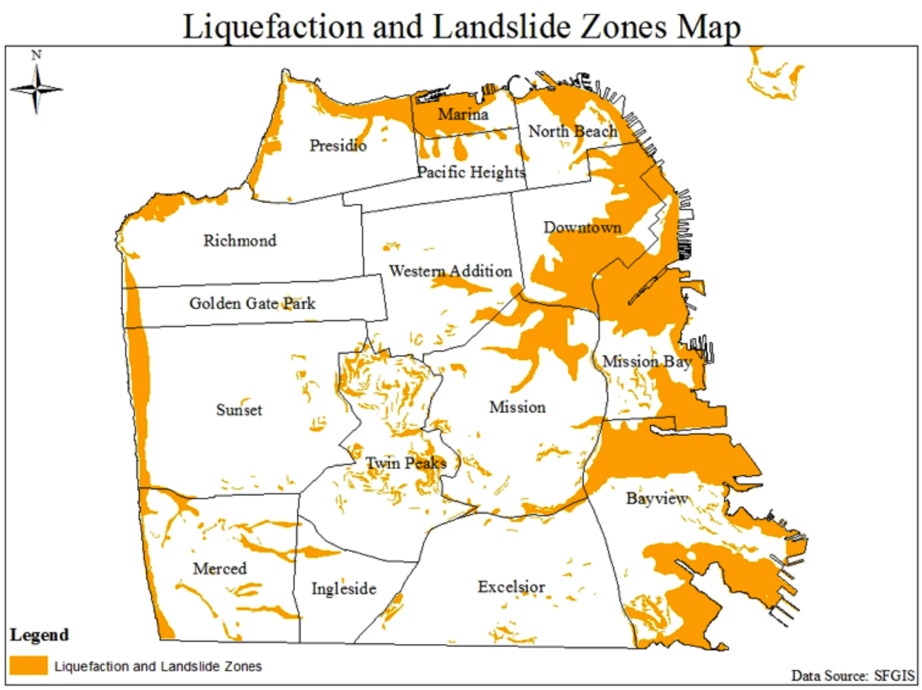

Figure 2.4 Liquefaction and landslide zone map.

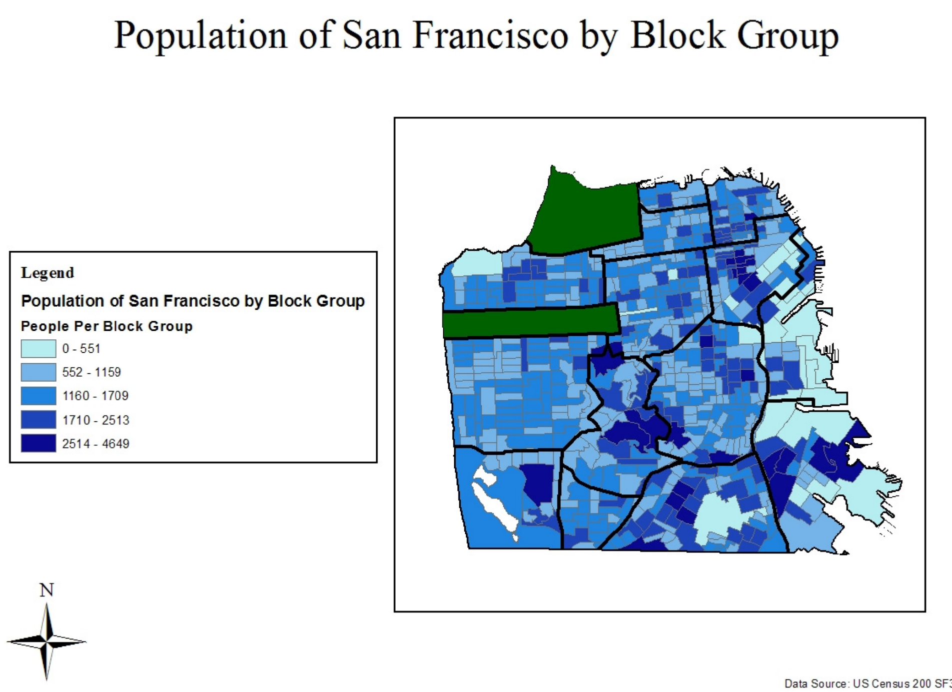

Figure 2.5 Population of San Francisco map

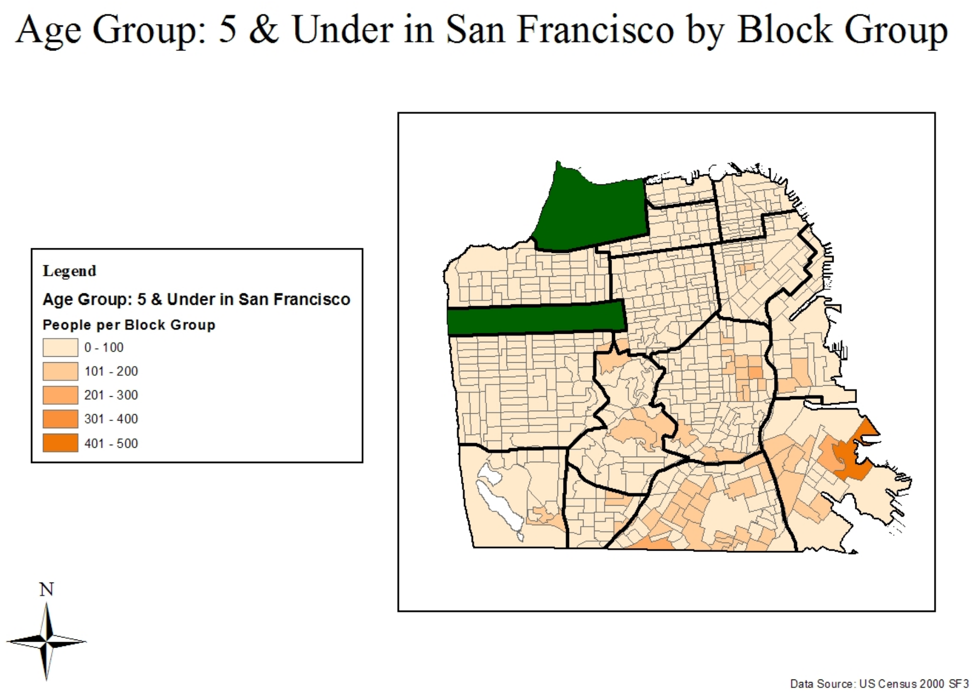

Figure 2.6 Map of age-group 5 and under in San Francisco.

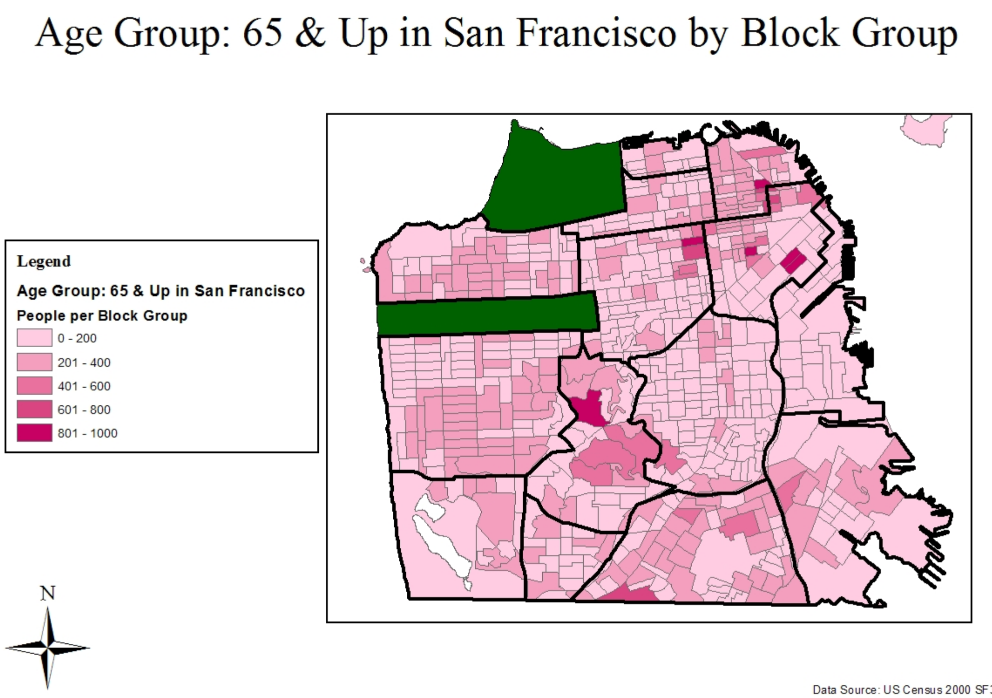

Figure 2.7 Map of age-group 65 and up in San Francisco.

2.3.5 Microsoft Excel

Microsoft Excel was very helpful for completing various mini tasks. For example, Excel was used to create charts and graphs that convey building usability information. Figure 2.8 displays an example of one of the charts created through Excel. Excel was also used to create a list that conveys various characteristics of demographic information that the mentors felt was better displayed in a list as opposed to a map and can be seen in Figure 2.9.

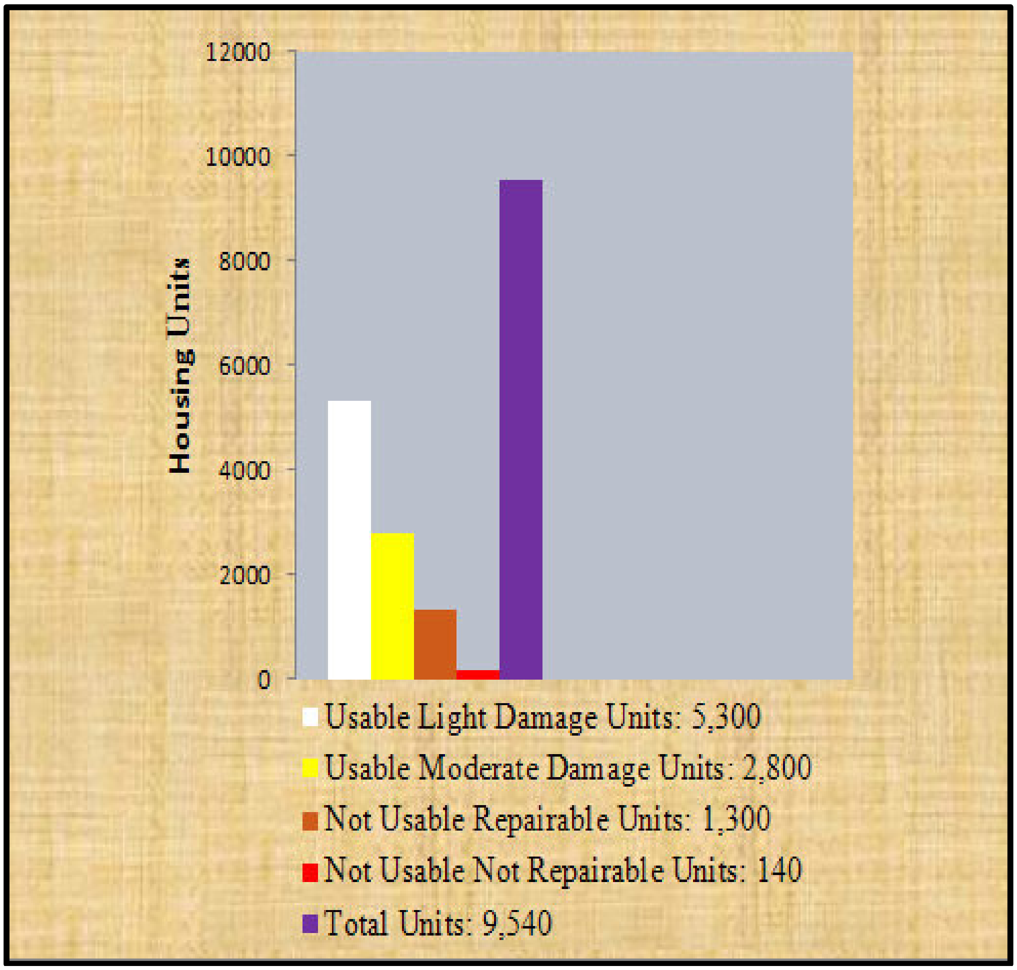

Figure 2.8 Graph displaying usability states in the Bayview District.

Total Population	33,000
Race: White	3,200
Race: Black	16,000
Race: Asian	8,100
Race: Other*	6,040
Male Population	16,000
Female Population	17,000
Age Under 5 Years Old	2,400
Age 5-17 Years Old	7,700
Age 18-21 Years Old	2,000
Age 22-29 Years Old	3,800
Age 30-39 Years Old	5,100
Age 40-49 Years Old	4,700
Age 50-64 Years Old	4,200
Age 65 Years Old & Up	3,500
Median Age	33 Years Old
Median Age Male	32 Years Old
Median Age Female	35 Years Old
Households	9,300
Average Household Size	3.5
Families	7,100
Average Family Size	3.9
Owners	4,800
Renters	4,500
Median Income	$43,000

Figure 2.9 List of demographic characteristics for the Bayview District.

2.3.6 Microsoft PowerPoint

Microsoft PowerPoint is another great software tool that has helped display the data that was collected throughout this research effort. The mentors felt creating multiple maps each conveying one demographic characteristic would make it difficult to fully comprehend the demographic information. Instead, they suggested making neighborhood documents which contain all the demographic information along with usability graphs for each neighborhood. The neighborhood documents were proposed in order to tie everything together and shrink it down to one document. Microsoft PowerPoint was very helpful in getting the documents together. It was a lot of work getting a lot of a whole bunch of information into a single page. However, the various tools in Microsoft PowerPoint made it a lot easier to get everything together. Figure 2.10 displays an example of one of the neighborhood documents.

Bayview Demographics

Total Population	33,000
Race: White	3,200
Race: Black	16,000
Race: Asian	8,100
Race: Other*	6,040
Male Population	16,000
Female Population	17,000
Age Under 5 Years Old	2,400
Age 5-17 Years Old	7,700
Age 18-21 Years Old	2,000
Age 22-29 Years Old	3,800
Age 30-39 Years Old	5,100
Age 40-49 Years Old	4,700
Age 50-64 Years Old	4,200
Age 65 Years Old & Up	3,500
Median Age	33 Years Old
Median Age Male	32 Years Old
Median Age Female	35 Years Old
Households	9,300
Average Household Size	3.5
Families	7,100
Average Family Size	3.9
Owners	4,800
Renters	4,500
Median Income	$43,000

Other*: Ameri_Es-American Indian/Alaska Native, Hispanic, Pacific Islander, Multi-race
Note: Data numbers are rounded

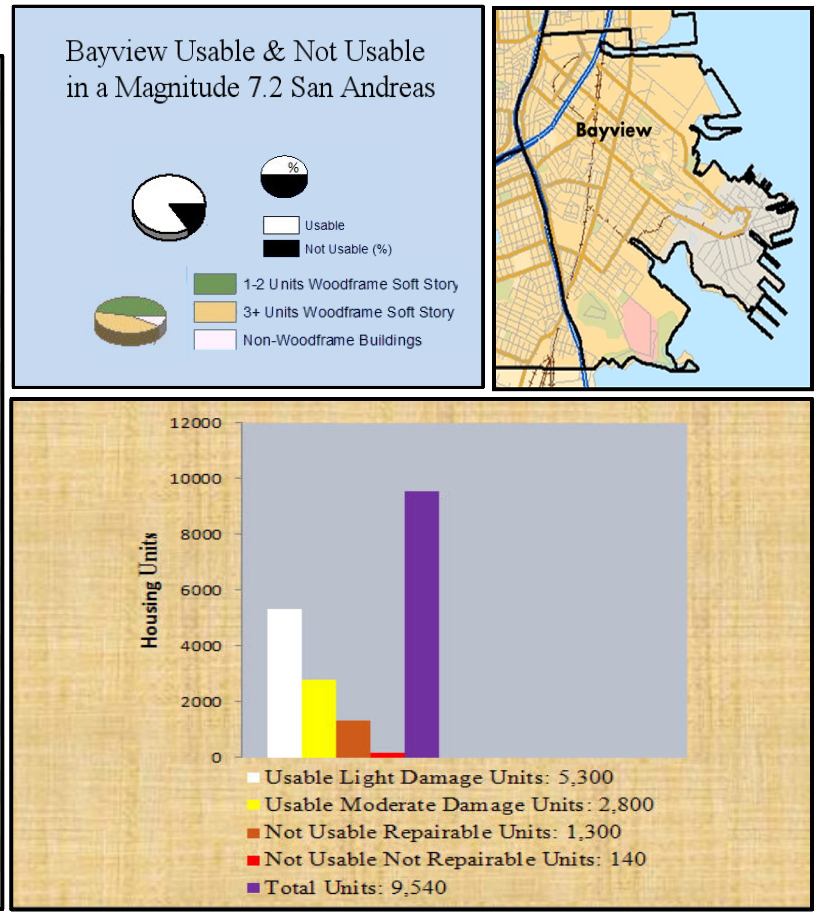

Figure 2.10 Neighborhood document for the Bayview District

2.3.7 Census-Demographic Data

Getting all of the necessary data from the census was not an easy task. Surprisingly, there is no database that has all of the census data. There are various sources from which the data was aggregated. A lot of the data was available from FactFinder.com. Other data was available from the Sf.gov, the official San Francisco government website for the city and county. The data that was unavailable online was attained through contacts such as employees at USGS and Seifel. Furthermore, it was also important to find the data in appropriate formats such as excel spreadsheets. Gathering the data took a few weeks and once all of the data was collected, it took a lot of trial and error to figure out the best way to display all of the demographic data. Finally, it was decided that the demographic documents would be the most visually clear and productive way to convey the information. (An example of one of these neighborhood documents is shown above in Figure 2.9)

2.4 RESULTS

This project was successful because the results show that it was able to accomplish the goals it set out. This project set out to map the usability states of buildings in the various neighborhoods in San Francisco. Also, the goal of the project was to tie in demographic information to the mapping scheme in order to understand the characteristics of the people that live in each neighborhood. Both of these goals were completed by the end of the ten-week research period. Furthermore, the results from this project will be published in the SPUR resiliency report that each member of the SPUR task force is working on. The information conveyed by the final maps and neighborhood documents was somewhat surprising to members of the task force and they said that the findings displayed in the maps and demographic documents will definitely influence their own piece of the Shelter-in-Place report they are writing (Figures 2.11 and 2.12). Thus, assuming from the response of the mentors and other members of the Shelter-in-Place task force, the project was a success. The research was completed on time and the final deliverables compiled beautifully and were very well received.

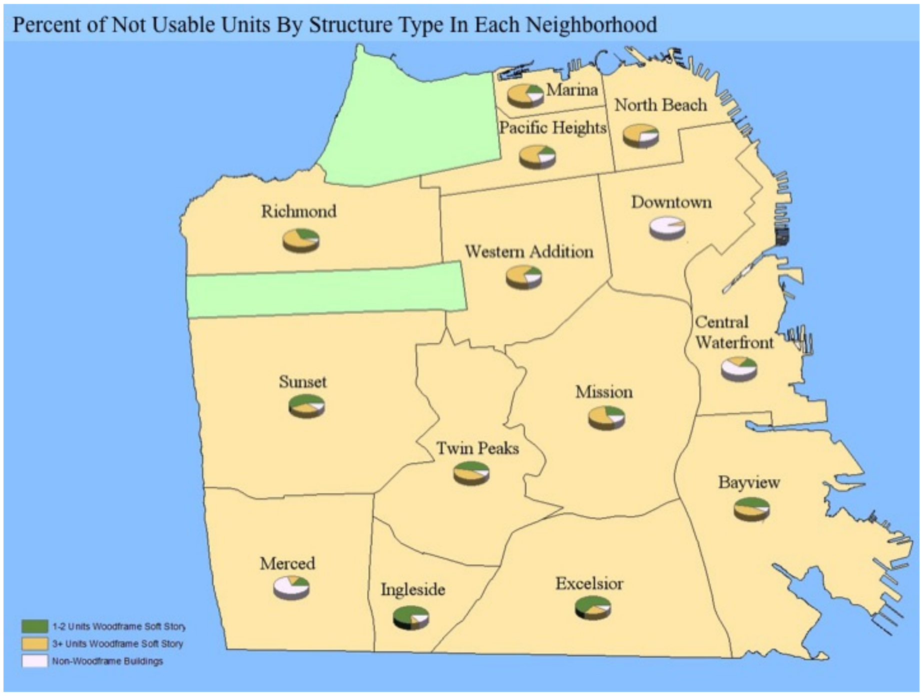

Figure 2.11 Percent of not usable units by structure type in each neighborhood.

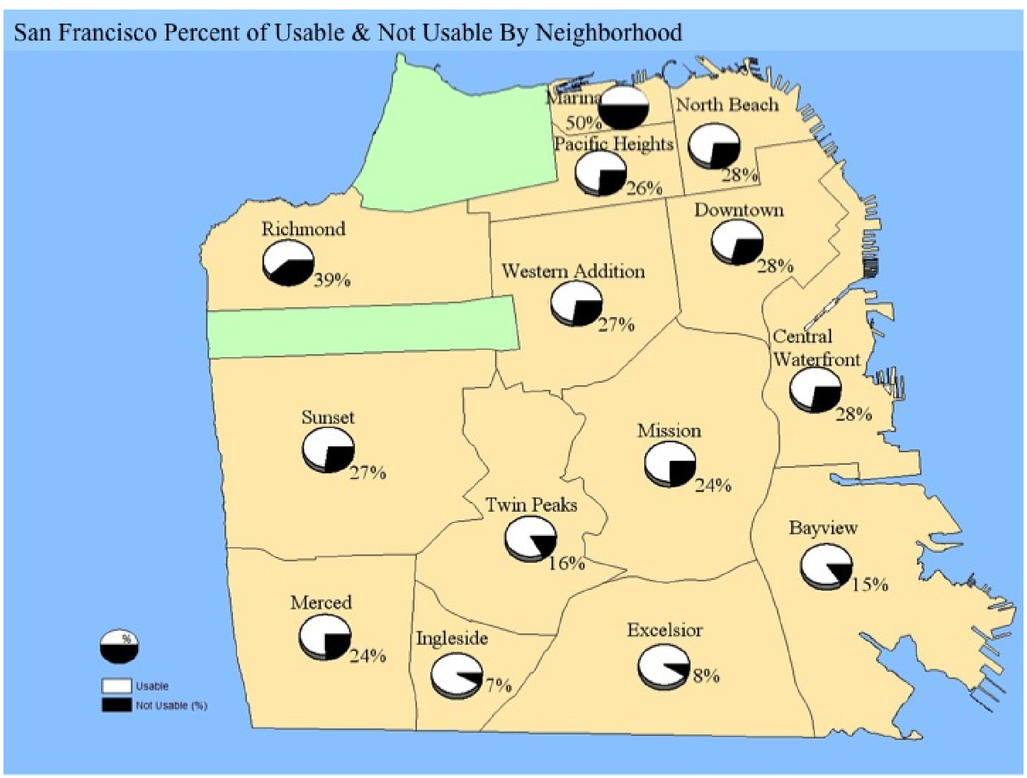

Figure 2.12 Percent of usable and not usable by neighborhood in San Francisco

2.5 CONCLUSIONS

In conclusion, this ten-week research effort was a complex yet wonderful learning experience. The project was a great way to get hands on experience in the field of research. For someone such as myself, who has never been part of a research effort, I found this to be a learning experience. I learned a lot through working with people from the planning field as well as people in consulting and engineering. I did not imagine I would get as much exposure as I did to how problems are solved in the real work world. Furthermore, I found this experience beneficial because I learned that even the work world; sometimes there are problems that have no solution and a new solution need to be created. Moreover, overall I would definitely look back at this experience as a positive learning opportunity that provided me the chance to gain valuable knowledge about how research is done and how a think tank like SPUR operates.

REFERENCES

Glaeser, E. L. [2005]. Should the Government Rebuild New Orleans, Or Just Give Residents Checks?, *The Economists' Voice*, 2(4):Article 4.

Karlinsky, S. [2010]. *The resilient city: a new framework for thinking about disaster planning in San Francisco,* Retrieved from http://www.spur.org/policy/the-resilient-city.

Nakata, J. K. (1999). *The October 17, 1989, Loma Prieta, California, earthquake*. Retrieved from http://pubs.usgs.gov/dds/dds-29/.

The Great 1906 San Francisco Earthquake, (n.d.), Retrieved from http://earthquake.usgs.gov/regional/nca/1906/18april/index.php.

Van Aalst, M. K. [2006]. The impacts of climate change on the risk of natural disasters, *Disasters*, 30:5–18. doi: 10.1111/j.1467-9523.2006.00303.x.

3 The Resilient City: San Francisco Shelter-in-Place Analysis

JOHN PHAM

ABSTRACT

In order to become a resilient city, San Francisco must improve the seismic resistance of its existing housing stock and build new housing to performance levels that allow residents to stay in their homes after the event of an earthquake. This is called "sheltering-in-place." As seen in recent natural disasters, cities are at risk to losing their communities when shelter-in-place standards are not met. Only 74% of San Francisco residents would be able to shelter-in-place if an earthquake strikes, according to a citywide analysis. This translates to over 200,000 residents needing temporary housing assistance. San Francisco does not have the capacity to shelter this many residents. The objective of this research is to assist in validating the need for a 95% shelter-in-place standard for San Francisco and to analyze San Francisco's residential building stock vulnerability with its demographic profiles at the neighborhood level to help formulate a strategy to meet this goal. The results indicated that the Downtown and Marina neighborhoods are of highest concern. The building type most vulnerable in this scenario was soft-story wood-frame buildings accounting for 47% of the unusable units.

3.1 INTRODUCTION

The San Francisco Planning and Urban Research Association (SPUR) launched an effort to achieve 95% "shelter-in-place" in San Francisco. In order to become a resilient city, San Francisco must improve the seismic resistance of its existing housing stock and build new housing to performance levels that allow residents to stay in their homes after the event of an earthquake. As seen in the recent Christchurch, New Zealand earthquake, and the New Orleans, Louisiana hurricane, cities are at risk to losing their communities when shelter-in-place standards are not met. The Community Action Plan for Seismic Safety (CAPSS) project analyzed the earthquake vulnerability of San Francisco's privately owned buildings at a citywide level. According to this analysis, if an earthquake occurred on the San Andreas Fault, 7.2 in magnitude, only 74% of the residential building stock would meet shelter-in-place standards. This means an estimated 200,000 residents would need temporary housing. With its limited space and high density, San Francisco does not have the capacity to shelter these many residents.

3.1.1 Background

Shelter-in-place is a term used when residents are allowed to stay in their homes after a natural disaster. The natural disaster for the scope of this research is an earthquake on the San Andreas Fault, 7.2 in magnitude. Liquefaction damage is taken into account with this earthquake scenario however landslide damage is not. CAPSS has data for four different earthquake scenarios which includes earthquakes on the San Andreas Fault 6.5, 7.2, and 7.9 in magnitude and on the Hayward Fault 6.9 in magnitude. The intent of this research was to prioritize a study on the 7.2 magnitude earthquake on the San Andreas Fault and publish a report to the public. If time allotted the other scenarios would be studied which did happen in the end. San Francisco is an area prone to earthquakes due to its location in between two active fault lines. The San Andreas Fault west of the city and the Hayward Fault east of the city. There are also characteristics of San Francisco that work against it in the event of an earthquake. This includes San Francisco's soft-story buildings, unreinforced masonry buildings, cliffs, liquefaction prone areas as well as other characteristics.

3.1.2 San Francisco Planning and Urban Research Association (SPUR)

The San Francisco Planning and Urban Research Association is a member-based nonprofit organization that promotes good government and good planning through research. In 2008, SPUR launched an effort to achieve 95% shelter-in-place in San Francisco. SPUR divided their shelter-in-place research project into four tasks shown in Table 3.1, each task with its own subcommittee.

Table 3.1 SPUR Research Task Forces

Task One	Validate the need to achieve 95% shelter-in-place and the most economical way to achieve it citywide
Task Two	Define the role and extent of post earthquake self-inspection
Task Three	Define a shelter-in-place standard using available documents such as ASCE31 and 41 and 7. Establish the proper planning case for the expected earthquake scenario and determine the impact of the geological hazards in the post-disaster period
Task Four	Develop policy recommendations

Each subcommittee is in charge of doing research relevant to their task and is responsible of holding regular subcommittee meetings. Each month all four subcommittees meet to discuss the progress on their research and help in terms of facilitating the direction of the final report. Each of the subcommittees is responsible for a write up of their research. The four write ups will be edited and composed to form the final report which is planned to be released in late fall of 2011.

3.1.3 Community Action Plan for Seismic Safety

The Community Action Plan for Seismic Safety (CAPSS) is a city project formed due to concerns of preventing earthquake damages in San Francisco. In 2010, CAPSS published four reports, ATC 52-1, ATC 52-2, ATC 52-3 and ATC 52-4. These reports describe the existing earthquake risks in San Francisco and a plan on how to reduce these risks. Part of the CAPSS research was to create and study the four earthquake scenarios described earlier on the San Andreas Fault and on the Hayward Fault. The earthquake scenarios were created by a program called HAZUS and these studies are reliable at a citywide level. It is the goal of this research to create data that is reliable at a neighborhood level from the given HAZUS study. CAPSS breaks down San Francisco into 16 neighborhoods in its report to describe soft-story prevalence. The same neighborhoods were used in this research with the exception of Presidio and Golden Gate Park. The neighborhood map for this research can be seen in Figure 3.1 below.

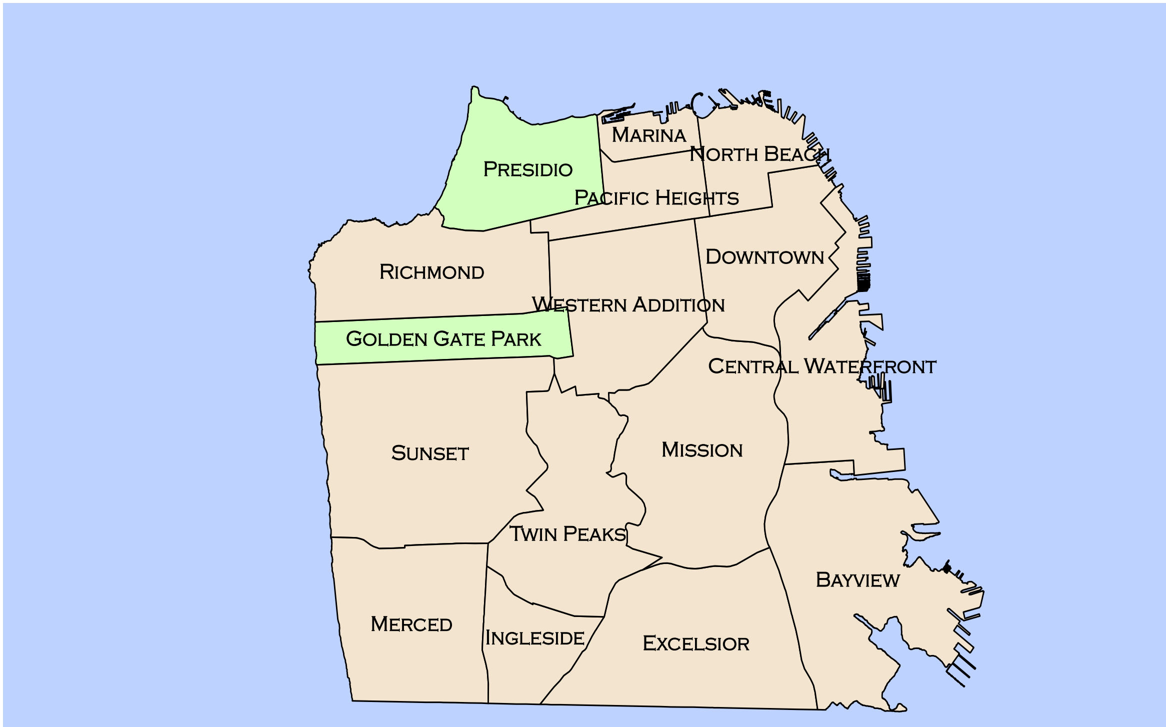

Figure 3.1 San Francisco neighborhood map.

3.2 RESEARCH OBJECTIVES

SPUR has four main research objectives described in Table 3.1. The intent of these four objectives is to better understand how to help mitigate shelter-in-place risks in San Francisco. Mitigation of shelter-in-place risks is important to quicken recovery efforts and to avoid community loss which was seen in recent natural disasters. The scope of this research falls under task one of SPUR's initiative, to validate the need for 95% shelter-in-place and the most economical way to achieve it citywide.

The objective of this research is to assist task one with an analysis of the HAZUS study performed by CAPSS. To better understand the allocation of damage in this earthquake scenario, the HAZUS data needed to be processed from the citywide level down to the neighborhood level. Census data also had to be analyzed to better understand the likely demographic of those effected in the event of an earthquake to help determine plausible post-earthquake shelter needs.

3.3 RESEARCH METHODS

The research methodology behind this report includes a technical portion and an analytical portion. The technical portion involved the use of three computer software programs: Microsoft Excel, ESRI ArcGIS and Microsoft Access. Integration of these three programs was crucial for interpreting the given HAZUS output data. Other data involved in the process includes Census data of 'Units in Structure' and Census data of demographic profiles. The analytical portion of the methodology involved an estimation of the building typology for San Francisco's residential building stock at a neighborhood level and also an interpretation of the demographic information from the Census data.

3.3.1 HAZUS Output Data

HAZUS is a computer software program used by the Federal Emergency Management Agency (FEMA) to estimate economic and social losses due to natural disasters. These natural disasters may include earthquakes, hurricanes or floods. The natural hazard that pertains to this research is earthquakes.

The CAPSS ran a HAZUS study for an earthquake scenario in San Francisco that was 7.2 in magnitude and occurred on the San Andreas Fault west of the city. According to the study, 26% of residential units failed at meeting shelter-in-place standards. One of the inputs accounted for was building typology. However, the structural make-up of San Francisco was only known at the citywide level thus only providing data applicable at the citywide level. For this information to be more beneficial, it needed to be broken down to a smaller scale which the neighborhood level was deemed appropriate.

The first step to breaking down the given HAZUS output data to a smaller scale was to understand what the data it displayed. The given HAZUS output data was separated into four files listed below:

- SA72wLiq HC STR DSD.csv
- SA72wLiq HS STR DSD.csv
- SA72wLiq LC STR DSD.csv
- SA72wLiq MC STR DSD.csv.

SA72wLiq stands for San Andreas Fault and 7.2 magnitude with liquefaction. HAZUS included the liquefaction risks that the earthquake entailed: HC, HS, LC, and MC stand for different building code levels. HC stands for high code. HS stands for high superior code which is mainly used for important facilities such as hospitals. LC stands for low code and MC stands for moderate code. The last section of the files STR DSD stands for structural damage state distribution.

In each file there were 8 columns, as shown in Figure 3.2. The first column labeled BLOCK describes the census block designation. The second column labeled TRACT describes the same information as the first but includes more information about the state and city. The third column MBT stands for model building type. The list of model building types and their descriptions can be found in Appendix 2. Then there are five columns, NONET, SLIGHTT, MODERATT, EXTNSIVT and CMPLETET which determine the damage state distributions depending on the building type (MBT) and location (TRACT). Important facts to note about the data is that it is simultaneously (1) building type specific and (2) location specific and also there is no data included for the count of buildings in each building type. The building typology is known at the citywide level as mentioned previously. In order to determine the building typology at a neighborhood level, we held a meeting with city experts which is explained in the following section. To account for the number of buildings, San Francisco 'Units in Structure' data was downloaded from Census to determine the count of units in the city.

	A	B	C	D	E	F	G	H
1	BLOCK	TRACT	MBT	NONET	SLIGHTT	MODERAT	EXTNSIVT	CMPLETET
59	4	60750004	URML_LC	0.03	0.09	0.24	0.34	0.29
60	4	60750004	URMM_LC	0	0.02	0.13	0.35	0.49
61	4	60750004	W2_LC	0.02	0.09	0.35	0.36	0.19
62	5	60750005	C3H_LC	0	0.02	0.2	0.37	0.41
63	5	60750005	C3L_LC	0.01	0.03	0.13	0.29	0.54
64	5	60750005	C3M_LC	0	0.02	0.16	0.39	0.42
65	5	60750005	MH_LC	0.26	0.35	0.21	0.14	0.04
66	5	60750005	PC2L_LC	0.01	0.04	0.17	0.38	0.39
67	5	60750005	RM1L_LC	0.03	0.03	0.17	0.39	0.38

Figure 3.2 Representative sample from the original HAZUS output data.

3.3.2 Mapping Scheme Meeting

The mapping scheme meeting is one of the analytical components of the research. This meeting was held with city experts from a variety of different fields which include structural engineering, architecture, building inspection, and district involvement. The term city expert is used to describe a person practicing in one of these professions for many years that have also lived in San Francisco for a majority if not all their life therefore they are familiar with the building typology of San Francisco. This meeting was held first on July 15, 2011 and then again on July 27, 2011.

The goal of these meetings was to determine the building typology in each neighborhood as descriptive as possible with the time given. All city experts that attended the meetings were there voluntarily so it was important to efficiently use time. The task they were handed was to determine the percentage of wood-frame units versus non-wood-frame units in each of the neighborhoods. These percentages were then multiplied to the building counts found from the Census data and then further distributed according to building types. There were 13 out of the 66 building types from CAPSS used in this research, which are highlighted in Appendix 2. The wood-frame units were broken down into different soft-story categories and distributed using percentages found from the windshield survey in a CAPSS report shown in Appendix 1. The non-wood-frame units were broken down into many categories which were distributed according to the CAPSS citywide results.

3.3.3 Microsoft Excel

Microsoft Excel is a popular software program used to store and manipulate data. There are many ways to manipulate data in Excel including the use of formulas, tables, charts and a variety of other useful tools. For the purpose of this research, Excel was used to render the given HAZUS output data compatible for ArcGIS and Access. Also, Excel was used to create tables presented in the final visuals.

The first step in Excel was to tag building code levels to the building types in the MBT column. _HC was added to high code building types, _HS was added on to high superior, _LC was added on to low code and _MC was added on to moderate code. The four given HAZUS output data files were then copied and pasted into one workbook excel file labeled SA72wLiq ALL STR DSD.xls. On this compiled file, nine new columns were added which can be seen in Figure 3.3. The column labeled TRACT1 is a modified version of TRACT to make the file compatible with a file used in ArcGIS.

	A	B	C	D	E	F	G	H	I	J	K	L	M	N	O	P	Q
1	BLOCK	TRACT	TRACT1	MBT	BUILDING	NONET	SLIGHTT	MODERAT	EXTNSIVT	CMPLETET	CHECK1	USABLELI(	USABLEM(	NOTUSAB	NOTUSAB	CHECK2	SQFT
193	4	60750004	0004	URML_LC	D	0.03	0.09	0.24	0.34	0.29	0.99	0.121212	0.276768	0.382323	0.219697	1	0
194	4	60750004	0004	URMM_LC	D	0	0.02	0.13	0.35	0.49	0.99	0.020202	0.166667	0.441919	0.371212	1	0
195	4	60750004	0004	W1_HC	A	0.01	0.09	0.31	0.35	0.24	1	0.1	0.625	0.239	0.036	1	0
196	4	60750004	0004	W2_HC	C	0.31	0.39	0.14	0.13	0.03	1	0.7	0.153	0.1395	0.0075	1	0
197	4	60750004	0004	W2_HS	C	0.48	0.32	0.05	0.12	0.03	1	0.8	0.062	0.1305	0.0075	1	0
198	4	60750004	0004	W2_LC	C	0.02	0.09	0.35	0.36	0.19	1.01	0.108911	0.382178	0.461881	0.04703	1	0
199	4	60750004	0004	W2_MC	C	0.14	0.3	0.32	0.2	0.04	1	0.44	0.34	0.21	0.01	1	0
200	5	60750005	0005	C1H_HC	D	0.01	0.08	0.48	0.35	0.08	1	0.09	0.515	0.335	0.06	1	0
201	5	60750005	0005	C1L_HC	C	0.02	0.02	0.18	0.37	0.42	1.01	0.039604	0.214851	0.641584	0.10396	1	0
202	5	60750005	0005	C1M_HC	C	0.24	0.37	0.22	0.14	0.03	1	0.61	0.234	0.1485	0.0075	1	0
203	5	60750005	0005	C2H_HC	D	0.03	0.24	0.48	0.21	0.04	1	0.27	0.501	0.199	0.03	1	0
204	5	60750005	0005	C2L_HC	D	0.3	0.35	0.17	0.15	0.03	1	0.65	0.185	0.1425	0.0225	1	0
205	5	60750005	0005	C2M_HC	D	0.13	0.37	0.32	0.15	0.03	1	0.5	0.335	0.1425	0.0225	1	0
206	5	60750005	0005	C3H_LC	D	0	0.02	0.2	0.37	0.41	1	0.02	0.237	0.4355	0.3075	1	0
207	5	60750005	0005	C3L_LC	D	0.01	0.03	0.13	0.29	0.54	1	0.04	0.159	0.396	0.405	1	0

Figure 3.3 Snippet from the Modified HAZUS Output Data

The column labeled BUILDINGTYPE assigns each MBT as a Single Family Home (A), Duplex (B), Multi-unit wood-frame (C), or Multi-unit non-wood-frame (D). The BUILDINGTYPE column is used to assess the usability equations for the damage state distributions. These equations can be found in Figure 3.4. The columns USABLELIGHT, USABLEMOD, NOTUSABLEREPAIR, and NOTUSABLENOTREPAIR are all calculated from these equations which are dependent on the building type and damage state distributions. The CHECK1 column and the CHECK2 column makes sure the rows that need to be normalized are normalized accordingly. Finally the last column labeled SQFT includes information about the square footage of the MBT in each TRACT according to the Tax Assessor's data of San Francisco. There are many implications of the Tax Assessor's data; therefore it was only used to create a preliminary usability map and to look at possibly weighting the average of damage levels when aggregated up to the block group scale. The mapping scheme determined by the city expert meeting was ultimately used for the results and not the square footage.

A. single family all types

	usable light	*usable mod*	*repair*	*no repair*
none	100%	0%	0%	0%
slight	100%	0%	0%	0%
moderate	0%	100%	0%	0%
extensive	0%	90%	10%	0%
complete	0%	0%	85%	15%

B. duplex all types

	usable light	*usable mod*	*repair*	*no repair*
none	100%	0%	0%	0%
slight	100%	0%	0%	0%
moderate	0%	100%	0%	0%
extensive	0%	50%	50%	0%
complete	0%	0%	85%	15%

C. wood-frame 3+ units residential

	usable light	*usable mod*	*repair*	*no repair*
none	100%	0%	0%	0%
slight	100%	0%	0%	0%
moderate	0%	100%	0%	0%
extensive	0%	10%	90%	0%
complete	0%	0%	75%	25%

D. non-wood-frame 3+ units residential

	usable light	*usable mod*	*repair*	*no repair*
none	100%	0%	0%	0%
slight	100%	0%	0%	0%
moderate	0%	100%	0%	0%
extensive	0%	10%	90%	0%
complete	0%	0%	25%	75%

Figure 3.4 Equations used to calculate usability.

3.3.4 ArcGIS by ESRI

Created by the Economic and Social Research Institute (ESRI), ArcGIS is a computer software program that is used to take a geographic approach to problem solving. In this research ArcGIS is used to spatially link the different geographic scales that each data set is presented in. HAZUS output data is at the city block scale, and Census data is at the block group scale and the structural mapping scheme of San Francisco's residential buildings is at a neighborhood scale. The boundary scales can be seen in Figure 3.5. Since there was no geographical connection between the HAZUS data, the Census data and the neighborhood boundaries, ArcGIS was used to create this spatial connection. This connection was done by geographically locating each scale (city block, block group, and neighborhood) and creating identifiers in the data that specify where each scale lies relative to each other. The identifiers created in the data were labeled as the following columns: TRACT1 for city block, CENSUSBG for block group, and NBRHOOD for neighborhood. The ArcGIS was also the tool used to present the final informational maps of San Francisco's residential building stock. This program was used because it has the ability to take information that is geographically specific and communicate the information on a map which can be displayed in many ways. The final maps created by ArcGIS are included in the results section of this report.

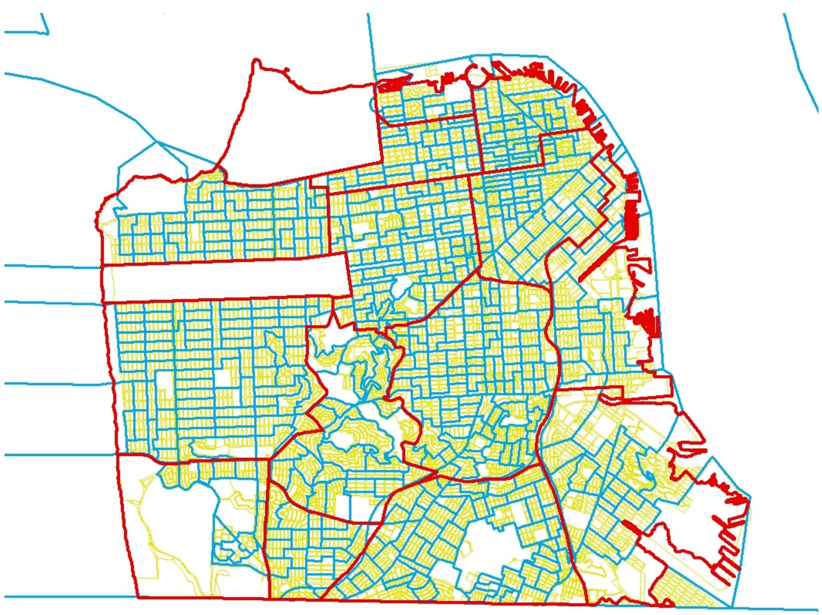

Figure 3.5 San Francisco map with different boundary scales: (Yellow = City Block, Blue = Block Group, Red = Neighborhood).

3.3.5 Microsoft Access

Microsoft Access is a database management program used to store data which is can be easily filtered with the use of queries to display particular information. The data can be stored in Access or it may be linked directly to other formatted data sets including those of Excel. For the purpose of this project, Access was used to integrate the previously manipulated data into one master file with location specific information about the building type, building counts, usability levels and demographic information. This master file incorporated the HAZUS output data, the Census data, the structural mapping scheme data.

3.4 RESULTS

There were two deliverables for this research project. The first deliverable was a database that contained geographic specific information about building types, the count of units in these building types distributed in four different usability levels, and lastly demographic information. This information was requested at the neighborhood scale. The database is also available at the smaller block group scale but would not be accurate enough to present to the public. The second deliverable was a presentation of the database information in a visual format. Again, the information was to be presented at the neighborhood scale. The calculations the HAZUS output data went through had uncertainties that would not make it appropriate to provide the public at a smaller scale.

3.4.1 Master Data File

The master data file, found in Appendix 3, is the final outcome of what was done with the original HAZUS output data. In summary, 35 columns of data were made for each of the 14 neighborhoods. The first column indentifies the neighborhood; the next five columns contain information on the usability of units, and the last 29 columns hold information taken from the Census which describes the demographic profiles who live in the neighborhood. This master file is only a portion of the database. The database was filtered with queries in order to output this information. There is more detailed information that can be outputted from this database, however for the scope of this research, only certain data was pulled out.

3.4.2 Citywide Maps

The citywide visuals for this research were created from the information in the master data file. ArcGIS was the program utilized to create maps and Microsoft PowerPoint was used to put together the visuals. The concept in designing the maps and the information displayed on the visuals was to educate the public. When the public audience sees these maps they should be more informed about the resiliency of their community. In order to make sure the audience understands the visuals, the graphics were made to be simple but informative and descriptive but not cluttered. Another thing to note is that the information at hand must be sensitively displayed. The visuals display information about the earthquake scenario and the viewers can interpret the visuals however they please. The first visual created was the "San Francisco Units in Usable Categories by Neighborhood" sheet shown in Figure 3.6. The information on this sheet displays the number of units in each usability category (Usable Light Damage, Usable Moderate Damage, Not Usable but Repairable, and Not Usable nor Repairable). These numbers were rounded to two significant digits.

San Francisco Units in Usable Categories by Neighborhood

San Andreas 7.2 Magnitude Earthquake Scenario

Citywide Information	
Population	776,731
Total Housing Units	344,121
Usable Light Damage Units	135,600 (39%)
Usable Moderate Damage Untis	120,300 (35%)
Not Usable, Repairable Units	76,020 (22%)
Not Usable, Not Repairable Units	12,201 (4%)

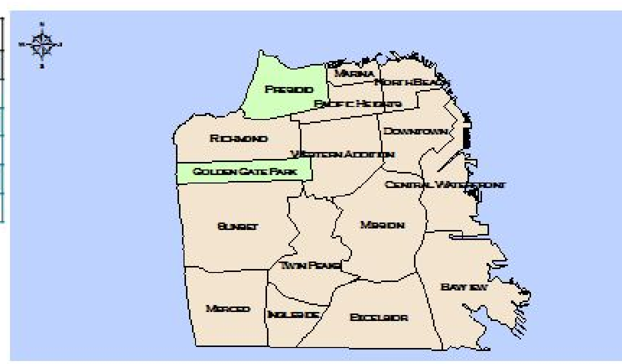

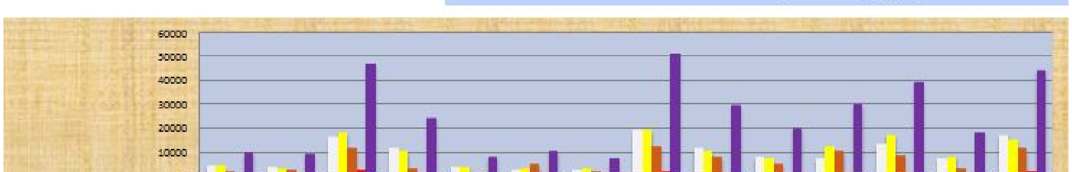

	Bayview	Central Waterfront	Downtown	Excelsior	Ingleside	Marina	Merced	Mission	North Beach	Pacific Heights	Richmond	Sunset	Twin Peaks	Western Addition
Usable Light Damage Units	4100	3300	16000	11000	3100	2000	2400	19000	11000	7500	7000	13000	7200	17000
Usable Moderate Damage Units	3700	3000	18000	10000	3600	3000	2900	19000	9800	7100	12000	17000	7900	15000
Not Usable Repairable Units	1500	2000	11000	2800	800	4500	1400	12000	7500	4700	10000	8100	2800	11000
Not Usable Not Repairable Units	170	510	2400	330	94	730	350	1400	1000	590	1200	1000	330	1400
Total Units	9470	8810	47400	24130	7594	10230	7050	51400	29300	19890	30200	39100	18230	44400

Source: SFGIS , Census 2000 and CAPSS Hazus Output Data

Figure 3.6 San Francisco units in usable categories by neighborhood sheet.

The second visual created was the “San Francisco Usable Units vs. Not Usable Units by Neighborhood” map shown in Figure 3.7. In this map, there are pie charts that display the percentage of usability in each neighborhood. The purpose of this map was to compare neighborhoods in terms of resiliency and shelter-in-place.

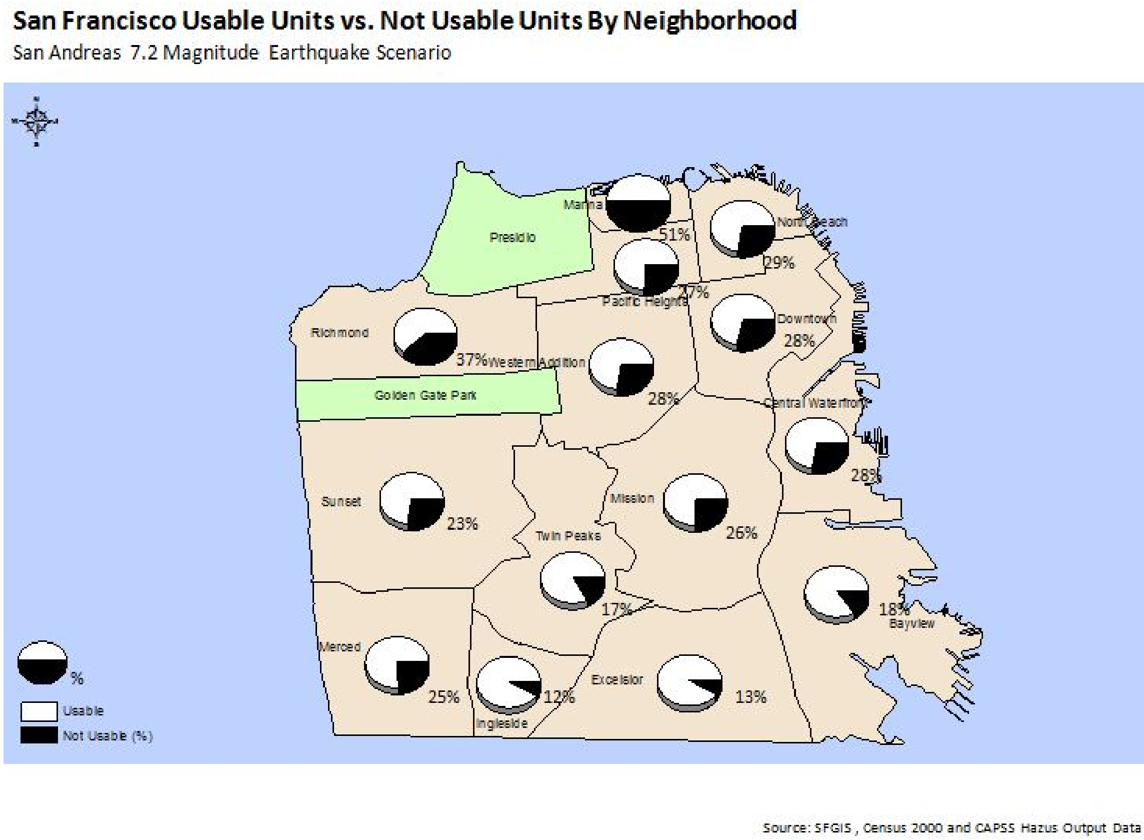

Figure 3.7 San Francisco usable versus not usable units by neighborhood map.

The third visual created was the “San Francisco Breakdown of Not Usable Units by Neighborhood” map shown in Figure 3.8. In this map, the percentage of building types for the units that were deemed not usable in each neighborhood was displayed. The purpose for this map was to show which buildings are most vulnerable in each neighborhood. The categories include 1-2 units soft-story buildings in green, 3+ units soft-story buildings in yellow and other non-wood-frame buildings in white.

San Francisco Breakdown of Not Usable Units By Neighborhood
San Andreas 7.2 Magnitude Earthquake Scenario

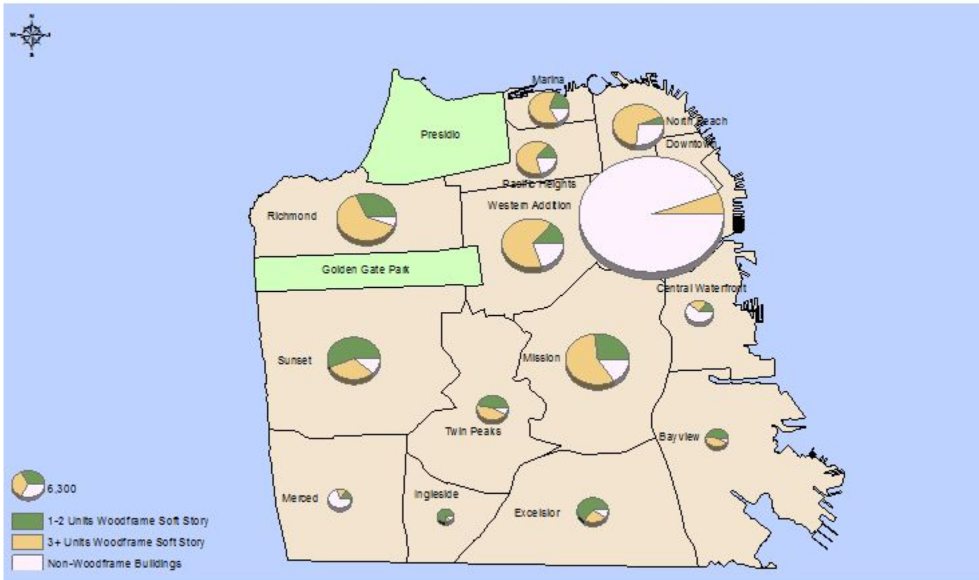

Source: SFGIS , Census 2000 and CAPSS Hazus Output Data

Figure 3.8 San Francisco breakdown of not usable units by neighborhood map.

3.4.3 Detailed Neighborhood Sheets

There were detailed sheets made for each of the 14 neighborhoods. Included in this sheet was a map of the neighborhood, the building usability levels, and demographic statistics. The purpose of these sheets was to provide detailed information about who would be affected and what type of buildings would be affected in each neighborhood. This way the audience can view the earthquake vulnerability information and the demographic information side by side and ultimately make their own conclusions and reactions. Figure 3.9 below is an example of one of the detailed neighborhood sheets.

Bayview Demographics

Total Population	33,000
Race: White	3,200
Race: Black	16,000
Race: Asian	8,100
Race: Other*	6,040
Male Population	16,000
Female Population	17,000
Age Under 5 Years Old	2,400
Age 5-17 Years Old	7,700
Age 18-21 Years Old	2,000
Age 22-29 Years Old	3,800
Age 30-39 Years Old	5,100
Age 40-49 Years Old	4,700
Age 50-64 Years Old	4,200
Age 65 Years Old & Up	3,500
Median Age	33 Years Old
Median Age Male	32 Years Old
Median Age Female	35 Years Old
Households	9,300
Average Household Size	3.5
Families	7,100
Average Family Size	3.9
Owners	4,800
Renters	4,500
Median Income	$43,000

Other*: Ameri_Es-American Indian/Alaska Native, Hispanic, Pacific Islander, Multi-race
Note: Data numbers are rounded

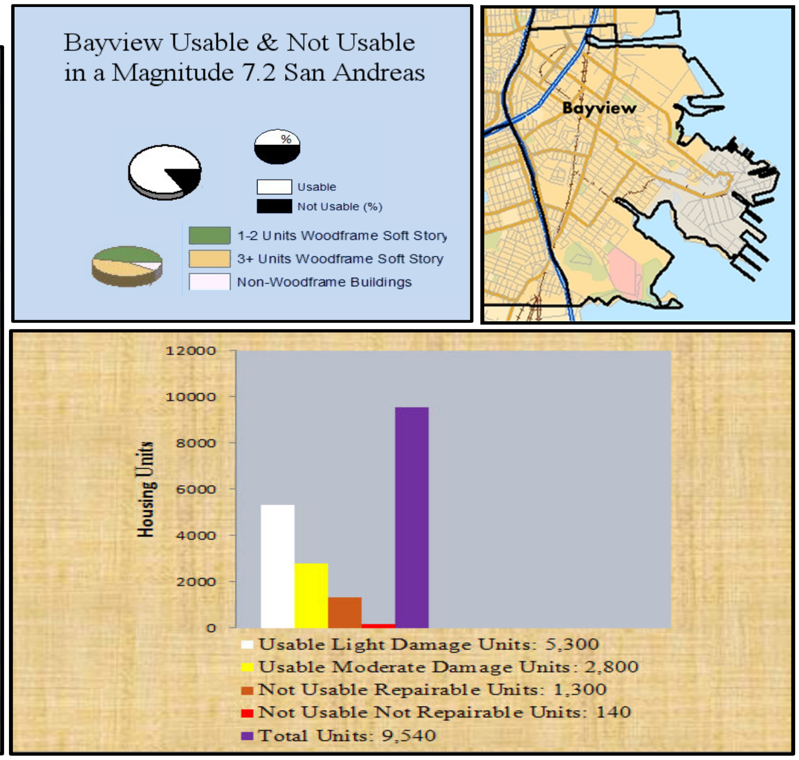

Figure 3.9 Detailed neighborhood sheet of Bayview District (A. Dhaliwal).

3.5 ANALYSIS

In analyzing the data, it is important to note that the raw data is visually difficult to interpret and to visualize. It does not display the geographic location of the neighborhoods, it does not display the relative impact citywide nor at the neighborhood level and it does not have the effect that a graphic or visual may have. Therefore the maps were vital in not only analyzing the data but also in displaying the analysis to a general audience.

3.5.1 Citywide Analysis

The citywide maps helped in analyzing the neighborhood vulnerability relative to each other and relative to the city as a whole. As seen from Figure 3.4, the Downtown, the Mission, and the Western Addition neighborhoods are the ones with the most units that did not meet shelter-in-place standards. Downtown had 13,400 units, Mission had 12,300 units, and Western Addition had 12,400 units that did not meet the standard.

From Figure 3.7, it is seen that the Marina neighborhood had the highest percentage of its units that did not meet the shelter-in-place standard at 51% which is almost twice the citywide percentage at 26%. The neighborhood with the next highest percentage of units that did not meet shelter-in-place standards is Richmond at 37% but had three times the total units that the Marina had. Eight neighborhoods did not diverge far from the citywide percentage of 26%, two neighborhoods were far greater and four neighborhoods were far less.

The map in Figure 3.8 describes the breakdown of the unusable units in each neighborhood. Each pie represents the total unusable units in the neighborhood which is reflective on their sizes on the map. It is clear on the chart that Downtown held the most unusable units with the majority of the units being in non-wood-frame buildings. This was interesting to see because it is apparent that the rest of the neighborhoods do not exhibit this characteristic with the exception of Central Waterfront. The other neighborhoods have the majority of their unusable units in wood-frame soft-story buildings. In total the city has 91,600 unusable units, 47% in wood-frame soft-story buildings and 53% in other building types. Looking at these numbers it would be more beneficial for the city to put a priority on retrofitting residential units that are in soft-story wood-frame structures. Hypothetically if all soft-story wood-frame residential buildings were retrofitted to shelter-in-place standards, San Francisco would up its 74% resiliency to 85%.

3.5.2 Neighborhood Analysis

There were a couple neighborhoods that exhibited apparent characteristics important to look at. The first neighborhood was Downtown. Downtown had the highest number of unusable units at 13,400 units. It is sitting on an area of prone to liquefaction which is one of the reasons why it has the most unusable units in this earthquake scenario. It has the lowest household median income in San Francisco at an estimated $31,000. With the most damage and the lowest income, Downtown was the neighborhood most affected.

Another neighborhood that exhibited important characteristics is the Marina. This neighborhood had the highest percentage of units that did not meet the shelter-in-place standards in the earthquake scenario. It is a neighborhood that sits at the northern end of the peninsula in a liquefaction prone area. Looking at the demographic information it is seen that the Marina has one of the highest household median incomes at $79,000. Knowing these types of statistics about the neighborhood can help facilitate policy recommendations. For example, a wealthy neighborhood may be able to better afford retrofitting their residential buildings.

The two neighborhoods described in the analysis are the ones that stood out from the rest of the neighborhoods, at least apparent from the visual maps. There are many interpretations that can be made for each of the 14 neighborhood detailed sheets but it is not within the scope of this research to interpret everything. The purpose of these detailed sheets was to provide the public with important information about the neighborhoods of San Francisco and how they would be impacted in the scenario if an magnitude 7.2 earthquake occurred on the San Andreas Fault. These sheets also serve as a tool for the other tasks forces in SPUR's effort to achieve 95% shelter-in-place in San Francisco, particularly task force four whose objective is to develop policy recommendations. The data from this research can be used to ground their reasoning.

3.6 CONCLUSIONS

An estimated 26% of San Francisco's residential housing stock did not meet shelter-in-place standards in this San Andreas earthquake scenario. This percentage translates in over 200,000 residents without shelter. San Francisco does not have the capacity to shelter these many people. Out of the residential units that did not meet shelter-in-place standards, 47% was due to soft-story wood-frame structures and 53% was due to other building types. The Marina neighborhood, with one of the highest median incomes, had the lowest percentage of its units meet shelter-in-place standards at 49%. The majority of these units were in soft-story structures. The Downtown neighborhood, with the lowest median income, had the most units that did not meet the shelter-in-place standard at 13,400 units. The majority of these units were in non-wood-frame buildings. It is shown from the visuals provided from this research that each of the neighborhoods was affected differently and the demographic profiles affected also varied. This concludes that the HAZUS output data was proven to be more useful at a neighborhood level to assist the mitigation efforts of shelter-in-place risks. The future work with the outcomes of this research will be done by task force four of SPUR's initiative. Their task is to develop policy recommendations to mitigate shelter-in-place risks partially grounding their input with this research contribution.

ACKNOWLEDGMENTS

This research was supervised and funded by the Pacific Earthquake Engineering Research Center as part of the 2011 Summer PEER Internship Program. The author would like to thank Sarah Karlinsky, Laura Samant and Mary Comerio for their mentorship in the duration of the program. Also a special thanks to Amy Dhaliwal for being a partner in this research. Any opinions, findings, and conclusions or recommendations in this material are those of the authors and do not necessarily reflect those of the sponsors.

REFERENCES

Applied Technology Council (2010). Potential earthquake impacts, *Report No. ATC 52-1*, Redwood City, CA.

Applied Technology Council (2010). A community action plan for seismic safety *Report No. ATC 52-2*, Redwood City, CA.

Applied Technology Council (2010). Earthquake safety for soft-story buildings, *Report No. ATC 52*-3, Redwood City, CA.

Applied Technology Council (2010). Post-earthquake repair and retrofit requirements, *Report No. ATC 52-4*, Redwood City, CA.

Poland, C. (2008). The Resilient City: before the disaster. *Report SPUR 2008/11*, San Francisco Planning and Urban Research Association, San Francisco, CA.

Poland, C. (2009). The Resilient City: defining what San Francisco needs from its seismic mitigation policies. *Report SPUR 2009/02*, San Francisco Planning and Urban Research Association, San Francisco, CA.

APPENDICES

APPENDIX 1: SOFT-STORY WINDSHIELD SURVEY FROM CAPSS

Table 4-17 Wood-Frame Windshield Survey Results by Neighborhood

Neighborhood	Adjacency	Soft Story	Not Soft Story
Bayview	No gap (adjacent building on both sides)	33%	21%
	Gap on 1 side	26%	9%
	Gap on 2 sides	3%	9%
	Total	62%	38%
Downtown	No gap	69%	0%
	Gap on 1 side	22%	8%
	Gap on 2 sides	0%	0%
	Total	92%	8%
Excelsior	No gap	35%	17%
	Gap on 1 side	11%	17%
	Gap on 2 sides	3%	17%
	Total	49%	51%
Ingleside	No gap	28%	13%
	Gap on 1 side	13%	13%
	Gap on 2 sides	2%	31%
	Total	43%	57%
Marina	No gap	63%	7%
	Gap on 1 side	23%	2%
	Gap on 2 sides	2%	4%
	Total	88%	12%
Merced	No gap	4%	2%
	Gap on 1 side	18%	4%
	Gap on 2 sides	9%	65%
	Total	30%	70%
Mission	No gap	32%	7%
	Gap on 1 side	30%	14%
	Gap on 2 sides	2%	14%
	Total	64%	36%
Mission Bay	No gap	32%	13%
	Gap on 1 side	30%	13%
	Gap on 2 sides	0%	11%
	Total	62%	38%
North Beach	No gap	58%	13%
	Gap on 1 side	16%	11%
	Gap on 2 sides	0%	2%
	Total	75%	25%

Neighborhood	Adjacency	Soft Story	Not Soft Story
Pacific Heights	No gap	29%	4%
	Gap on 1 side	37%	8%
	Gap on 2 sides	4%	19%
	Total	69%	31%
Richmond	No gap	40%	12%
	Gap on 1 side	40%	6%
	Gap on 2 sides	0%	2%
	Total	80%	20%
Sunset	No gap	33%	8%
	Gap on 1 side	25%	10%
	Gap on 2 sides	2%	22%
	Total	60%	40%
Twin Peaks	No gap	16%	6%
	Gap on 1 side	25%	7%
	Gap on 2 sides	16%	28%
	Total	58%	42%
Western Addition	No gap	19%	5%
	Gap on 1 side	27%	8%
	Gap on 2 sides	13%	27%
	Total	60%	40%

APPENDIX 2: FULL MODEL BUILDING TYPE LIST

MBT	CATEGOF	DESCRIPTION
MH_LC*	A	Single family without soft story (stored as MH/low code RES1), wood-frame (CAPSS Custom MBT)
S1M_HC*	A	Single family soft story pounding one side (stored as S1M/High Code, RES1), wood-frame (CAPSS Custom MBT)
S3_HC*	A	Single family soft story freestanding (stored as S3/High Code), wood-frame (CAPSS Custom MBT)
W1_HC*	A	Single family soft story pounding both sides (stored as W1/High Code), wood-frame (CAPSS Custom MBT)
MH_HC*	B	Duplex without soft story (stored as MH/High Code RES2), wood-frame (CAPSS Custom MBT)
S1M_LC*	B	Duplex/flat with soft story (stored as S1M/Low Code, RES2), wood-frame (CAPSS Custom MBT)
C1L_HC*	C	Multi-family soft story (stored as C1L/High Code), wood-frame (CAPSS Custom MBT)
C1M_HC*	C	Multi-family not soft story (stored as C1M/High Code), wood-frame (CAPSS Custom MBT)
W2_HC	C	Wood, all other occupancies, high code
W2_HS	C	Wood, all other occupancies, superior code
W2_LC	C	Wood, all other occupancies, low code
W2_MC	C	Wood, all other occupancies, moderate code
C1H_HC	D	Concrete building high-rise, high code
C2H_HC*	D	Concrete shear walls high-rise, high code (High seismic design level only, not considered non-ductile in CAPSS Phase
C2L_HC	D	Concrete shear walls low-rise, high code (High seismic design level only, not considered non-ductile in CAPSS Phase 1)
C2M_HC	D	Concrete shear walls mid-rise, high code (High seismic design level only, not considered non-ductile in CAPSS Phase 1)
C3H_LC	D	Concrete frame with unreinforced masonry infill walls high-rise (considered non-ductile in CAPSS Phase 1), low code
C3L_LC*	D	Concrete frame with unreinforced masonry infill walls low-rise (considered non-ductile in CAPSS Phase 1), low code
C3L_MC*	D	Concrete frame with unreinfroced masonry infill walls low-rise (considered non-ductile in CAPSS Phase 1), moderate coc
C3M_LC*	D	Concrete frame with unreinforced masonry infill walls mid-rise (considered non-ductile in CAPSS Phase 1), low code
C3M_MC	D	Concrete frame with unreinfroced masonry infill walls (considered non-ductile in CAPSS Phase 1), moderate code
PC1_HC	D	Pre-cast concrete tilt-up walls, high code
PC1_MC	D	Pre-cast Concrete tilt-up walls, moderate code
PC2H_MC	D	Pre-cast concrete frames with concrete shear walls high-rise (considered non-ductile in CAPSS Phase 1), moderate co
PC2L_LC	D	Pre-cast concrete frames with concrete shear walls low-rise (considered non-ductile in CAPSS Phase 1), low code
PC2L_MC	D	Pre-cast concrete frames with concrete shear walls low-rise (considered non-ductile in CAPSS Phase 1), moderate cod
PC2M_MC	D	Pre-cast concrete frames with concrete shear walls mid-rise (considered non-ductile, stored as PC2M), moderate code
RM1L_HC	D	Reinforced Masonry bearing walls with wood or metal deck diaphragms low-rise, high code
RM1L_LC	D	Reinforced masonry bearing walls with wood or metal deck diaphragms low-rise, low code
RM1L_MC	D	Reinforced Masonry bearing walls with wood or metal deck diaphragms low-rise, moderate code
RM1M_HC*	D	Reinforced Masonry bearing walls with wood or metal deck diaphragms mid-rise, high code
RM1M_MC*	D	Reinforced Masonry bearing walls with wood or metal deck diaphragms mid-rise, moderate code
RM2H_MC	D	Reinforced masonry bearing walls with pre-cast concrete diaphragms high-rise, moderate code
RM2L_LC	D	CAPSS Custom MBT: Retrofitted URML, Unreinforced masonry bearing walls
RM2L_MC*	D	CAPSS Custom MBT: Retrofitted URMM, Unreinforced masonry bearing walls (low- and mid-rise)
RM2M_LC	D	Reinforced masonry bearing walls with pre-cast concrete diaphragms mid-rise low code
RM2M_MC	D	Reinforced masonry bearing walls with pre-cast concrete diaphragms mid-rise, moderate code
S1H_HC*	D	Steel moment frame high-rise, high code
S1H_MC	D	Steel moment frame high-rise, moderate code
S1L_HS	D	Steel moment frame low-rise, superior code
S1L_LC	D	Steel moment frame low-rise, low code
S2H_HC	D	Steel braced frame high-rise, high code
S2H_LC	D	Steel braced frame high-rise, low code
S2H_MC*	D	Steel braced frame high-rise, moderate code
S2L_HC	D	Steel braced frame low-rise, high code
S2L_HS	D	Steel braced frame low-rise, superior code
S2L_LC	D	Steel braced frame low-rise, low code
S2L_MC	D	Steel braced frame low-rise, moderate code
S2M_HC	D	Steel braced frame mid-rise, high code
S2M_LC	D	Steel braced frame mid-rise, low code
S4H_HC	D	Steel frame with cast in place concrete shear walls high-rise, high code
S4H_MC	D	Steel frame with cast in place concrete shear walls high-rise, moderate code
S4L_HC	D	Steel frame with cast in place concrete shear walls low-rise, high code
S4L_LC	D	Steel frame with cast-in-place concrete shear walls low-rise, low code
S4L_MC	D	Steel frame with cast in place concrete shear walls low-rise, moderate code
S4M_HC	D	Steel frame with cast in place concrete shear walls mid-rise, high code
S4M_HS	D	Steel frame with cast-in-place concrete shear walls mid-rise, superior code (used for RES6/Nursing Homes only)
S4M_MC	D	Steel frame with cast in place concrete shear walls mid-rise, moderate code
S5H_LC*	D	Steel frame with unreinforced masonry infill walls high-rise, low code
S5H_MC	D	Steel frame with unreinforced masonry infill walls high-rise, moderate code
S5L_LC	D	Steel frame with unreinforced masonry infill walls low-rise, low code
S5L_MC	D	Steel frame with unreinforced masonry infill walls low-rise, moderate code
S5M_LC	D	Steel frame with unreinforced masonry infill walls mid-rise, low code
S5M_MC	D	Steel frame with unreinforced masonry infill walls mid-rise, moderate code
URML_LC	D	Unreinforced masonry bearing walls low-rise, low code
URMM_LC	D	Unreinforced masonry bearing walls mid-rise, low code

APPENDIX 3: MASTER DATA FILE

SAN ANDREAS 7.2M and CENSUS 200 DATA												
Neighborhood	Usable Light	Usable Moderate	Not Usable Repair	Not Usable Not Repairable	Sum	Pop	White	Black	AmeriEs	Asian	Hawaiian Pacific Islander	Other
Bayview	4100	3700	1500	170	9500	33000	3200	16000	140	8100	1200	3300
Central Waterfront	3300	3000	2000	510	8800	17000	11000	2700	120	1800	170	700
Downtown	16000	18000	11000	2400	47000	77000	36000	5900	650	27000	270	3600
Excelsior	11000	10000	2800	330	25000	90000	22000	6100	340	44000	970	12000
Ingleside	3100	3600	800	94	7600	26000	5600	6000	100	11000	120	1900
Marina	2000	3000	4500	730	10000	12000	11000	58	22	1200	11	100
Merced	2400	2900	1400	350	7100	17000	8800	780	37	6100	39	430
Mission	19000	19000	12000	1400	51000	120000	74000	4600	1000	14000	390	21000
North Beach	11000	9800	7500	1000	29000	49000	24000	630	77	22000	64	590
Pacific Heights	7500	7100	4700	590	20000	32000	28000	430	50	3300	46	330
Richmond	7000	12000	10000	1200	31000	68000	33000	1100	150	30000	73	1000
Sunset	13000	17000	8100	1000	39000	100000	46000	1300	220	48000	160	1400
Twin Peaks	7200	7900	2800	330	18000	41000	26000	2200	120	9800	91	1300
Western Addition	17000	15000	11000	1400	44000	86000	54000	13000	390	12000	230	2300
Neighborhood	Multi Race	Males	Females	Age Under 5	Age 5_17	Age 18_21	Age 22_29	Age 30_39	Age 40_49	Age 50_64	Age 65_Up	Med Age
Bayview	1400	16000	17000	2400	7700	2000	3800	5100	4700	4200	3500	33
Central Waterfront	730	9900	7500	660	1200	540	3200	5200	3200	2300	1100	37
Downtown	3800	44000	32000	1900	4600	3200	14000	15000	12000	13000	13000	41
Excelsior	4400	44000	46000	5300	15000	4800	11000	14000	13000	14000	13000	36
Ingleside	1100	13000	13000	1400	4100	1300	3300	4100	4000	4300	3600	37
Marina	260	5700	6600	360	340	93	2500	4300	1400	1500	1700	35
Merced	910	7900	9200	650	1700	2100	2900	2600	2100	2300	2800	39
Mission	7200	66000	57000	5700	13000	4700	22000	30000	20000	16000	11000	35
North Beach	1200	24000	25000	1300	3200	1200	8600	10000	6800	8300	9600	40
Pacific Heights	740	15000	17000	1100	1700	460	6100	9300	4400	5200	4200	37
Richmond	2400	32000	36000	2600	7300	2300	11000	13000	11000	11000	11000	39
Sunset	3600	49000	52000	4100	12000	3800	15000	18000	16000	16000	16000	39
Twin Peaks	1800	21000	20000	1700	4300	1000	4100	7700	7300	7800	6900	43
Western Addition	3800	45000	41000	2400	5400	3800	21000	21000	12000	11000	9900	35
Neighborhood	Med Age Male	Med Age Female	Households	Avg Household Size	Families	Avg Family Size	Housing Units	Owner Occupied	Renter Occupied	Med Income		
Bayview	32	35	9300	3.5	7100	3.9	9600	4800	4500	43000		
Central Waterfro	37	36	8100	1.9	2900	2.5	8900	3100	5100	77000		

nt												
Downtown	41	40	44000	1.7	11000	2.7	48000	3100	40000	31000		
Excelsior	34	38	24000	3.7	19000	4.1	25000	16000	7800	55000		
Ingleside	36	39	7500	3.4	5500	3.8	7700	5500	2000	64000		
Marina	35	35	8000	1.5	2000	2.4	8300	1700	6300	79000		
Merced	38	40	6900	2.4	3700	3	7100	2000	4900	64000		
Mission	35	35	50000	2.5	20000	3.2	51000	16000	33000	62000		
North Beach	40	41	26000	1.9	9400	2.8	28000	5000	21000	57000		
Pacific Heights	37	37	19000	1.8	5800	2.5	20000	5300	14000	100000		
Richmond	38	40	28000	2.4	15000	3.1	29000	10000	18000	65000		
Sunset	38	41	38000	2.7	23000	3.2	39000	21000	16000	66000		
Twin Peaks	42	44	18000	2.3	8900	2.9	18000	12000	6100	91000		
Western Addition	35	35	43000	2	12000	2.7	44000	9100	33000	58000		

4 Overburden Correction Factor and the Effect of Fines Content on the Limiting Compression Curve of Intermediate Soils

CHRSTOPHER KISSICK

ABSTRACT

The Overburden Correction Factor (C_N) is used to normalize Cone Penetration Test (CPT) resistance to an equivalent overburden stress of one atmosphere. This normalization is necessary to calculate the liquefaction potential of a soil. The C_N is a function of effective stress and relative density; current practices for calculating C_N are unreliable at high confining stresses and for soils with a range of fines contents. The combination of MIT-S1, using the Limiting Compression Curve (LCC), and Cylindrical Cavity Expansion Analysis [Pestana and Whittle 1999; Jaeger et al. 2011] can help to develop more concise relationships for C_N in the future. The combination of MIT-S1 and Cylindrical Cavity Expansion uses the slope of a soil's Limiting Compression Curve (LCC), ρ_c, as an input to simulate a CPT test. Tests were performed on various soil mixtures from clean sands to Perris Dam Samples. From these samples; LCC slopes were obtained, disturbed versus undisturbed specimens were compared and relationships between fines content and relative breakage were observed.

4.1 INTRODUCTION

4.1.1 Overview of Delta Levee System

The Sacramento-San Joaquin Delta system is a diverse and crucial expanse of water systems that over two thirds of California's population relies on [California Department of Water Resources 2008]. The Sacramento-San Joaquin Delta, as seen in Figure 4.1, is the west coast's largest estuary and is home to 500 plant and animal species, 20 of which are endangered (California

Department of Water Resources). The Delta is used by 12 million recreational users per year. In addition to afore mentioned uses, the delta's water is crucial to California's industry and population. The delta water helps irrigate agriculture within the delta region and the central valley. The water is also sent to Southern California through the State Water Project which helps supply one of the nation's largest urban populations with freshwater necessary to survive.

A series of levee failures in the delta region would be disastrous to California. With so much of the state dependent upon the levee system for their jobs, food and drinking water the potential for a catastrophe in the state of California is very high. California's agricultural and industrial sections would suffer if the freshwater supply were damaged. Many residents of southern California would have to live an alternate lifestyle or be removed from their home due to a lack of fresh water.

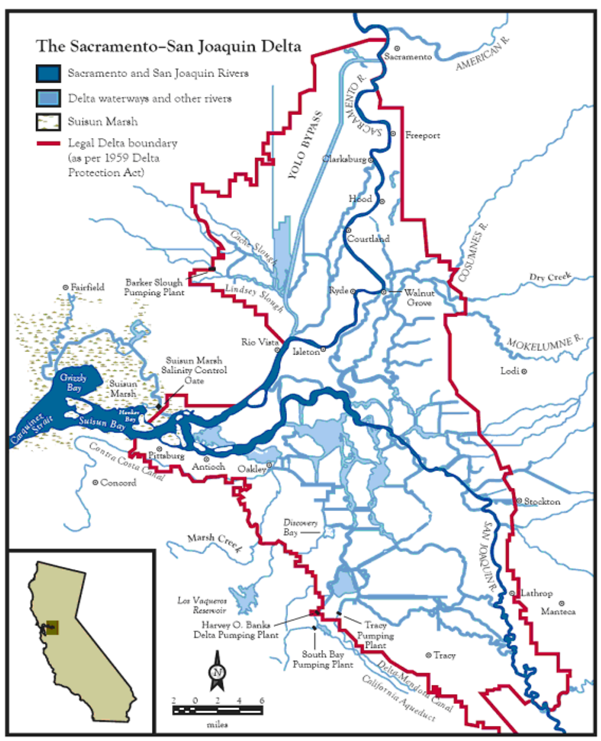

Figure 4.1 Sacramento-San Joaquin Delta [Boulanger 2011].

4.1.2 Cone Penetration Test Importance and Need for Improved Soil Characterization Techniques

Levee failures can be induced from liquefied soils due to seismic events, peak rains, and even gopher holes. Levees can breach during a heavy storm year when large amounts of water have accumulated. The levees can also liquefy during an earthquake, which are always a possibility in the delta region of California due to the close proximity of numerous fault lines. Soil liquefaction occurs when the pore water pressure is increased due to soil settlement in an earthquake. When the effective stress between soil particles becomes less than the pore water pressure, the soil loses the ability to withstand shear forces. Levee failure is a very unfortunate event, Figure 4.2 displays the terrible consequences. The Sacramento-San Joaquin delta region has been very fortunate to date, to not have the combination of high waters and large seismic activity at the same time.

Cone Penetration Testing (CPT) can help the Sacramento-San Joaquin Delta region become more resilient by identifying which soils will be susceptible to soil liquefaction. Soil liquefaction in the Delta region is a serious threat to California's well being and soils that are susceptible need to be characterized more accurately to avoid a major disaster. The CPT drilling has become a popular, rapid, accurate and affordable way to characterize *in situ* soils (e.g., Mayne et al. [2007]). CPT drilling provides a soil profile for the drilling location; recording the tip resistance, the sleeve resistance and the pore water pressure at a given depth. These tip resistances are then used during the calculation of liquefaction potential. When calculating the liquefaction potential of a soil, the CPT resistances are corrected to a pressure of one atmosphere using the overburden correction factor (C_N). Current practices for determining C_N are not dependable at high effective stresses and require extrapolation for determination.

Figure 4.2 Flooded delta island [Boulanger 2011].

4.1.3 Limiting Compression Curve Relation to CPT resistance

At high vertical effective stresses, soil particles begin to crush and this behavior is best displayed by the Limiting Compression Curve (LCC) of a soil. As seen in Figure 4.3, under high effective stresses the particles should reach the same crushing slope if the samples consist of the same mineralogy, independent of the initial void ratio. Soil samples that are deep in the ground or under large structures, like a levee, may experience crushing while CPT probes are being inserted.

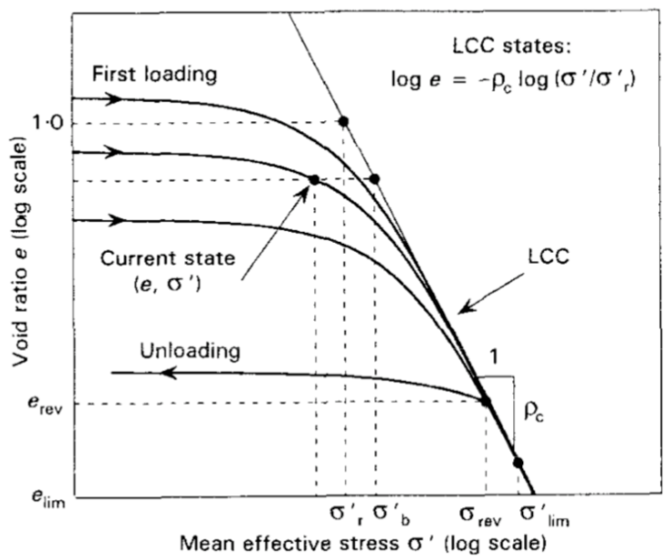

Figure 4.3 LCC behavior [Pestana and Whittle 1995].

The slope of the LCC (ρ_c) is an important soil characteristic for developing a more concise C_N relationship. The slope of the LCC is one of many soil parameters used in the MIT-S1 model [Pestana and Whittle 1999; Jaeger et al. 2011]. The MIT-S1 [Pestana and Whittle 1999; Jaeger et al. 2011] model combined with cylindrical cavity expansion analysis can simulate CPT tests and help to develop a more concise and site specific relationship for the calculation of C_N in soil samples that need to be identified.

4.2 SPECIMEN PROFILE

4.2.1 Sample Mixtures

Various soil mixtures were crushed in the structural lab at U.C. Davis. Ottawa sand was crushed first to compare to known results from DeSouza [1958]. The LCC tests have been performed on

Ottawa sand numerous times and past results were used to validate crushing techniques being performed on new samples. Clean Nevada sand and mixtures of Nevada sand and Yolo loam were crushed next. Nevada sand was chosen instead of Ottawa to mix with the Yolo loam because the results of this study can be compared to previous work done with this mixture by a former graduate student at UC Davis, Ogul Doygun. Nevada sand is also a better graded sand than Ottawa and will better represent intermediate *in situ* soils. The mixtures of Nevada sand and Yolo loam created were 10, 20, and 35% by weight. These samples help to clarify the behavior that different fines contents have on particle crushing behavior. Pure Yolo loam fines were also crushed to observe the sample behavior at higher stresses then a typical consolidation test would allow. Pure Yolo loam also served as a lower limit to compare to the Nevada-Yolo mixtures. Finally, disturbed and undisturbed Perris Dam samples were crushed to observe whether sample placement had an effect on LCC behavior.

4.2.2 Sample Placement

All samples, dry and saturated, were placed in the compression device with metal filters above and below the sample as shown in Figure 4.4. The perforated filters placed on the outermost part of the specimen helped the sample perform as desired. The perforated screen helped to prevent shear angles from propagating through the soil. The perforated screen was one of two screens stiff enough to not fail during compression testing. Without this screen the grooves in the top and bottom caps would have created failure planes in the soil lowering the sample's compressive strength. The second function of the perforated screens performed was to maintain proper drainage during saturated tests. Without the stiffness that the perforated screens provided the other filters would have been pressed into the top cap ridges, making the only drainage path for the sample through the small hole in the center. This would not have been a proper simulation of saturated ground conditions. The other three screens; number 30, 200, and 400 sieve size were used to prevent fine particles, already in the sample and created during crushing, from leaving the specimen during testing.

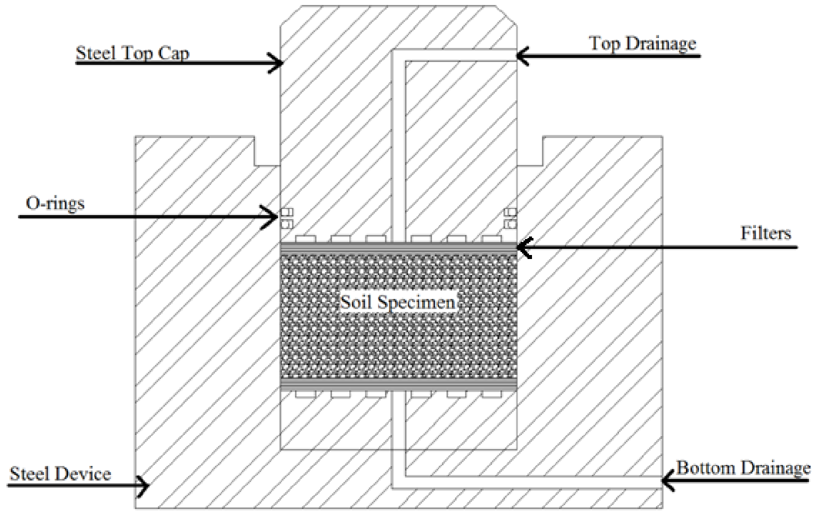

Figure 4.4 Testing device cross section.

Figure 4.5 From left to right; perforated screen, 30 screen, 200 screen, 400 screen, top cap.

Dense samples were placed with a pressurized air vibrator. After the bottom layer of filters were placed in the device, the dense samples were air pluviated through a small screen to make the sample as dense as naturally possible (see Figure 4.5). After the initial pluvation the device was then vibrated with the air pressurized vibrator to make the sample as dense as possible without the use of compression.

Loose samples were placed using a funnel. Through a series of trial and error experiments, it was determined that using a funnel to place the sample returned the best results.

The bottom of the funnel was placed in contact with the bottom layer of filters. Then the sample was placed in the funnel, and the funnel was raised very slowly to achieve the loosest density possible.

All wet samples were saturated in the same fashion. Prior to saturation, the sample was placed in the device dry, and the properly lubricated top cap and filters were placed on top. The sample was then saturated from the bottom up with deionized water to help air escape the specimen. Water was added until both the bottom and top drainage tube's heads were equal.

4.2.3 Seating Technique

To obtain an initial void ratio, samples were seated to approximately 0.1 MPa. After complete sample saturation a total weight of 32.28 kg was added to the top cap of the testing device as shown in Figure 4.6. This was the minimum compression load that the testing load cell would read accurately. After the weights were added and leveled samples were given 30 minutes to consolidate. After ample consolidation time, a measurement of the top cap height was taken to calculate the initial void ratio. Without use of the weights to anchor the stress/displacement location there was far too much variability in the initial void ratio and repeatability was not possible.

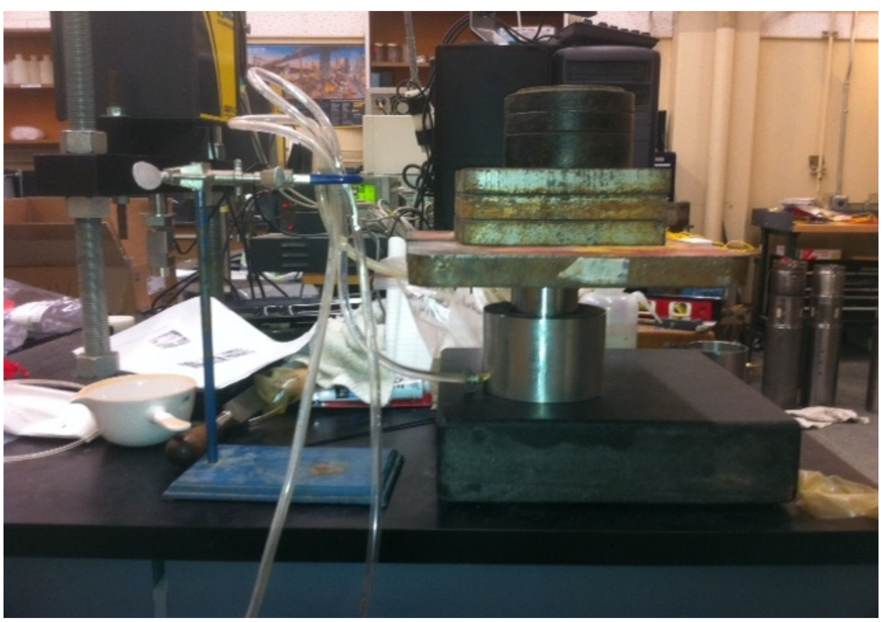

Figure 4.6 Seating of specimen.

4.2.4 Sample Testing

Saturated samples were tested slowly to assure accurate results (see Figure 4.7). Saturated samples were compressed at a rate of 0.0007 in./min to allow for proper pore pressure dissipation. The run rate was calculated with the help of Ogul's thesis, it was stated consolidation tests were run at a rate of 5% strain an hour or approximately 0.0007 in./min for this test. If samples were compressed quickly, the pore pressure could not dissipate fast enough due to the permeability of the soil and the LCC would become the elastic compression curve of the pore water, not the effective stress that was desired. Sample displacements were read using a GEO-TAC Linear Variable Differential Transformer (LVDT). The LVDT was placed perpendicular to the moving surface of the MTS compression machine and readings were taken throughout the duration of the test. Saturated samples were tested to 15–25% strain because samples with higher fines contents would tend to consolidate more and not reach crushing pressures as quickly as those with a poorly graded profile.

Dry samples were crushed quickly. Dry coarse grained samples were tested at a rate of 0.025 in./min because pore pressure had no effect on specimen testing. Dry Specimens were crushed to pressures of 100MPa.

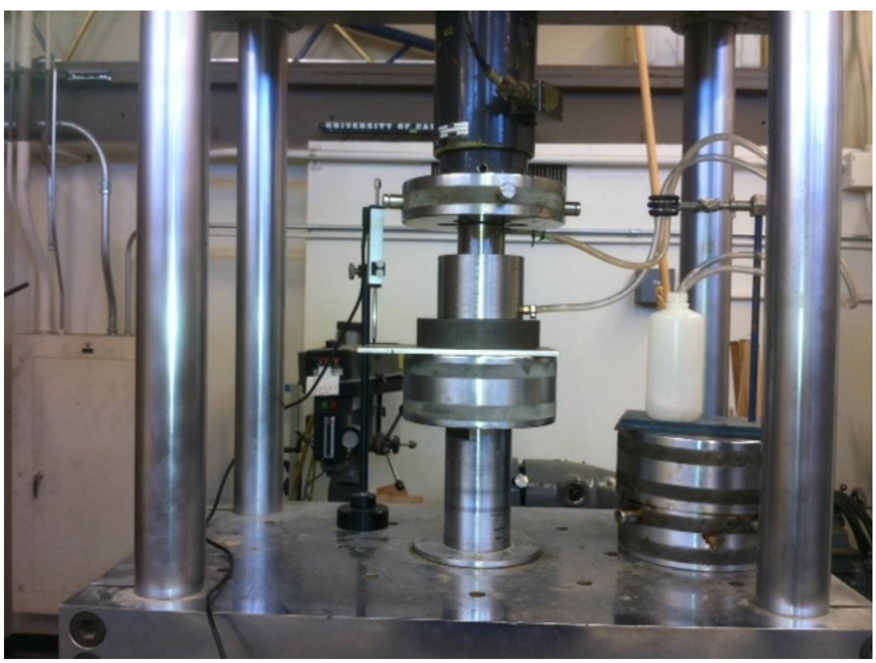

Figure 4.7 Sample testing

4.3 LCC SLOPES AND TRENDS

4.3.1 LCC Background and Comparisons to Accepted Results

Ottawa Sand was crushed prior to all other soil specimens to verify the testing methods. While the results were not identical to what DeSouza recorded in 1958 properties such as gradation of the sand and basic mineralogy can have effects on the recorded results.

Table 4.1 LCC slopes and Effective Vertical Reference Stresses comparison

Property	Kissick, Maki [2011]	DeSouza [1958]
AVG ρc: (unitless)	0.499	0.44 to 0.46
AVG $\sigma'vr$: (Mpa)	8.73	9.5 to 11.5

4.3.2 Effect of Fines Content

Soils exhibited very intuitive behavior as fines contents increased. As seen in Figure 4.8, clean Nevada sand withstood large amounts of pressure before experiencing large crushing deformations. As more Yolo Loam fines were added to the samples, the LCC progressively moved downward and had a greater compressibility in a lower range of stresses as seen by the 35% and 20% fines content samples in Figure 4.8. Soils are able to consolidate more as fines content is increased because the smaller particles can rearrange to bear the load. Those poorly graded soils rearrange until pressures become large enough that crushing occurs.

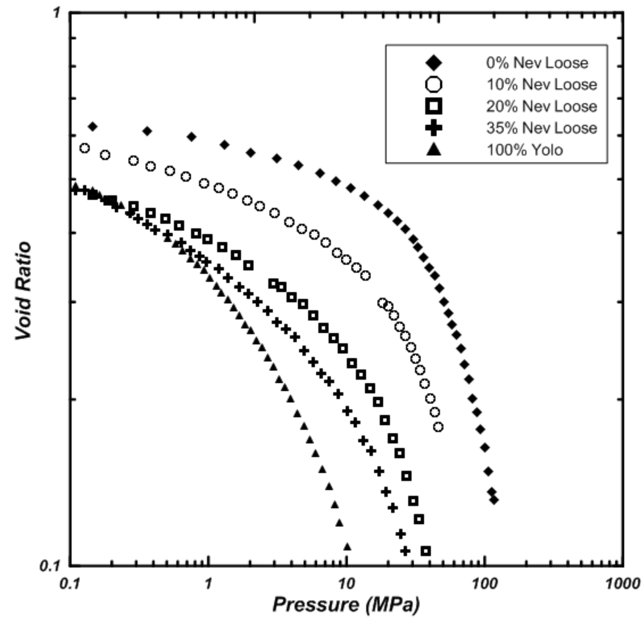

Figure 4.8 LCC of Nevada Sand, Yolo Loam trials.

4.3.3 Slopes and Effective Vertical Reference Stress

As fines content increased the slope of the LCC decreased because deformation did not take place in such a rapid fashion. The samples with high fines contents experienced deformations almost immediately due to the range of stresses at which testing was performed, making the shape of the LCC more gently curved and also decreasing the slope of the LCC. The clean sand samples reached a much higher effective stress before crushing. When crushing did occur large deformations ensued changing the void ratio dramatically and made the slope of the LCC very steep.

The Effective Vertical Reference Stress decreased as fines content increased (see Table 4.2). The reference stresses behaved in this fashion because as fines content increased the LCC's were moved toward lower effective stresses making the reference stresses lower as well.

Table 4.2 **LCC slopes and Effective Vertical Reference Stresses of Nevada Sand, Yolo Loam trials.**

Sample:	ρ_c:	σ'_{vr}: (MPa)
Nevada Loose	0.65	8.5
Nevada Dense	0.65	8.1
10% Nevada	0.61	3.2
20% Nevada	0.6	1.2
35% Nevada	0.55	0.55
100% Yolo	0.55	0.189

4.4 PARTICLE CRUSHING

4.4.1 Relative Breakage Overview

Relative Breakage [Hardin 1985], is a method used to analyze the difference in grain size distribution pre and post crushing (see Figure 4.9). The Relative Breakage analysis only takes into account those particles above the number 200 size sieve. This method utilizes the area above the pre-crushing percent finer curve as the breakage potential (B_P). After LCC testing, the total breakage (B_T) is found by determining the difference in area between the pre- and post-crushing grain size distribution curves. The total breakage is then divided by the breakage potential and is used to determine the relative breakage.

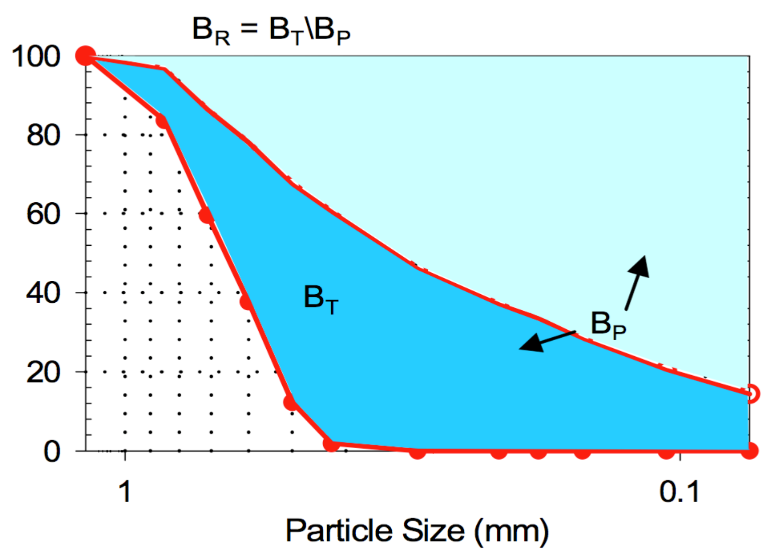

Figure 4.9 **Relative Breakage [DeJong and Christoph 2004].**

4.4.2 Relative Breakage versus Fines Content

Nevada Sand mixtures experienced less relative breakage as fines content increased. The higher fines contents allowed for soil particles to rearrange and increase the points of contact between particles to endure the load. As the contact area between particles grew, more effective stress could be endured forcing water to leave from the sample as pore size shrank.

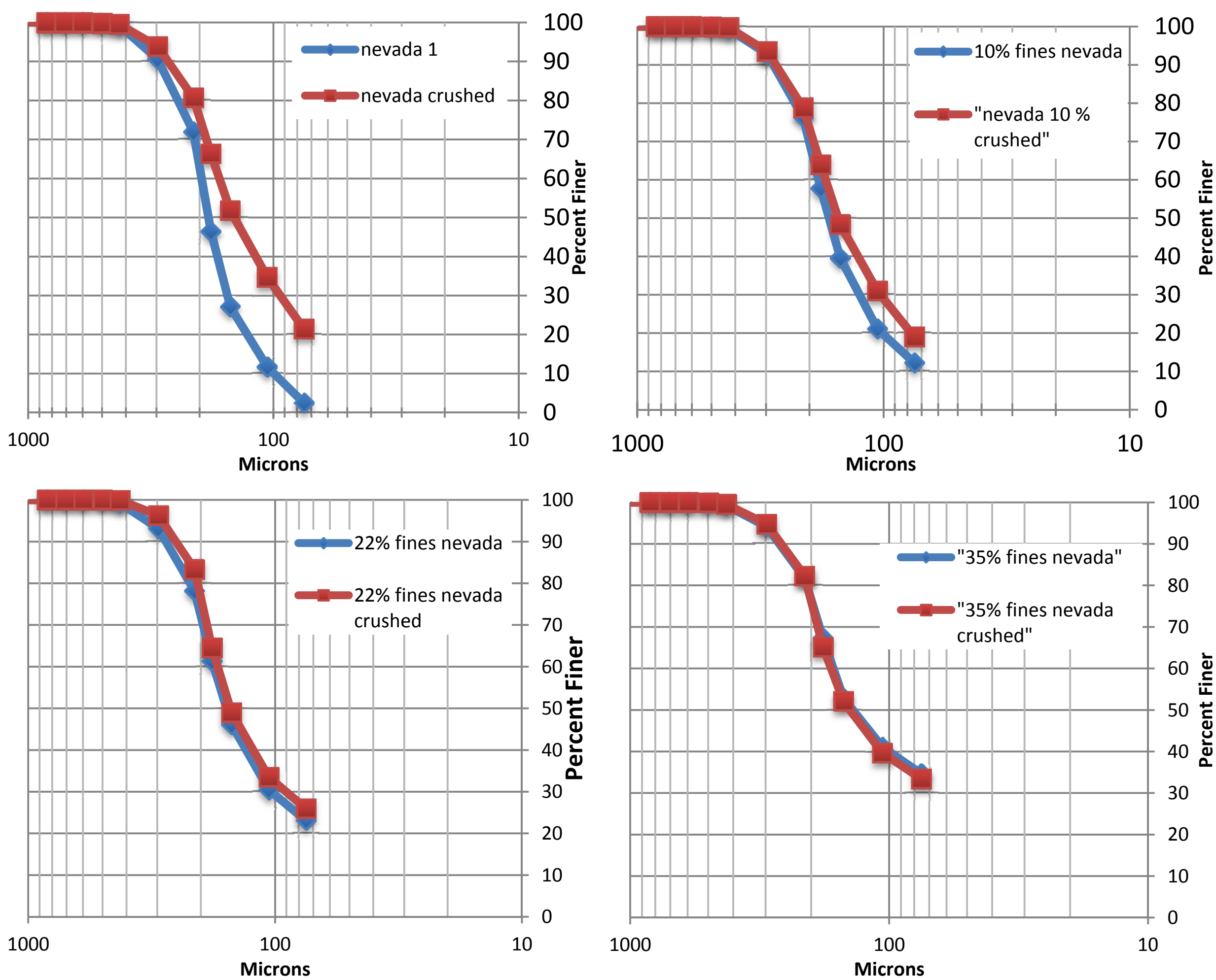

Figure 4.10 Gradation curves of pre- and post- crushed Nevada Sand, Yolo Loam mixtures.

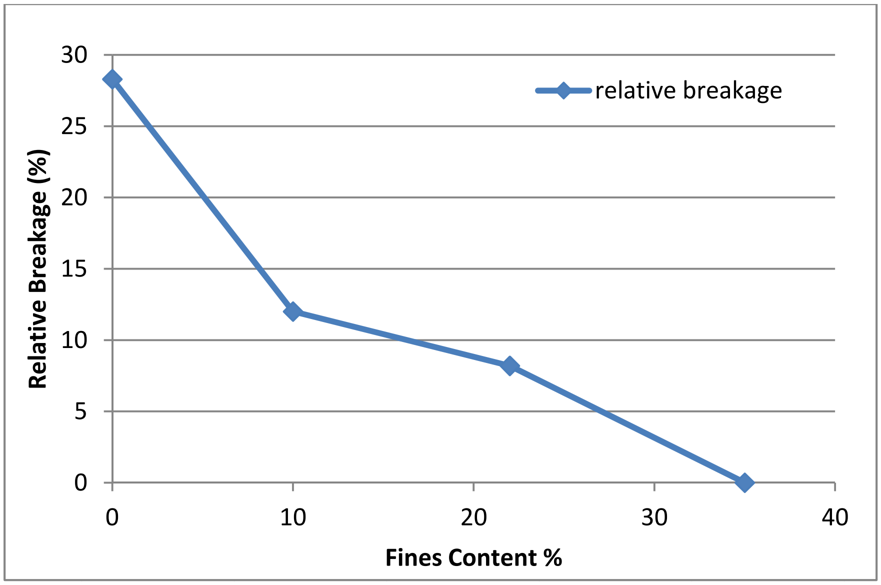

Figure 4.11 Relative breakage versus fines content.

Perris Dam samples experienced large amounts of crushing due to the amount of particles larger than number 16 sieve size present in the soil. Larger soil particles experience more crushing, the particles bear most of the compression load due to the fact that they are not able to rearrange freely.

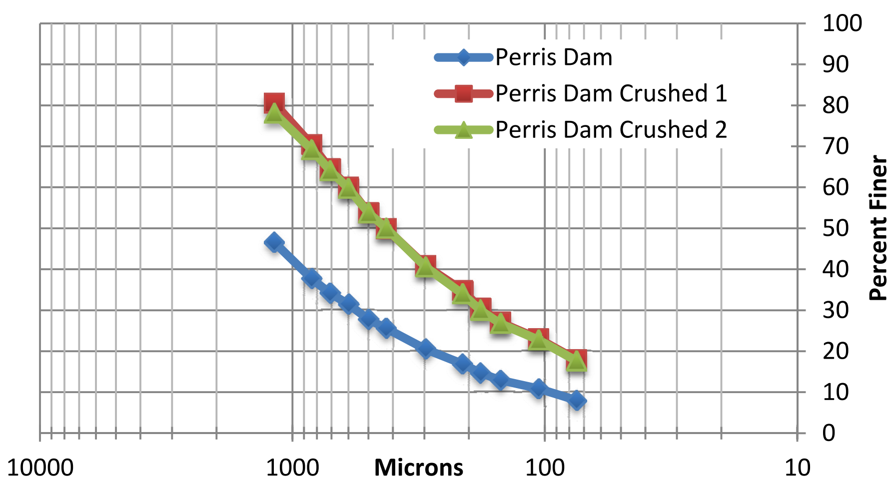

Figure 4.12 Gradation curve of pre and post crushed Perris Dam samples.

4.5 SAMPLE DISTURBANCE

4.5.1 Undisturbed Perris Dam Samples

Undisturbed Perris Dam samples were extruded very carefully as to not disturb the in situ soil characteristics. After the Perris Dam Shelby Tubes were removed from the UC Davis humidifier, the tubes were cut and samples were promptly extruded and trimmed so that little moisture was lost. Once trimming was complete excess soil was shaved off and the sample was placed into the testing device and saturated. Tests were then run in an identical way to the Nevada sand, Yolo loam mixtures.

4.5.2 Reconstituted Perris Dam Samples

Reconstituted Perris Dam samples were taken from the trimmings of the undisturbed samples. The trimmings were dried and ground lightly to remove bonds formed during oven drying. The sample was then pluviated into the device using the funnel method discussed earlier. Once the top cap had been placed the sample was saturated, weighted and tested exactly as the Nevada Sand, Yolo Loam mixtures.

4.5.3 Undisturbed versus Reconstituted LCC Comparison

From the tests observed in Figure 4.13 it can be observed that there is little effect on the LCC when comparing reconstituted and undisturbed samples. While samples started at very similar void ratios samples crushed with approximately the same slope and to the same vertical effective stress. But, based on other trials performed on Perris Dam samples, the non-uniformity of the soil makes it difficult to display the effects of sample disturbance on the LCC because soils of different gradations are being compared. The difference in gradation will have an effect on the reference stress but not the slope of crushing [Pestana and Whittle 1995].

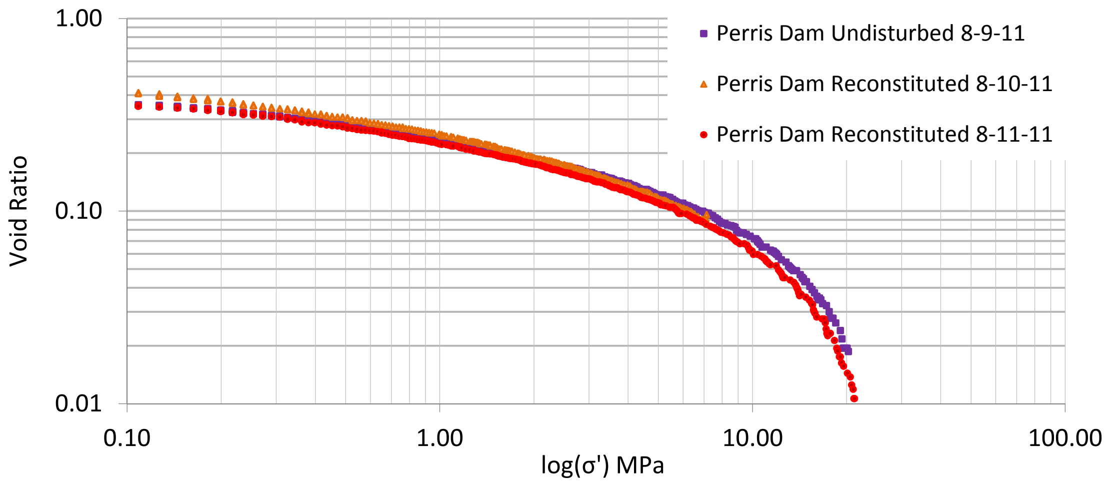

Figure 4.13 LCC trials of undisturbed and reconstituted Perris Dam samples.

4.6 FUTURE RESEARCH POTENTIAL

Using the slopes and effective vertical reference stresses determined in the LCC trials a more comprehensive C_N standard can be developed. The MIT-S1, cavity expansion analysis model [Pestana and Whittle 1999; Jaeger et al. 2011] uses the soil parameters found to simulate CPT testing. Once the slope of the LCC and effective vertical reference stresses for Perris Dam samples are determined CPT tests can be simulated and C_N exponents can be verified by comparison to known results. If verified, the simulation can be used to develop C_N standards for other soil types helping to improve design efficiency and improving the resiliency of levee designs.

REFERENCES

California Department of Water Resources (2008). Where rivers meet – the Sacramento-San Joaquin Delta. CA, <http://www.water.ca.gov/swp/delta.cfm>

DeJong, J. T., and G. G. Christoph (2004). Relation of initial specimen state and particle properties to the breakage potential of granular soils. *Proc*., 57th Canadian Geotech. Conf. and 5th joint CGS-IAH Conf., Quebec City, Canada.

Desouza, J. M. [1958]. Compressibility of quartz sand at high pressure, M.Sc. thesis, Massachusetts Institute of Technology, Cambridge, MA.

Doygun, O. [2009]. Monotonic and cyclic undrained loading behavior of intermediate soils, M.Sc. thesis, Dept. of Civil and Environmental Engineering, University of California, Davis, CA.

Jaeger, R. A., DeJong, J. T., Boulanger, R. W., Whittle, A. J., and Pestana, J. M. [2011]. A modified MIT-S1 constitutive model implemented in FLAC, *Inter. J. Numerical Analytical Methods in Geomechanics*, in press.

Mayne, P. W. [2007]. Cone penetration testing state-of-practice. Washington, D.C., IDEA and Synthesis Studies, Transportation Research Board.

Pestana, J. M., and A. J. Whittle [1995]. Compression model for cohesionless soils, *Geotechnique* 45(4):611-613.

Pestana, J. M., and A. J. Whittle [1999]. Formation of a unified constitutive model for clays and sands, *Inter. J. Numerical Analytical Methods in Geomechanics,* 23:1215–1243.

5 How Well Are Fines and Plasticity Represented in Liquefaction Triggering Curves?

CHRISTOPHER KRAGE

ABSTRACT

Recent attempts to develop liquefaction correlations for the Cone Penetration Test (CPT) reveal a need to investigate parameters that have an uncertain influence on liquefaction. Seismic induced liquefaction is the failure of subsurface soils due to cyclic loading and in-situ tests are needed to determine the soil's resistance to liquefaction since sampling of cohesionless soils results in excessive disturbance. Analysis of the CPT-based liquefaction database proposed by Moss et al. [2006] was used to evaluate the representation of fines and plastic fines within the case history database. The results indicate a shortage of case histories with high fines content and plastic fines. This report reviews available cases with plastic fines to evaluate any relationship between these cases.

5.1 INTRODUCTION

Many of the 1100 miles of levees in the California Delta have been found to be at risk of damage due to earthquakes [DWR, 2009]. One area of concern is the possible strength loss within the levee or foundation due to liquefaction of sandy soils. The reduction in soil strength due to liquefaction may lead to slumping and cracking of the levees, which could turn catastrophic if the water breaches the damaged section.

The potential for liquefaction can be evaluated using triggering curves that are derived using case histories, but their accuracy depends on the quality of the source data. Different types of soil will behave differently under cyclic loading and this may affect the likelihood and consequence of liquefaction. How well soils with high fines and plastic fines are represented in these correlations is not well recognized and provides impetus for this research. Improved procedures and understanding of CPT-based liquefaction correlations will lead to better evaluation of liquefiable soils and enable design and management practices that produce more resilient systems, such as levee systems in the California Delta.

5.1.1 Liquefaction

Liquefaction in granular soils occurs due to an increase in pore water pressure in response to cyclic loading, leading to a reduction in the effective stress and strength loss. This type of failure may be evident by the presence of ground cracks, lateral spreading, settlement, and sand boils. Liquefaction is a complicated phenomenon which has been studied by many researchers and is only briefly described here. Kramer [1996] or Idriss and Boulanger [2008] provide a more detailed description of liquefaction behavior and its evaluation.

Liquefaction in cohesionless soils occurs when cyclic shear stresses, such as those from an earthquake, exceed the cyclic strength of the soil. One common measure of cyclic strength is the Cyclic Resistance Ratio (CRR) which is often related to the penetration resistance of the soil. The Cone Penetration Test (CPT) is one method which can be used to determine the CRR in combination with a triggering curve (e.g. Moss et al.[2006] and Idriss and Boulanger [2008]). The strength of earthquake shaking can be represented through the Cyclic Stress Ratio (CSR) (Eq. 4.1) developed by Seed and Idriss [1971],

$$CSR = 0.65 \cdot \frac{a_{max}}{g} \cdot \frac{\sigma_v}{\sigma_v'} \cdot r_d \tag{5.1}$$

where a_{max} is the peak ground acceleration, g is the gravitational constant, σ_v is the vertical stress, σ'_v is the vertical effective stress, and r_d is the shear mass participation factor which accounts for non-linear soil response. The CSR* [Moss et al. 2006] is the magnitude weighted cyclic stress ratio which normalizes the cyclic stress to an earthquake magnitude of 7.5. Liquefaction can occur whenever the applied stress (CSR) exceeds the soil strength (CRR). Depth ranges where this occurs are often referred to as the critical layer within a soil profile.

5.1.2 Cone Penetration Test

In situ testing is used to measure the properties of soil deposits in the ground without the effects of disturbance which may occur when sampling and testing cohesionless soils. The CPT is one such in-situ test and the results from this test may be correlated to soil properties, such as shear strength or liquefaction resistance. One CPT sounding can continuously record data for tip resistance, pore fluid pressure, and sleeve friction. Two benefits of the CPT are the high degree of repeatability and relatively low cost, however parallel soundings must be made if soil samples are desired. Robertson [1990] used both the tip resistance and the friction ratio to determine the soil behavior type (Figure 5.1) which can be used to estimate the stratigraphy in the absence of soil samples.

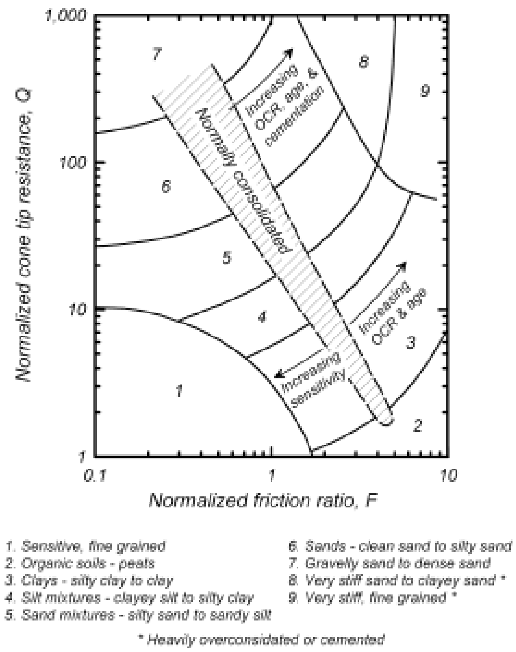

Figure 5.1 ***In-situ*** **soil behavior chart [Robertson 1990].**

5.1.3 Effects of Fines and Plasticity on Liquefaction Resistance

Sands and non-cohesive fines behave differently than clays and plastic silts do under cyclic loading [Idriss and Boulanger 2008]. The soils with the highest potential for liquefaction are sands and non-plastic fines, while plastic silts and clays are less likely to undergo what is traditionally defined as liquefaction and may experience cyclic softening instead. The plasticity index (PI) is one soil property which may be used to delineate sand-like behavior from clay-like behavior as shown by Bray and Sancio [2006] and Idriss and Boulanger [2008].

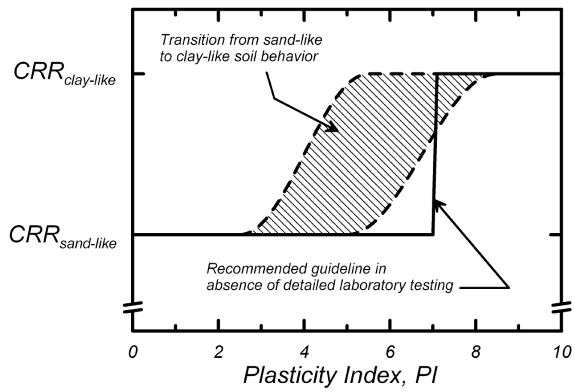

Figure 5.2 **Example of using PI to determine cyclic soil behavior [Idriss and Boulanger 2008].**

5.1.4 Liquefaction Triggering

Triggering curves are one method to evaluate the liquefaction potential of susceptible soils (e.g., Moss et al. [2006], Idriss and Boulanger [2004], and Robertson and Wride [1998]). These curves are empirically derived to provide a boundary between liquefied and non-liquefied cases (Figure 5.3) and are traditionally used to evaluate sandy soils with low fines contents. If these curves are to be used for soils with higher fines content or plastic fines, it is important to understand how well high fines and plastic fines are represented in the current case history database.

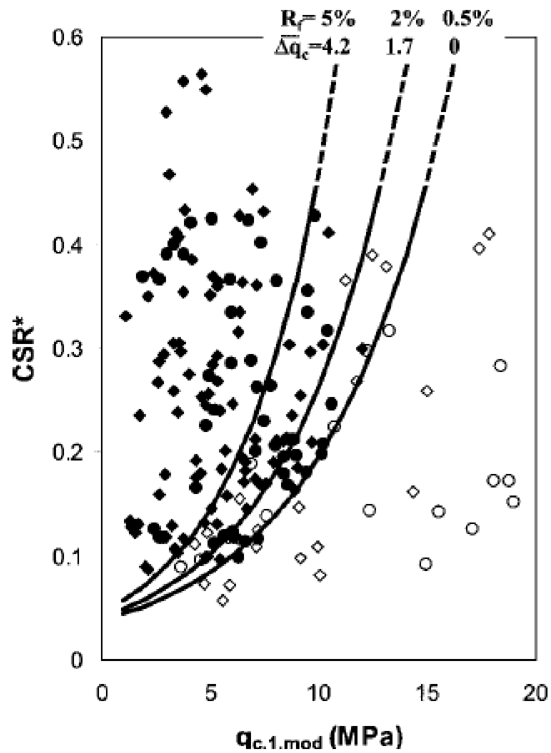

Figure 5.3 Probabilistic liquefaction triggering curves [Moss et al. 2006].

5.2 EXAMINING LIQUEFACTION DATABASE

The CPT-based liquefaction triggering database compiled by Moss et al. [2006] contains 182 cases of liquefied and non liquefied sites from several earthquake events. This database was used in the current study to investigate the presence of case histories with high fines or plastic fines. For case histories with more than 20% fines, the primary source was examined to determine the level of site damage, fines, plasticity, and site characteristics. From this analysis, there are 56 cases with fines content larger than 20% and 14 cases with measured plasticity (PI>0). Forty-five of the 182 cases did not have corresponding borings; therefore it was not possible to determine the fines content of the soils.

Non-liquefied and marginal liquefaction sites make up 10 out of the 56 cases with more than 20% fines (Figure 5.4). All of these case histories have a $q_{c1,mod}$ less than 10 MPa. This makes it difficult to constrain the triggering curves in regions of high fines contents and high tip resistances.

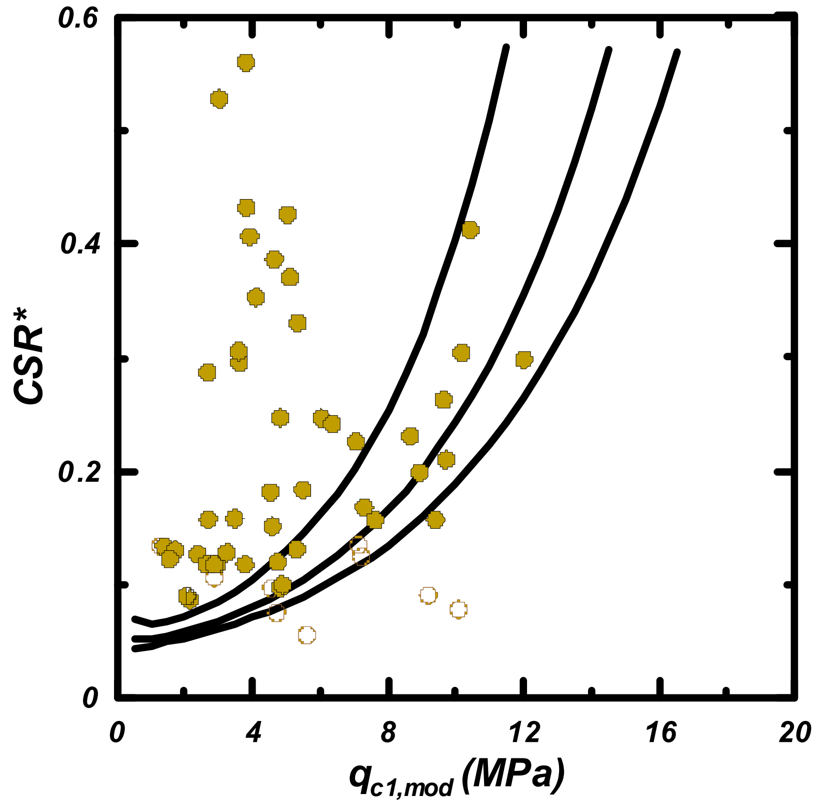

Figure 5.4 **Distribution of cases with greater than 20% fines. Open symbols represent non-liquefied cases and closed symbols represent liquefied cases.**

5.2.1 Primary Source Analysis

The original papers were reviewed for each case history with greater than 20% fines. The purpose of this review is to gather as much site specific information as possible by gathering the original author's observations of site damage, fines content, plasticity index, critical layer interpretation, and any relevant site irregularities. For many of the cases the original author's interpretation matched the descriptions in the Appendix of Moss [2003]. There were a few sites where the original author's interpretation differed from what was recorded in the database and these sites were recorded and noted for further evaluation. This paper presents the results for the cases which contain plastic fines, listed individually in Table 5.1.

Table 5.1 Cases with plastic fines.

Earthquake	Site	Magnitude[1]	Liquefied?[2]	CSR*[3]	Friction Ratio[1]	$q_{c,1,mod}$[3]	%Fines[2]	PI[2]
1975 Haicheng, China	17thMiddleSchool	7.30	No	0.13	1.02 ± 0.44	1.29	80	14
1975 Haicheng, China	PaperMill	7.30	Yes	0.13	1.28 ± 0.56	1.72	72	13
1976 Tangshan, China	TientsinF13 [1]	8.00	No	0.11	2.62 ± 0.74	2.87	75	10
1976 Tangshan, China	TientsinY21 [1]	8.00	Marginal	0.10	2.50 ± 1.84	2.06	50	10
1976 Tangshan, China	TientsinY24 [1]	8.00	Yes	0.12	0.72 ± 0.15	2.15	75	10
1976 Tangshan, China	TientsinY28 [1]	8.00	Yes	0.12	0.78 ± 0.33	3.78	75	10
1976 Tangshan, China	TientsinY29 [1]	8.00	Yes	0.10	0.91 ± 0.59	2.95	75	10
1983 Borah Peak, USA	WhiskeySprings Site1 [2]	6.90	Yes	0.41	1.83 ± 1.89	10.42	20	2
1983 Borah Peak, USA	WhiskeySprings Site2 [2]	6.90	Yes	0.30	3.90 ± 3.11	10.17	30	1
1994 Northridge, USA	BalboaBlvd.UnitC [1]	6.70	Yes	0.31	2.58 ± 1.62	8.66	43	11
1994 Northridge, USA	MaldenSt.UnitD [1]	6.70	Yes	0.25	2.36 ± 1.28	4.82	25	10
1999 Chi-Chi, Taiwan	WuFengSiteA	7.60	Yes	0.57	2.14 ± 0.66	3.02	88	5
1999 Kocaeli, Turkey	AdapazariSiteJ [2]	7.40	Yes	0.42	0.80 ± 0.46	4.11	82	3
1999 Kocaeli, Turkey	AdapazariSiteK [2]	7.40	Yes	0.38	0.91 ± 0.49	4.64	86	9

Superscript [1] are values taken from Table 1 (Moss et al., 2006), [2] for values taken from primary sources and [3] for values calculated using equations in Moss et al. (2006). CSR*=magnitude weighted cyclic stress ratio; $q_{c1,mod}$=calculated adjusted normalized average cone tip resistance for fines content (Moss et al., 2006).

5.2.2 Discussion

The current database contains few case histories with fines content greater than 40% and tip resistance larger than 5 MPa. Case histories with plastic fines are shown in red in Figure 5.5 and account for eleven out of the twenty-three case histories with fines content greater than 40%. Of the 14 cases with plastic fines, 2 are non-liquefied and 1 is marginal liquefaction.

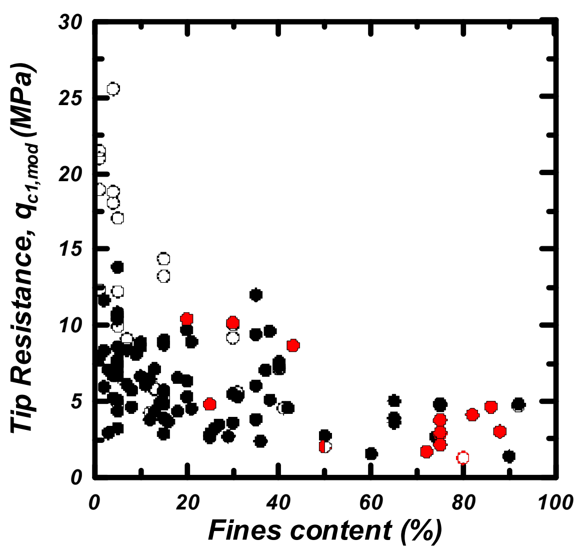

Figure 5.5 **Normalized tip resistance and fines content for all available cases. Open symbols represent non-liquefied cases, half open half closed symbols represent marginal liquefaction, and closed symbols represent liquefied cases. Red symbols are the cases with mentioned plastic fines.**

5.3 PLASTIC FINES ANALYSIS

The 14 cases with plastic fines have PIs ranging from 1 to 14 and fines contents from 20% to 88% (Figure 5.6). Each of these cases was reviewed in detail to determine how well plastic fines are represented in the CPT-based liquefaction database. The goal of this analysis is to provide confidence where appropriate and to understand the quality of each case with plastic fines. Each site is methodically reviewed for descriptions of the original author's interpretation, soil type, site behavior, and any site uncertainty.

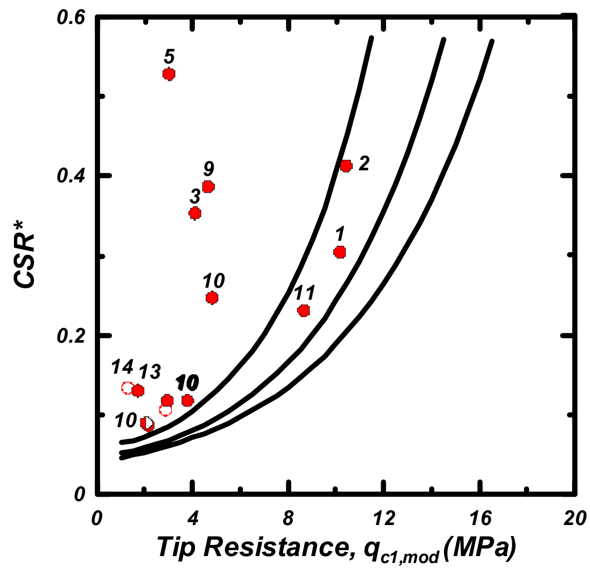

Figure 5.6 **Distribution of cases with plastic fines. Open symbols are non-liquefied, half open are marginal liquefaction, and closed symbols are liquefied sites. The labels are the corresponding PI.**

5.3.1 17th Street Middle School

The 17th street Middle School was investigated and examined by Earth Technology Corporation [1985] and Arulanandan et al. [1986] following the 1975 Haicheng, China, earthquake. The original authors noted no surface manifestation of liquefaction. The soil consisted of clayey silt to silty clay with a fines content of 80% and an average PI of 14. The original authors did not think surface manifestation of liquefaction was hidden by a thick overburden layer, but rather this was a non-liquefaction site. Arulanandan et al. [1986] suggested the lack of surface evidence is due to sufficiently high salt concentrations in the pore fluid that may have produced significant cementation to resist liquefaction.

The Moss et al. [2006] database lists the site as liquefied, the PI as not available, and the fines content as 80%. There were several samples in the critical layer that described the plasticity of the soil, but there is variability in assigning the given fines content to the critical layer due to uncertainty of sampling for the gradation curves.

5.3.2 Paper Mill

The Paper Mill was investigated and examined by Earth Technology Corporation [1985] and Arulanandan et al. [1986] following the 1975 Haicheng, China, earthquake. The original authors noted surface manifestation of liquefaction. The soil consisted of clayey silt to silty clay with a fines content of 72% and an average PI of 13.

The Moss et al. [2006] database lists the site as liquefied, the PI as not available, and the fines content as 72%. There were several samples in the critical layer that described the plasticity of the soil, but there is variability assigning the given fines content to the critical layer due to uncertainty of sampling for the gradation curves.

5.3.3 Tientsin F13

Tientsin F13 was investigated and examined by Arulanandan [1982] following the 1976 Tangshan, China, earthquake. The original author noted no surface manifestation of liquefaction. The soil consisted of clayey sandy silt with a fines content of 75% and an average PI of 10. The average PI of 10 is assigned to all 5 Tangshan cases. The non-liquefaction of site F13 is attributed to a sufficiently thick clay and silty clay overburden layer [Arulanandan 1982]. The site specific gradation curve does not provide a corresponding depth for the sampled soils. The PGA reported for this site by the original authors was 0.09 g.

The Moss et al. [2006] database listed the case as non-liquefied, the PI as 10, and the fines content as 75%. The PGA was reevaluated to 0.12 g by Moss et al. [2011], which will result in an increase in CSR*.

5.3.4 Tientsin Y21

Tientsin Y21 was investigated and examined by Arulanandan [1982] following the 1976 Tangshan, China, earthquake. The original author noted marginal surface manifestation of liquefaction; the site was on the border between zones of liquefaction and non-liquefaction. The soil consisted of clayey sandy silt with a fines content of 50% and an average PI of 10. The average PI of 10 is assigned to all 5 Tangshan cases. The site specific gradation curve does not provide a corresponding depth for the sampled soils. The PGA reported for this site by the original authors was 0.08 g.

The Moss et al. [2006] database listed the case as liquefied, the PI as 10, and the fines content as 50%. The PGA was reevaluated to 0.12 g by Moss et al. [2011], which will result in an increase in CSR*.

5.3.5 Tientsin Y24

Tientsin Y24 was investigated and examined by Arulanandan [1982] following the 1976 Tangshan, China, earthquake. The original author noted surface manifestation of liquefaction in the form of sand boils. The soil consisted of clayey sandy silt with a fines content of 75% and an average PI of 10. The average PI of 10 is assigned to all 5 Tangshan cases. The site specific gradation curve does not provide a corresponding depth for the sampled soils. The PGA reported for this site by the original authors was 0.09 *g*.

The Moss et al. [2006] database listed the case as liquefied, the PI as 10, and the fines content as 75%. The PGA was reevaluated to 0.12 g by Moss et al. [2011], which will result in an increase in CSR*.

5.3.6 Tientsin Y28

Tientsin Y28 was investigated and examined by Arulanandan [1982] following the 1976 Tangshan, China, earthquake. The original author noted surface manifestation of liquefaction in the form of sand boils. The soil consisted of clayey sandy silt with a fines content of 75% and an average PI of 10. The average PI of 10 is assigned to all 5 Tangshan cases. The site specific gradation curve does not provide a corresponding depth for the sampled soils. The PGA reported for this site by the original authors was 0.09 g.

The Moss et al. [2006] database listed the case as liquefied, the PI as 10, and the fines content as 75%. The PGA was reevaluated to 0.12 *g* by Moss et al. [2011], which will result in an increase in CSR*.

5.3.7 Tientsin Y29

Tientsin Y29 was investigated and examined by Arulanandan [1982] following the 1976 Tangshan, China, earthquake. The original author noted surface manifestation of liquefaction in the form of sand boils. The soil consisted of clayey sandy silt with a fines content of 75% and an average PI of 10. The average PI of 10 is assigned to all 5 Tangshan cases. The site specific gradation curve does not provide a corresponding depth for the sampled soils. The PGA reported for this site by the original authors was 0.08 g.

The Moss et al. [2006] database listed the case as liquefied, the PI as 10, and the fines content as 75%. The PGA was reevaluated to 0.12 g by Moss et al. [2011], which will result in an increase in CSR*.

5.3.8 Whiskey Springs Site 1

Whiskey Springs Site 1 was investigated and examined by Andrus et al. [1987] following the 1983 Borah Peak, U.S. earthquake. The original author noted surface manifestation of liquefaction in the form of lateral spreading. The soil consisted of gravelly-sand to sandy-gravel with a fines content of 20%. Two sample borings were made in the critical layer, one with a PI of 2 and the other is characterized as non-plastic.

The Moss et al. [2006] database listed the case as liquefied, the PI as 2, and the fines content as 20%. There are concerns regarding the large uncertainty of the friction ratio, which may be attributed to the gravelly soil [Robertson 2009].

5.3.9 Whiskey Springs Site 2

Whiskey Springs Site 2 was investigated and examined by Andrus et al. [1987] following the 1983 Borah Peak, U.S. earthquake. The original author noted surface manifestation of liquefaction in the form of lateral spreading. The soil consisted of gravelly-sand to sandy-gravel with a fines content of 30%. Three sample borings were made in the critical layer, one with a PI of 1 and the other two are characterized as non-plastic.

The Moss et al. [2006] database listed the case as liquefied, the PI as 1, and the fines content as 30%. There are concerns regarding the large uncertainty of the friction ratio, which may be attributed to the gravelly soil [Robertson 2009].

5.3.10 Balboa Boulevard Unit C

Balboa Boulevard Unit C was investigated and examined by Bennett et al. [1998] and Holzer et al. [1999] following the 1994 Northridge, U.S. earthquake. The original authors noted surface manifestation of liquefaction in the form of ground cracks. The soil consisted of layers of sandy silt, silty sand, and lean clay with a fines content of 43%. A total of ten sample borings were made in the critical layer, three with PIs of 2, 5, and 26 for an average PI of 11. The seven other samples were characterized non-plastic.

The Moss et al. [2006] database listed the case as liquefied, the PI as 11, and the fines content as 43%. The critical layer consisted of interbedded layers of sands, silts, and clays, making it difficult to use average values to describe the layer.

5.3.11 Malden Street Unit D

Malden Street Unit D was investigated and examined by Bennett et al. [1998] and Holzer et al. [1999] following the 1994 Northridge, U.S. earthquake. The original authors noted surface ground cracks and attributed them to shear failure in the soft clays [Holzer et al. 1999]. The underlying Pleistocene soils consisted of sandy lean clay with a fines content of 25%. A total of five samples were obtained from this Pleistocene sandy clay and clayey sand, three with PIs of 7, 12, and 10 for an average PI of 10. The two other samples were characterized non-plastic.

The Moss et al. [2006] database listed the case as liquefied, the PI as 12, and the fines content as 25% for the Pleistocene clayey sand layer. A low strength, lean clay layer overlies this Pleistocene clayey sand layer which introduces uncertainty as to which layer lead to the observed ground failure.

5.3.12 Wu Feng Site A

Wu Feng Site A was investigated and examined by PEER [2000b] and Stewart et al. [2001] following the 1999 Chi-chi, Taiwan, earthquake. The original authors noted surface manifestation of liquefaction in the form of building settlement and sand boils. The soil composition is unknown but has a fines content of 88% and a PI of 5. The appendix containing CPT and sample borings was not available at the time of this research; therefore this site lacks a thorough review of the critical layer and its composition.

The Moss et al. [2006] database listed the case as liquefied, the PI as 5, and the fines content as 88%.

5.3.13 Adapazari Site J

Adapazari Site J was investigated by PEER [2000a] following the 1999 Kocaeli, Turkey, earthquake. The original author noted surface manifestation of liquefaction in the form of building settlement and sand boils. The soil consisted of clayey silt to silty sand with a fines content of 82% and an average PI of 3.Two sample borings were made in the critical layer, one with a PI of 7 and the other characterized as non-plastic.

The Moss et al. [2006] database listed the case as liquefied, the PI as 7, and the fines content as 82%. The PEER [2000a] report provided only CPT logs and sample borings which were used to validate the information in the database.

5.3.14 Adapazari Site K

Adapazari Site K was investigated by PEER [2000a[following the 1999 Kocaeli, Turkey, earthquake. The original author noted surface manifestation of liquefaction in the form of building settlement and sand boils. The soil consisted of clay, silt, and fine sand with a fines content of 86% and a PI of 9.

The Moss et al. [2006] database listed the case as liquefied, the PI as 7, and the fines content as 82%. The PEER [2000a] report provided only CPT logs and sample borings which were used to validate the information in the database. The sample provided was taken from just below the critical layer because there were no samples within the defined critical layer.

5.3.15 Discussion

Of the 14 cases with reported plastic fines, 11 had some form of significant uncertainty. Ambiguity in the sampling location for the Tangshan event and averaging of the PI for 6 of the 14 cases produces significant uncertainty. It is potentially inaccurate to assign an average PI to an entire critical layer, let alone to five different critical layers from five different sites, as was the case with the five Tangshan sites. The potential for misrepresentation of the soil characteristics in a heterogeneous environment (e.g., Balboa Blvd) means that these cases provide a rather poor constraint of cases with plastic fines.

Two case histories have significant uncertainty in the measured friction ratio. These sites are from the Borah Peak event, for which the presence of gravelly soils can adversely affect the measurement of sleeve friction. The gravelly soil type distinguishes these two cases from the other fourteen.

Ground failure at Malden Street was attributed to shear failure in the soft clays by Holzer et al. [1999]. They further concluded that the underlying Pleistocene silty and clayey sands were not likely the source of failure. The Moss et al. [2006] database lists the Pleistocene clayey sands as having liquefied. This case history illustrates the uncertainty that can come from interpreting the source of ground failure in heterogeneous environments.

The presence of uncertainty in the majority of cases shows how poorly plastic fines are represented in CPT-based liquefaction correlations. Many factors play a role in seismic induced liquefaction, so uncertainty in one or two variables does not bring into question the validity of the entire site. Triggering curves try to incorporate all of these variables, but there is still a lack of information that hinders this process.

5.4 CONCLUSIONS

Liquefaction often causes significant damage and researchers are often drawn to sites that show signs of liquefaction. The absence of a problem, such as ground failure, is not as well sampled which leads to poor sampling of non-liquefied or non-ground failure sites. Only 3 of the 14 cases with plastic fines within the critical layer and 10 of the 56 cases with fines content greater than 20% are either non-liquefaction or marginal liquefaction sites. If this database is intended for use with plastic fines or high fines, several more non-liquefied or non-ground failure sites with high fines or plastic fines need be documented. This is especially noticeable for cases with greater than 40% fines content and 5 MPa tip resistance.

Cases with high fines are not well constrained in the database. The data is very limited in high fines content if cases with plastic fines are treated separately. There are 23 cases with greater than 40% fines content and 11 of these are cases have plastic fines. More research and site surveys with high fines content are needed to adequately constrain the derived relationships.

Plastic fines are not well represented in the CPT-based liquefaction database. Only 14 of the 137 reviewed cases noted plastic fines. The cases that are available do not follow any observable pattern in their relationship with triggering curves. In order to improve the accuracy and usability of these cases the various sources of uncertainty must be addressed. The quality of the source data reflects the quality of the triggering correlation for cases with plastic fines.

5.5 FUTURE RESEARCH

There is need to continue standardizing a mechanics based approach to evaluate CPT sites for use in liquefaction correlations. The current trend in CPT-based liquefaction correlations is to provide a user-based interpretation of the critical layer and average the values in the critical layer. This can oversimplify the actual in-situ parameters. Overcoming this limitation may require standard methods for determining the critical layer, developing accounting methods for average values, etc. The database by Moss et al. [2006] is a valuable compilation of documented case histories. The database illustrates the limitations and uncertainty in the quality of data for some sites. Standardizing procedures will help reduce uncertainty and variability in the interpretation of case histories and increase the usability of CPT-based liquefaction triggering correlations for many different subsurface conditions.

ACKNOWLEDGMENTS

This research was made possible through funding and support from PEER. I am grateful to Jack Montgomery for encouraging me and teaching me what research is all about. Thanks to Professor Ross Boulanger for his insight and direction and to Doug Wahl for giving me valuable experience assisting with CPTs.

REFERENCES

Arulanandan, K., B.J. Douglas, Y.Z. Qu, X. Junfei, W. Chengchun, and H. Qizhi (1982). Evaluation of Earthquake induced liquefaction in Tientsin during the Tangshan earthquake P.R.C., *Proc*., U.S.-P.R.C. Bilateral Workshop on Earthquake Engineering (E-3-1)-(E-3-42).

Arulanandan, K., C. Yogachandran, N.J. Meegoda, L. Ying, and S. Zhauji (1986). Comparison of the SPT, CPT, SV and electrical methods of evaluating earthquake induced liquefaction susceptibility in Ying Kou City during the Haicheng earthquake, Use of In Situ Tests in Geotechnical Engineering, *Geotechnical Special Publication No. 6*, 389-415.

Andrus, R.D., and T.L. Youd (1987). Subsurface investigation of a liquefaction-induced lateral spread Thousand Springs Valley, Idaho, *Misc. paper GL-87-8*, U.S. Army Corps of Engineers.

Andrus, R.D., K.H. Stokoe, II, and J.M. Roesset (1991). Liquefaction of gravelly soil at Pence Ranch during the 1983 Borah Peak, Idaho earthquake, *Soil Dyn. and Earthq. Engng. V*, Computational Mechanics Publications and Elsevier Applied Science, London.

Bennett, M.J., D.J. Ponti, J.C.I. Tinsley, T.L. Holzer, and C.H. Conaway (1998). Subsurface geotechnical investigations near sites of ground deformation caused by the January 17, 1994, Northridge, California, earthquake, *Open File Report 98-373*, U.S. Geological Survey, Menlo Park, CA.

Bray, J.D. and R.B. Sancio (2006). Assessment of the liquefaction susceptibility of fine-grained soils, *J. Geotech. Engrg*., 132(9):1165-1177.

Department of Water Resources (2011). *Delta Risk Management Strategy*, Viewed Sept. 1, 2011, http://www.water.ca.gov/floodmgmt/dsmo/sab/drmsp/

Earth Technology Corporation (1985). In Situ Testing II, Peoples Republic of China, 84-141-13.

Holzer, T.L., M.J. Bennett, D.J. Ponti, and J.C.I. Tinsley (1999). Liquefaction and soil Failure during 1994 Northridge earthquake, J. Geotech. Engineering, 125(6), 438-452.

Idriss, I.M., and R.W. Boulanger (2008). Soil liquefaction during earthquakes. *Monograph MNO-12*, Earthquake Engineering Research Institute, Oakland, CA, 261 pp.

Kramer, S L. (1996). *Geotechnical Earthquake Engineering*, New Jersey: Prentice Hall.

Moss, R.E.S. (2003). *CPT-based Probabilistic Assessment of Seismic Soil Liquefaction Initiation*, Doctoral Thesis, University of California, Berkeley, CA.

Moss, R.E.S., R.B. Seed, R.E. Kayen, J.P. Stewart, A.D. Kiureghian, and K.O. Cetin (2006). CPT-Based probabilistic and deterministic assessment of in situ seismic soil liquefaction potential, J. Geotech. Engrg., 132 (8):1032-1051.

PEER (2000a). *Documenting Incidents of Ground Failure Resulting from the Aug. 17, 1999, Kocaeli, Turkey Earthquake*, http://peer.berkeley.edu/publications/turkey/adapazari/index.html.

PEER (2000b). Documentation *of Soil Conditions at Liquefaction Sites from 1999 Chi-Chi, Taiwan Earthquake*, PEER Lifelines Project 3A02. http://peer.berkeley.edu

Robertson, P.K. (1990). Soil classification using the Cone Penetration Test, *Canadian Geotech. J*., 27 (1):151-158.

Robertson, P.K., and C.E. Wride (1998). Evaluating cyclic liquefaction potential using the Cone Penetration Test, *Canadian Geotech. J*., 35(3)442-59.

Robertson, P.K. (2009). *Performance Based Earthquake Design using the CPT*, Gregg Drilling and Testing Inc., Signal Hill, CA.

Seed, H.B., and I.M. Idriss (1971). Simplified procedure for evaluating soil liquefaction potential, *J. Soil Mech. and Foundations Division, ASCE*, 97(SM 9):1249-1273.

Shengcong, F., and F. Tatsuoka (1984). Soil liquefaction during Haicheng and Tangshan earthquake in China; a review, *Soils and Foundations, J. Japanese Soc. Soil Mech. and Foundation Engrg*., 24(4):11-29.

Stewart, J.P. coordinator (2001). Chapter 4: Soil Liquefaction. Chi-Chi, Taiwan Earthquake of September 21, 1999 Reconnaissance Report, *Earthq. Spectra*, 17, Supplement A:37-60.

6 Microbial Induced Calcite Precipitation in Partially Saturated Soils

ANDREW MAKDISI

ABSTRACT

Among the more prominent issues in the California Delta is the potential of liquefaction in any of its sand levees under a cyclic shear load or sudden shear load. Both of these loads are associated with large earthquake stresses. Many of these issues are being addressed via artificial grouting techniques to increase the shear stiffness of soil. Artificial grouting creates a toxic aqueous environment near the treatment site, hence the need for Microbial Induced Calcite Precipitation. Using bacteria to facilitate the precipitation of Calcium Carbonate at particle contacts in weak, subsaturated sands will increase the shear stiffness of the soil by speeding up the formation of sandstone. Treating via a surface-down percolation approach can create a substantial layer of liquefaction-resistant sand, thus improving the resiliency of the Delta's extensive levee system in the event of major seismic activity in the region.

6.1 INTRODUCTION

The California Delta is extremely vulnerable to several potentially catastrophic failures, most of which are related to the strength (or lack thereof) of its extensive levee system. Failure of any number of key levees can cause a myriad of economic and ecological problems in the region. Levee breaches, depending on the location and degree, can destroy farmland, flood cities and towns, and cause saltwater intrusion to what are normally freshwater channels. Levees can fail gradually for any number of reasons: high water levels, erosion, or poorly designed embankments. Additionally, there is the threat of sudden failure due to seismic activity. Levees experiencing high shear stresses can be at risk for soil liquefaction, or a complete loss of shear strength in the soil. This could potentially result in catastrophic levee failure and significant overtopping.

Artificial grouting techniques have been the primary method of treating soil over the last century. While these injections are effective in increasing shear stiffness of soil, they tend to produce harmful environmental side effects. Various injection solutions have been shown to alter subsurface pH in soils and create a toxic environment.

Alternatively, a microbiological injection method has been developed to treat soils. This method uses microorganisms native to the soil as well as external bacteria to facilitate a chemical reaction that produces calcium carbonate at particle contacts in a soil matrix. By treating sands with bacteria, bacteria nutrients, Urea, and Calcium Chloride, geologists and engineers can effectively speed up conversion of uncemented sands to sandstone. Sandstone formation is a natural geological process that occurs over thousands of years. This microbiological process, known as Microbial Induced Calcite Precipitation (MICP) can shorten that time and be used to cement weak sand levees in a much less harmful manner than traditional grouting methods would.

Extensive research has been performed to test the response of sand to MICP treatment, and the results have been positive. However, the common treatment methods used have would not be applicable to treatment of levees. The aim of this research was to develop an *in situ* treatment technique to increase shear stiffness in sands using a surface-down approach. The methods described here involved testing two vastly different soil types to assess the viability and versatility of MICP Percolation in a wide range of environments. Development of an effective, practical, and ecologically innocuous treatment method should improve resistance to liquefaction in sand levees, and thus their resiliency in response to a large earthquake.

6.2 BACKGROUND

6.2.1 MICP

Central to this bio-cementation treatment is a process known as Microbial-Induced Calcite Precipitation, or MICP for short. As the name indicates, this process utilizes bacteria to catalyze a chemical reaction between Urea and Calcium Chloride:

$$Ca^{2+} + CO_3^{2-} \leftrightarrow CaCO_3$$

The bacteria used for this process is bacillus pasteurii, which uses urea as an energy source to produce ammonia. The presence of ammonia causes a rise in pH to about 8 to 8.5. This pH level is sufficiently high enough to cause Calcium Carbonate to precipitate at particle contacts in the soil matrix where bacteria are present. (Figure 6.1)

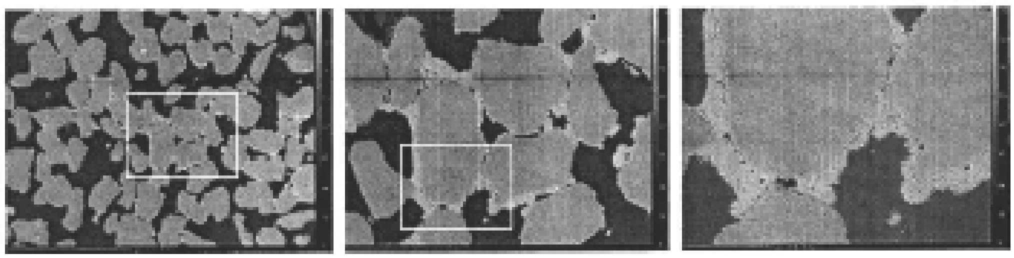

Figure 6.1 Heavily microbially cemented sand. Scanning electron microscopy imaging [DeJong et. al. 2006].

A number of environmental parameters effect the cementation, and thus the overall effectiveness of treatment. It has been shown that MICP is robustly effective over a wide range of soil types, ammonium chloride concentrations, and salinity of water present. However, calcium carbonate has been observed to precipitate at higher rates in coarser and well-graded sands. These optimal sand properties are characteristic of most of the natural sand levees in the Delta. Additionally, sites with higher seawater concentrations also exhibit greater rates of precipitation. This is an encouraging observation, allowing for the potential of treatment in areas of the Delta experiencing increased salinity. Regardless of the circumstance, past research has shown that MICP can be a viable and effective treatment method in most environments in the California Delta.

6.2.2 Liquefaction and Other Hazards Associated with Levee Systems

Soil liquefaction is the most direct and catastrophic result of supercritical shear stresses on a foundation, dam, levee, or any other type of soil-based entity. Liquefaction describes the phenomenon of a saturated soil losing its stiffness and strength under severe shear stresses. Under these conditions, soils will lose their structural stability and essentially behave as a liquid.

Soils are considered saturated when their water content, denoted as θ, equals the porosity φ. This means that the pore volume is equal to the volume of water in the soil, and that the soil cannot take on any more water.

When experiencing a load, the water pressure in the pores increases, causing the water to flow to zones of lower pressure, usually towards the surface. However, under rapid cyclic shearing, which is associated with earthquake stress, pore water may not have enough time to diffuse to regions of lower pressure before the soil matrix experiences the next period of shear loading. This causes the pore pressure to increase, instead of diffusing towards the surface. Liquefaction occurs when this pore pressure buildup exceeds the contact stresses between grain particles. This causes the soil to lose its ability to transfer shear stresses, which is the criterion for soil failure.

When liquefaction occurs in soil foundations, the results can be interestingly disastrous. Structures themselves may not fail, but will still collapse above liquefied soil. Such was the case in the Niigata Earthquake of 1964. (Figure 6.2). In dams and levees, liquefaction can lead to severe breaches and significant overtopping. Liquefaction is most susceptible in young, poorly graded sands, particularly along riverbeds. The risk to subsaturated soils is even greater, hence the need for research pertaining to treatment of sands that are partially saturated or unsaturated.

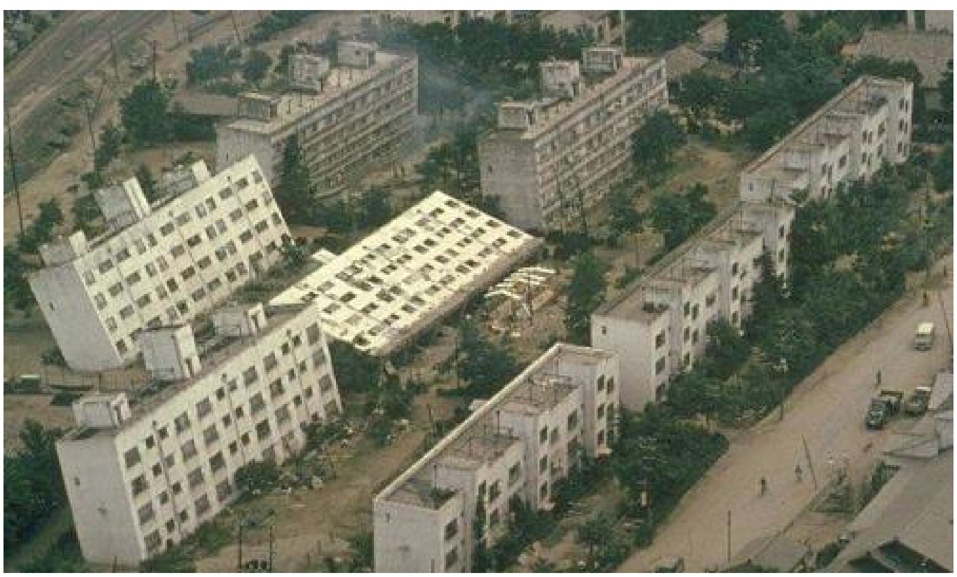

Figure 6.2 Liquefaction during the 1964 earthquake in Niigata, Japan, (photo courtesy of the PEER Library, University of California, Berkeley).

6.2.3 Potential of Percolation Treatment

Most of the MICP research to date has dealt with treatment procedures that are difficult to implement *in situ.* Treatment performed by DeJong et. al. [2006] and Mortensen et. al. [2011]

consisted of injection of the bacterium *bacillus pasteurii* into the base of the specimen via peristaltic pumping. The cementation medium was then introduced to the specimen in a similar manner. While these methods proved to be very effective, treatment of a sand levee simply does not allow for injection at the base.

An alternative approach is to prepare the treatment solution initially without bacillus pasteurii. This solution contains Urea, Calcium Chloride, and a nutrient broth for bacteria growth. On site, the treatment solution is then inoculated with bacteria and allowed to percolate deep into the soil from the surface. This process can repeated as many times as necessary, and the goal of the research presented here is to determine how many treatment cycles are needed to produce a nominal increase in shear stiffness at lower depths.

Bacterial concentration, which will be shown to be an important parameter in MICP Percolation, can be controlled such that precipitation does not begin until the treatment solution has reached sufficient depths in the soil. Optimal bacteria concentration minimizes the precipitation gradient due to depth and ensures adequate improvements in shear stiffness at adequate depth.

6.3 RESEARCH METHODS AND MATERIALS

6.3.1 Optimization of Treatment Concentration

Treatment of unsaturated or sub-saturated sand via MICP Percolation requires inoculation of the treatment solution with microbes *before* it is applied to the sand sample. The time between inoculation and the onset of calcium carbonate precipitation is controlled by the amount of bacteria with which the aqueous mixture of Urea, Calcium Chloride, and nutrient broth is inoculated.

In order to characterize the relationship between bacteria concentration and precipitation time, a beaker test was devised. Five different recipes of treatment solution were prepared in triplicate, each contained the same concentrations of Urea, Calcium Chloride, and Difco. Difco serves as a nutrient broth medium to facilitate bacteria growth. This is especially important in a beaker test, as the bacteria have not soil matrix to which they can adhere and multiply.

Table 6.1 **Ingredient concentrations for 5 different recipes. Included is a control group, which was not inoculated with bacteria.**

Ingredient	Recipe 1 (Control)	Recipe 2 (2X)	Recipe 3* (10X)	Recipe 4 (100X)	Recipe 5 (1000X)
Bacteria (*S. pasteruii*)	0 cells/mL	$5E10^6$ cells/mL	10^6 cells/mL	10^5 cells/mL	10^4 cells/mL
- OD_{600}	0.000	1.000	~0.100	~0.010	~0.001
Bacto (nutrient broth)	3 g/L	3 g/L	3 g/L	3 g/L	3 g/L
Urea (60 g/L)	1 M	1 M	1 M	1 M	1 M
$CaCl_2$-$2H_2O$ (141 g/L)	0.5 M	0.5 M	0.5 M	0.5 M	0.5 M

The pH of each beaker was measured before inoculation and every 10 minutes after inoculation. A sudden jump in pH from its starting point (usually between 6 and 7) to above 8 indicated the onset of calcite precipitation.

Optical Density was also measured using a Shimadzu UV160U UV-visible recording spectrophotometer at a wavelength of 600 nm. OD was taken before inoculation and every 20 minutes during testing. Again, a sharp rise in OD indicates the onset of precipitation. Beakers were monitored until precipitation had occurred in all beakers. Besides the sharp increases in Optical Density and pH, change in color (as calcite visibly begins to form at the bottom of the beaker) is also an indicator of the onset of precipitation.

Figure 6.3 **Calcite precipitation is exhibited by the darker hue and increased turbidity of recipe 2A. Recipe 1A, the control beaker, exhibits no precipitation, due to the absence of bacteria.**

6.3.2 Large Sample Percolation

The Sample Container

Two cylindrical containers were constructed from PVC piping. Each container is 4 ft (1.22 m) high and 1 ft (0.305 m) in diameter. The bottom cap of each tank was drilled to allow effluent to flow out of the tank through an elbow pipe and ball valve. Drilled into the side of the containers were 10 holes: five on each side at various depths, directly opposite each other to allow for the insertion of Bender Elements into the soil samples (detailed description of bender elements is presented in the next section). Two nylon string filters were placed on the bottom of the tank, followed by one black felt filter. A layer of coarse gravel was added, followed by a layer of angular sand.

Two types of sand were tested for this percolation experiment. Felt sand is a well-graded, coarse sand that closely resembles many naturally occurring sands in the Delta. Ottawa 50-70 represents the other end of the spectrum. It is a poorly-graded, fine-grained, manufactured sand. It consists of mostly uniformly sized, relatively small particles. Each sand type was pluviated into its respective tank at a degree of 20. Pluviating at this degree achieves a uniform, relatively loose density throughout the tank. Thus, the only initial parameter that varies with depth is the overburden, or load above a certain cross-section of sand. At lower depths, the overburden will be greater than near or at the surface, causing initial shear wave velocities to be greater at lower depths.

Table 6.2 Sample preparation for both percolation tanks. Note: Each sand type was pluviated at 20º.

	Tank I	**Tank II**
Sand Type	Ottawa 50-70	Felt Sand
Volume of Gravel	0.0674 ft^3	0.0614 ft^3
Volume of Angular Sand	0.0258 ft^3	0.0297 ft^3
Volume of Pluviated Sand	2.247 ft^3	2.287 ft^3
Total Mass of Pluviated Sand	111.41 kg	118.2 kg
Total Density	1.75 g/cm^3	1.83 g/cm^3
Specific Gravity	2.65	2.65
Void Ratio	0.51	0.45

.

Bender Elements and Shear Wave Velocity

The shear wave velocity, V_s, through a particular cross section of soil is a valuable parameter in determining the shear stiffness of soils. Shear wave velocity is a function of the density of the soil and its shear modulus, and is characterized by the following equation:

$$V_s = (G_0/\rho)^{1/2}$$

where G_0 is the shear modulus of the soil layer and ρ is the density of the soil, derived from its unit weight.

Physically, a shear wave is an elastic deformation within a cross-section of soil. The elastic deformation propagates through the sand as a transverse wave. It eventually reaches its terminus at the end of the cross section, or in cases of a seemingly infinite propagation medium, when its amplitude degrades to zero over long distances.

For experimental purposes, a bender element pair can control the disturbance that prompts the shear wave. A bender element pair consists of two small, rectangular, piezoceramic transducers that are embedded in the soil. The transmitting bender is controlled by a remote signal, and converts electrical energy into mechanical energy. When prompted, the transmitting bender vibrates very slightly, depending on the applied voltage (usually 10 V), producing a shear wave. The receiving bender, positioned on the opposite end of the cross-section, detects the shear wave and converts mechanical energy back into electrical energy. Using data acquisition software, sufficient grounding of excess sources of signal noise, and signal filtering devices, the propagation time of the shear wave can be determined, and then divided by the separation distance between the benders to calculate shear wave velocity.

Five pairs of benders were fabricated for each percolation tank. Placed at increasing depths, these benders were used to measure the increase in shear stiffness in the soil that would result from calcite precipitation. Shear wave readings were the primary indicator of the progress and improvements that MICP percolation would have on the shear stiffness of the sand.

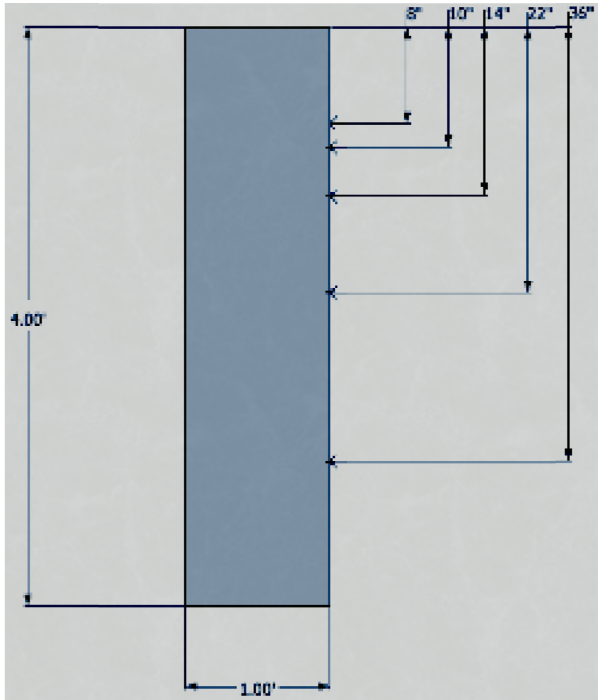

Figure 6.4 **Schematic of dimensions and bender positioning on percolation tank.**

Percolation

In order to achieve percolating flow, a gravity-driven drip system was developed. A versatile percolator was fabricated out of acrylic material. The percolator consists of a small cylindrical well with a diameter of under 1ft, with a top cap with a diameter over 1 ft, allowing it to rest on the top edge of the tank. The percolator was thus suspended above the surface of the sand. Ninety-six holes were drilled radially into the bottom of the well. The holes were 1/8 in. in diameter, and were filled with 1.5 in. segments of irrigation tubing. Treatment solution was prepared in an external tank, which was then placed above the percolator and percolation tank rig. Flow was sufficiently consistent throughout the percolation process.

The treatment solution was prepared by combining Difco nutrient broth, Urea, and Calcium Chloride in an aqueous solution equal to one-half the pore volume of the sand.

Treatment was applied via percolation on 24-hour cycles. This time allowed for complete percolation, draining of effluent, and the completion of calcite precipitation in the soil. Once the system was deemed no longer transient, treatment was applied again. Treatments were repeated until surface cementation occurred to the extent that solution pooled at the top of the container for more than 1.5 hours.

Figure 6.5 **Percolation tank rig. The percolator rests on top of the tank on the left. DAQ boxes are responsible for sending and receiving the signal and processing it into a visual graph.**

6.3.3 Post-Treatment Analysis

After percolation was completed, each sample was dried out using a vacuum attached to the bottom effluent port. The tank, made of PVC was then cut from around the sample of sand, and using a hammer and chisel, 4-in.-diameter and 6-in-high core samples were then extracted from the center of the cross-section. These core samples, 8 in total for each sand type, were then dried overnight in an oven, and then further filed down to meet ASTM Standards for unconfined compression. ASTM Standards specifically require a sample diameter of no less than 1.4 inches, and a height-to-diameter ratio between 2 and 3. Compression tests were performed using a GeoJac Automated Load Actuator, made by GeoTac, on each core sample for various depths, as further means to determine the extent of cementation with respect to depth.

6.4 TEST RESULTS AND DISCUSSION

6.4.1 Optimal Bacteria Concentration

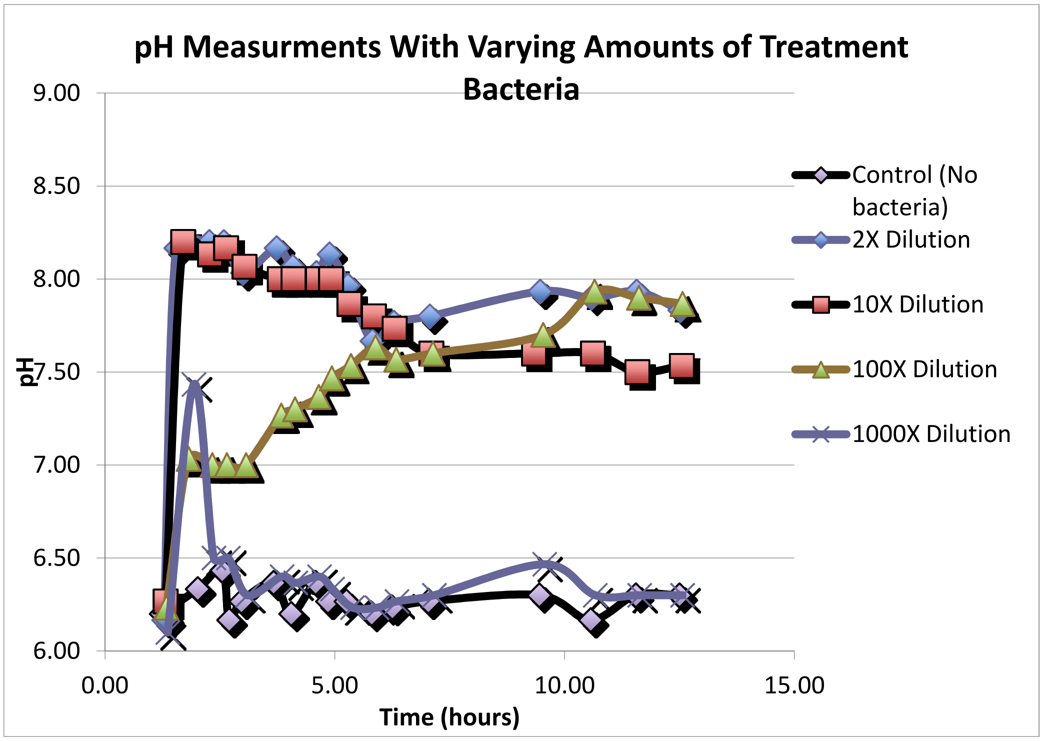

Figure 6.6 **Beaker test results for pH versus time for each bacteria concentration, including control.**

The first pH readings after inoculation with bacteria indicate the onset of precipitation in both a 2x and 10x dilution of bacteria. This sort of binary result is undesirable in percolation treatment, as it is clear that such a concentration of bacteria would likely cause rapid cementation only at or near the surface of the sand. As a result, the surface would seal off the rest of the sand, vastly decreasing the rate at which treatment solution would percolate through the sand. The 100x dilution however, appears to reach a pH of 8 at about 13 hours after inoculation. Additionally, it appears that the increase in pH was more gradual with lower concentrations. This concentration is closer to the optimal amount of bacteria, as it allows the treatment solution to percolate completely through the sand before the chemical reaction occurs. The 1000x dilution did not precipitate calcium carbonate within the time frame of this experiment, thus a bacterial concentration on the order of 10^4 cells/mL appears to be neither robust nor time-efficient for percolating large volumes of sand.

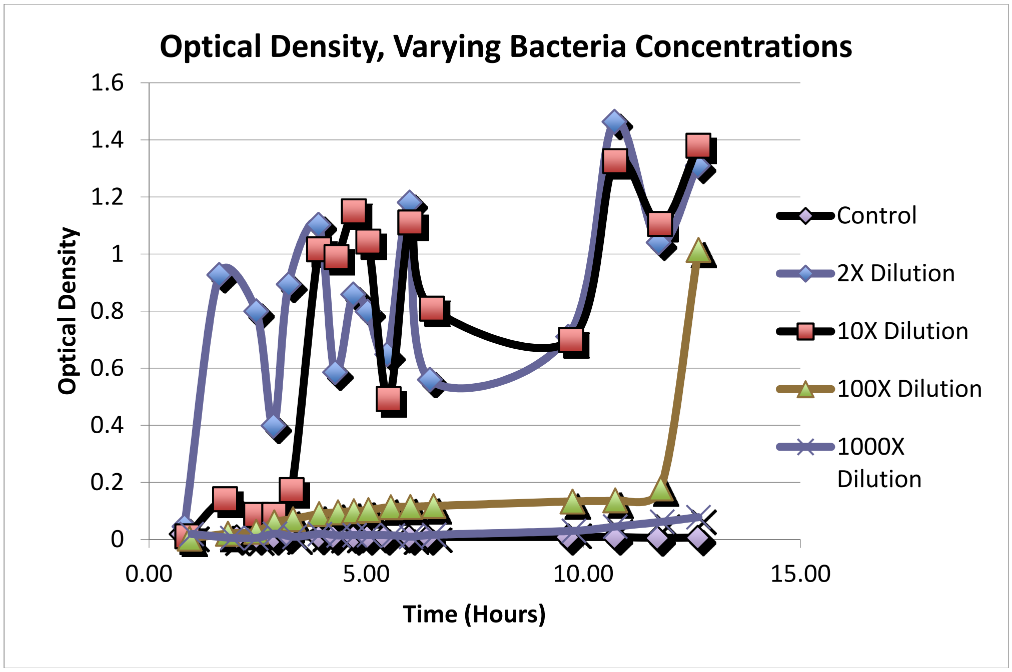

Figure 6.7 **Beaker test results for OD versus time for each bacteria concentration, including control.**

The time plot for Optical Density supports the conclusions drawn from the pH data. It is, however, somewhat limited in what it indicates in the hours *after* the onset of precipitation. Once again, a sharp increase in optical is density is observed shortly after inoculation in both the 2x and 10x diluted recipes. It is after this increase though, where the data loses its utility, due to settling of calcite particles in the cuvette.

Therefore, optical density data serves as only a confirmation of what the pH data already shows. This is indeed true for the precipitation times of each recipe. Once again, the 2x and 10x dilutions cause binary and near-binary results, respectively; and the 100x dilution takes about 13 hours to precipitate. Additionally, the optical density data confirms that 1000x dilution does not precipitate calcite in a substantial or efficient manner.

6.4.2 Shear Wave Velocities in Large Percolation Tanks

A total of 8 percolation treatments were performed on each type of sand. For the first 5 treatments, a bacterial concentration of $5x10^5$ cells/mL was used. The next three used a 100x dilution, or $1x10^5$ cells/mL. After the eighth treatment, solution had begun to pool significantly above the surface of both sands. In the Ottawa 50-70 tank, treatment solution took about 2 hours to drain completely after treatment began. The Felt Sand tank only pooled for about 45 minutes after percolation began.

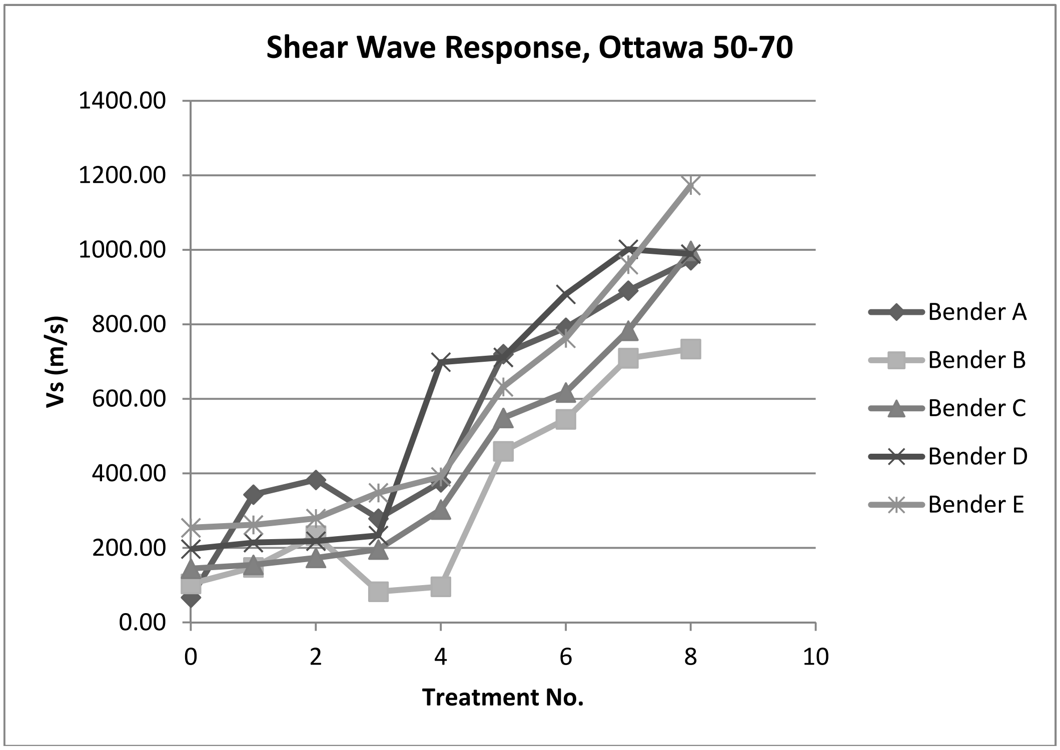

Figure 6.8 **Changes in shear wave velocity for each bender depth for Ottawa 50-70. Bender A corresponds to the bender element closest to the surface.**

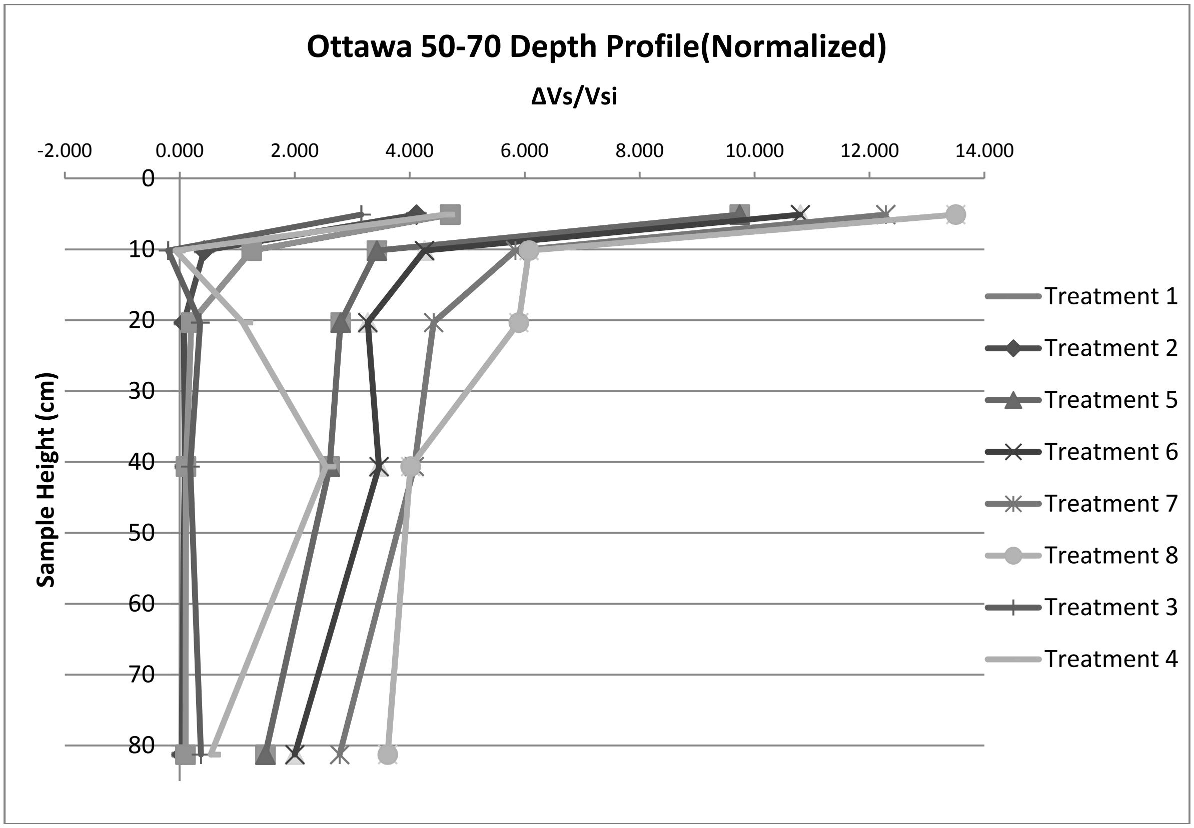

Figure 6.9 **Changes in shear wave velocity for each bender depth for Felt Sand. Bender A corresponds to the bender element closest to the surface**

The time plots for each type of sand show the largest increases in V_s near the surface occurring during the earlier treatments. Also note the initial shear wave readings. They confirm the effect on V_s due to overburden. Generally, the lower benders exhibited significantly higher initial shear wave velocities due to the stresses associated with increased overburden. Lower depths in the sand do not see significant increases in V_s until the fourth or fifth treatments. Once significant cementation occurs at all depths (generally after the fifth treatment for both sand types), V_s continues to increase moderately throughout the tank. At this point during the treatment, it is believed that there are significant amounts of bacteria and nutrients throughout the tank, and hence cementation can occur with the addition of more Urea and Calcium Chloride. The permeability has certainly decreased, but adequate treatment solution is still reaching the bottom of the tank, and significant amounts of effluent were observed for each treatment.

It is clear that significant cementation is possible at depth by percolation treatment. What is also clear is that there appears to be a cementation gradient with respect to depth. Comparing the initial (baseline) and final V_s readings for the bender elements near the surface with those at lower depths supports this notion.

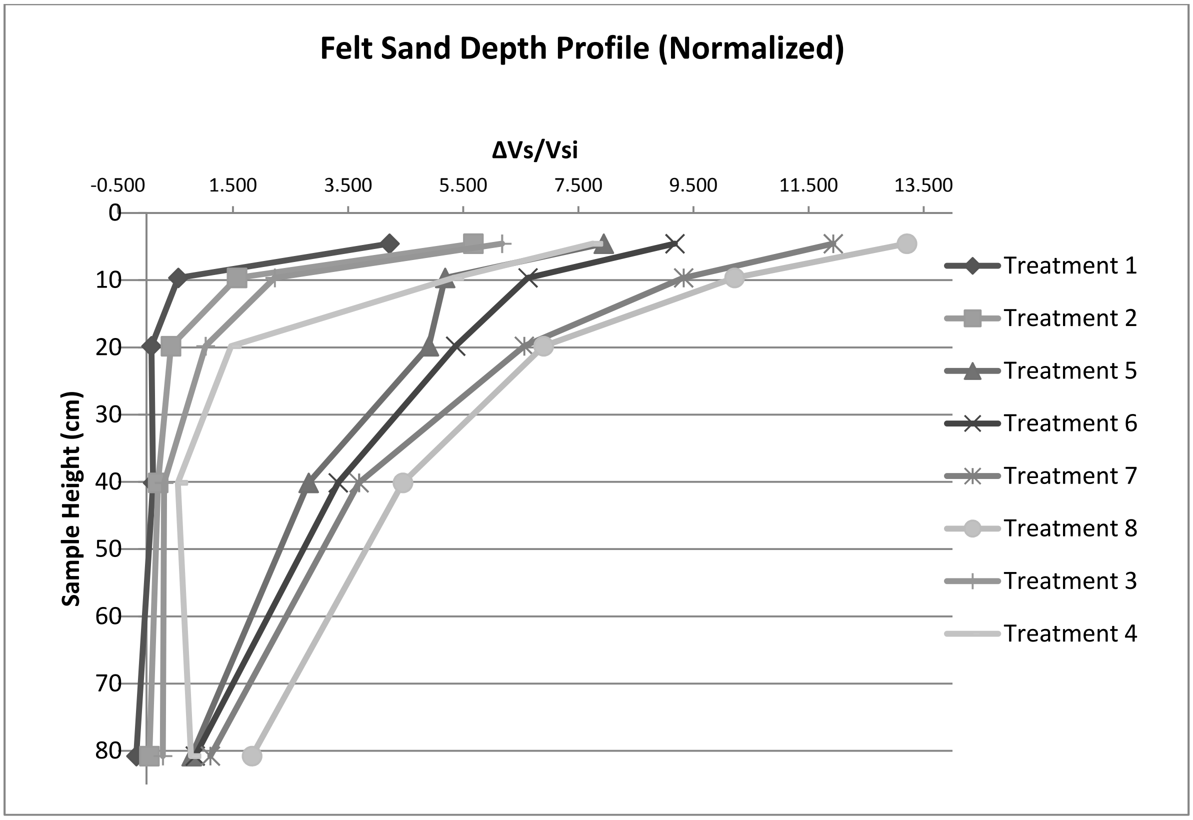

Figure 6.10 Normalized shear wave response versus depth for felt sand and Ottawa 50-70.

Near the surface, we see a final shear wave velocity that is about 14 times the baseline reading. Closer to the bottom of the tank, the final V_s is only about twice the initial reading for the Felt Sand and 4 times the initial for the Ottawa 50-70. While it appears that the Ottawa 50-70 responded better to treatment, it is important to note that the Felt Sand could probably have been treated further, however desirable shear stiffness was achieved in both sands and time didn't allow for treatment to continue.

6.4.3 Sample Coring and Compression Testing

Post-treatment coring revealed a number of things about the nature of MICP percolation for different sand types. Firstly, the sandstone formed from MICP percolation, despite exhibiting substantial shear stiffness, proved to be quite brittle when subjected to a hammer and chisel. This type of low-contact-area pressure is would generally not be experienced by sand levees in nature, hence the brittle nature of the treated sands is not alarming.

Table 6.4 Unconfined compression test results for Felt Sand after 8 MICP percolation treatments.

Sample #	Avg. Distance from Surface (cm)	Sample Height (in.)	Sample Diameter (in.)	Compressive Strength (psi)	Comments
1	5.00	1.5	1.5	25.92	1:1 aspect ratio, small transverse crack in sample before testing
2	10.75	1.5	1.5	49.33	1:1 aspect ratio, no visible cracks
3	17	3.875	2.0	165.44	Strongest sample available, no visible cracks
4	21.5	4	1.75	25.53	Longitudinal crack 2 in long visible in midsection
5	24.5	3.75	1.75	35.62	No visible cracks, sample integrity maintained throughout coring process

It was during the coring process that the Ottawa 50-70 and Felt Sand began to differentiate from one another. Chiseling the felt sand required a high degree of precision, and even so, 2 of the core samples had to be tested at a 1-to-1 aspect ratio due to failure of the sample during coring and/or filing the initial coring sample down. The Ottawa 50-70, however, was impossible to core. When enough pressure was applied from the chisel the sand failed completely.

It is important to note that the sand below Sample 5 (at depths lower than 26.5 in.) was not cohesive enough for coring in the Felt Sand. The cementation at this depth had formed small clusters of sandstone, but the sand below the 5th bender lacked the overall cohesiveness seen in sand closer to the surface.

It is also pertinent to discuss how a lower sample aspect ratio (one that is less than ASTM standards) affects compression data. When a cylindrical sample is subjected to an axial compressive load, two "cones" develop from each load surface. When critical stress is reached, failure generally occurs along and x-shaped plane known as a shear band.

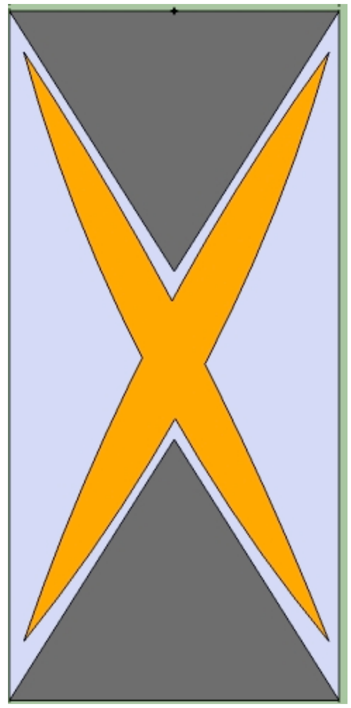

Figure 6.11 Visual representation of localized failure along a shear plane in a cylindrical sample under compressive stress.

For failure to occur in this manner, the sample height must be at least twice the diameter, as stated in ASTM standards. When the ratio is below this limit, the "cones" shown above tend to overlap each other, and no localized shear band develops. Thus, failure doesn't occur in a localized manner and the compressive strength in samples such as these tend to be significantly lower.

The results in Table 6.4, while scattered, do support a few trends in data. Samples 3 and 5, both up to ASTM Standards and showing no visible failures, illustrate the gradient in compressive strength due to depth. The midsection of the percolation tank exhibited a compressive strength 5 times greater than the sand closer to the bottom of the tank. All in all, sample coring and subsequent compression testing revealed the brittle nature of MICP-percolated sand. The unconfined compression testing, while somewhat inconsistent, did reveal an apparent decrease in compressive strength with respect to sample depth.

6.5 CONCLUSIONS

6.5.1 Feasibility of Percolation Treatment

The data presented here has shown that bio-cementation of sand-based levees via MICP percolation treatment is very effective in improving the resiliency of levees in the California Delta. The probability of failure of a sand due to liquefaction from cyclic shearing (or any other sudden shear stress associated with earthquake loads) can be decreased significantly by treating weaker, loose sands with microbes, Urea, and Calcium Chloride. Shear stiffness increased at least five times its initial dry reading at depths as low as 40 cm from the surface. Closer to the surface, the increase was at least tenfold.

While the Ottawa 50-70 was treated to a near maximum capacity and failed under low-contact area pressure, Felt Sand, which is well-graded and exhibits qualities closer to natural sand, had potential for even more treatment. As it is, its shear wave velocity was above 800 m/sec for each bender reading, and exhibited adequate cohesion when cored. Compression test data showed a severe gradient with respect to depth, yet the compressive strength near the bottom of the tank is about 35 psi, equal to that of most polyurethane grouts.

Despite the decrease in treatment response with depth, it is important to note that the entire depth of sand need not be uniformly cemented, or even at optimal resistance to liquefaction. In many cases of liquefaction at subsurface levels, the effects and damage will not be observed at the surface if the liquefied layer is 3 m or less and the cover layer is 3 m or more (for a particular case of an earthquake of magnitude 7.5). What this means is that if MICP percolation can be tailored to ensure adequate cementation to a depth that prevents surface damage from liquefaction at lower depths, then the weaker sand near the bottom of a levee won't cause catastrophic failure even it liquefies.

6.5.2 Future Research

It may be constructive in future experiments to find the optimal usage of treatment solution in terms of bacteria concentration and volume of solution. Limited the amount of effluent, or excess solution not taken up by the soil would lessen any potential harmful impacts from treatment and save money and resources.

In that same vein, a lifecycle analysis would be extremely helpful in determining the cost and benefits of MICP percolation. Knowing the effect of having a Urea-based effluent remain in the soil on the environment is an important factor in determining how good of an alternative MICP percolation really is to artificial grouting. As it stands, MICP is indeed a much more natural process of creating sandstone, and there is little reason to believe that it would have any substantial toxic effects on an aqueous environment. A lifecycle analysis would hopefully confirm that or uncover any unexpected consequences.

ACKNOWLEDGMENTS

This research would not have been possible without the funding and support of PEER. Special thanks to Heidi Faison for her facilitation of this process through PEER. I am also eternally grateful for the mentorship, guidance, and patience of Brian Martinez, who oversaw my first research experience and gave me a valuable crash course in research. Additional thanks to Jason DeJong and the rest of the Soil Interactions Lab at UC Davis.

REFERENCES

ASTM International. Standard Test Method for Unconfined Compressive Strength Index of Chemical- Grouted Soil, Designation: D 4219–93a.

DeJong, J.T.; M.B. Fritzges; and K. Nusslein (2006). Microbially induced cementation to control sand response to undrained shear, ASCE, J. Geotech. Enviro. Engrg.,132, (11).

Mortensen, B.M.; M.J. Haber, J.T. DeJong; L.F. Caslake; and D.C. Nelson (2011). Effects of environmental factors on microbial induced calcium carbonate precipitation*, J. Applied Microbiology*, Manuscript No. 5065.

Terzaghi, K.; R.B. Peck, and G. Mesri (1996). *Soil Mechanics in Engineering Practice.* John Wiley and Sons, Inc., Chichester, U.K.

7 The Effect of Microbially Induced Calcite Precipitation on the Liquefaction Resistance of Sand

DOUGLAS SPITZER

ABSTRACT

The California Delta levee system is vulnerable during a seismic event. One issue that may lead failure of the levee system during an earthquake is the potentially liquefiable loose sands found underlying many of the levees within the Delta region. Ground improvement techniques can be used to prevent the soils from liquefying during an earthquake. A novel ground improvement method, Microbial Induced Calcite Precipitation (MICP) may have the potential to increase the liquefaction resistance of loose sands. The improvement in the sand's properties from MICP was investigated using cyclic and monotonic one dimensional direct simple shear tests. Specimens of loose Ottawa 50-70 sand were treated with MICP and compared to untreated specimens. CSR vs. N curves were constructed comparing the MICP treated and untreated sand. Results demonstrate that MICP treatment significantly increases the strength and liquefaction resistance of the sand. MICP treatment also prevents the development of shear induced pore water pressure.

7.1 INTRODUCTION

7.1.1 Motivation

East of Suisun Bay in Northern California at the confluence of the San Joaquin and Sacramento Rivers is a delta sometimes referred to as the California Delta. This massive hydrologic system is vital to the entire state. More than twenty-five million peoples' drinking water comes from the delta; water that also sustains agriculture and other industries in the state. Farmers, manufacturers and the public rely on more than 1100 miles of levees in and around the delta. A 2007 report found that there was a two in three probability of a catastrophic levee failure in the next fifty years if new programs to improve the levees were not implemented [BDPAC 2007]. One source for such a failure might be a large earthquake. A large earthquake might trigger liquefaction of sands underlying the levees.

One effective way to prevent liquefaction is to improve sands using artificial cement or grout [Clough et al. 1989]. Unfortunately grouting is expensive and may involve toxic and hazardous chemicals [Karol 2003]. Bio-cementation might prove to be an economical, safe way to increase the resiliency of the levees by making underlying sands stronger and more resistant to liquefaction.

7.1.2 Objectives

The increase in strength and liquefaction resistance of MICP treated sands needs to be evaluated to demonstrate its potential use as a ground improvement or liquefaction mitigation method. To do this treated and untreated soils are tested in monotonic and cyclic direct simple shear. This data will demonstrate that MICP bio-cements, like artificial cements, can be effective at preventing liquefaction. The testing will also investigate how bio-cemented sands behave in shear so that future tests can be better designed. Finally, the testing should complement triaxial [Mortensen and DeJong 2011] and geotechnical centrifuge [Mortensen 2011] results from previous studies.

7.1.3 Background

7.1.3.1 Shear Behavior of Sands

Sands behave one of two ways in shear. Dense sands typically dilate, while loose sands contract. This behavior is controlled by the structure of the sand. In loose sands there are larger volumes of open pore space between the grains. When the loose sand is sheared the individual sand grains will move into these open spaces and the soil mass contracts. Dense sand grains are initially packed tightly with relatively little open space. When the dense sand is sheared the grains will roll over one another and the soil mass dilates.

7.1.3.2 Pore Water Pressure and Liquefaction

Unlike air, water is relatively incompressible so saturated sands behave differently in shear. During shear, instead of contracting, the saturated loose sand transfers the stress from the grains to the water filling the pore spaces; the water develops a stress that pushes back against the grains [Idriss and Boulanger 2008]. The shear induced pressure applied by the fluid is called to as excess pore water pressure, Δu. Typically this stress dissipates quickly in sands as the water drains from the pores and the sand contracts. If the stress is applied rapidly across a large area, such as during an earthquake, the pore water will be unable to drain quickly and a large excess pore water pressure can develop. If the excess pore water pressure is large enough it will push the grains of sand apart. When the grains lose contact with one another the soil mass rapidly loses strength and behaves like a liquid. This phenomenon is called liquefaction. Cementation mitigates the development of shear induced pore water pressures. In cemented sands, the cement between the grains holds the grains in place. During shear in order to develop excess pore water pressure the sand must begin to contract, in order to for the sand to contract the cement must be degraded or broken. Because the excess pore water pressure does not develop in the cemented sand, the risk of liquefaction is mitigated.

7.1.3.3 Microbially Induced Calcite Precipitation

Microbially induced calcite precipitation or MICP is the process by which biologic activity from bacteria changes the chemistry of pore water which causes the precipitation of calcium carbonate at the grain-grain contacts. In this research, ureolytic bacteria, *Sporosarcina pastuerii,* hydrolyze urea to produce ammonia and bicarbonate ions which increase the pH of the pore fluid [Mortensen et al. 2011]. In the more alkaline pore fluid, calcium carbonate rapidly precipitates cementing the grains of sand together.

7.1.3.4 Direct Simple Shear Apparatus and Test

The Direct Simple Shear test is used to test a thin section of soil in shear. Specimens are tested in load cells consisting of cylinders of soil held by stacks of polished rings between two end caps. The rings can move only in the horizontal plane during shear; the specimen's volume is held constant by fixing the height of the rings. The load cell is fixed at the base to a base plate and at its top to a crosshead. The crosshead is laterally confined; the base plate is vertically constrained.

The test has two phases. In the first phase the sample is consolidated. The crosshead lowers, loading the specimen to the prescribed consolidation stress, $\sigma_{cv}^{'}$. In the second stage of the test the specimen is sheared. During shear one or more actuators move the base plate. In the monotonic shear test the base plate moves at a constant rate in the positive direction, shearing the specimen, until a prescribed strain is reached. In the cyclic shear test the specimen is sheared at a constant rate in the positive direction until the resistance to shearing reaches a prescribed cyclic shear stress, τ_{cyc}. At this time the test reverses displacing the base of the sample at a constant rate in the negative direction. Once the prescribed stress limit is reached in the negative direction the direction of displacement the direction of shear reverses again, and a new cycle begins. The ratio of the prescribed stress in the cyclic test to the consolidation stress applied in the first phase of the DSS test is called the cyclic stress ratio or *CSR*; Equation 9.1.

$$CSR = \frac{\tau_{cyc}}{\sigma_{vc}^{'}} \tag{7.1}$$

The earthquake induced *CSR* can also be derived from the seismic shear stress applied to the ground during an earthquake [Idriss and Boulanger 2008]. The test can also be used to measure the excess pore water pressure developed during shear. The excess pore water pressure is equal to the decrease in the vertical stress required to hold the specimen at a constant volume during shear [Terzaghi et al. 1996]. A cyclic DSS testing program is used to investigate the liquefaction of loose sands through the construction of a *CSR* versus N curves, where in N is the number of cycles required to reach a given shear stress using a prescribed *CSR* value.

7.2 METHODS

7.2.1 Specimen

Specimens were prepared using Ottawa 50-70 sand, see Table 7.1. Ottawa 50-70 sand is a clean, uniform, well rounded, quartz sand mined in LaSalle County, Illinois. The specimens were pluviated through air. Specimens had a diameter of 2.3 in. and a target pre-consolidation height of approximately .72 in. Specimens were saturated during treatment or proceeding consolidation. The target relative density of the specimens was 40%. Specimens were to be grounded during or immediately preceding pluviation. Prior to consolidation untreated specimens were saturated by flushing at least 3 pore volumes of deionized water through the specimen; treated specimens were dry during consolidation. Treatment took place at the end of consolidation.

Table 7.1 Properties of Ottawa 50-70 sand [DeJong et al. 2006].

Mineralogy	D_{50}	C_U	C_C	G_S	e_{min}	e_{max}	Shape	Hardness (Mohs Hardness Scale)
Quartz	0.12mm	1.6	0.8	2.65	0.55	0.87	Well Rounded	7

7.2.2 Treatment

Specimens were treated under a 100 kPa normal stress. Treatment consisted of flushing 150 mL of solution through the specimen via both the top and bottom treatment ports in the load cell's end caps. The treatment was monitored using shear wave velocity measurements and effluent pH measurement. When treatment appeared to be stagnating the effluent solution would be flushed through the system or a new solution would be flushed through the system. The target shear wave velocity for the treated specimens was 650 m/sec; see Figure 7.1. Once this velocity was reached, the specimen would be flushed with at least 3 pore volumes of 5mM NaCl to completely saturate the specimen. Deionized water was not used as it is slightly acidic and would react with the precipitated calcite.

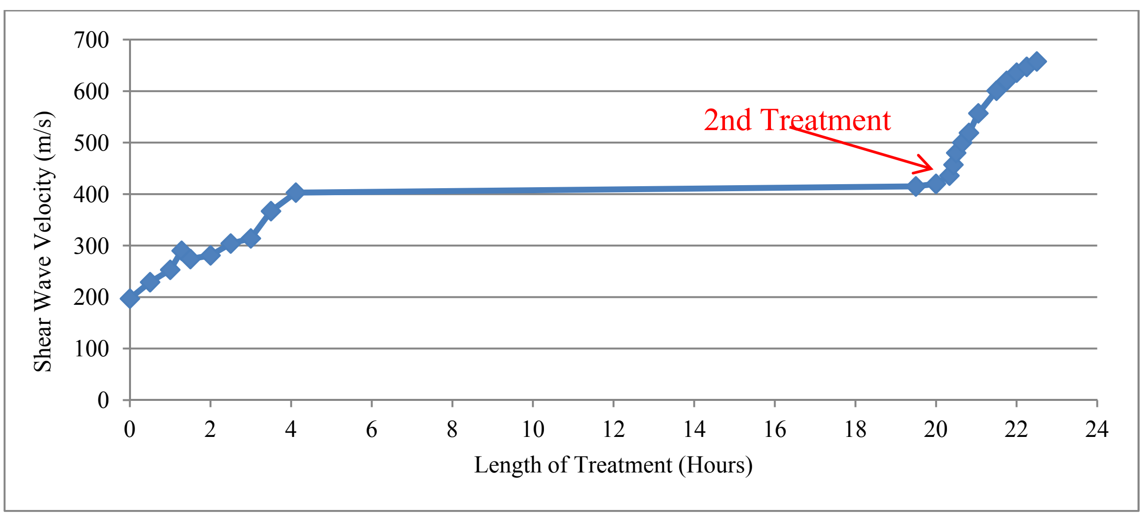

Figure 7.1 The shear wave velocity is increased by the MICP treatment; this plot is from the data collected during treatment in test 11072901-DSSc.

7.2.2.1 Treatment Solution

150	mL	Deionized Water
11 or 8.32	Grams	Dihydrate or Anhydrous Calcium Chloride respectively
9.0	Grams	Urea
0.5	Grams	Difco Nutrient Broth
10^7	mL^{-1}solution	Bacteria cells

7.2.3 Direct Simple Shear Test

In the first phase of the test specimens were consolidated under 100kPa (2088psf) using incremental loads of 100psf, 200psf, 400psf, 800psf, 1600psf for 5 to 6 minutes each and 2088psf for at least 15 minutes. In the second phase of the Direct Simple Shear (DSS) test specimens were either sheared monotonically (tests are referred to as DSS tests) or cyclically (tests are referred to as DSSc tests); see Figure 7.2. Monotonic shear was applied at a displacement rate of 5% shear strain per hour of shear. Cyclic tests were conducted at a displacement rate of 50% shear strain per hour of shear. If after a significant number of cycles shear wave velocities and test data indicated the specimen had neither yielded nor changed structurally, the load limits were increased to accelerate the test. The results in such a case are conservative. The number of cycles needed to strain the sample at the initial and later *CSR*s is lower than the number of cycles that would be needed had the *CSR* not been increased.

Figure 7.2 **The Direct Simple Shear Apparatus; the test is being set up, the top sensor has yet to be placed.**

7.2.4 Shear Wave Velocity and Calcium Carbonate Content Measurement

The effect of the treatment and shearing on the structure of the treated and untreated specimens was observed by measuring the velocity of shear waves traveling through the specimens. Bender elements embedded in the top and bottom end cap of the load cell were used to send and receive shear waves across the specimen. Shear wave velocity is a function of the medium through which the wave travels. As the stiffness of the medium increases shear wave velocity increases [DeJong et al. 2010]. As treatment progresses shear wave velocity increases; Figure 7.1. During shear the shear wave velocity falls as the cementation breaks down and particles contacts are pushed apart by excess pore water pressure.

Upon the completion of testing the level of cementation was measured using a using a gravimetric acid washing technique. The mass of calcium carbonate was measured as the difference between the dry mass of the treated specimen and the dry mass of the specimen after acid washing. The specimen is rinsed several times with 5 molar hydrochloric acid (HCl); after each rinsing the acid and dissolved solids are drained through a number 200 sieve. The carbonate cement reacts with the acid and dissolves passing through the sieve. The quartz sand is unaffected and too large to pass through the sieve.

7.2.5 Software and Equipment

Equipment and software used belongs to the University of California Davis's Soil Interactions Laboratory. Direct simple shear tests were performed using a Digishear Automated Direct Simple Shear System. Shear wave measurements were made using a National Instruments data acquisition system and bender elements fabricated in the laboratory. Microsoft Excel was used to analyze the data.

7.3 RESULTS AND ANALYSIS

7.3.1 Monotonic Tests

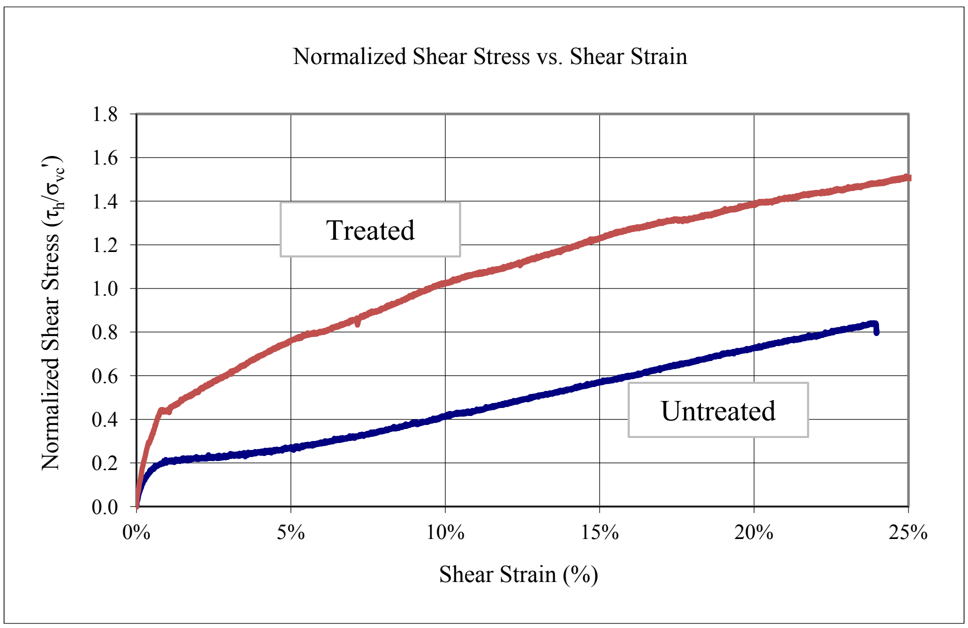

Figure 7.3 Monotonic Direct Simple shear test results show the treated specimen (top curve) is stiffer and has a higher strength than the untreated specimen (bottom curve).

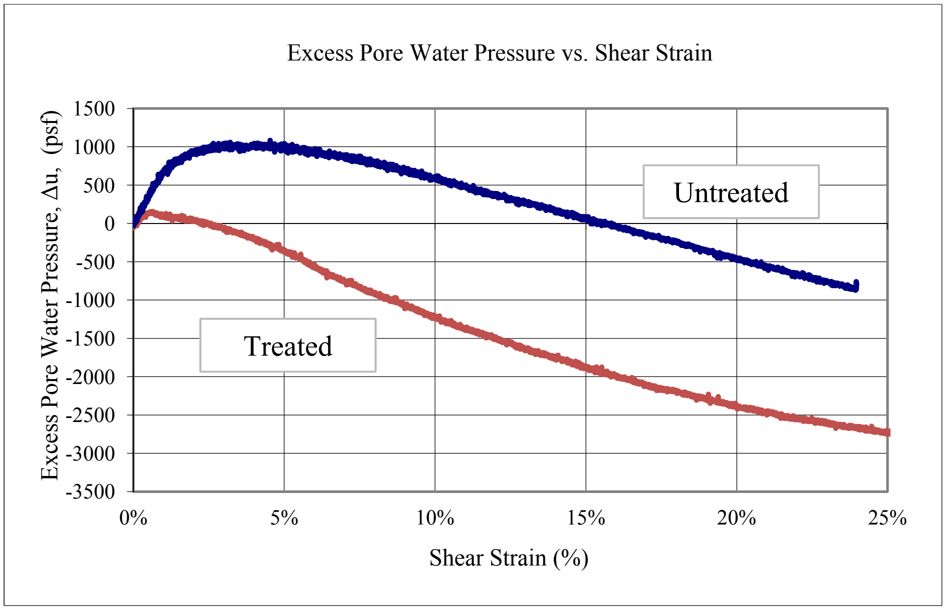

Figure 7.4 **Monotonic direct simple shear tests results show that the MICP treated specimen (bottom curve) developed smaller excess pore water pressures than the untreated specimen (top curve).**

7.3.2 *CSR* versus N Curve

The *CSR* versus Curve, Figure 7.5 demonstrates that the MICP cemented sand would be less susceptible to liquefaction as it requires more cycles at higher stresses to strain 3%. Not only did the treated sand take more cycles and stress to deform; the monotonic tests indicated the cemented sand developed smaller pore water pressures, and was stronger; Figures 7.3 and 7.4.

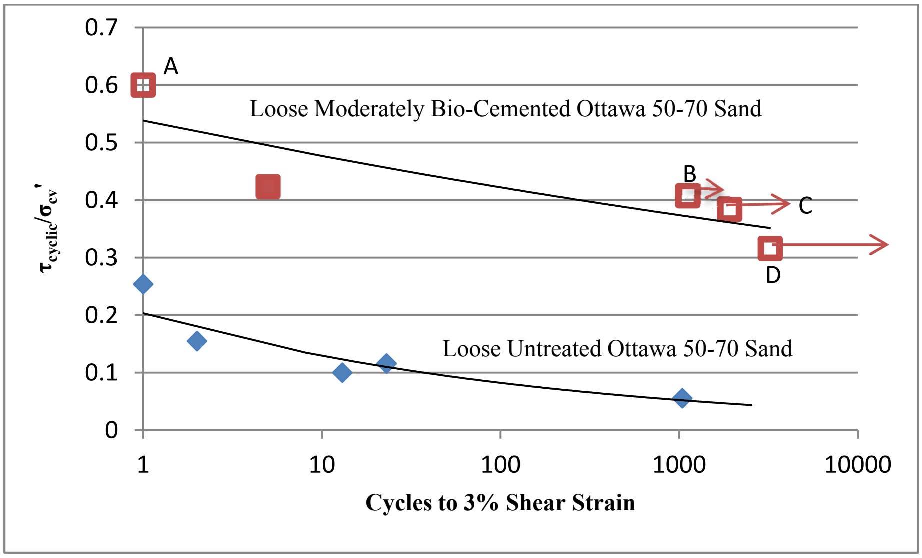

Figure 7.5 **The MICP cemented sand (squares) must be cycled more times at higher stresses to shear as much as the untreated sand (diamonds).**

Due to time constraints only 4 MICP treated specimens were tested, one of which was unsuccessful. The data point labeled A in Figure 7.5 is an estimate made from the stress at which the treated specimen tested in monotonic direct simple shear had strained approximately 3%. This *CSR* of 0.6 is an upper bound, it is the lowest stress ratio at which the specimen would strain 3% in the first half of the first cycle. Specimens sheared at a lower *CSR* might strain 3% in the second half of the first cycle. Data points B, C, and D, also in Figure 10.5, likewise have some additional uncertainty. The specimen plotted at point D cycled 1300 times without significant changes in shear wave velocity or shear strain. Taking time constraints into consideration the decision was made to increase the *CSR* of the specimen from the target 0.30 to 0.37. The data point referring to this higher *CSR* test is labeled C. After 814 cycles at a *CSR* of approximately 0.37 the specimen had not shown a significant increase in strain from one cycle to the next nor did the shear wave velocity or normal stress change significantly. The *CSR* was increased again to a target stress ration of 0.40. At this stress the specimen strained 3% after 1115 cycles. All of these results are conservative but there uncertainty supports the conclusion that the MICP treated sand is more resistant to liquefaction than the untreated sand. Data point B would have a greater number of cycles had the specimen not been subjected to an unmeasured disturbance during the previous 2114 cycles. Results C and D come from specimens which surely would have required significantly more cycles had the *CSR* not been increased mid test.

7.3.3 Reliability of Data

Direct simple shear tests can often be unreliable especially compared to other geotechnical tests. These tests though are reliable. In all the tests the vertical displacement was monitored to ensure the volume was kept constant. The specimens were all initially in a similar condition because they had comparable shear wave velocities and relative densities. This may hold less true for a few specimens where grounding was likely ineffective; these specimens had the lowest relative density and didn't consolidate as much during the first phase of testing compared to the other specimens. Figure 7.6 demonstrates the reliability of these tests. The plot shows the beginning of each cyclic test and the beginning of each monotonic test for the untreated specimens. The similarity between the curves indicates that the samples are comparable at the beginning of shearing and have a similar initial stress-strain behavior.

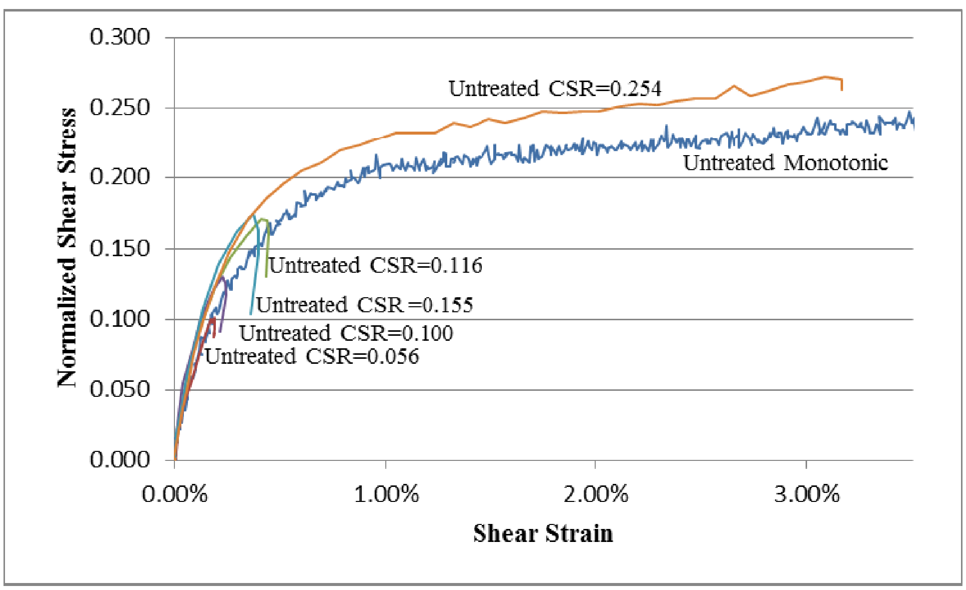

Figure 7.6 The initial stress-strain behavior is similar in all of the untreated tests so comparisons between the tests are valid.

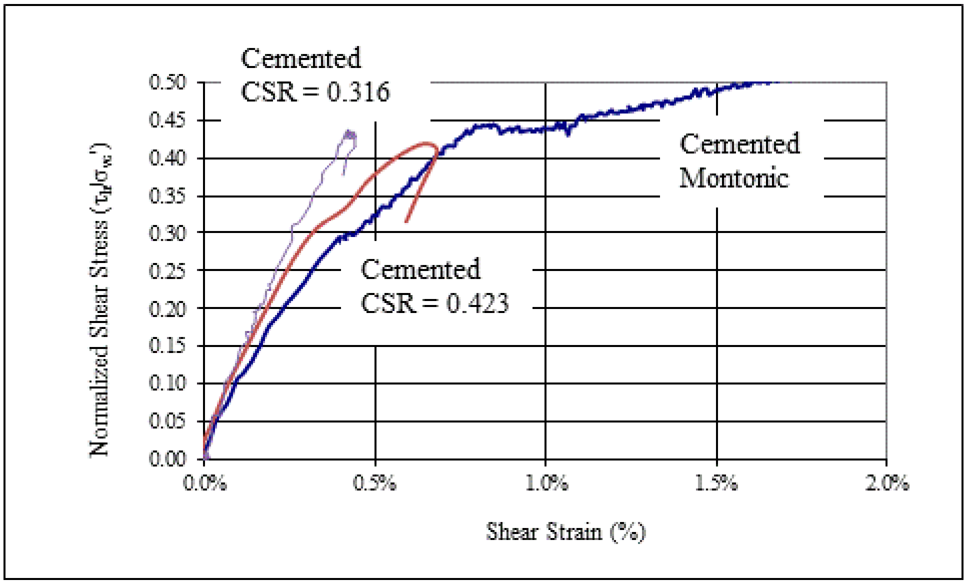

Figure 7.7 The initial stress-strain behavior of the cemented tests.

The reliability of the data from the treated specimens is harder to demonstrate. This was the first time DSS specimens were being treated with MICP so the effectiveness and rate of treatment was variable. Because of time constraints not all of the specimens obtained a level of treatment such that their shear wave velocities were 650m/sec. Additionally the specimen used in tests with the three lowest *CSR*s was significantly disturbed immediately preceding the beginning of the shearing phase of the DSSc test. After this disturbance the sample was re-treated but could not achieve a shear wave velocity as high as the one recorded prior to the disturbance, see Table 7.2. Despite having a lower measured shear wave velocity the specimen was stiffer than the previous treated tests, Figure 7.7, and calcite measurement after testing revealed it had a calcium carbonate content of 7.11% by weight. The previous treated specimens were 1.85% and 2.05% calcium carbonate for comparison, see Table 7.2. All of the tests on the cemented sands indicated increased strength and stiffness compared to untreated specimens.

7.4 CONCLUSIONS

7.4.1 Findings

1. MICP bio-cementation significantly increases the strength of clean, well rounded, uniform quartz sand.

2. MICP bio-cementation increases the resistance of clean, well rounded, uniform sand to liquefaction. The MICP bio-cementation decreases the magnitude of shear induced pore water pressures. The MICP treatment also increases the magnitude of cyclic shear and number of cycles required to deform specimens in simple shear.
3. Direct simple shear testing complements the findings of triaxial tests and geotechnical centrifuge tests on effects of MICP treatment on clean, well rounder, uniform, quartz sand.

7.4.2 Future Studies

1. Additional DSS and triaxial tests are needed to resolve uncertainty in the *CSR* versus N curve especially for treated specimens under relatively smaller *CSR*s.
2. Additional testing is needed to demonstrate whether or not the treatment will be effective on other types of sand. Comparisons should be made to other ground improvement methods such as compaction and chemical grouting.
3. The effectiveness and feasibility of MICP treatment in the field needs to be investigated. Costs, reliability, and environmental impact need to be assessed before MICP treatment can be used commercially.

ACKNOWLEDGMENTS

I would like to thank the Pacific Earthquake Engineering Research Centers, PEER, for providing me with this research opportunity and funding this research. This research would not have been possible without my graduate mentor Brina Mortensen whose experience and instruction guided me through my research and taught me more than I ever expected to learn in 10 short weeks; and whose vast knowledge and interest in MICP, biology, and soil mechanics gave me confidence and motivation to work through the countless challenges that arose during testing. I am also thankful for the guidance, time, and experience shared by Professor Jason DeJong. Additional thanks go to Daniel Bernardi and Dyana Picache who prepared the bacteria used in this research; and to Michael Alcantara who contributed to this research by acid washing the treated specimens. Finally, I am grateful to my fellow interns and researchers in the Soil Interactions Laboratory at UC Davis whose experience and guidance were invaluable.

REFERENCES

BD PAC (2007). Program Performance Assessment Executive Summary Final Draft as of August 20, 2007, State of California, Sacramento, CA.

Clough, R.G., J. Wayne, N. Iwabuchi, R, Shafii, and T. Kuppusamy (1989). Influence of cementation on liquefaction of sands, *J Geotech. Engrg*., 115(8):1102–1117.

DeJong, J.T., M. B. Fritzges, and K. Nüsslein (2006). Microbially induced cementation to control sand response to undrained shea, J. Geotech. Geoenviro. Engrg., 132(11):1381–1392.

DeJong, J.T., B.M. Mortensen, B.C. Martinez, and D.C. Nelson (2010). Bio-mediated soil improvement, Ecologogical Engrg., 36(2):197–210.

Idriss, I.M., and R.W. Boulanger (2008). *Soil Liquefaction During Earthquakes*, Earthquake Engineering Research Institute, Oakland, CA.

Karol, R.H. (2003). *Chemical Grouting and Soil Stabilization*, New York, New York: Marcel Dekker.

Mortensen, B.M., and J.T. DeJong (2011). Strength and stiffness of MICP treated sand subjected to various stress paths, *Proc*., ASCE, Geo-Frontiers 2011 Conference, Dallas, TX.

Mortensen, B.M., M.J. Haber, J.T. DeJong, L.F. Caslake, and D.C. Nelson (2011). Effects of environmental factors on microbial induced calcium carbonate precipitation, *J. Applied Microbiology*, 111(2): 338-349.

Mortensen, B.M. (2011). Bio-mediated soil improvement and the effect of cementation on the identification, behavior, improvement, and performance of sand, *Ph.D. dissertation*, Dept. of Civil and Enviro. Engrg., University of California, Davis, CA.

Terzaghi, K., R.B. Peck, and G. Mesri (1996). *Soil Mechanics in Engineering Practice*, 3rd ed., New York, New York: John Wiley & Sons.

APPENDIX

Table 7.2 Initial conditions and results.

<table>
<tr><th>Test</th><th>Test Number</th><th>Dry Relative Density</th><th>Shear Wave Velocity at the Start of Shear (m/sec)</th><th>Moisture Content By Mass</th><th>$CaCO_3$ Content By Mass</th><th>Mass of $CaCO_3$ (grams)</th><th>Cycles to γ = 3%</th><th>Figure Number</th></tr>
<tr><td>Untreated Monotonic</td><td>11070601-DSS</td><td>53.0%</td><td></td><td>25.0%</td><td>0.00%</td><td></td><td></td><td>10.13</td></tr>
<tr><td>Untreated CSR = 0.056</td><td>11072001-DSSc</td><td>56.0%</td><td>205</td><td>24.5%</td><td>0.00%</td><td></td><td>1036</td><td>10.8</td></tr>
<tr><td>Untreated CSR = 0.100</td><td>11072801-DSSc</td><td>53.4%</td><td></td><td>23.9%</td><td>0.00%</td><td></td><td>13</td><td>10.9</td></tr>
<tr><td>Untreated CSR = 0.116</td><td>11071401-DSSc</td><td>52.2%</td><td>186</td><td>25.4%</td><td>0.00</td><td></td><td>23</td><td>10.10</td></tr>
<tr><td>Untreated CSR = 0.155</td><td>11071301-DSSc</td><td>49.0%</td><td>222</td><td>23.8%</td><td>0.00%</td><td></td><td>2</td><td>10.11</td></tr>
<tr><td>Untreated CSR = 0.254</td><td>11071201-DSSc</td><td>66.4%</td><td>222</td><td>24.2%</td><td>0.00%</td><td></td><td>1</td><td>10.12</td></tr>
<tr><td>Treated Monotonic</td><td>11072901-DSS</td><td>43.8%</td><td>637</td><td>25.6%</td><td>1.85%</td><td>6.66</td><td></td><td>10.18</td></tr>
<tr><td>Treated CSR = 0.316</td><td>11080801-DSSc</td><td rowspan="3">41.8%</td><td>(609[4]) 440</td><td rowspan="3"></td><td rowspan="3">7.11%</td><td>6.66</td><td>3227</td><td>10.14, 10.19</td></tr>
<tr><td>Treated CSR = 0.384</td><td>11081501-DSSc</td><td>401</td><td>6.66</td><td>1915</td><td>10.15, 10.19</td></tr>
<tr><td>Treated CSR = 0.408</td><td>11081801-DSSc</td><td>380</td><td>1.74</td><td>1115</td><td>10.16, 10.19</td></tr>
<tr><td>Treated CSR = 0.423</td><td>11080101-DSSc</td><td>37.0%</td><td>550</td><td>22.4%</td><td>2.05%</td><td>1.57</td><td>5</td><td>10.17</td></tr>
</table>

[4] Test 11080801-DSSc was initially treated to a shear wave velocity of 609 m/s. During the transition from the first phase to the second phase of the DSSc test the apparatus malfunctioned and significantly disturbed the sample. The specimen was reconsolidated under 101.3kPa. The specimen was also flushed with a 1M Urea, .5M CaCl solution. This solution reached a maximum shear wave velocity after re-treating of about 440m/s. This additional treatment is likely the reason for the significantly higher calcium carbonate content measured after the test.

Test 11072001-DSSc Untreated CSR = 0.056

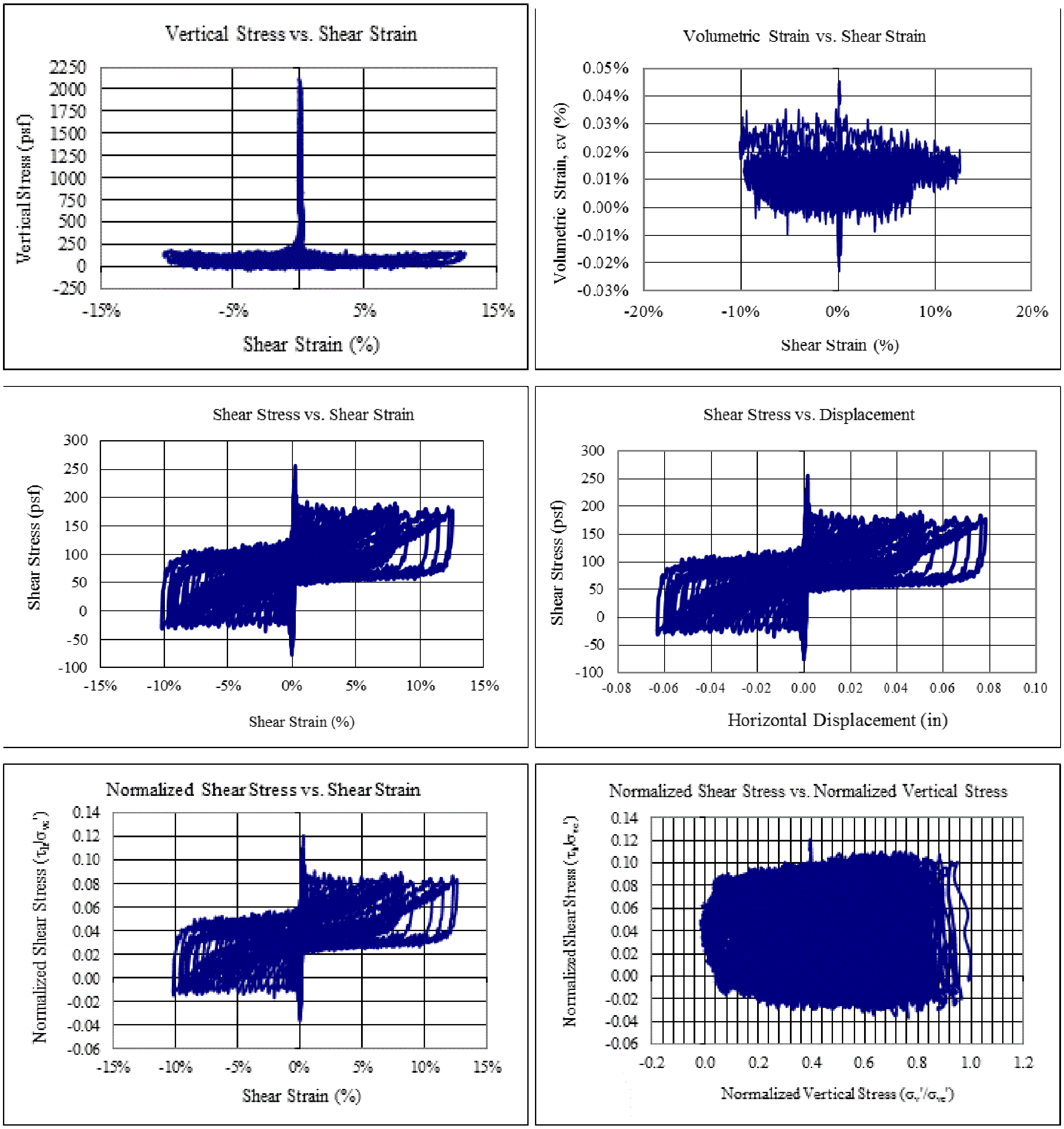

Figure 7.8 Data plots from loose untreated cyclic DSS test.

Test 11072801-DSSc Untreated CSR = 0.100

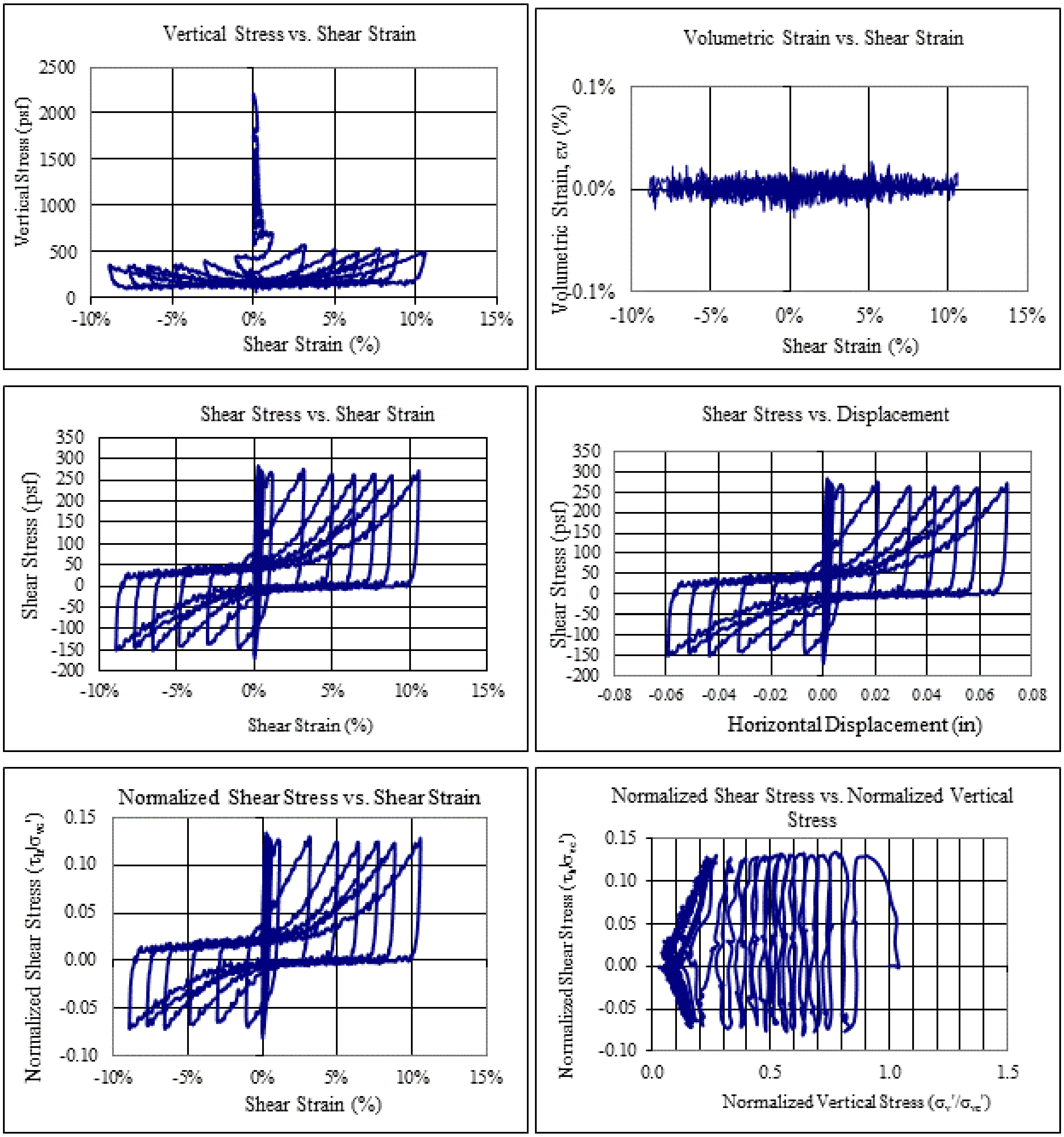

Figure 7.9 Data plots from loose untreated cyclic DSS test.

Test 11071401-DSSc Untreated CSR = 0.116

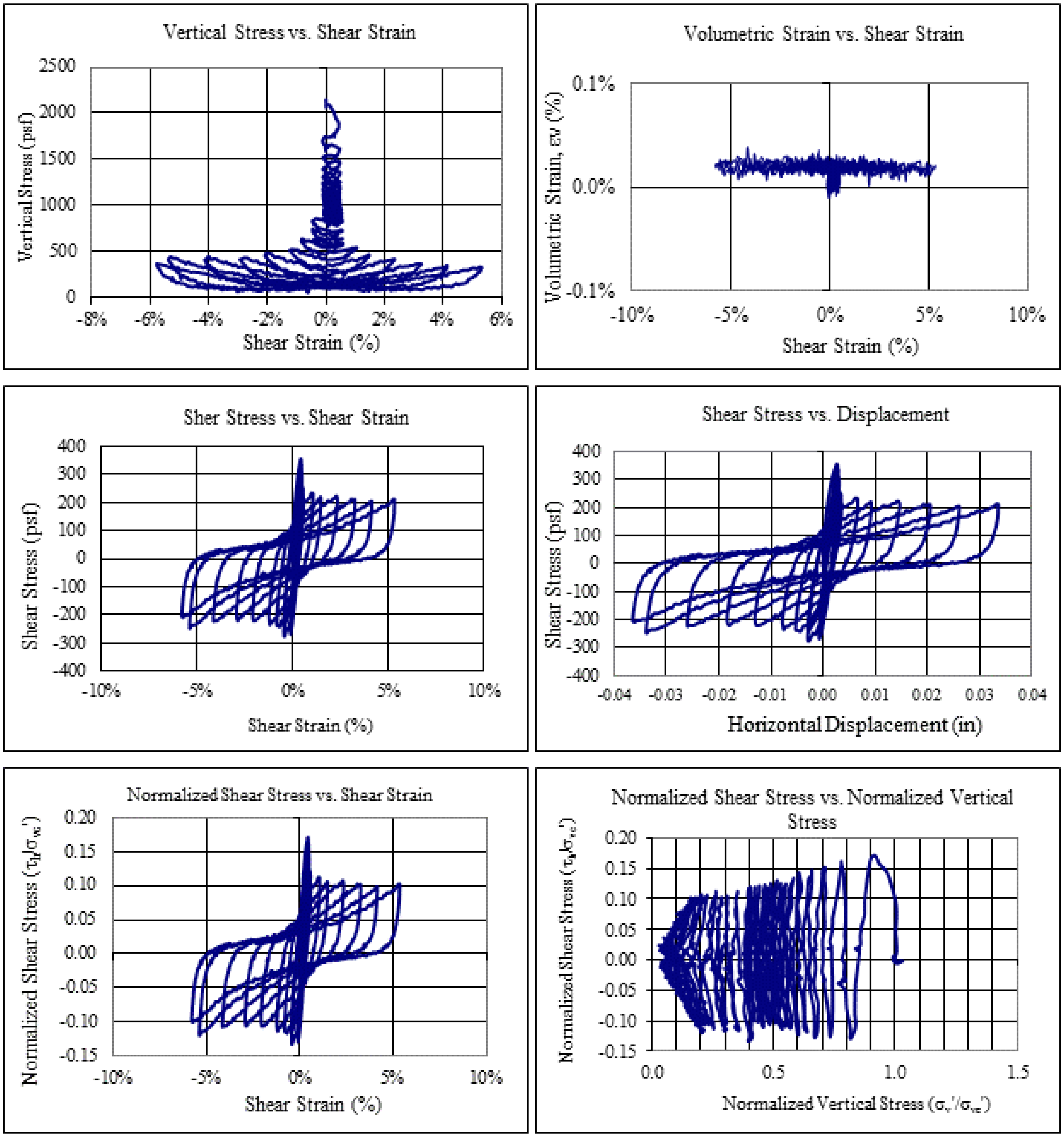

Figure 7.10 Data plots from loose untreated cyclic DSS test.

Test 11071301-DSSc Untreated CSR=0.155

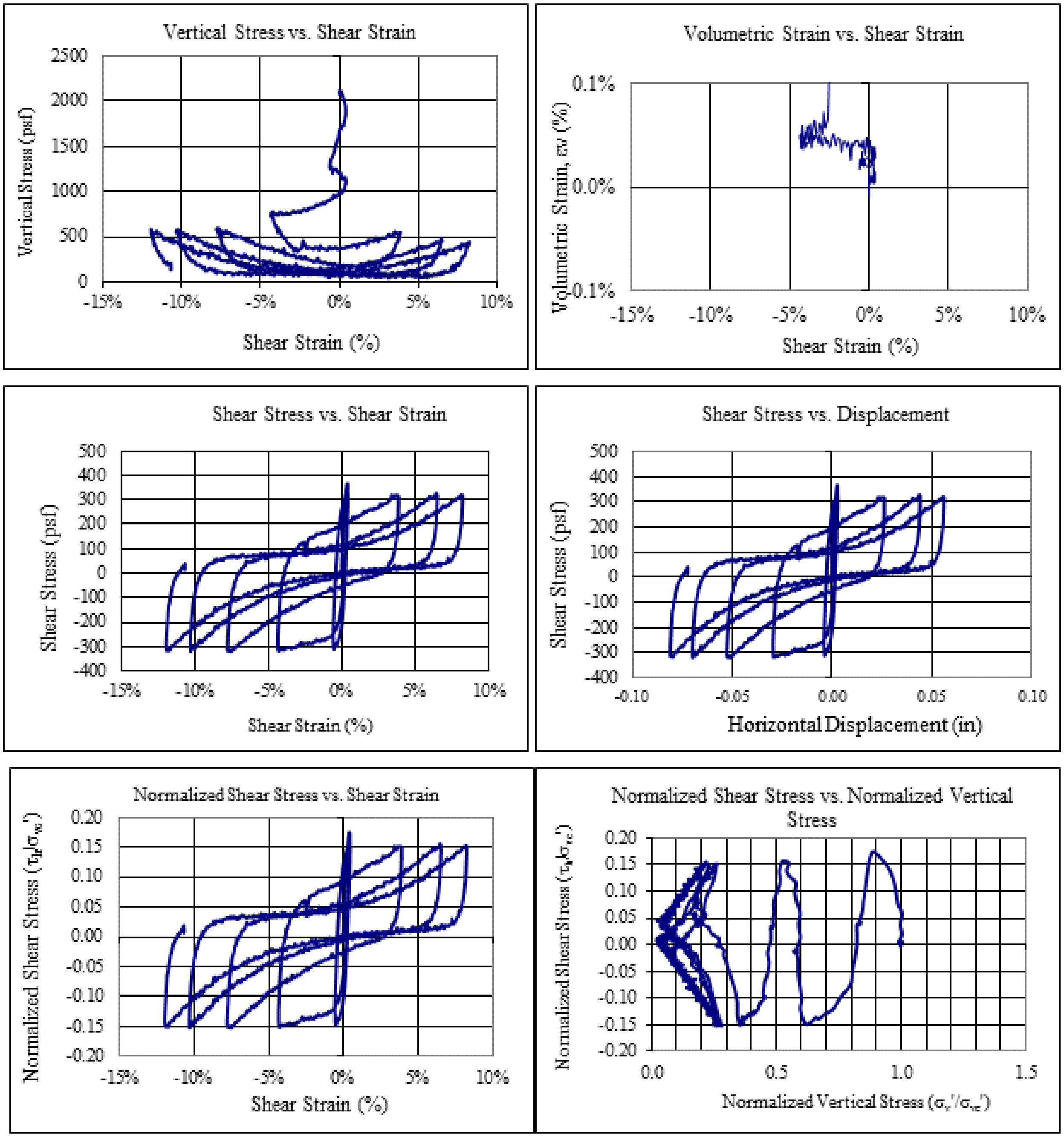

Figure 7.11 Data plots from loose untreated cyclic DSS test.

Test 11071201-DSSc Untreated CSR = 0.254

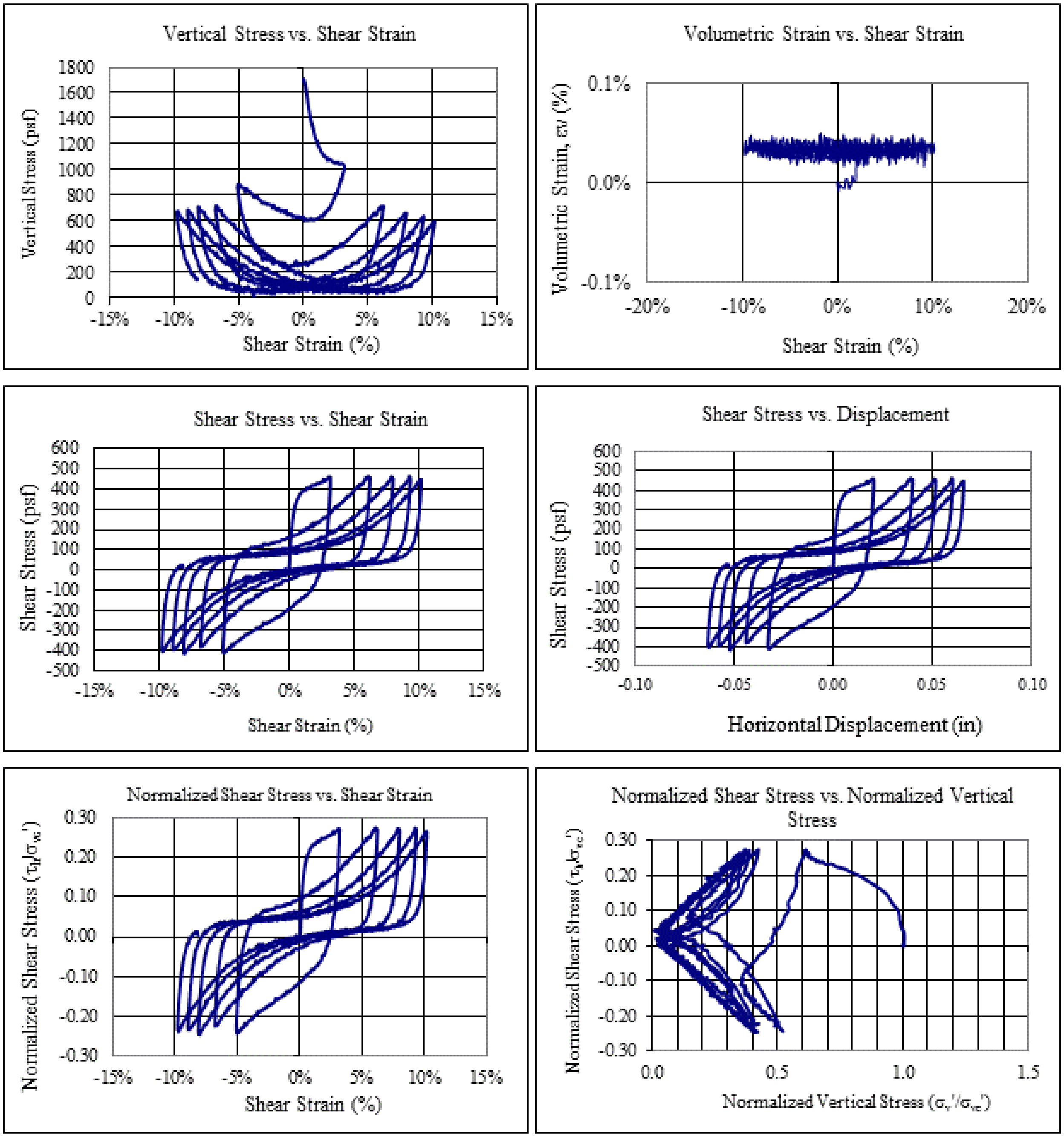

Figure 7.12 Data plots from loose untreated cyclic DSS test.

Test 11070601-DSS Untreated Monotonic Shear Test

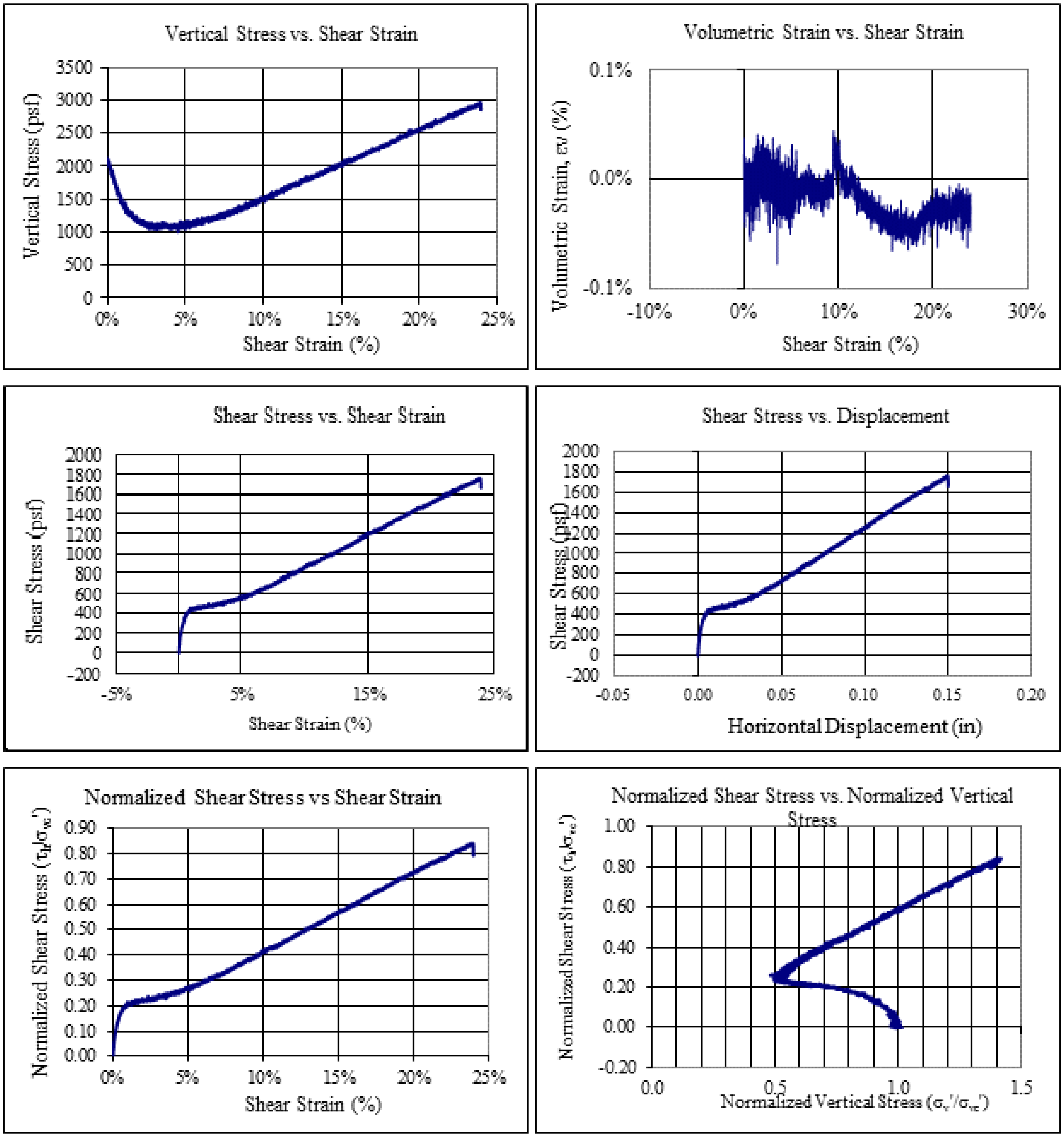

Figure 7.13 Data plots from loose untreated monotonic DSS test.

Test 11080801-DSSc Treated CSR = 0.316 (Partial Data; Cycles 1-558)

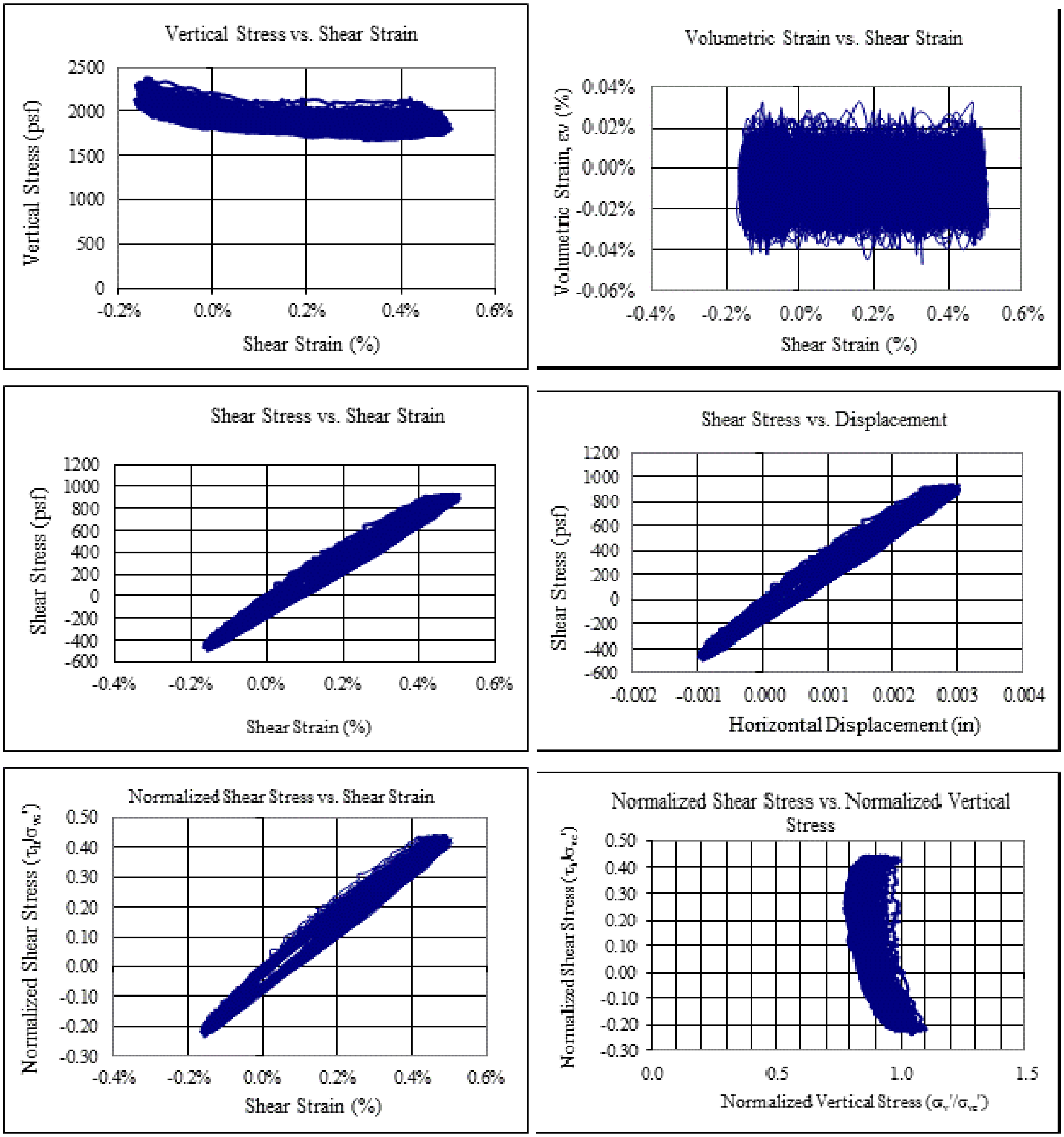

Figure 7.14 Data plots from loose moderately cemented cyclic DSS test. Partial data shown, after 1300 cycles at *CSR* = 0.316 the *CSR* was increased to 0.384, Shear strain versus cycle number shown in Figure 7.19.

TEST 11081501-DSSC TREATED CSR = 0.384 (PARTIAL DATA; CYCLES 1-814)

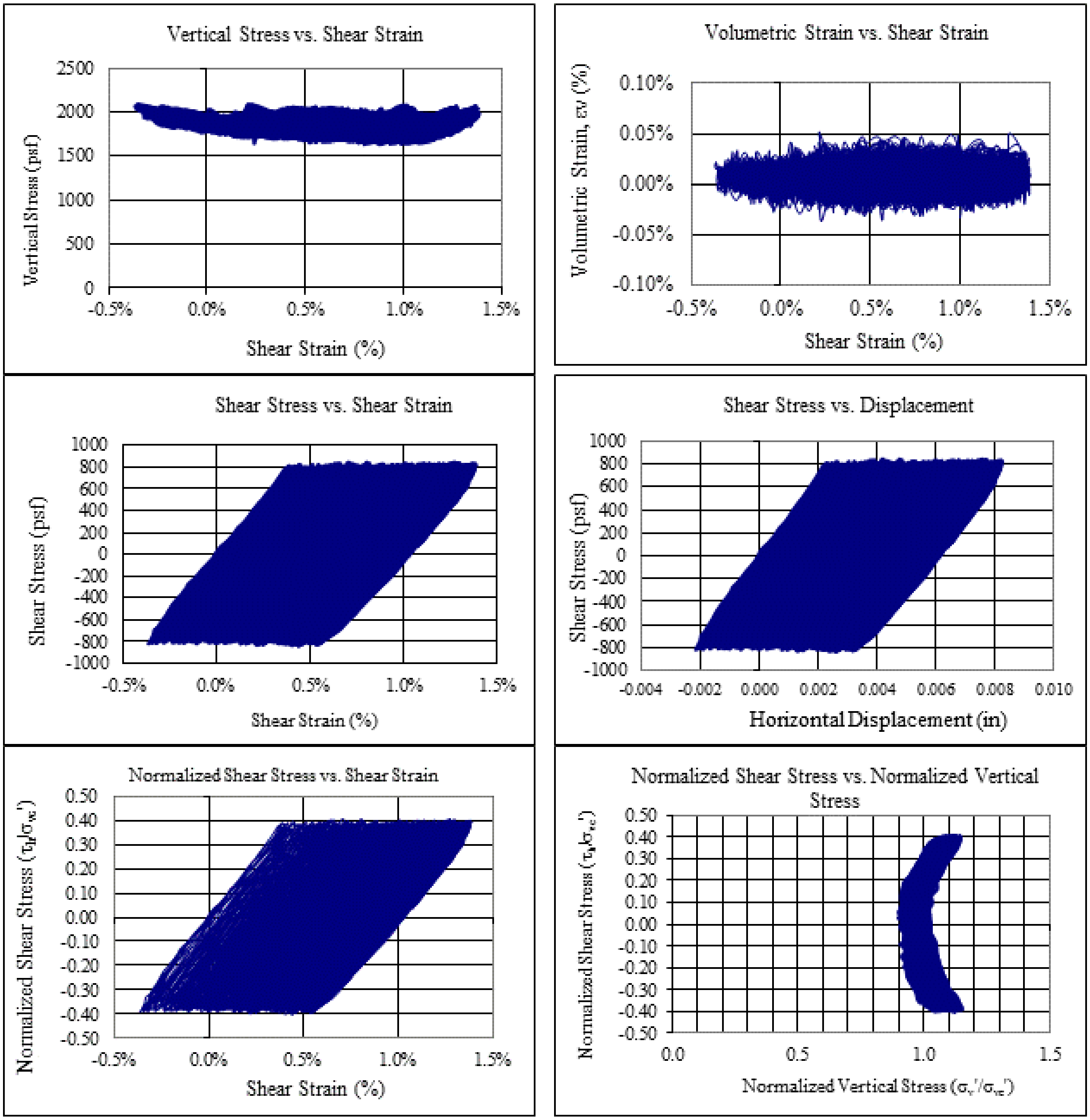

Figure 7.15 **Data plots from loose moderately cemented cyclic DSS test. Partial data shown, this test continues at a higher CSR. The mechanical behavior is identical cycle to cycle, there appears to be an increase in strain because the specimen drifted to the right.**

TEST 11081801-DSSC TREATED CSR = 0.408 (PARTIAL DATA; CYCLES 1-944)

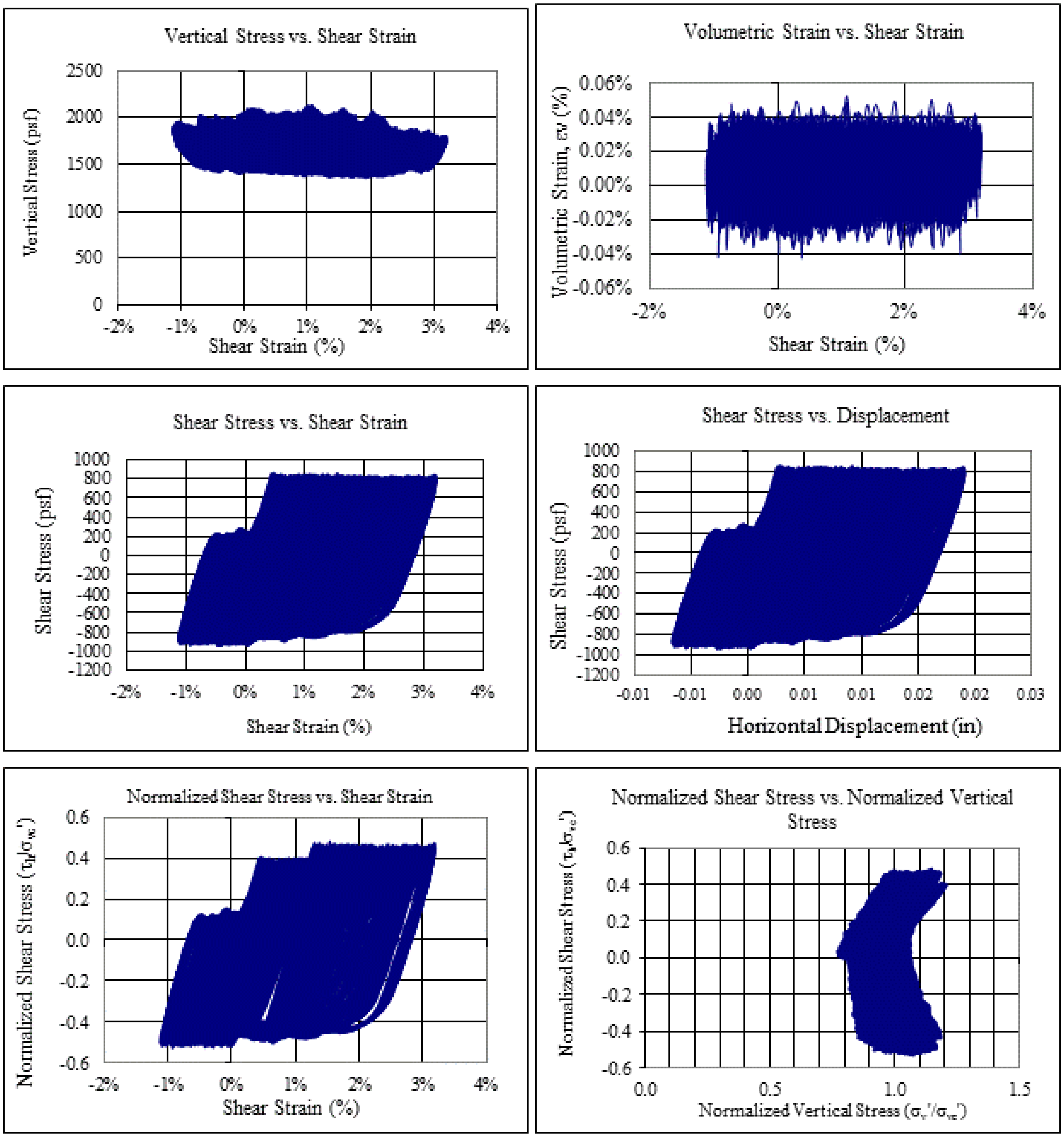

Figure 7.16 Data plots from loose moderately cemented cyclic DSS test. Data begins when the *CSR* was increased during test 11081501-DSSc and continues until the backup data stream finished collecting data. More limited data collection continued until the specimen reached a shear strain of 3% after 1115 cycles.

TEST 110801-DSSC TREATED CSR=0.423

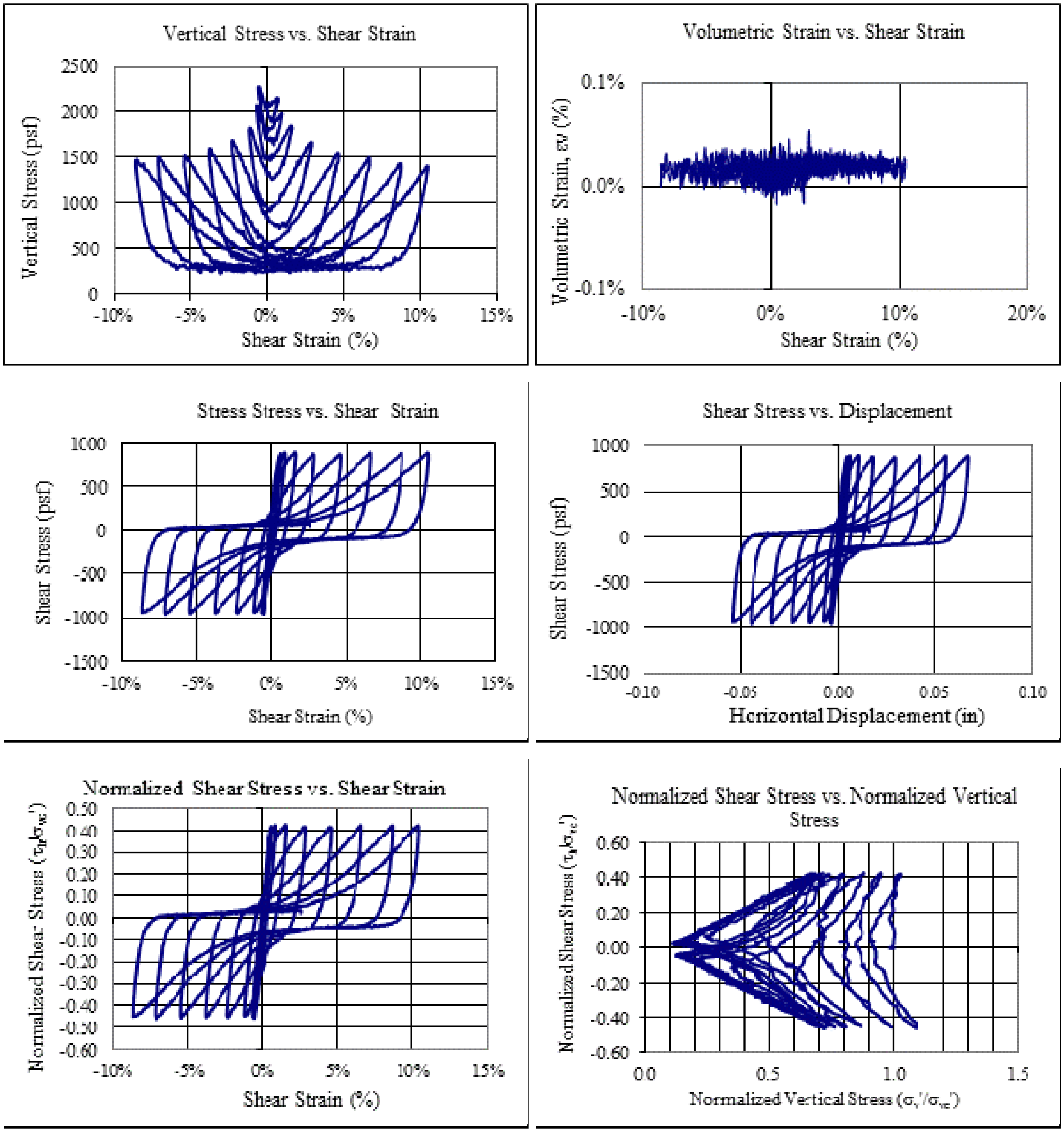

Figure 7.17 Data plots from loose moderately cemented cyclic DSS test.

TEST 11072901-DSS TREATED MONOTONIC SHEAR TEST

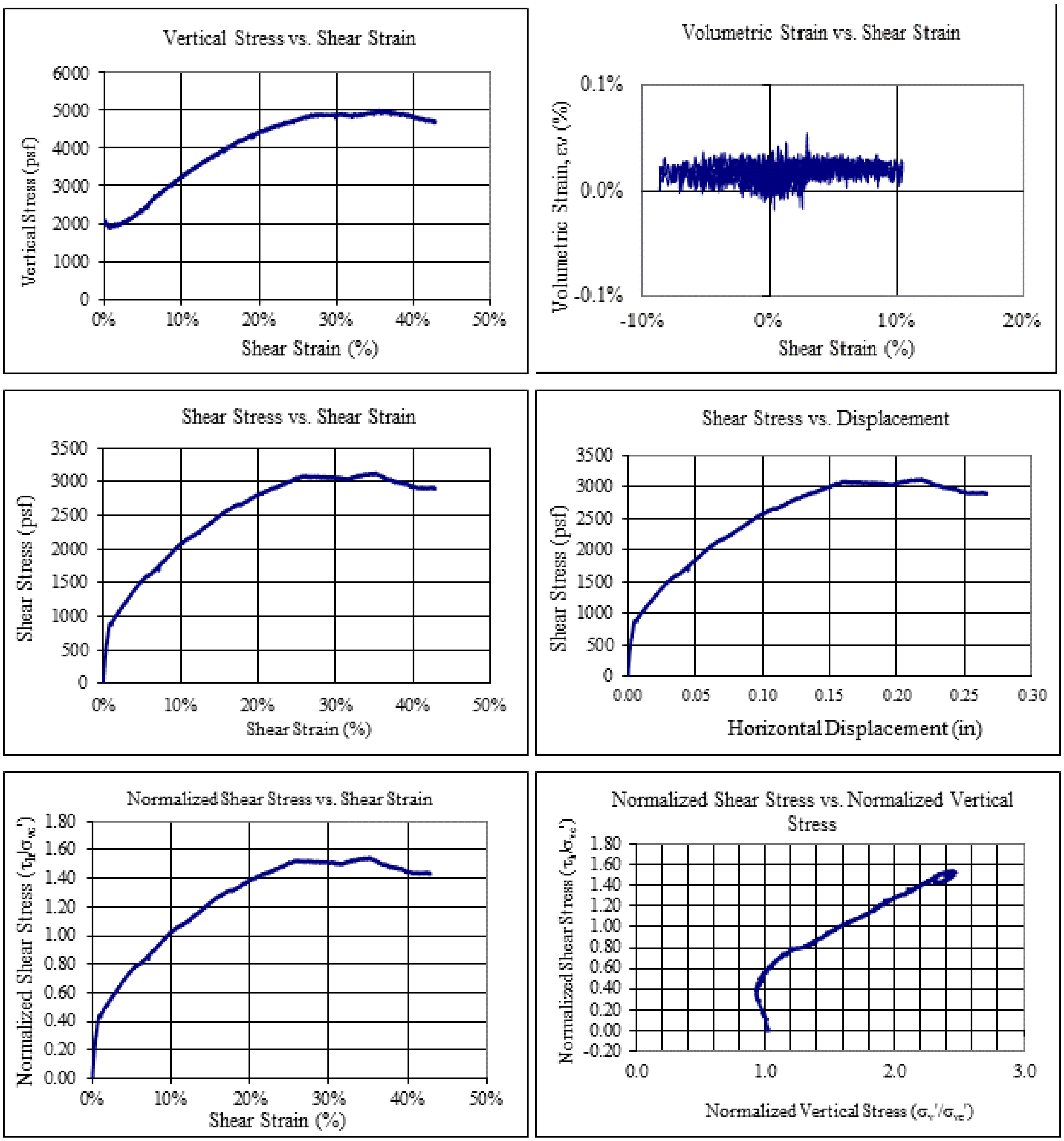

Figure 7.18 Data plots from loose moderately cemented monotonic DSS test.

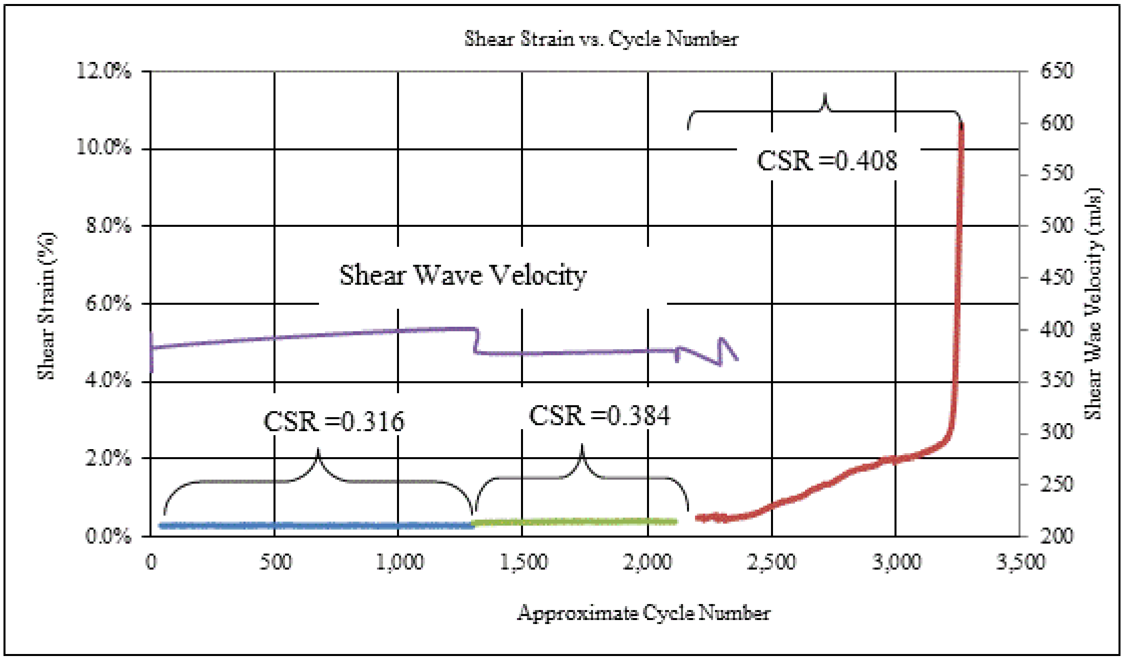

Figure 7.19 **Shear Strain VS Cycle Number; Tests 11080801-DSSc, 11081501-DSSc, 11081801-DSSc. Notice that the shear wave velocity doesn't decrease and the shear strain doesn't increase for the duration of testing at the lower *CSR*s; because these values did not change the decision was made twice to increase the *CSR*.**

8 High-Volume SCM Concrete in Composite Construction

GULZAT ATYMTAYEVA

ABSTRACT

Although Portland cement contributes to high strength concrete, it is important to acknowledge that cement production is a major source of CO_2 emissions worldwide. It is possible to develop more sustainable and durable structures by utilizing supplementary cementitious materials (SCMs) such as fly ash and slag in concrete. Concrete that contains a high volume of such materials has low early strength development; as a result, they are often avoided in the reinforced concrete construction. In contrast, concrete-filled steel tubes, used as composite columns in buildings, are suitable candidates for the use of cement replacement because the steel jacket takes on the initial loading, thus an early concrete strength is not required. This research is a follow-up study of the mechanical properties of the high-volume SCM concrete, conducted by G.M. Hannesson in 2010. The primary objective of this research is to investigate the time-dependent behavior of concrete with a high level of cement replacement in composite construction such as concrete-filled steel tubes. The project consisted of compressive strength, drying shrinkage, and creep tests. The compressive strength as well as the drying shrinkage tests were performed using small-scale cylinders; the long-term (5 months) creep tests were performed using both small-scale cylinders and full-scale concrete-filled steel tubes. Because of time constraints, this paper includes only the results for the first 36 days of the tests since the initial setup. The results revealed that the time-dependent deformation in the tubes tended to stabilize in 14 to 21 days. The concrete with a high volume of SCMs exhibited a high initial strain upon loading but less creep than the self-consolidating concrete made with mostly Portland cement. This suggests that SCMs may serve as suitable alternatives to Portland cement in

concrete-filled tubes. In addition, because the deformations are quite low in the tubes, neglecting the shrinkage in design may be appropriate.

8.1 INTRODUCTION

Concrete-filled tubes (CFTs) are widely used in high-rise buildings and bridges in Asia because of their high strength, high ductility, large energy absorption capacity, and construction efficiency [Wang et al. 2009]. Concrete-filled tubes are known to perform well under axial as well as lateral loading due to the composite action that takes place between the steel and concrete, thus delivering high earthquake-resistant structures. The concrete fill delays local buckling of the steel tube and increases its compressive strength [Roeder 2010].

Although Portland cement used in most of the CFTs contributes to high strength concrete, it is important to acknowledge that cement production is a major source of CO_2 emissions worldwide [Hannesson 2010]. There is extensive research on CFTs that are made with Portland cement based concrete, but very limited study of CFTs that have a high volume of supplementary cementitious materials (SCMs) such as fly ash and slag. The main advantages of using SCM concrete in structural applications include reduction in green house gases and air pollutants, reduction in waste (otherwise directed to landfills), and reduction in virgin material use. Therefore, utilizing SCMs in concrete should help develop more sustainable systems.

Since one of the challenges in utilizing CFTs in structural applications includes achieving a full shear force transfer between the steel and concrete via natural adhesion, it is crucial to know the mechanical properties of concrete such as compressive strength, creep, and drying shrinkage. In addition, the majority of creep tests performed on CFTs are relatively small scale, conducting a full-scale creep test should give better perspectives on the performance of these tubes.

This research is a follow-up study on the mechanical properties of high-volume SCM concrete, investigated by G.M. Hannesson in 2010. The aim of the research is to evaluate the time-dependent behavior of self-consolidating concrete (SCC), used primarily in CFTs, with a high volume of fly ash and slag under constant loading. Using SCC has advantages in reinforced concrete and composite construction by facilitating rapid construction [Hannesson 2010]. Concrete filled tubes are a composite structural component that can resist gravity and seismic loadings. Although concrete containing SCMs tends to have slower strength development, especially at high cement replacement rates, high early strength is not a requirement for the concrete-filled tubes, as the steel tube takes on the initial loading. Therefore, one of the objectives of this research is to examine the influence of high cement replacement level on long-term deformation response (creep) for concrete-filled tubes, whereas the research, completed by G.M. Hannesson, focused only on the mechanical properties of concrete at material levels.

The research consisted of two parts. In the first part, a small-scale creep test was conducted using 6×12 in. cylinders. This part of the test was mostly based on the test setup and procedures employed by Hannesson in his research. The second part of the test was unique to this research, as two full-scale CFTs were investigated for creep strain.

8.2 PREVIOUS RESEARCH

A considerable amount of research has been done on the time-dependent behavior of steel tubes filled with Portland cement based concrete, however there has been very limited study of CFTs that are made with high-volumes of supplementary cementitious materials such as fly ash and slag. Because the present research is a continuation of the study by G.M. Hannesson, developed to determine the mechanical properties of high-volume SCM concrete, it is important to review the results of past research.

G.M. Hannesson in 2010 investigated the time-dependent behavior of high-volume SCM concrete by developing several binary (cement and one SCM such as fly ash or slag) and ternary (cement and two SCMs, both fly ash and slag) concrete mixes with different cement replacement levels. The research consisted of two phases: in the first phase, twenty binary mixes made with 20%, 40%, 60%, and 100% cement replacement and one control mix (only Portland cement) were tested for the compressive strength and time of initial set. In the second phase, the compressive strength as well as elastic modulus test, shrinkage test, and creep tests were performed on both binary and ternary mixes. Later in the project, SCM' efficiency was evaluated using the modified Bolomey strength equation. A model of the creep behavior of concrete mixes was developed using the combined Maxwell and Bingham rheological model.

A concrete mix with 90% cement replacement with 50/50 fly ash-to-slag ratio with different curing levels was chosen for the creep and shrinkage tests. Both sealed and unsealed cylinders were used in this part of the research. Figures 8.1 and 8.2 show the elastic and creep strain of the sealed and unsealed cylinders, respectively, since the initial loading. Note from the graphs that the SCM concrete cured for 7 days exhibited the highest creep strain, and the SCM concrete cured for 28 days exhibited the lowest creep strain among the four mixes. Based on the results of Hanesson's research, the following was concluded:

- The creep strains of the sealed specimens were less than the unsealed specimens. This trend was expected because less water evaporation occurs in the sealed specimens.
- The same mix with higher stress/strength ratio showed higher creep strains, which was also expected.
- Shrinkage strains of the unsealed specimens were less than the sealed specimens.

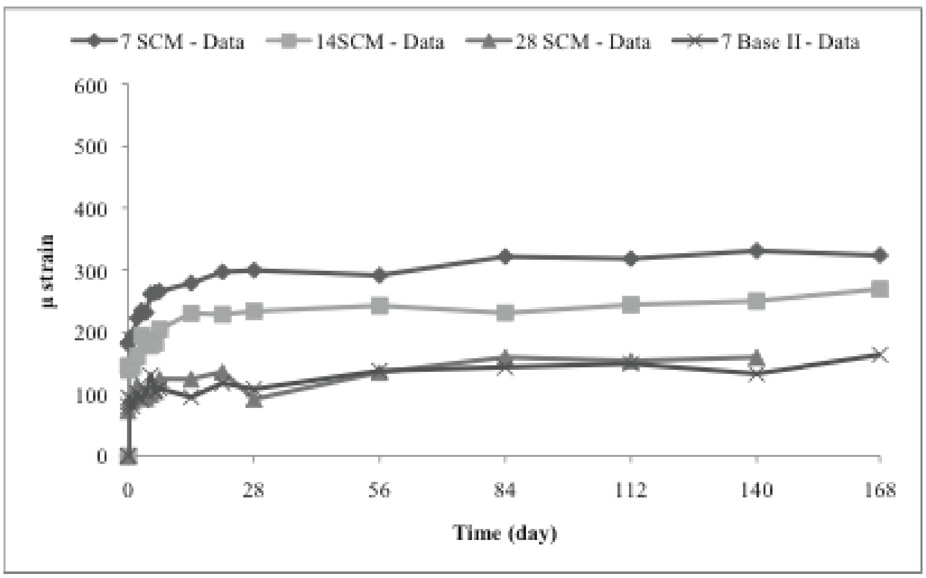

Figure 8.1 Elastic and creep strain of the sealed cylinders since initial loading [Hannesson 2010].

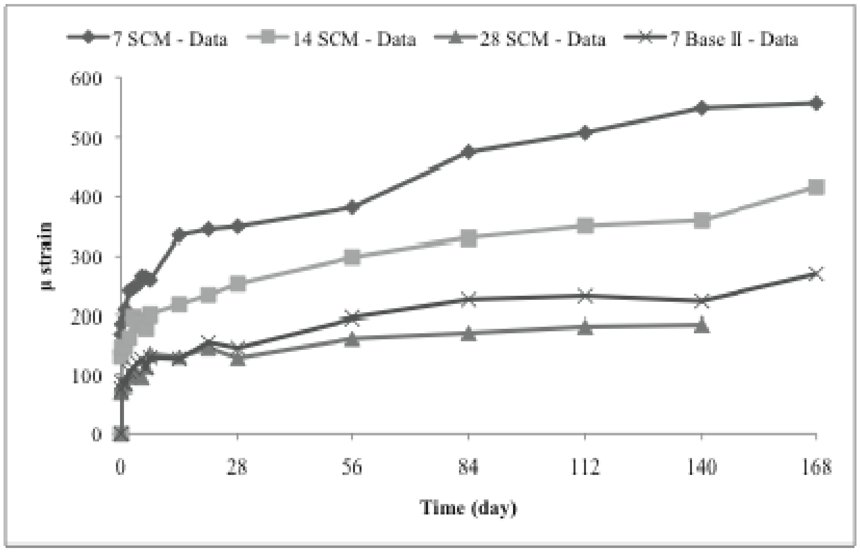

Figure 8.2 **Elastic and creep strain of the unsealed cylinders since loading [Hannesson 2010].**

In general, all the creep strains were low, which was probably due to a large portion of fly ash and slag remaining unreacted in the concrete and, therefore, acting as fine aggregates that provided higher resistance against creep.

8.3 TEST PREPARATION

Two concrete mixes, both containing self-consolidating low-shrinkage concrete, were prepared for test: one binary mix with 35% cement replacement using Portland cement and slag (denoted as SCC concrete), and one ternary mix with 80% cement replacement using fly ash and slag (SCM concrete). The water-to-binder ratio of the mixes was 0.327. The 50:50 fly ash to slag ratio was chosen for the cement replacement since it gave the most reliable strength development in previous research.

8.3.1 Materials

The Portland cement used for the concrete mixes was ASTM I-II Ash Grove Cement (ASTM C150). The two cementitious materials used for the cement replacement were Class F fly ash (ASTM C-618) from ENX. Alberta, Canada and Lafarge slag (Lafarge GGBFS). The concrete mixes were ordered through Stoneway Concrete, a supplier from Renton, Washington, by specifying the desired 28-day concrete compressive strength, f'_c, along with cement replacement levels (Appendix A). The target compressive strength for SCC concrete was 6000 psi, whereas for SCM concrete it was 8000 psi.

A spiral seam steel tube was used for the full-scale creep testing. Northwest Pipe delivered a 40-ft-long, 20-in.-diameter, 1/4-in.-thick steel tube, designated as AWWA C200 ASTM A1018-07 SS, to the University of Washington testing site. It was further cut into two 102-in. steel tubes for the full-scale creep test setup. The specified yield stress for the steel was 50 ksi.

8.3.2 Specimen Preparation and Curing

Both concrete mixes were mixed and delivered by Stoneway Concrete to the University of Washington structural engineering laboratory. The specimen preparation for the creep testing consisted of two parts. In the first part, samples were cast into 6×12 in. (152.4 × 304.8 mm) cylindrical molds for determination of compressive strength, creep, and shrinkage strains. Once the strength of the cylinders was sufficient enough, the specimens were demolded and stored at 100% relative humidity for 14 days. In order to ensure flat surfaces at both ends of the cylinders, sulfur capping was used; see Figure 8.3. Because a rough surface may result in stress concentration and uneven loading of the cylinders, the sulfur cap was a requirement. The second part of the specimen preparation consisted of two 20-in.-diameter concrete-filled tubes anchored into a concrete footing. Figure 8.4 shows the photograph of the full-scale specimens.

Figure 8.3 Photo of sulfur-capped concrete cylinders.

Once the steel tubes were anchored into the footing, one tube was filled with SCC concrete and the other tube with SCM concrete. To ensure moist curing of the concrete and prevent it from plastic shrinkage, the exposed ends of the tubes were covered with wet burlap sacks. This method of curing took place during a seven-day period to ensure 100% relative humidity.

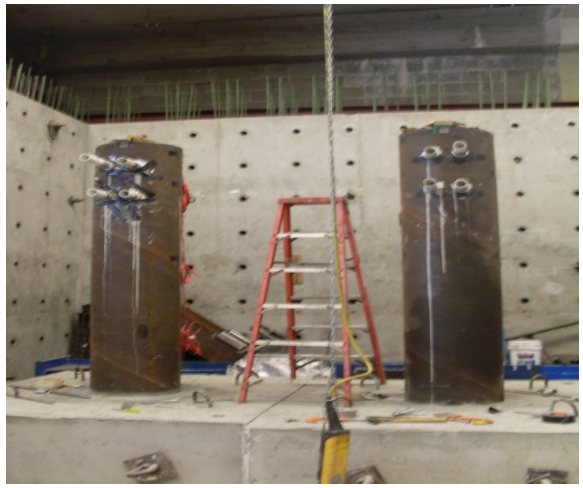

Figure 8.4 Specimen layout.

8.4 TEST PROCEDURES AND SETUP

8.4.1 Compressive Strength

Compressive strength is essentially the most important engineering property of concrete, as it performs best in a compressive mode rather than tensile. The other properties of concrete such as tensile strength and modulus of elasticity are based on the compressive strength because it is an easy test to perform. It is important to note that the compressive strength tests should be conducted at successive time intervals, as it is a time-dependent property. In this research, the compressive strength of the concrete mixes was measured by applying axial load, according to ASTM C 39 standard. The strength of the concrete mixes was determined at 7, 14, 28, and 56 days.

The standard configuration for the compressive strength test is such that the specimen is under axial loading until failure. It is crucial to ensure that the loading is exactly perpendicular to the ends of the specimens. Figure 8.5 shows photographs of the test apparatus used for determining the compressive strength. A pivoting head is used in order to make sure that the loading is not eccentric. The maximum load applied to the specimen is applied via hydraulic testing machine, which is directly connected to the apparatus. The average value of three (or two) cylinders tested at each age was recorded as the compressive strength of the mix (Appendix B).

Figure 8.5 Photograph of the test apparatus at University of Washington.

8.4.2 Creep and Shrinkage Strain Monitoring

Concrete undergoes volume changes while in service, due to factors such as applied stress, change of moisture content, and change in temperature [Mindess et al. 2003]. The time-dependent behavior of concrete is a major concern in construction, as deformations may result in a structure performing poorly. Two of the main types of deformations that were investigated in this project are creep and drying shrinkage strains of concrete mixes. Creep is a time-dependent deformation that occurs on the prolonged application of stress, whereas the drying shrinkage represents the strain caused by the loss of water from the hardened material [Mindess et al. 2003]. In composite construction, creep and drying shrinkage are the possible stimuli that can compromise the full shear stress transfer between steel and concrete, thus they require a special attention [Roeder 2010].

8.4.3 Small-Scale Creep Test Setup

Creep and shrinkage strains in the small-scale creep test were measured according to ASTM C 512. There were two types of strain gauges employed in this test setup: the mechanical strain gauge and vibrating wire strain gauge. A total of sixteen 6x12 in. cylinders were used in the creep and shrinkage tests. The cylinders were instrumented with four sets of targets (for the mechanical strain gauge) that were spaced 10 in. (254 mm) apart, and two vibrating wire strain gauges. Figure 8.6 shows the layout of the targets as well as vibrating wire gauges. Once the targets and mounting blocks were glued on the cylinders, 8 of the 16 cylinders were sealed with two layers of low viscous clear coat epoxy (System Three Epoxy).

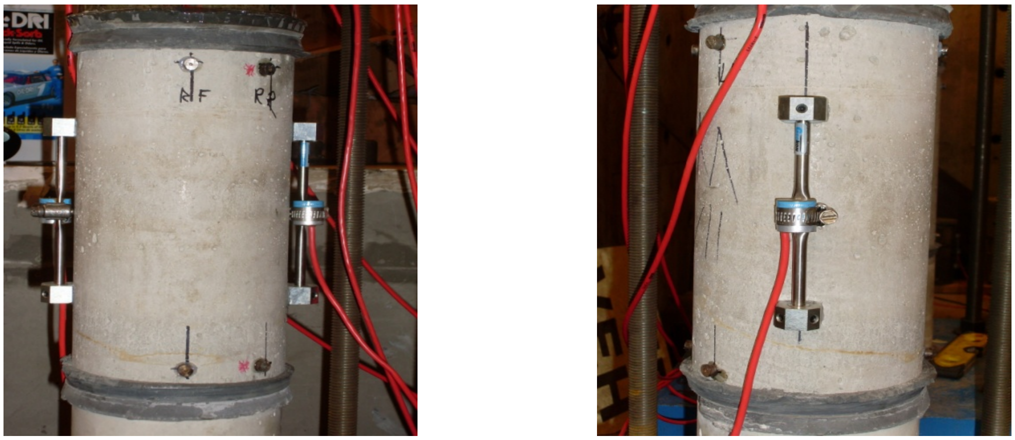

Figure 8.6 Photograph of the strain gauge layout.

Figure 8.7 Photograph of the creep rigs with the installed cylinders.

To measure the deformations caused by a constant load, a total of four cylinders (two sealed and two unsealed) were stacked in each creep rig shown in Figure 8.7. To maintain a nearly constant load as the specimens shortened, each rig had 4 coil springs. They were concentrically placed around holes that accommodated steel rods ensure an even distribution of the spring stiffness. Throughout the test, the tension in the rods was maintained by adjusting the nuts below the bottom plate. The prescribed stress of 1.2 ksi to the concrete cylinders in the creep rigs was applied by means of a single 60-kip jack. The remaining eight cylinders, 2 sealed and 2 unsealed for each concrete mix, were kept at the footing of the full-scale CFTs so that they would be at a relatively similar temperature and relative humidity as the ones used for the creep test. These cylinders were used to determine the shrinkage strain, thus they remained unloaded throughout the test.

In order to measure the strains of the concrete mixes using the mechanical strain gauge, two conical studs of the mechanical gauge were placed in the divots of the target. Prior to taking readings, the mechanical gauge was calibrated using a mild steel calibration bar. The elastic strain readings were taken immediately before and immediately after the initial loading followed by another reading taken 2 hours later. The creep strain readings were taken every day for the first week, every week for one month, and then every month until the end of the test. Prior to each strain reading, the applied load on the rig was adjusted with the hydraulic jack. The average of the four sides was taken as the strain for each cylinder. The strain in the shrinkage cylinders was measured using the same schedule as for the specimens placed in the creep rig.

The strain readings from the vibrating wire gauges were obtained by simply collecting the data via the data acquisition system MultiLogger. One of the advantages of using vibrating strain gauge is that the strain is automatically displayed in microstrain, whereas the mechanical gauge requires a few conversions before the final strain value is achieved (see Appendix C). The temperature is recorded as well, so there is no need for thermometers. Once all of the vibrating wire strain gauges were labeled, the data was collected every day for the first week, then twice a week for the following weeks. Because the vibrating wire gauges display strain values at specified time intervals, the total strain for each cylinder was obtained by: first transporting the data into an Excel spreadsheet, then taking the difference between two consecutive strain values, and finally taking the average of the two strain gauges.

Total creep was calculated using the following equation:

$$\varepsilon_C = \varepsilon_T - \varepsilon_S \tag{8.1}$$

where ε_C is the total creep strain, ε_T is the strain of the specimens under loading, and ε_S is the strain of the shrinkage specimens.

8.4.4 Full-scale Creep Test Setup

Figure 8.8 shows the full-scale creep test setup. In order to apply stress to the tubes, a standard 60-ft (18.3 m) W24×94 steel beam was cut into two 10-ft segments. The flanges of the two beams were bolted together with six 3×10-in. (76.2×254 mm) plates. Two Williams bars, used in place of the rods employed in the small-creep test, were cut to a length of 16 ft (4.9 m). The bars had a thread diameter of 2 in. (50.8 mm). Once the steel tubes, anchored into the footing, were arranged in the structural engineering laboratory, the Williams bars were placed into the strong floor on each side of the tubes.

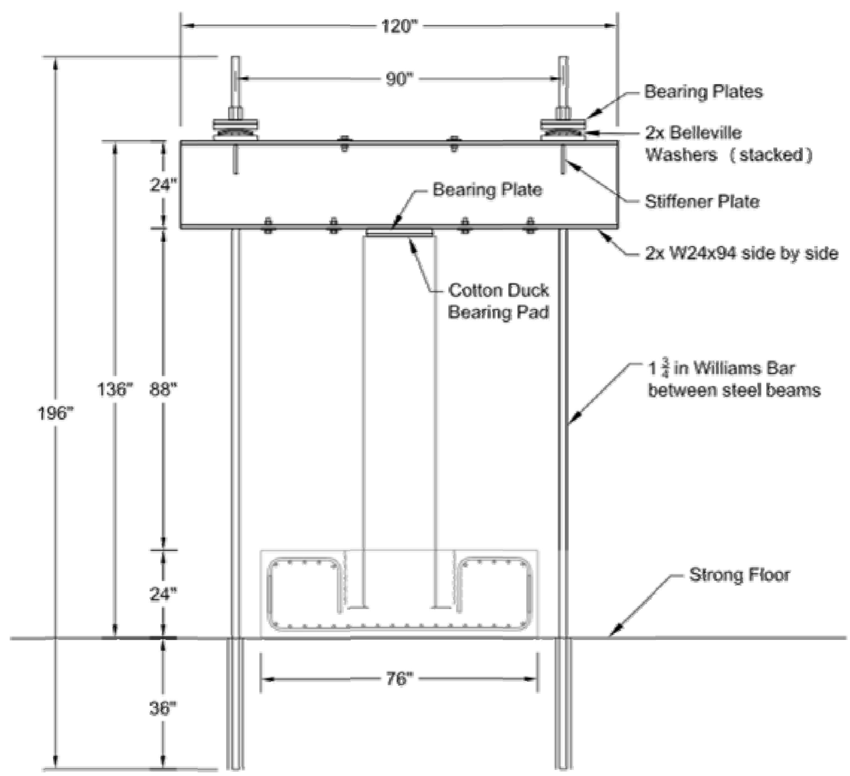

Figure 8.8 Full-scale creep test setup.

To ensure even loading of the specimens, the tubes were leveled using gypsum mortar called Hydrostone. To avoid edge load deformation, cotton duck bearing pads were placed on top of the Hydrostone. The two steel beams were raised up and placed on top of 18 in. (457.2 mm) diameter, ¾-in.- (19.1-mm)-thick steel bearing plates. Two 2-in. thick 12×12 in. (304.8×304.8 mm) bearing plates were bolted onto the beams. The Williams bars ran through the plates.

Figure 8.9 Photograph of the full-scale creep test setup.

Only vibrating wire gauges were used for this setup. The main reason for doing so was that it was necessary to measure the time-dependent deformation of both the concrete fill and steel tube. It is crucial to know how each component responds to a constant load, as the composite action takes place between the two. Thus, it was required to attach the strain gauges not only on the outside surface of the tubes but also inside of the tubes, in the concrete fill. Vibrating wire strain gauges were welded to the outside surface of the steel tube at approximately the same height as the internal gauges. As the dimensions of the full-scale tubes were significantly larger than that of the cylinders used for the small-scale creep test, three rows of vibrating strain gauges were constructed in order to measure the deformations along the full length of the tubes. Four sets of vibrating wire strain gauges were welded to the Williams bars in order to monitor the load in the bars. Because the creep in steel members is negligible, the readings from these gauges were intended to reflect any changes in the load.

To load the specimens, a 300-kip hydraulic ram was used. The ram was raised up to the level of the bearing plates on top of the steel beams using an electrical lift. Next, the pump was expanded until the Williams bar on one side of the tube was stressed to 180 kips, resulting in a 180-kip force in the other Williams bar and a 360-kip force in the concrete filled tube.

The time-dependent deformation in the CFTs was measured by collecting the data in Multilogger. The vibrating wire strain gauges provided all the necessary information needed to determine the height changes in the concrete fill and steel tube. The load was kept constant by stressing the bars approximately once a week since the initial loading. The creep strain was calculated in the same manner as the small cylinders with the exception of the shrinkage strain calculation. Since the full-scale creep test setup did not include full-scale concrete tubes for shrinkage monitoring, the shrinkage strain of the sealed cylinders was used to measure the creep strain in the concrete filled tubes.

8.5 TEST CHALLENGES

8.5.1 Constant Load

In actual structures, the loads do not remain constant due to the redistribution of stress resulting from creep and relaxation phenomena [Ichinose et al. 2001]. However, standard creep tests are conducted under a sustained load in order to keep the variables separate. Creep is still far from being completely understood, as it is a very complex engineering property of concrete. Thus, it is best to keep the load constant if the goal is to determine the effect of applying stress to the concrete as opposed to moisture and temperature.

One of the challenges in the full-scale creep test was keeping the load constant throughout the whole test. In the small-scale creep test, the applied load in the rig was adjusted prior to each strain reading. Although concrete mixes in CFTs were expected to creep significantly immediately after the initial loading thus causing a slight drop in the load, the amount of load that needed to be adjusted each week was quite large in the full scale test. This was surprising, as the readings taken from vibrating wire strain gauges indicated that the total strain in the concrete mixes tended to stabilize in approximately three weeks.

Therefore, a further investigation was conducted to determine the reason why the load in the tubes was decreasing so drastically. After a careful examination of the tube, it was noted that there were traces of oil at the top of the both tubes. In addition, the cotton duck pads (CDPs) seemed to deform a lot since the initial loading, which could explain the significant load drops in the CFTs. Figure 8.9 is a photograph of the findings during the tube examination. Thus, several compression tests were performed on these pads in order to determine if they were responsible for the radically changing load.

Figure 8.9 Photograph of the CFT during examination.

8.5.2 Cotton Duct Pad Compressive Tests

Lehman, et al. [2003] conducted research on the cotton duck bearing pads in 2003 to develop design guidelines and to establish the variation in behavior expected with different bearing pad manufacturers. The cotton duck pad used in the full-scale creep test, further designated as CDP A, was among the pads investigated by Lehman, et al. Based on the results from past research, it was concluded that the compressive stress limits of 3000 psi for maximum stress due to total dead plus live load and 2000 psi for stress due to live load must be recommended. Delamination or secretion of oil and wax from the CDP were found to be the common serviceability limit states for CDP [Lehman et al. 2003].

Furthermore, short-term static compressive load tests revealed that the peak stress for CDP A with a pad size 12x12x0.75 was 11.6 ksi. It is important to note that the CDP A used for the full-scale creep test had the same thickness as the one tested in the past CDP research. The damage state at the peak stress was described as pad fracture. The peak stress for the pads with different dimensions but the same thickness of 0.75 in. ranged from 7.3 to 13.4 ksi, and the damage states included oil secretion, damage within 5 to 15% of edge, and pad fracture. Based on the results of CDP creep tests, the peak stress was found to vary between 8 and 13 ksi for all manufacturers.

According to past research, the deformation of the cotton duck pads in the full-scale creep test should not take place since the stress level in the full-scale test was maintained at about 1.5 ksi. The several short-term cotton duck pad tests performed after discovery of oil traces in the tubes revealed that the peak stress for these pads was about 10 ksi, thus confirming the results obtained by Lehman, et al. A slight oil secretion and tear along the diagonal direction were noted, however the overall damage state was significantly less pronounced than that of the cotton duck pads in the CFTs. Possible causes of large deformations in CDP A in the full-scale tests could be the uneven loading of the tubes in the beginning of the test as well as the configuration of the beams mounted on top of the pads. Because it is hard to directly examine the cotton duck pads used for the full-scale test, it is recommended that an investigation of the damage state of the pads be conducted after the test is complete.

8.6 MEASURED ENGINEERING RESPONSE OF HIGH-VOLUME SCM CONCRETE

8.6.1 Compressive Strength

Figure 8.10 shows the compressive strength development of both concrete mixes. Although the results presented in this graph are not final, it can be noted that there is a steady strength development in the SCM mix. As was expected, concrete with a high-volume of fly ash and slag exhibited a low early strength in comparison to the SCC concrete. The compressive strength tests were conducted at 7, 14, 28, and 56 days.

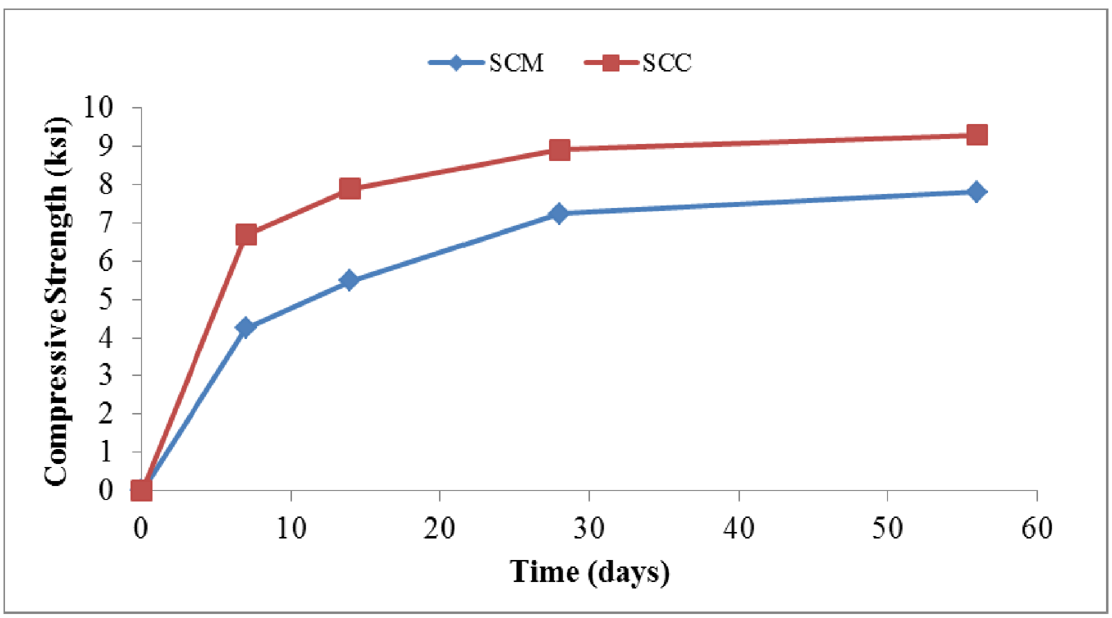

Figure 8.10 Compressive strength of the concrete mixes.

8.6.2 Creep and Shrinkage Response

All the rigs in the small-scale creep test were subjected to the same load of 34 kips, which resulted in a stress of 1.2 ksi in the cylinders. The load in the tubes was maintained at approximately 360 kips, which created a stress of 1.2 ksi in the tubes, thus producing the same stress level as in the cylinders. Because of time constraints, this section provides the results for only the first 36 days of the creep test since the initial loading.

Total strain is the sum of elastic, creep and shrinkage strain. The total strains of the unsealed and sealed specimens are shown in Figure 8.11 and Figure 8.12, respectively. The plots depict the results obtained from vibrating wire strain gauges only. As one of the objectives of this research is to compare the small-scale creep test results with the full-scale creep test results, only the data from the vibrating wire strain gauges were used in order to be consistent throughout the analysis. The mechanical strain gauge readings were used later in the project to verify the strain measurements taken from the vibrating wire strain gauges in the cylinders (Appendix D).

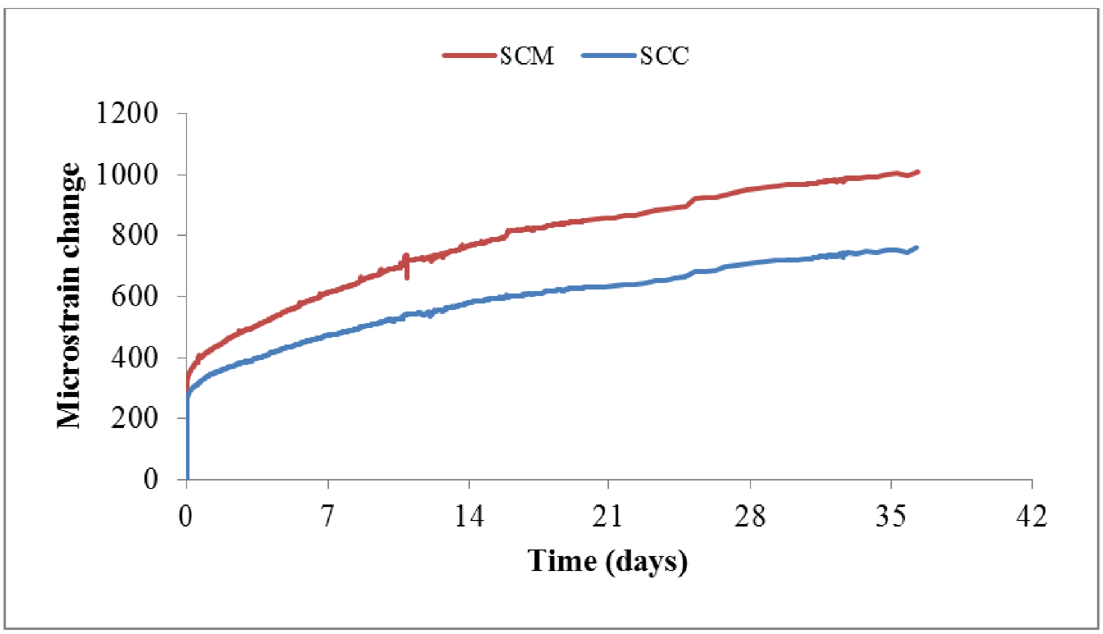

Figure 8.11 Total strain of the unsealed cylinders.

The total strain of the concrete-filled tubes is shown in Figure 8.13. It is important to note that the total strain of the concrete-filled tubes was measured using the middle row of the vibrating strain gauges located inside the tubes in order to capture the deformations caused by the load only.

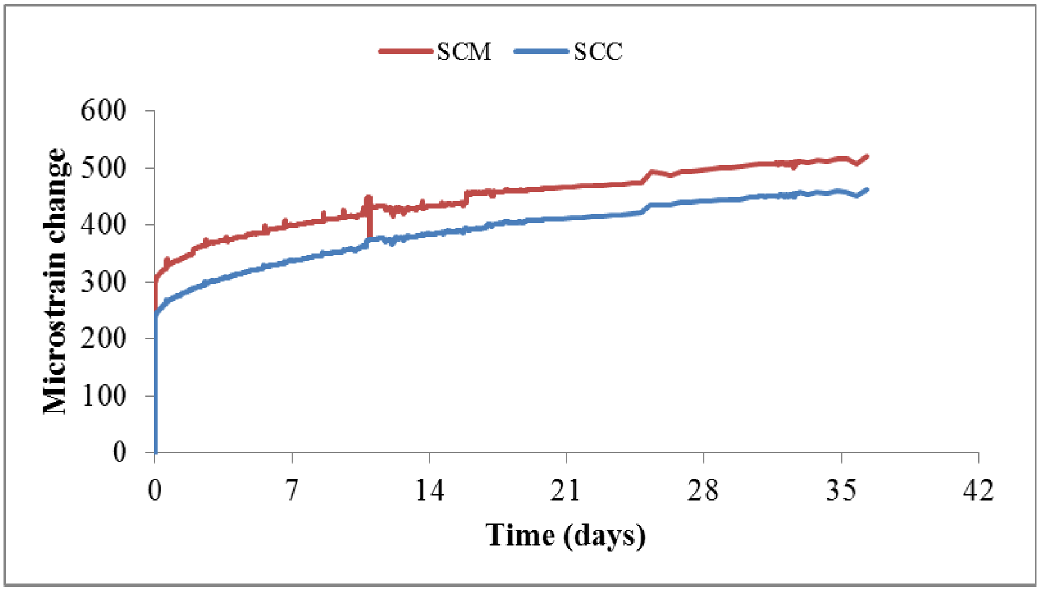

Figure 8.12 **Total strain of the sealed cylinders.**

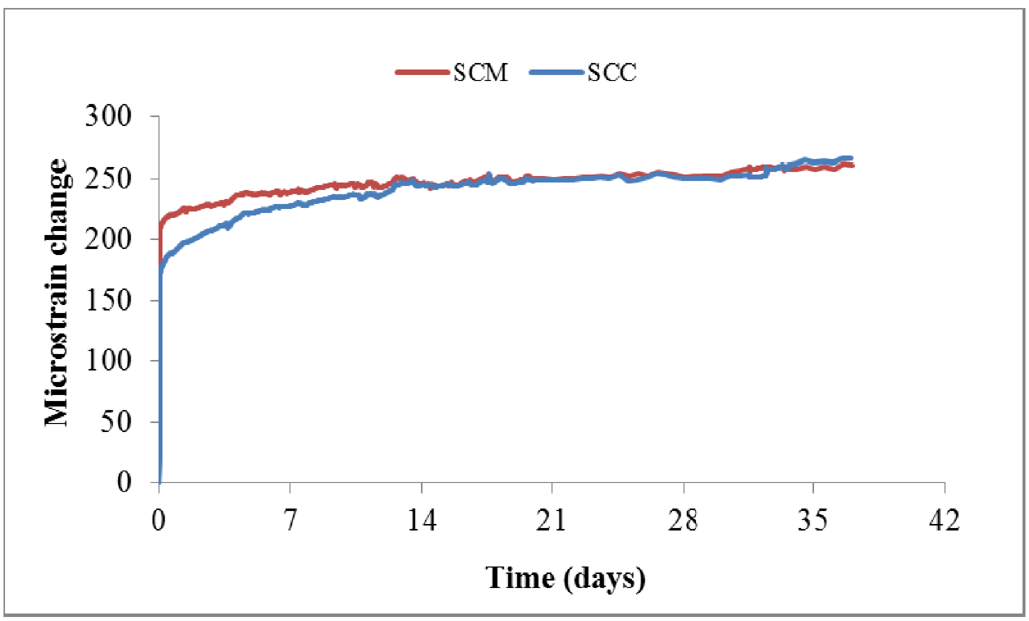

Figure 8.13 **Total strain of the concrete-filled tubes.**

As expected, the plots of total strain are characterized by an initial strain (elastic concrete response) followed by a gradual increase in strain with time. The total strain of the unsealed cylinders was larger than that of the sealed cylinders, which confirmed the findings of Hannesson [2010]. Less shrinkage occurs in the sealed cylinders because excess water in the concrete cannot fully evaporate. Generally, in the sealed cylinders, the initial strain in the SCM concrete was larger than the initial strain in the SCC concrete; however the creep strain in the SCM concrete tended to be smaller than in the SCC concrete. The lower creep strains might result from the larger unreacted portion of fly ash and slag, which act as a fine aggregate, providing higher creep resistance [Hannesson 2010]. From the plot of the total strain in the CFTs, it can be observed that the process tends to stabilize after about 14 to 21 days. Furthermore, as expected, the total strain in the tubes was smaller than that in the sealed cylinders. The steel jacket does not allow the free water to evaporate resulting in less total strain. In addition, it can be seen from the plot of the total strain in the CFTs that even though the SCM concrete exhibited a high initial strain, there was less long-term deformation than in the SCC concrete.

The creep strain plots of the cylinders were similar to the shrinkage strain as well as the total strain plots in that the sealed cylinders experienced less deformation than the unsealed cylinders. Figure 8.14 shows the shrinkage strain in the sealed cylinders. The creep strain of the CFTs was obtained by subtracting the shrinkage strain of the sealed cylinders for each concrete mix from the total strain in the tubes. Figure 8.15 shows the creep strain in the full-scale concrete-filled tubes.

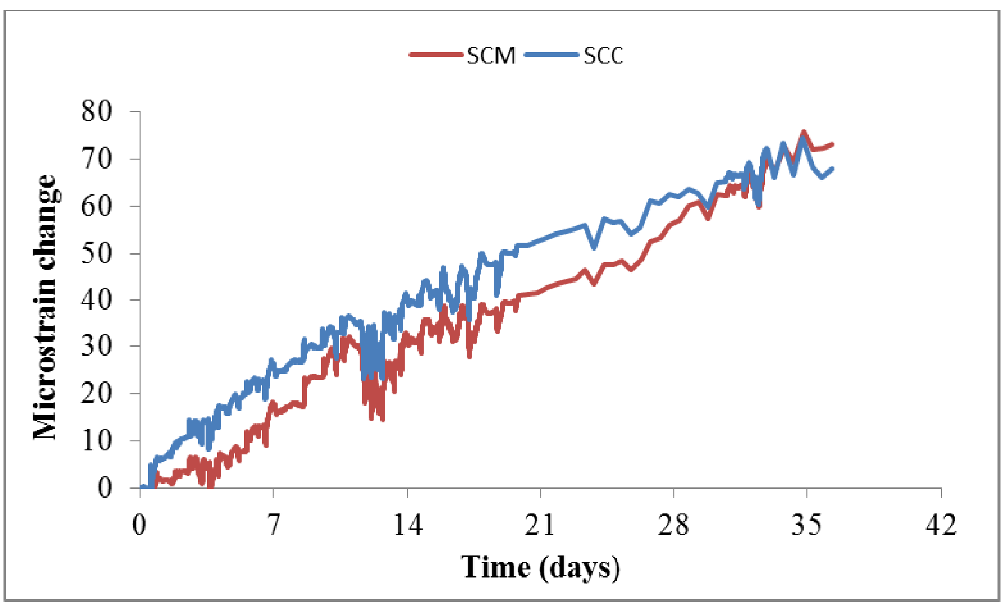

Figure 8.14 Shrinkage strain in the sealed cylinders.

.

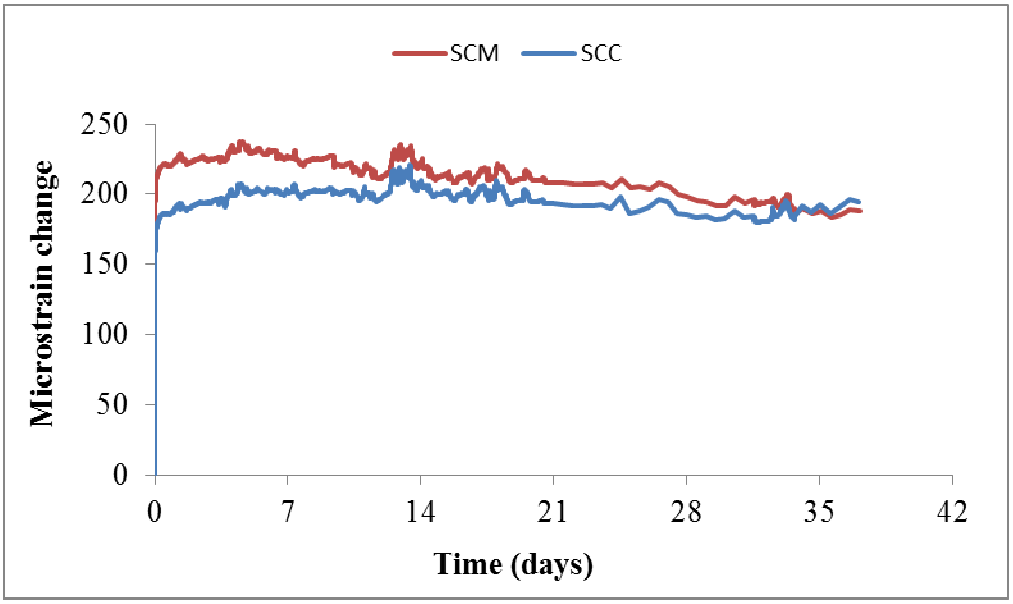

Figure 8.15 Creep strain of the concrete-filled tubes.

The plot of creep strain in the CFTs revealed curves with negative slopes, thus producing creep coefficients (the ratio of creep strain after very long time to the elastic strain) of less than one. Although the test setup did not include full-scale concrete tubes for the shrinkage measurement, the assumption that the shrinkage strain in the concrete-filled tubes was significantly smaller than the shrinkage strain in the sealed cylinders might seem viable. In fact, by taking a look at the plot of total strain in the tubes, one can easily conclude that the shrinkage strain in the tubes may be negligible (or close to zero).

8.7 CONCLUSIONS AND RECOMMENDATIONS

This research program was undertaken to determine the time-dependent behavior of SCC with a high volume of SCMs in composite construction, as they have had limited attention in the literature. This research was performed in two parts. In the first part, the small-scale cylinders were tested for compressive strength, drying shrinkage, and creep. In the second part, two full-scale concrete-filled steel tubes were tested for creep only.

Based on the results obtained from the first 36 days of the project, the following has been concluded:

- The SCM had an early low compressive strength but a steady strength development. This trend was expected since the hydration reaction for the SCM concrete is slower than the hydration reaction for SCC concrete.
- Shrinkage strains of the unsealed specimens were more than the sealed specimens. This verified the results obtained by G.M. Hannesson since less water evaporation occurs in the sealed specimens.
- The total strain in the tubes was significantly smaller than the sealed specimens. This suggests that the time-dependent deformation depends on the dimensions of the specimens. In addition, it may be possible that the steel jacket in the tubes prevents evaporation of free water to a greater degree than the epoxy coating of the cylinders.
- The SCM concrete in the tubes exhibited a higher initial strain but a lower long-term deformation than the SCC concrete. This was expected because the SCM had a slow strength development.

Based on this investigation, a few recommendations for future research can be made:

- Full-scale shrinkage specimens are needed to verify that the shrinkage strains in the concrete-filled tubes are negligible.
- Specimens with different dimensions are needed to examine the influence of the size of the specimens on the time-dependent deformation of concrete.
- Further research should be performed on the creep behavior of high-volume SCM concrete in composite construction
- Expressions that predict long-term creep strain without performing tests are needed.

ACKNOWLEDGMENTS

This research work was overseen and partially supported by the Pacific Earthquake Engineering Research (PEER) Center as a part of the 2011 PEER Internship Program. Financial support was provided by TransNow and the National Science Foundation (NSF). The author would like to thank Dr. Charles Roeder, Dr. Dawn Lehman, Kenneth O'Neil, and Arni Gunnarsson for their mentorship during the research process. Any opinions, findings, and conclusions or

recommendations expressed in this material are those of the authors and do not necessarily reflect those of the sponsors.

REFERENCES

Hannesson, G.M. (2011). *Mechanical Properties of High-volume SCM Concretes*. Thesis. University of Washington, 2010. Seattle, WA.

Ichinose, L.H., E. Watanabe, and H. Nakai (2001). An experimental study on creep of concrete-filled steel pipes, *J. Constructional Steel Res.,* 57:453–66.

Lehman, D.E., C.W. Roeder, and K. Curtin (2003).. *Cotton Duck Bearing Pads: Engineering Evaluation and Design Recommendations*, Rep. No. WA-RD 569.1. Seattle: U.S. Department of Transportation Commission, Washington, D.C.

Mindess, S. J. F. Young, and D. Darwin (2003). *Concrete*. 2nd ed. Upper Saddle River, NJ: Prentice Hall.

Roeder, C.W., D.E. Lehman, and E. Bishop (2010). Strength and stiffness of circular concrete-filled tubes, *J. Struct. Engrg*.,136(12): 1545–553.

Wang, Y.F., B. Han, and D.J. Zhang (2009). Advances in creep of concrete-filled steel tube members and structures, *Creep, Shrinkage and Durability Mechanics of Concrete and Concrete Structures: Proceedings of the Eighth International Conference on Creep, Shrinkage and Durability of Concrete and Concrete Structures, Ise-Shima, Japan, 30 September-2 October 2008*, by T. Tanabe. Boca Raton: CRC Press, pp. 595–600.

APPENDIX A

Table 8.1 Mix proportions for SCC concrete .

Material	Source	Destination	ASTM	Spec. Gravity	oz.	cu.ft.	Weight(lb)
#8	Glacier Pit #B-335	AASHTO #8 (3/8)	C33	2.67	0.00	8.76	1,460
Fine Aggregate	Glacier Pit #B-335	Concrete Sand	C33	2.63	0.00	9.37	1,538
Type I-II	Ash Grove	Type I-II	C150	3.15	0.00	2.73	536
Type F High Range Water R	W.R.Grace	ADVA 170	C494	1.10	74.25	0.00	
Type A Water Reducer	W.R.Grace	WRDA64	C494	1.20	33.00	0.00	
Slag	LAFARGE	Lafarge GGBFS 120	C 989	2.87	0.00	1.61	289
City	City	Water	C94	1.00	0.00	4.32	270
Air						0.41	
					TOTAL	27.20	4,093
Specified F'c:	6,000	PSI					
Specified Slump:		in.	Designed Unit Weight:			150.50	lbs./cu.ft.
Specified Air:	1.00 To 3.00	%	Designed W/C + P Ratio:			0.33	
Designed Air:	1.5	%	Designed Volume:			27.20	cu.ft.

Table 8.2 Mix proportions for SCM.

Material	Source	Destination	ASTM	Spec. Gravity	oz.	cu.ft.	Weight(lb)
#8	Glacier Pit #B-335	AASHTO #8 (3/8)	C33	2.67	0.00	8.39	1,399
Fine Aggregate	Glacier Pit #B-335	Concrete Sand	C33	2.63	0.00	8.97	1,473
Type I-II	Ash Grove	Type I-II	C150	3.15	0.00	0.84	165
Type A Water Reducer	W.R.Grace	WRDA64	C494	1.21	33.00	0.00	
Type F High Range Water R	W.R.Grace	ADVA 170	C494	1.10	74.25	0.00	
Fly Ash	ENX Alberta, Canada	Fly Ash	C-618	2.20	0.00	2.40	330
Slag	LAFARGE	Lafarge GGBFS		2.84	0.00	1.86	330
City	City	Water	C94	1.00	0.00	4.32	270
Air						0.41	
					TOTAL	27.20	3,967
Specified F'c:	8,000	PSI					
Specified Slump:		in.	Designed Unit Weight:			145.80	lbs./cu.ft.
Specified Air:	0.00 To 3.00	%	Designed W/C + P Ratio:			0.33	
Designed Air:	1.5	%	Designed Volume:			27.20	cu.ft.

APPENDIX B

Table 8.3 Compressive strength results for SCC concrete.

Cylinder#	Curing Time (days)	Force (lb)	Stress (ksi)	Average Stress (ksi)	Notes
1	7	195830	6.926	6.683	7 Day Strength Test
2	7	182090	6.440		
3	14	224150	7.928	7.887	14 Day Strength Test
4	14	221830	7.846		
5	28	256540	9.073	8.907	28 Day Strength Test
6	28	247150	8.741		
7	56	269400	9.528	9.301	56 Day Strength Test
8	56	253260	8.957		
9	56	266250	9.417		

Table 8.4 Compressive strength results for SCM concrete.

Cylinder#	Curing Time (days)	Force (lb)	Stress (ksi)	Average Stress (ksi)	Notes
1	7	119850	4.239	4.242	7 Day Strength Test
2	7	119180	4.215		
3	7	120780	4.272		
4	14	147080	5.202	5.490	14 Day Strength Test
5	14	158160	5.594		
6	14	160430	5.674		
7	28	207560	7.341	7.233	28 Day Strength Test
8	28	198880	7.034		
9	28	207080	7.324		
10	56	206810	7.314	7.814	56 Day Strength Test
11	56	218390	7.724		
12	56	237580	8.403		

APPENDIX C

The original length of the calibration bar is 254 mm (10 in.) at 20°C, however it must be corrected using the thermal expansion coefficient if the ambient temperature is either higher or lower than 20°C. The following equation is used to correct the length of the calibration bar:

$$L_c = 254(1+\Delta T\alpha_L) \qquad \text{(C1)}$$

where L_c is the corrected length of the calibration bar (mm), ΔT is the difference of ambient temperature from 20°C (°C) and α_L is the thermal expansion coefficient for mild steel and is equal to 0.0000126 1/°C. The equation used to find the distance between the targets relative to the bar is as follows:

$$L_T = \left(\frac{\varepsilon_t - \varepsilon_c}{10000}\right)25.4(mm) + L_C \qquad \text{(C2)}$$

where L_T is the distance between the targets (mm), ε_T is the strain value between the targets using the mechanical gauge (mm/mm) and ε_C is the strain value of the calibration bar using the mechanical gauge (mm/mm). Figure 8.16 shows a photograph of the mechanical strain gauge used to measure the strains.

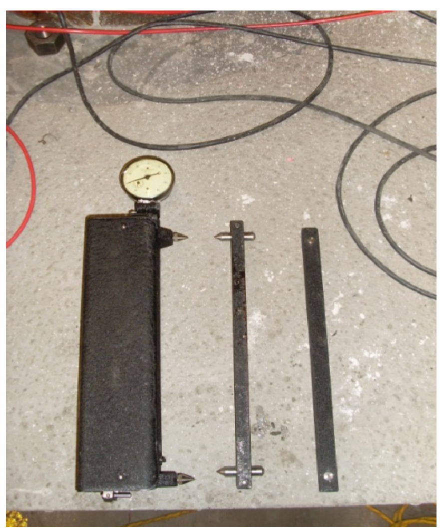

Figure 8.16 Photograph of the Whittemore strain gauge.

APPENDIX D

Table 8.5 Sample sheet for the mechanical strain gauge.

Day: 07.12.11	1	2	3	Notes:
Temerature (T)	71	72		
Relative Humidity (RH	46	46		
Calibration bar	720	720	720	

Ram on	Unsealed (1)			Sealed (1)			Unsealed (2)			Sealed (2)		
	1	2	3	1	2	3	1	2	3	1	2	3
Left Rear (LR)	620	620	620	655	656	655	555	555	556	637	638	637
Left Front (LF)	685	686	686	649	650	650	602	602	602	664	665	664
Right Front (RF)	619	616	615	663	664	665	624	624	624	668	667	668
Right Rear (RR)	614	612	612	658	657	658	630	630	632	678	678	679
Ram off	Unsealed (1)			Sealed (1)			Unsealed (2)			Sealed (2)		
	1	2	3	1	2	3	1	2	3	1	2	3
Left Rear (LR)	620	620	620	655	656	655	555	555	556	637	638	637
Left Front (LF)	685	686	686	649	650	650	602	602	602	664	665	664
Right Front (RF)	619	616	615	663	664	665	624	624	624	668	667	668
Right Rear (RR)	614	612	612	658	657	658	630	630	632	678	678	679
Shrinckage samples	Unsealed (1)			Sealed (1)			Unsealed (2)			Sealed (2)		
	1	2	3	1	2	3	1	2	3	1	2	3
Left Rear (LR)	662	663	665	711	711	710	683	683	682	705	710	704
Left Front (LF)	668	670	670	700	695	694	675	675	675	726	727	726
Right Front (RF)	680	682	680	721	722	721	675	675	673	700	700	700
Right Rear (RR)	660	662	662	683	683	684	668	668	669	712	712	710

9 CFT Bridge Pier Connections

ZHI LONG LIU

ABSTRACT

Concrete-filled tubes (CFTs) are composite structural members made of steel tubes with concrete infill. The steel tube serves as both the formwork and reinforcement to the concrete fill, and the fill can increase the compressive strength of the tube. The increased stiffness from the fill also delays local buckling if composite action is achieved. Circular CFT provides better performance than rectangular CFT because greater confinement is achieved, resulting in better composite interaction between the two materials. CFTs can be rapidly constructed and provide significant compression, bending, and shear resistance compared to conventional massive reinforced concrete. The time and material savings make them ideal for bridge piers and building columns. However, connection design for circular CFT is more difficult than other structural elements. Recent research is investigating a simple and economical connection between circular CFT piers and reinforced concrete foundations. The connection provides a logical sequencing process in actual construction. In addition, the connection is proved to be able to develop the full capacity of the composite column, with great ductility and inelastic deformation capacity under seismic loading.

9.1 INTRODUCTION

9.1.1 Concrete-Filled Tube (CFT)

Concrete-filled tubes (CFT) are composite structural members made of a rectangular or circular tube and a concrete infill. Figure 9.1 shows a typical circular CFT. The steel tube serves as the reinforcement and formwork for the concrete infill. The concrete infill, on the other hand, braces the steel tube and thus delays the local buckling.

Concrete filled tubes are efficient in material use compared to traditional reinforced concrete. Steel is strong in tension and compression but weak in buckling; Concrete is strong in compression but susceptible to shear and spalling damage. By placing steel tube at the extreme fiber of a concrete column, large strength and stiffness can be achieved. With the same capacity requirement, CFT columns are smaller in size compared to reinforced concrete, which lowers the material cost. Second, labor costs related to formwork and reinforcement are eliminated in CFT compared to reinforced concrete. Thus, CFT is more economical.

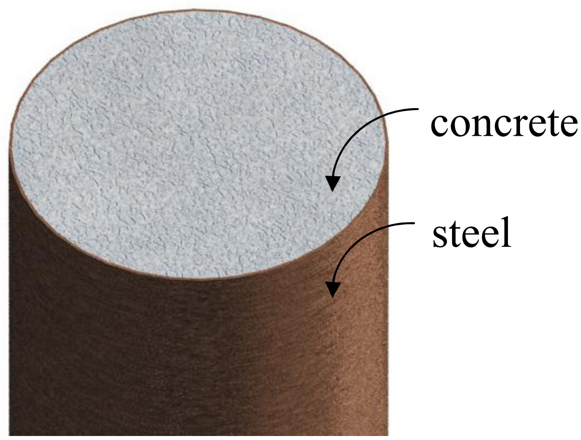

Figure 9.1 A typical circular CFT.

Rapid construction is another advantage of CFT. First, there is no time required in constructing concrete formwork. Second, the steel tube has a high initial strength. Once erected, there is no need to wait for the concrete to develop its strength before going into the next construction sequence. Third, since self-consolidating concrete is used to achieve composite action, the time associated with casting is also reduced.

However, CFT are not commonly used in modern construction due to the limited understanding of workable connections and complicated design methods. Therefore, developing a simple and economical base connection becomes necessary.

9.1.2 Base Connections for CFTs

Currently, two types of CFT base connections, namely the monolithic connection and the isolated connection, are under investigation in University of Washington. Figure 9.2 shows an overview of these connections. In a monolithic connection, the footing is cast around the erected column; while in an isolated connection, the column is erected and grouted into the footing. In this test, only the isolated type is used. The construction sequence is illustrated in Section 9.3.2.

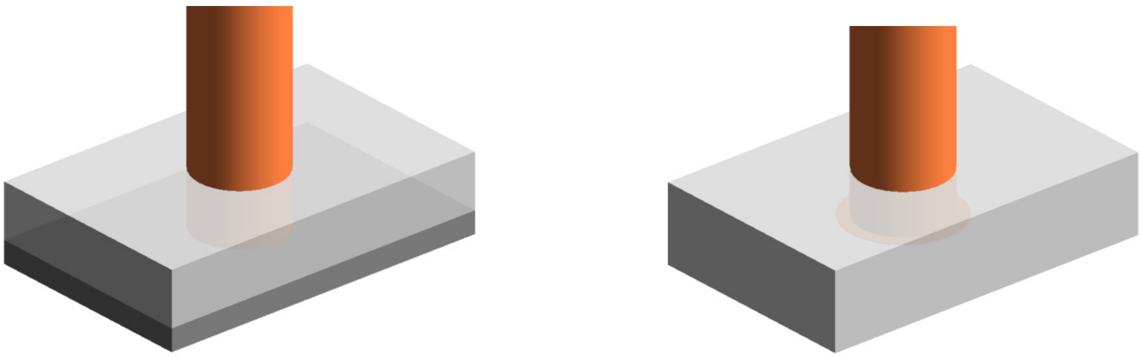

(a) Monolithic (b) Isolated

Figure 9.2 CFT base connections.

9.2 LITERATURE REVIEW

This research is the last part of an ongoing program at the University of Washington focusing on the development of CFT connection. Table 9.1 summarizes the previous research performed by several students.

In 2005, Kingsley tested specimen I ~ IV to investigate the effect of embedment depth. Several conclusions were drawn in his analysis. First, shallow embedment (0.6D) resulted in severe damage of the footing and deterioration of lateral capacity. Second, an embedment depth of 0.9D developed the full flexural strength of the CFT column. Third, the isolated connections provided improved deformation capacity and reduced footing damage compared to the monolithic connections. Lastly, vertical reinforcement in the footing did not affect the strength too much, but it did reduce the damage at drift level larger than 2%.

In 2006, Williams tested specimen V ~ VIII to investigate the flexible underlay. The main difference of these specimens from Kingsley's was that they had flexible underlay. First, he concluded that the isolated connection with 0.75D embedment reached full flexural capacity of the CFT. Second, large combined compressive stress from axial load and moment resulted in a punching shear failure in the footing below the column. Third, energy dissipation was mainly provided by the steel tube prior to buckling. Lastly, local buckling of the steel tube lowered the stiffness, but not the strength.

Table 9.1 Summary of specimens tested.

Specimen	Embed. Depth l_e/D	Connection	Test Loading	Specific Goals	Max. Drift	Failure Mode
I	0.600	Monolithic	Flexural	No Shear Reinf.	8.5%	Cone Pullout
II	0.600	Monolithic	Flexural	Embedment Depth	9.5%	Cone Pullout
III	0.900	Monolithic	Flexural	Embedment Depth	8.0%	Ductile Tearing of Tube
IV	0.600	Isolated	Flexural	Connection Type	7.8%	Cone Pullout
V	0.900	Monolithic	Flexural	Flexible Underlay	9.0%	Ductile Tearing
VI	0.750	Isolated	Flexural	Flexible Underlay, Embedment	9.6%	Ductile Tearing
VII	0.750	Isolated	Punching Shear	Monotonic Axial Loading	N/A	Punching Shear w/225mm depth
VIII	0.750	Isolated	Punching Shear	Cyclic Axial Loading	N/A	Cyclic Punching w/225mm depth
IX	0.900	Isolated	Flexural	Galvinization	8.5%	Ductile Tearing
X	0.900	Isolated	Flexural	Galvinization, Drift History	10.5%	Ductile Tearing
XI	0.900	Isolated	Flexural	Axial Load P/Po = 0.15	10.4%	Ductile Tearing
XII	0.900	Isolated	Flexural	Axial Load P/Po = 0.20	9.5%	Ductile Tearing
XIII	0.800	Monolithic	Flexural	Straight Weld	12.2%	Ductile Tearing
XIV	0.775	Isolated	Flexural	Straight Weld	12.3%	Ductile Tearing
XV	0.775	Isolated	Flexural	Spiral Weld	10.7%	Ductile Tearing
XVI	0.800	Monolithic	Flexural	Spiral Weld	10.5%	Ductile Tearing
XVII	0.700	Isolated	Flexural	Spiral Weld	10.7%	Ductile Tearing
XVIII	0.600	Isolated	Flexural	Spiral Weld	10.8%	Ductile Tearing

In 2007, Chronister tested specimen IX ~ XII to examine axial load ratio and drift history. Asymmetrical axial loadings and corrosion-resistant material were applied in these specimens. The first conclusion was that corrosion resistant material delayed each damage state to a higher drift ratio. Second, asymmetric drift history revealed a similar performance with increased drift ratios for each respective damage state. Third, delayed ductile tearing resulted in an increased deformation capacity of the footing connection.

In 2011, Lee tested specimen XIII ~ XVIII to compare (1) the capacity of monolithic and isolated connections, and (2) the behaviors of straight-seam-welded tubes with spiral-welded tubes under a constant axial load and a cyclic horizontal lateral load. He first concluded that isolated connections provided sufficient strength and ductility compared to monolithic connection. Second, straight-seam-welded tubes provided a 25% more drift ductility. Third, about 46% of the energy dissipation occurred at the connections and 26% from the local buckling of the tubes. Lastly, the modified stiffness expression proposed by Bishop was proved to be within 6% error compared to the experimental results.

9.3 OBJECTIVE

This research is the last part of an ongoing program at the University of Washington focusing on the development of CFT connection. This test is intended to compare previous results, Lee's in particular, with a full scale CFT specimen. Since isolated connections are preferred in construction, it is the only type of connections being investigated. Other key parameters, such as embedment depth, may also be examined.

9.4 TEST PROGRAM

9.4.1 SPECIMEN OVERVIEW

The specimens modeled a cantilever bridge column. The column consisted of a spiral-seam-welded steel tube with self-consolidating, low shrinkage concrete. Figure 9.3 shows an overview of the full scale 30-in-diameter specimen. Shear reinforcement is not shown in the figure for clarity. Material properties are shown in Table 9.2. The yield stress of the steel tube was 50 ksi, and the compressive strength of the concrete was 6 ksi. Table 9.3 shows several key parameters of this specimen. From the table, the D/t ratio is 120, which is the largest among all the test specimens tested so far.

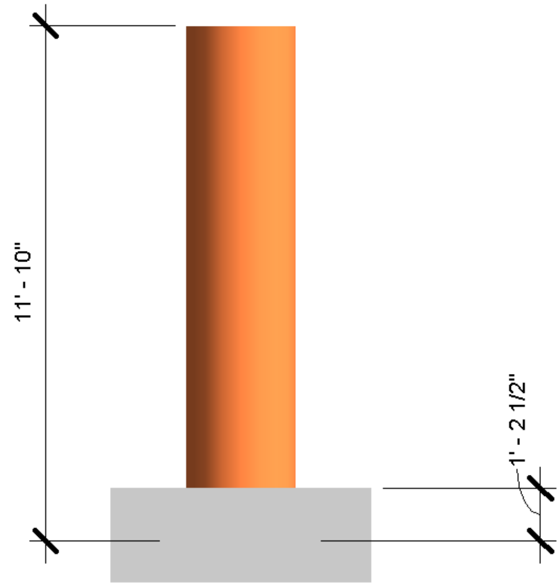

Figure 9.3 Test specimen.

Table 9.2 Material properties of test specimen.

Item	Designation
Spiral Seam Steel Tube	ASTM A1018-07 SS, F_y = 50 ksi
Reinforcing Steel	ASTM A615M-08b Grade 60
Concrete	Self Consolidating, Low Shrinkage, 6 ksi
High Strength Grout	ASTM C-1107

Table 9.3 Key parameters of test specimen.

Tube Diameter (D)	30 in.
Tube Thickness (t)	¼ in.
Embedment Depth	14.5 in.
Annular Ring Thickness	¼ in.
Annular Size	3 ft-2 in. O.D., 2 ft-1.5 in. I.D.
Footing Size	6 ft-0 in. X 9 ft-4 in. X 2 ft-2 in.

9.4.2 Construction Sequence of CFT Isolated Connections

To construct the isolated connection, the rectangular footing was first cast into the formwork with a 3 ft-6-in. diameter void defined by corrugated steel pipe. The footing was reinforced with No. 8 and No. 10 rebar in one direction, and No. 5 and No. 8 rebar in the other orthogonal direction. The reinforcement configuration is shown in Figure 9.4. Then, the tube was erected into the void with an annular ring welded on the bottom. Third, the void was grouted into place using a fiber-reinforced grout. Finally, the concrete was poured into the steel tube. The process of construction is shown in Figure 9.5.

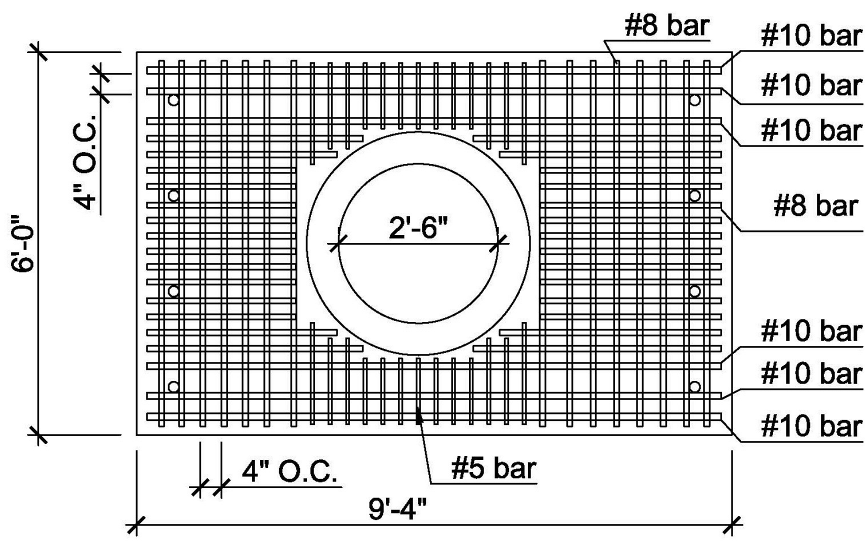

Figure 9.4 Reinforcement plan of footing.

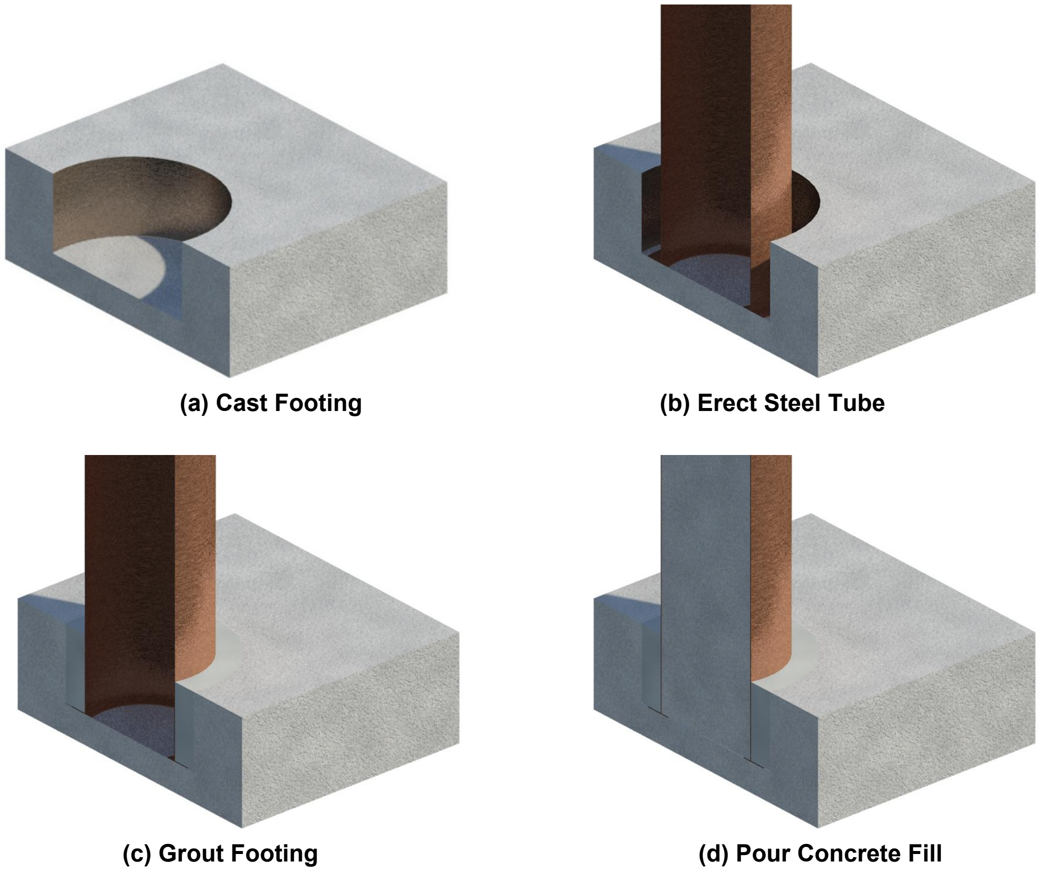

Figure 9.5 Construction sequence of isolated connection.

9.4.3 Experimental Test Setup

The experiment was performed on a self-reacting test rig designed by Kingsley (Figure 9.6). The rig was centered underneath a Baldwin Universal Testing Machine with a compressive capacity of 2400 kips. The specimen was leveled and grouted into place using a gypsum mortar called Hydrostone. The actuator was attached 6 ft. above the footing top surface.

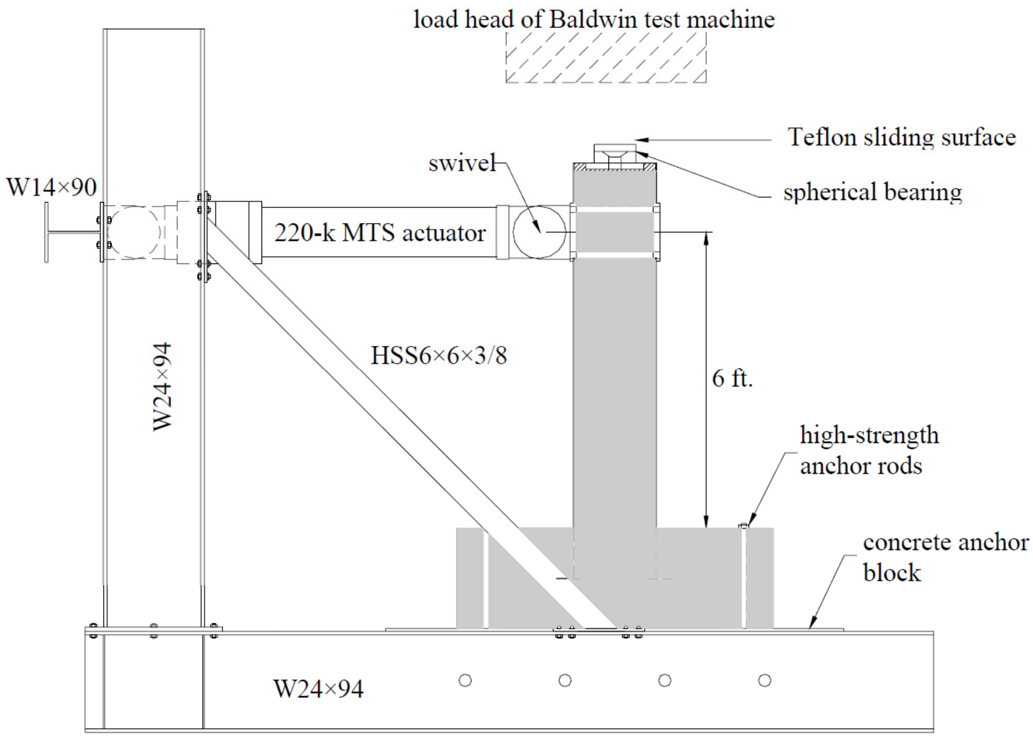

Figure 9.6 Experimental test rig (Kingsley).

9.4.4 Loading Configurations

The specimen was under a compressive axial load and a cyclic horizontal lateral load. The magnitude of the compression load was based on 5% of the gross axial capacity of the CFT specimen, which is about 333.6k, and it was held constant throughout the test. It was exerted by the Baldwin Testing Machine [Figure 9.7(a)]. The lateral load, however, was displacement-controlled and was exerted by the actuator [Figure 9.7(b)]. The cycles loosely followed the ATC24 guideline. The magnitude of the low-amplitude cycles were based on the yield displacement of 0.78 in. The post-yielding cycles were adjusted to follow the history of the previous specimens. The lateral load was oriented in the north-south direction, and the south direction was considered positive. Due to the elastic deformation of the rig frame, the proposed loadings varied from the actual loadings.

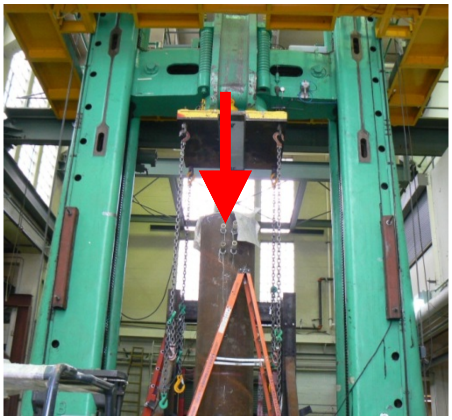

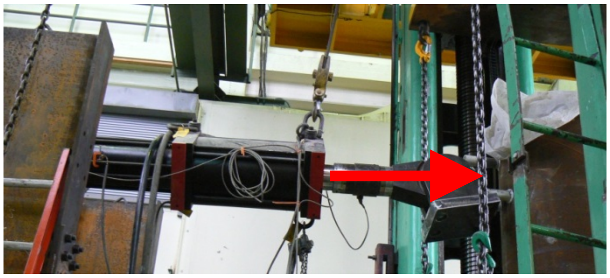

(a). Axial Compression (Baldwin) **(b). Cyclic Lateral Load (Actuator)**

Figure 9.7 Loading configurations.

9.4.5 Instrument Locations for LabView Setup

A variety of instruments, including potentiometers, inclinometers, and strain gauges were used in the LabView setup during the testing. In this section, the locations of each instrument will be discussed.

9.4.5.1 Strain Gauges

Two types of strain gauges were placed into the specimen: the steel type and the concrete type. Steel strain gauges were placed longitudinally on the steel tube centered on both the north and south sides. Above the footing, there were a total of six gauges symmetrically placed on each side of the tube. Below the surface of the footing, two gauges were placed in each cardinal direction. A detail configuration is shown in Figure 9.8(a). Concrete strain gauges were placed on the top surface of the footing. The configuration is shown in Figure 9.8(b).

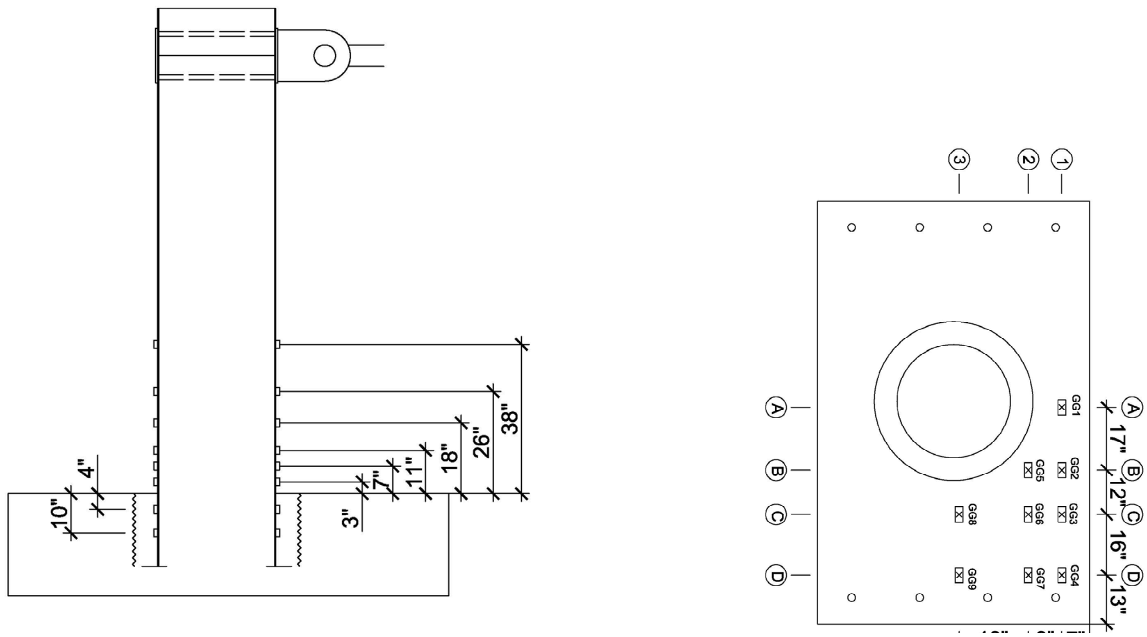

(a) Steel Gauge Locations. (b) Concrete Gauge Locations.

Figure 9.8 Location of strain gauges on the CFT Specimen.

9.4.5.2 Potentiometers

Two types of potentiometers were used in this test: string potentiometers and potentiometers made by Duncan Electronics. Duncan potentiometers were placed on the rig anchor block and the footing to account for relative horizontal and vertical movements occurred during the test. The average range of a Duncan potentiometer is about 1 in.

String Potentiometers were placed to measure horizontal and vertical movement of the column. The average range of them is 10 in. The housing of the potentiometers was fixed to either the foundation footing or a reference column bolted on the test floor.

9.4.5.3 Inclinometers

A total of four inclinometers were placed to the east side of the column to measure its rotation. To ensure the stability of the attachment, a 9-in-deep hole was drilled in each defined position, and then a 1-ft-long metal thread was placed inside the hole with epoxy filling. Finally, the inclinometer is rotated into position. Each inclinometer was calibrated to a range of $\pm 15^{\circ}$. They were centered at locations 2 in., 6 in., 14 in., 22 in. above the surface of the footing (Figure 9.9).

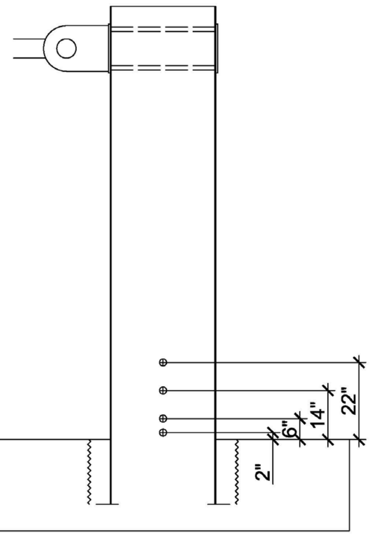

Figure 9.9 Inclinometer locations on the CFT specimen.

9.4.6 Instrument Locations for Optotrak Setup

The Optotrak Certus motion capture system was used to capture the buckled shape of the tube. The LED markers were attached to the surface of the tube with adhesive foam. In conjunction with the markers, two Optotak sensors were placed in the line of sight of the markers. Each sensor has three cameras. The sensor triangulates the position of each marker to obtain their positions in a manually-defined coordinate. A detailed configuration of the LED markers is shown in Figure 9.10.

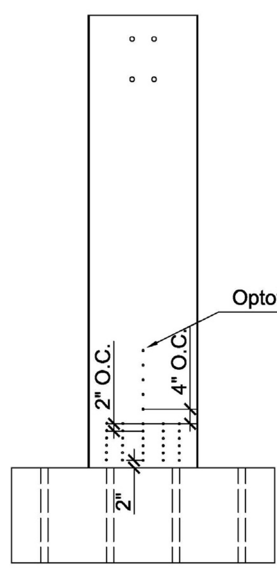

Figure 9.10 Optotrak LED marker locations on the CFT specimen.

9.5 RESULTS AND ANALYSIS

9.5.1 LabView Data

In the force versus displacement plot shown in Figure 9.11, the horizontal axis is the horizontal displacement measured by a string potentiometer, which is located at the center of the horizontal actuator. The vertical axis is the horizontal actuator force. The CFT column was loaded until failure, and a total of 26 cycles were recorded. From the figure, the load capacity at that height was about 170 to 180 kips in both the positive and the negative directions. As the displacement got larger, the load capacity remained essentially constant until Cycle 24, during which the initial tear occurred. After that, the capacity dropped significantly with only a small displacement increment. This result indicates that buckling does not affect the capacity significantly, and the single most important factor that reduces the load capacity is tearing.

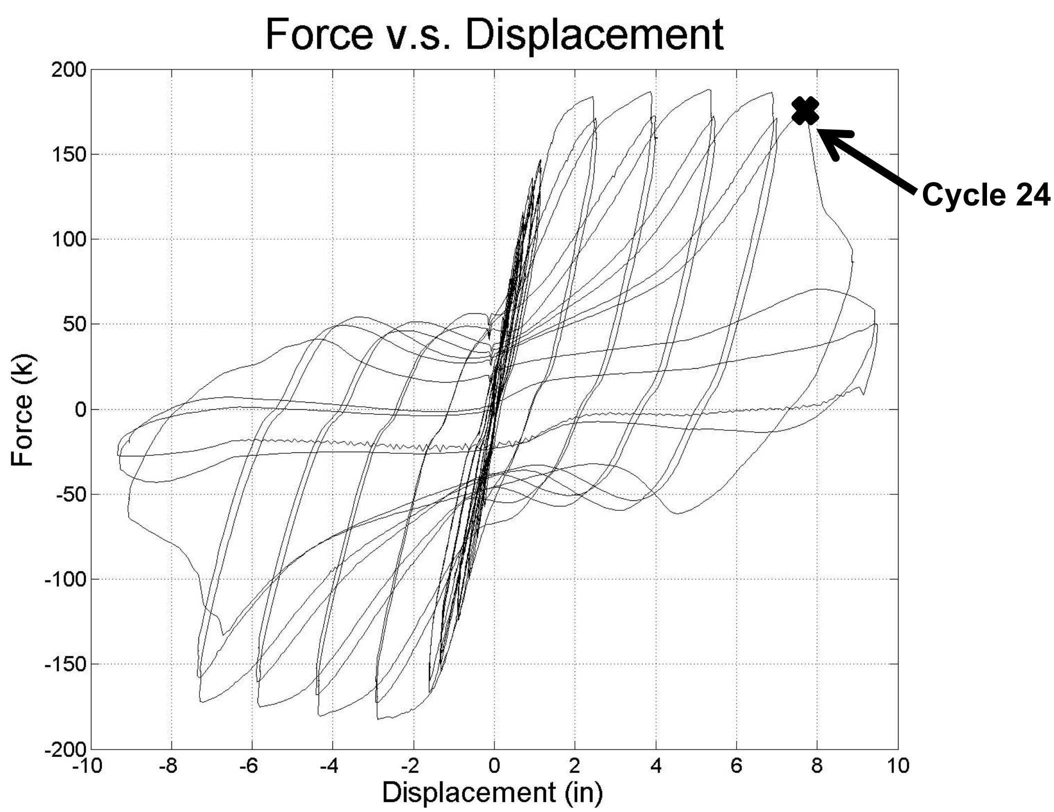

Figure 9.11 Force versus displacement plot.

The moment versus drift ratio plot in Figure 9.12 shows a similar result. In this plot, the horizontal axis is drift ratio, which is the ratio of horizontal displacement and actuator height. The vertical axis measures moment. Notice that a comparison was made between actuator moment and total moment, which include P-Delta effect. From the figure, the total moment capacity at that height was about 23,000 k-in, or 1917 k-ft, in the positive direction, and about 22,000 k-in, or 1833 k-ft in the negative direction. The actuator moments are a little lower. Thus, the moment capacities in both directions are approximately the same. As the drift ratio got larger, the load capacity remained essentially constant until Cycle 24, during which the initial tear occurred. After that, the capacity dropped significantly with only a small drift increment. This result indicates, again, the initial tear, instead of buckling, was the main cause of capacity drop.

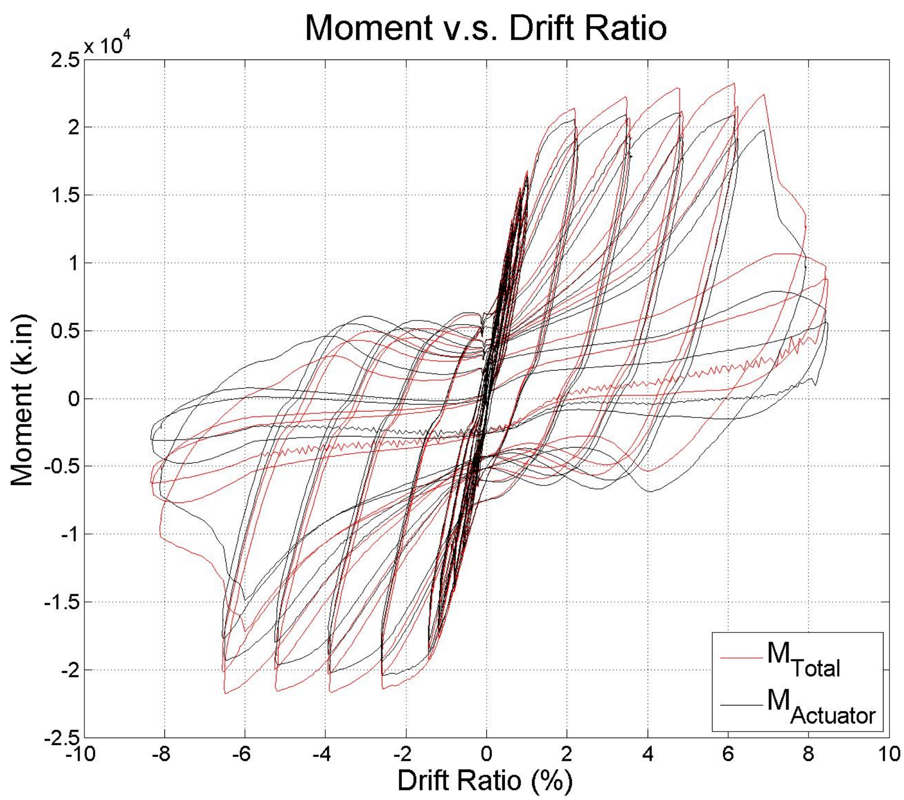

Figure 9.12 Moment versus drift ratio plot.

The next result to be examined is the relationship between drift and strain. With a yield stress of ~50 ksi and modulus of 29,000 ksi, the yield strain of the tube is about 0.0017, which is indicated by red dotted line in Figure 9.13. The yield strain was reached at about 0.8 to 1.0% drift. Notice that a positive strain value corresponds to tension, while a negative strain value represents compression. These strain patterns make sense because one side is in tension while the other side was in compression under lateral loading. In addition, the strain switched signs when the column was loaded in the other direction.

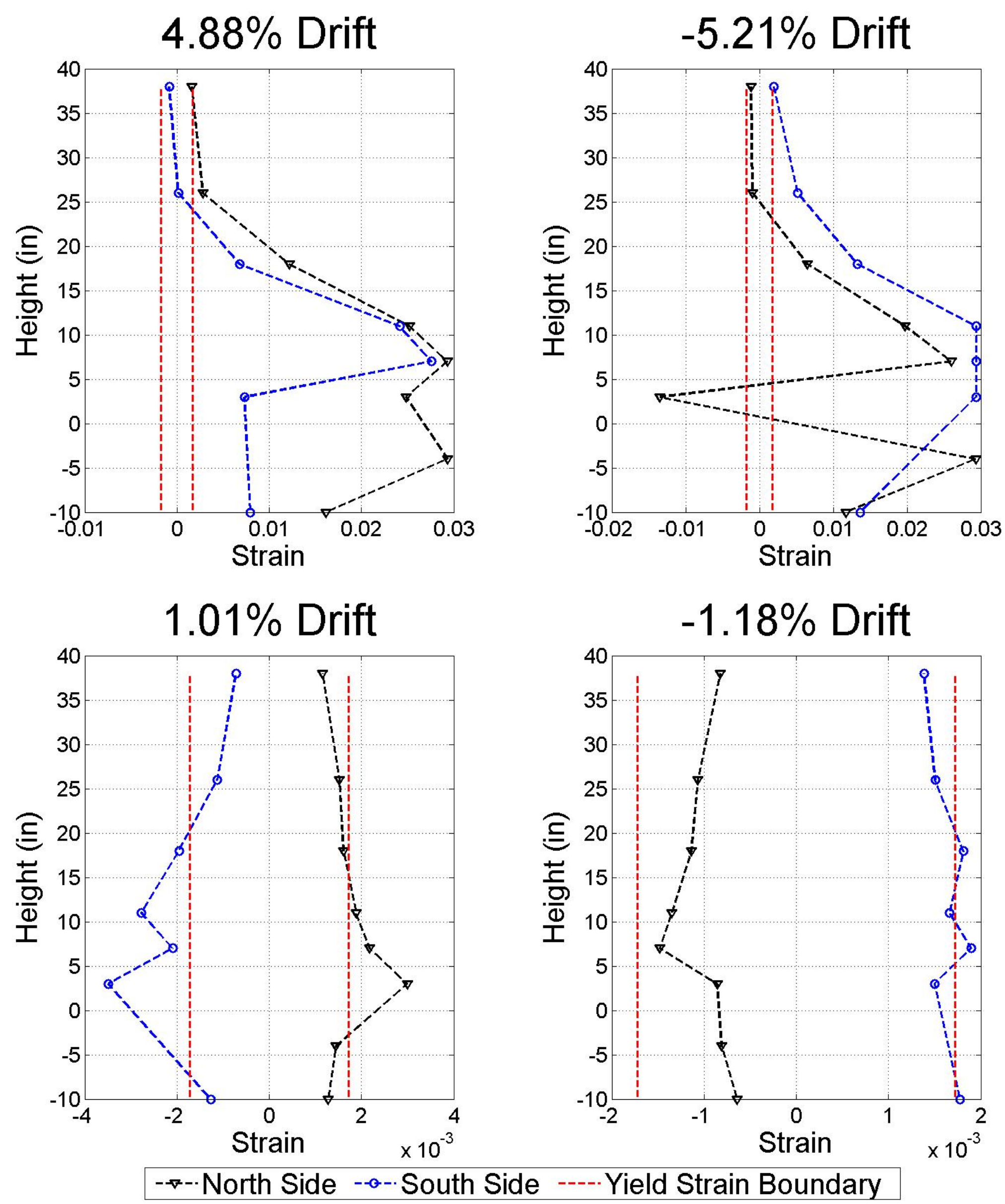

Figure 9.13 Determination of yielding drift.

After exceeding the yielding (Figure 9.14), the strain curves appear to be randomly distributed. However, the distinct pattern at 8.5% drift can be explained as following. For the strain gauges located 10 in. below the footing, the outside face of the tube is always in excessive tension, thus a positive strain makes sense. For the strain gauge at 3 in. level, it is located on top of the outside face of the buckling region, and thus in compression. A negative number also makes sense.

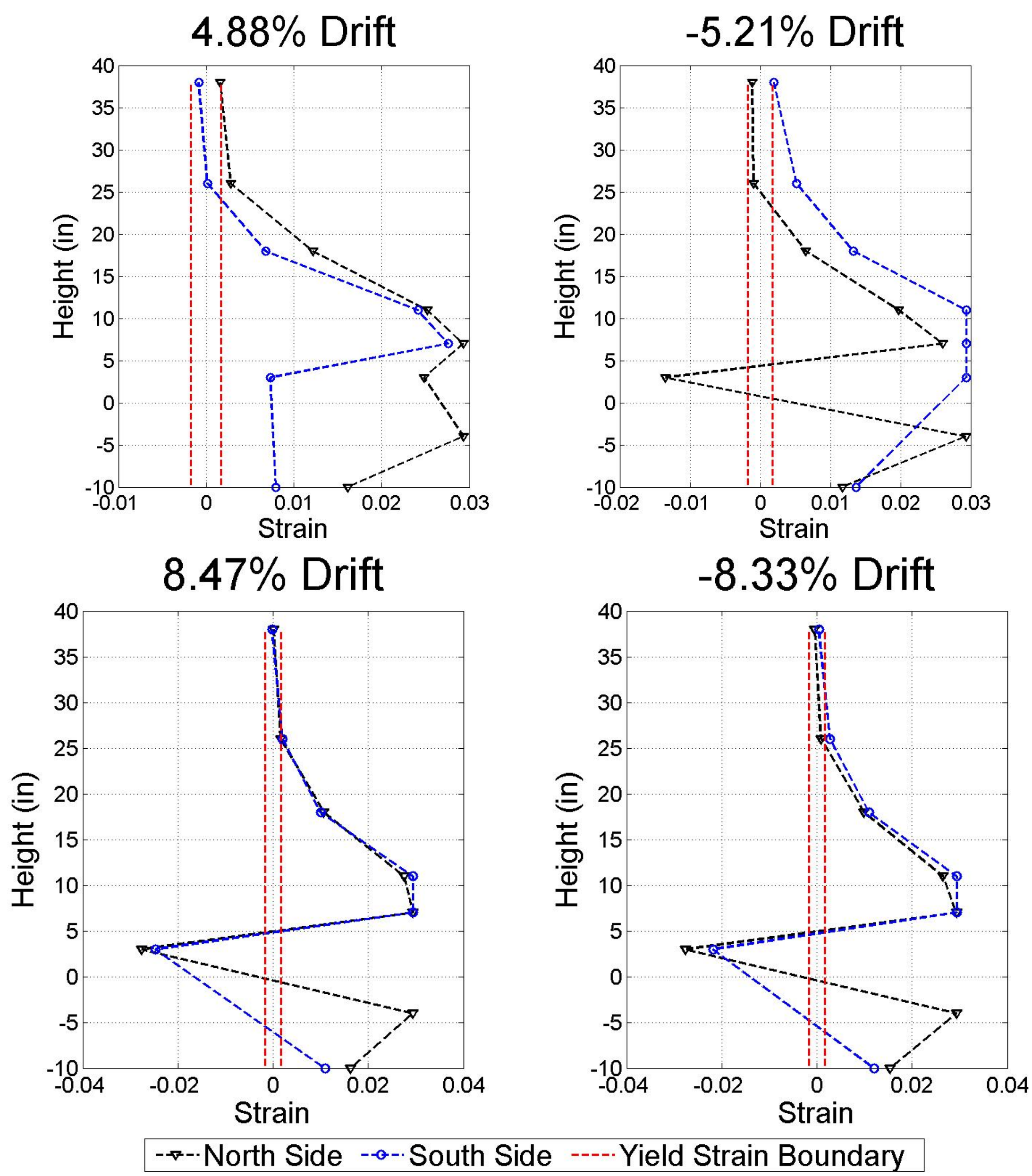

Figure 9.14 Sample strain plots after yielding.

9.5.2 Optotrak Data

The main purpose of the optotrak system is to observe the local buckling at the CFT connection. Figure 9.15 is a sample section of the tube. Since the graph is exaggerated, the middle portion of the tube is partially removed. As a result, the left plot shows the deflected shape in the south boundary, and the right plot shows the one in the north. The red dotted line shows the original tube position, while the black solid line shows the deflected position. The corresponding drift ratio is the title of the plot. In addition, some of the data points were missing (blocked LED's) due to inevitable human interference and tube deterioration in the test.

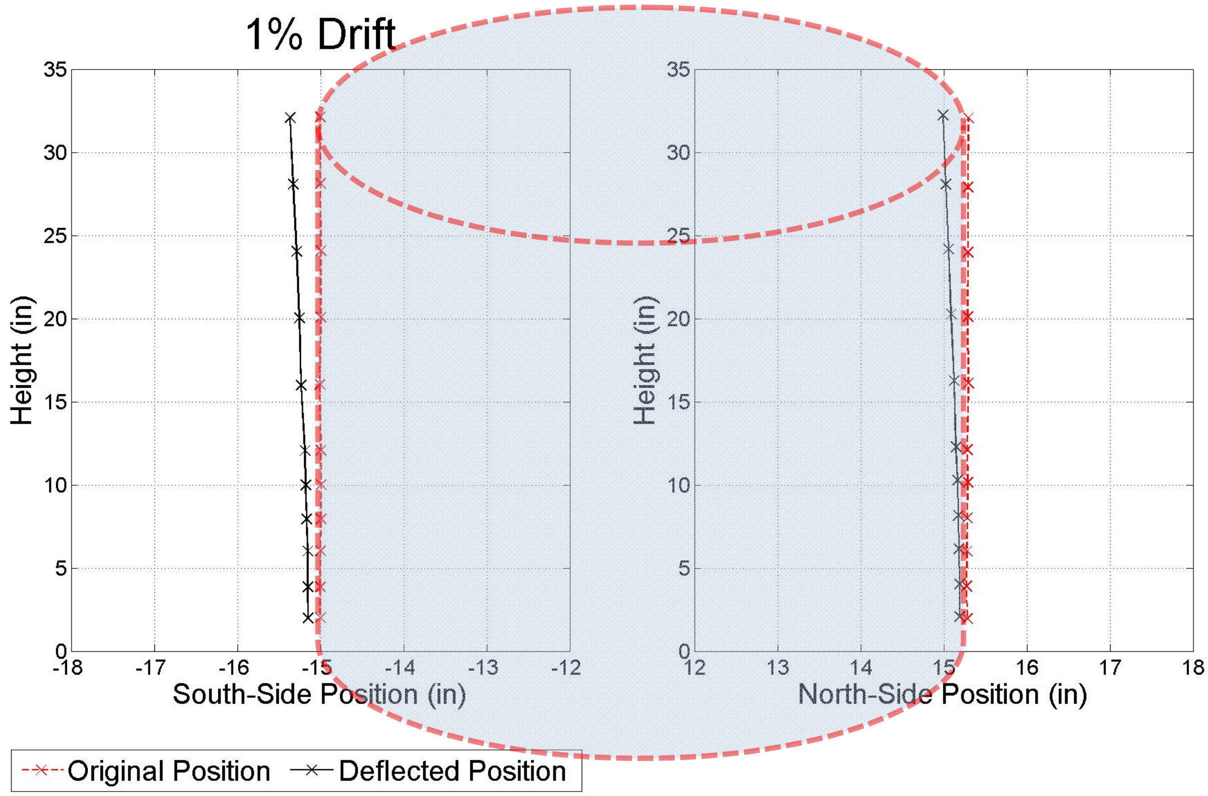

Figure 9.15 Sample Optotrak section plot.

Before discussing buckling, let's define observable buckling. In this test, the tube was about ¼ in. thick. Let's define the initial buckling occurred when the tube buckled twice as much as the tube thickness, which is about ½ in., then initial local buckling at the bottom of the column was observed at about 2.3% drift in both directions, as is shown in Figure 9.16. Notice that a positive deflection is to the north due to the nature of the instruments. By examining the subsequent plots, we can tell that the maximum vertical uplift before tearing occurred (Cycle 23) was about 1.3 in. on the tension side, while the maximum subsidence was about 0.5 in. on the compression side. At this point, the drift had already reached 6.2%.

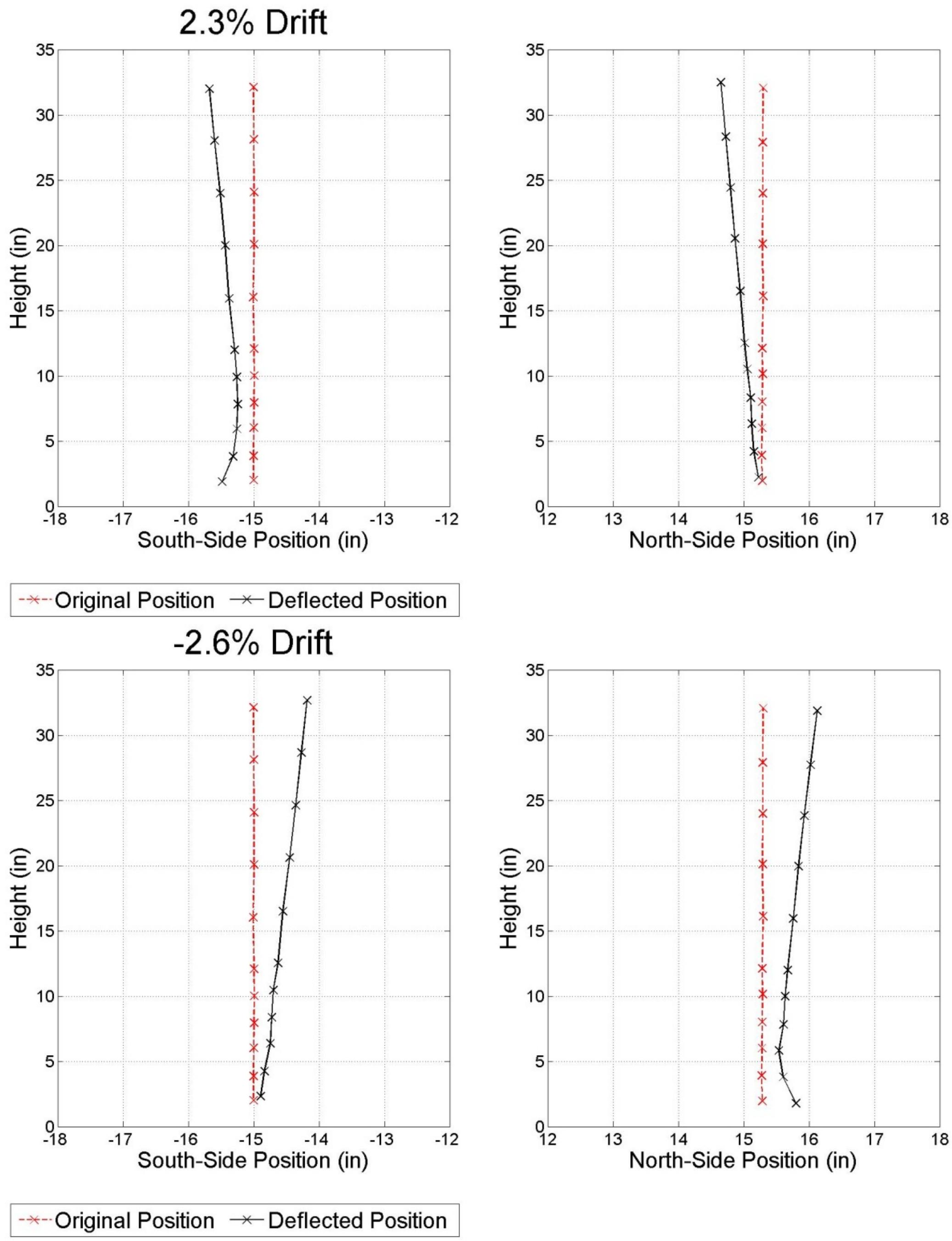

Figure 9.16 Optotrak section plots showing initial buckling.

Figure 9.17 shows the tube position right after final tearing (Cycle 26). Notice that after tearing occurred, the vertical deflection on the tension side reached about 2.1 in., which is greater than the one right before initial tearing. However, the maximum subsidence on the compression side was only around 0.6 in, which is about the same as the one before initial tearing.

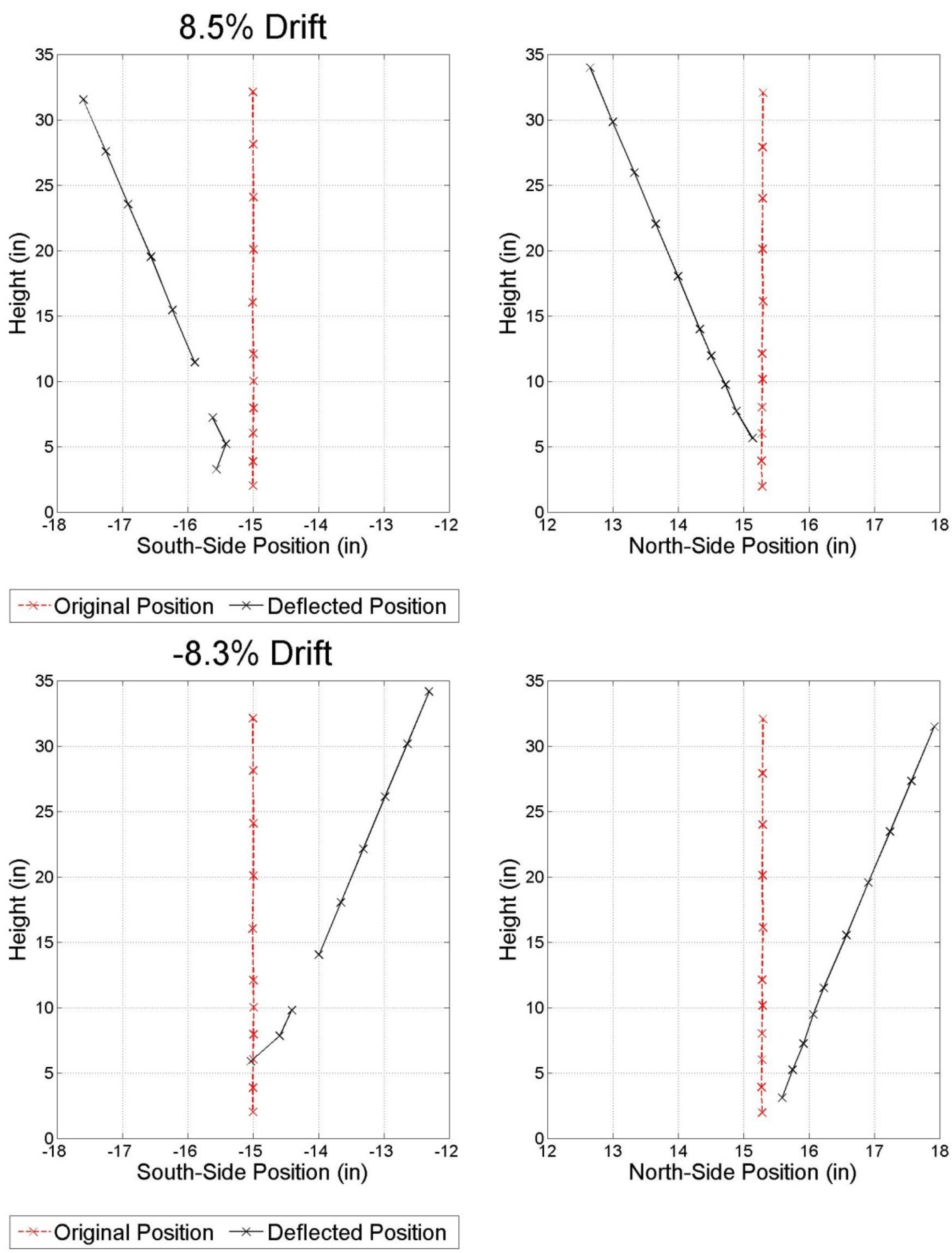

Figure 9.17 Optotrak section plots showing final tearing.

Another Important observation obtained from the Optotrak data is residual buckling. One measure for residual buckling is the residual displacement, which is the elongation of the tube when it comes back to the original position after several complete cycles of lateral loading. In Figure 9.18 is a simple illustration, and the residual displacement is represented by ΔZ.

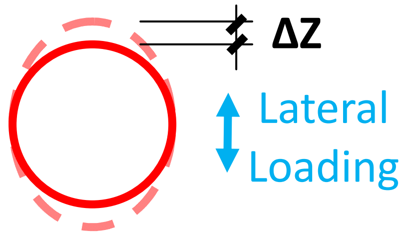

Figure 9.18 Plan view of residual displacement.

In the test, residual displacement was only significant at the buckled region, and thus measuring the residual displacement at the level of the buckled region, or about 2 in. above the footing surface, is a perfect illustration of residual buckling. Figure 9.19(a) shows the residual displacement (ΔZ) with respect to each cycle at 2" above the footing surface. The red solid line shows ΔZ at the beginning of each cycle, and the black solid line shows ΔZ at the end of each cycle. It makes sense that the red line is one cycle behind the black line because the end of Cycle # (n) is the beginning of Cycle # (n+1). The maximum ΔZ is about 1.0 in. in the north, and 0.8 in. in the south.

Above the 2 in. level, the residual displacement drops to essentially negligible. Figure 9.19(b) shows that ΔZ_{max} drops to about 0.12 in. in the north, and 0.4" in the south. Above the 4 in. level, the residual displacements are essentially zero.

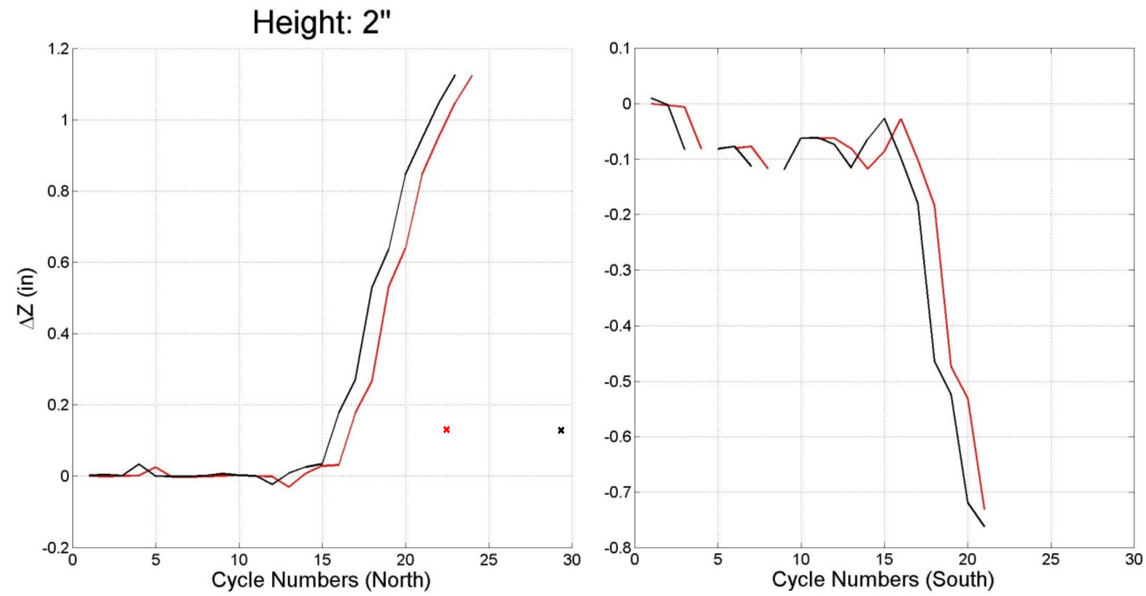

(a). At 2 in. level.

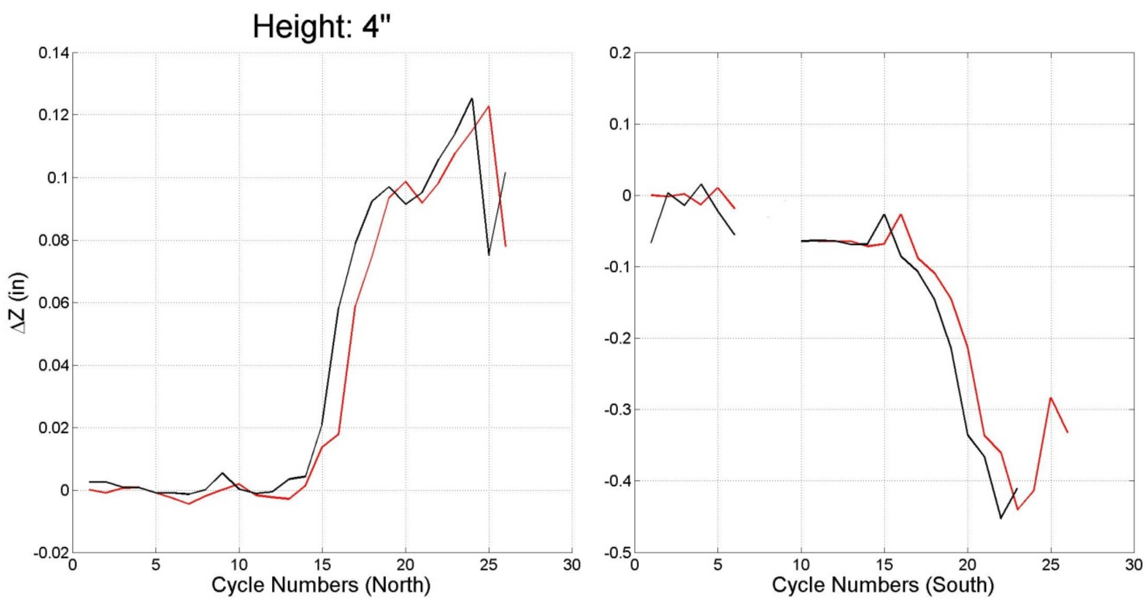

(a). At 4 in. level.

Figure 9.19 Residual displacement versus cycle numbers.

Lastly, let's examine the relationship between vertical uplift at the centerline of the tube and horizontal drift. The vertical uplift values along the centerline are obtained by averaging the vertical displacements on both principal sides. Figure 9.20(b) shows the relationship in both the 2 in. level and the 4 in. level. By comparison, it can be observed that the 4-in.-level plot is more complete. Since a lot of the data points were missing at the 2 in level, and the results obtained at each level are approximately the same, the results at the 4 in. level will be discussed instead. At maximum drift, which is about 8.5%, the maximum uplift at the centerline (ΔY) was about 0.6 in. in both principal directions.

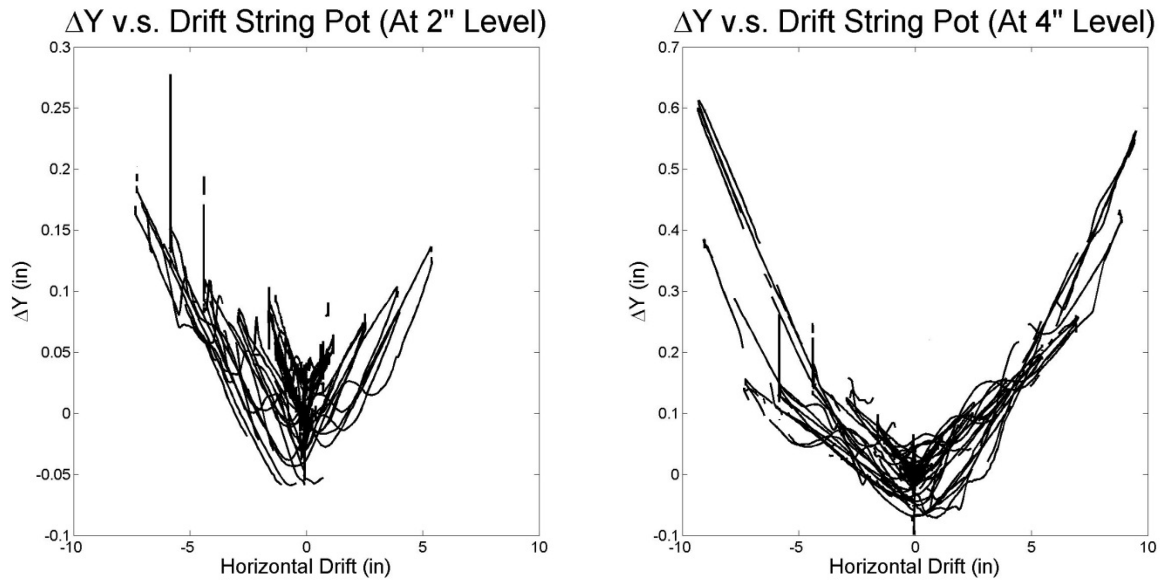

(a) (b)

Figure 9.20 Vertical displacement (ΔY) versus horizontal drift.

9.6 CONCLUSIONS

The following conclusion could be drawn from this test.

1. For a CFT column with a large D/t ratio, it still behaves fairly ductile. The 8% maximum drift is an eloquent proof.
2. As a newly-adopted instrument, the Optotrak Certus motion capture system works exceptionally well during the test, after overcoming two major problems. Overall, it captures the deflected shapes and buckled shapes well and thus advances the study.
3. Buckling is not a major concern in capacity deterioration. Both the force and moment resisting capacity does not drop even though buckling has already taken place.
4. The length of the buckle and the magnitude of the "out-of-surface" deformation appear to be a strong function of tube thickness, but not as much for the tube diameter.

5. The AISC Plastic Stress Distribution Method under-predicts the moment capacity of the 30 in. CFT, even though the D/t ratio = 120 with the limiting D/t ratio (per AISC) for this tube of 87 (120/87 = 1.38).

ACKNOWLEDGMENTS

This research was supported by Pacific Earthquake Engineering Research (PEER) Center. Funding was provided by NSF Network for Earthquake Engineering Simulation (NEES). The author would like to thank Professor Charles Roeder and Professor Dawn Lehman for their mentorship, and graduate student Kenneth O'Neill for his detailed instruction and great support, all other related undergraduate and graduate students for their generous support in the lab, and finally Heidi Faison at UC Berkeley for her support.

REFERENCES

American Institute of Steel Construction (2005). *Specification for Structural Steel Buildings*, Chicago, IL.

Kingsley, A. (2005). Experimental and analytical investigation of embedded column base connections for concrete filled high strength steel tubes, a thesis submitted in partial fulfillment of the degree of Master of Science in Civil Engineering, University of Washington, Seattle, WA.

Lee, J. (2011) Experimental investigation of embedded connections for concrete-filled steel tube columns subjected to combined axial-flexural loading, a thesis submitted in partial fulfillment of the degree of Master of Science in Civil Engineering, University of Washington, Seattle, WA.

Williams, T. (2007). Experimental investigation of high strength concrete filled steel tubes in embedded column base foundation connections, a thesis submitted in partial fulfillment of the degree of Master of Science in Civil Engineering, University of Washington, Seattle, WA.

10 Earthquake Resiliency: Managing Waste Water Sector Vulnerabilities through Green Infrastructure and Related Policies

JASON NAANOS

ABSTRACT

The disposal and treatment of waste water are essential processes for modern urban communities. Waste water infrastructure not only provides citizens with proper waste water services, but also prevents diseases from spreading. However, the effects of a powerful earthquake strong enough to disrupt infrastructures could potentially pose devastating threats and vulnerabilities to any urban area. I address how environmental land use planning with "green" infrastructure and community cooperation through environmentally-conscious related policies with the local government create a stronger waste water infrastructure as well as a more resilient Seattle in terms of economics, the environment, and social conditions.

10.1 RELATED POLICIES

10.2 INTRODUCTION

Critical infrastructures are necessary for the everyday tasks we perform, and without them, the tasks would be impossible to undertake. Table 10.1 is a list of all critical infrastructures according to the federal government. According to the Department of Homeland Security (DHS), critical infrastructure are "the assets, systems, and networks, whether physical or virtual, so vital to the United States that their incapacitation or destruction would have a debilitating effect on security, national economic security, public health or safety, or any combination thereof." Thus, the federal, as well as local governments, scrutinize efforts to help not only protect, but strengthen infrastructures.

Table 10.1 List of U.S. critical infrastructure [DHS 2007].

Critical Infrastructure		
Agriculture and Food	Banking and Finance	Chemical
Commercial Facilities	Communications	Critical Manufacturing
Dams	Defense Industrial Base	Emergency Services
Energy	Government Facilities	Healthcare and Public Health
Information Technology	National Monuments and Icons	Nuclear Reactors, Materials and Waste
Postal and Shipping	Transportation Systems	Water

As one can observe from viewing the table above, there are several critical infrastructures to account for. However, some are more necessary to the overall well-being of the health of the general human population. These are called "life-line" systems and include: electrical power, natural gas, liquid fuel, highways, railroads, airports, marine facilities, water, and waste water [USGS 2010]. My study will focus on the strengthening and protection of one of the most necessary infrastructures for urban areas around the world: waste water.

The focus of engineering mitigation methods to accommodate the possibility of an earthquake is a topic that has been discussed extensively. Engineering advancements have made great strides to ensure safety and security and to increase the resiliency of even the most vulnerable waste water pipes throughout cities. However, waste water infrastructure protection and resiliency, just like any other infrastructure, is beyond purely structural stability and sturdiness. With coordination from local governments and knowledge instilled within communities, resiliency of infrastructures can be enhanced.

In order for local governments and communities to respond, prepare, and improve their communities from earthquake vulnerabilities related to the waste water sector, this study suggests using "green" initiatives through land use management and policies, enhancing the protection of waste water systems while simultaneously improving the preparedness of a community. Previous studies have looked into environmental benefits of green infrastructure, not necessarily how it makes cities more resilient. This report will examine the effects of green infrastructure and related policies on waste water infrastructure (pipes, drains, and waste water treatment plants) as well as the resiliency effects on the city of Seattle's economy, environment, and citizens.

10.2.1 Purpose Statement

This report summarizes my research on the effects of low-impact development (green infrastructure), an alternative method to storm water management, and programs and policies that encourages environmental and sustainable efforts that increase the resiliency of waste water infrastructure as well as the city itself from earthquake hazards. Although the study was developed to further research of incorporating the natural environment with structural infrastructure (and the built environment) of earthquake prone vicinities, I chose to focus on Seattle for the setting of the research due to its progressive stance on environmentally-friendly programs and the proximity to the research center where I was based at; the University of Washington, Seattle (UW).

10.3 RESEARCH DESIGN

Data were collected in two different fashions: literature review/analysis and contacting industry specialists.

In approaching the research, I sought to gain an understanding of the issues and to learn from relevant experts and the Seattle experience. The documents I reviewed focused on: disaster resilience, earthquake mitigation, the water sector, functions of waste and storm water systems, sustainable infrastructure, green and low-impact development, secondary hazards of earthquakes and the geography of Seattle.

During the data collection period, several entities and individuals were contacted, either through electronic mail, phone calls, or in-person. Note taking was the only form of data collecting at this period. No recordings were developed. Entities contacted included: United States Environmental Protection Agency: Region 10 (USEPA), Seattle Public Utilities (SPU), Seattle Department of Planning and Development (DPD), the Office of Emergency Management (Seattle), Washington State Department of Ecology, the Cascadia Green Building Council, and University of Washington Department of Planning faculty and graduate students.

Individuals were selected through internet research and "snowball sampling," receiving contact information from previous contacts. Interviews lasted no longer than 30 minutes. Based upon their expertise, interviewees were asked questions from the following topics:

- Decision-making and land use planning for green infrastructure
- Earthquake mitigation strategies
- Emergency earthquake preparedness
- Connection(s) between green infrastructure and hazard mitigation
- Vulnerabilities of green and conventional infrastructure
- Policy enforcement (local and federal)

10.4 BACKGROUND

By way of background, it is useful to consider the effects of earthquake hazards for infrastructure and the design and location of conventional waste water infrastructures.

10.4.1 Pacific Ring of Fire

According to the United States Geological Survey [USGS 1999], the Pacific Ring of Fire, also known as the Circum-Pacific belt, is an area that surrounds the Pacific Ocean (see Figure 10.1) and is a zone where over 90% of the world's earthquakes occur. Due to the constant shifting of the Pacific Ocean Plate underneath the ocean floor, geologic and seismic activity is prevalent within the area.

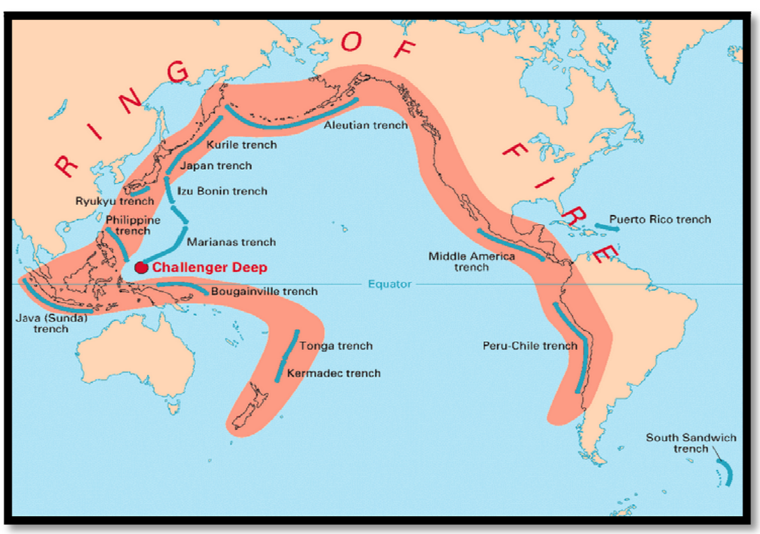

Figure 10.1 Map of the Pacific Ring of Fire [USGS 1999].

On top of the constant movement of the ocean floor, several cities along this region also deal with seasonal rainfalls. Table 10.2 shows the annual rainfall totals of urbanized areas along the rim. Rainfall has the ability to: add weight to slopes which causes stress on the soils, leading to slope instabilities; oversaturation of loose sediment; or transforming soil into plastic states or even liquids which provides little to no load-bearing ability [Nelson 2011]. With the combination of earthquake potential and severe rain storm seasons throughout much of the countries that surround the Pacific Ocean, it is important to see how cities manage its storm water, which goes along with waste water management as well. By observing the waste water infrastructure, policies, and possible hazards caused by seismic activity, we can develop a better understanding of the weaknesses and issues that make this sector vulnerable to earthquakes.

Table 10.2 Cities around the Pacific Ring of Fire and average rainfall totals, (weather.com).

City	Avg. rainfall/year (inches)
Manila (Philippines)	83.1
Guatemala City (Guatemala)	83.0
San Salvador (El Salvador)	68.3
Jakarta (Indonesia)	65.2
Kobe (Japan)	51.9
Quito (Ecuador)	47.6
Seattle, Washington (US)*	**38.2**
Mexico City (Mexico)	33.5
Christchurch (New Zealand)	25.5
San Francisco, California (US)	22.3
Los Angeles, California (US)	15.1
Santiago (Chile)	12.3

***Case study city**

10.4.2 Traditional Waste Water Infrastructure

The importance of protecting and increasing the resiliency of critical infrastructures can be the difference between a minor event and a catastrophe. One of the most important sectors of any nation's critical infrastructures is the Water Sector. Drinking water supplies and waste water systems are vulnerable to a variety of attacks, including contamination with deadly agents and physical and cyber-attacks. If these attacks were to occur, the result could be large numbers of illnesses, casualties, or a denial of service that would also affect public health and economic vitality. Critical services such as firefighting and health care (hospitals), and other dependent and interdependent sectors such as energy, transportation, and food and agriculture, would suffer negative impacts from a denial of Water Sector service [DHS 2007].

A population's ability to obtain water from a fresh-water source is the difference between sustaining livable conditions and moving on to a region where the resource is available. However, the exponential growth of populations worldwide is not only leading to less space to move to, but also potable water shortages and the inability to treat waste water in a sustainable and effective fashion. These in turn lead to harmful effects that may disrupt populations' current ways of life. Already apparent in several developing countries, human-beings are witnessing the fatal effects of aging sewer lines and outdated methods of managing waste and storm water. With sewage systems reaching their designed life expectancy and the lack of advancing methods of dealing with storm water in the United States, the effects of an earthquake can lead to devastating secondary-effects that may be difficult to recover from.

10.4.2.1 U.S. History of Traditional Waste Water Infrastructure

During the development of waste and storm water infrastructure throughout cities in the US, the main strategy was to develop systems to convey waste water (including storm water) away from the more populated city centers and residences into nearby waterways to avoid deadly outbreaks of disease. During the late nineteenth century, bacterial analysis confirmed the link between sewage pollution in rivers and epidemics of certain diseases. As a result, views on the safety of discharging untreated waste water directly to receiving waters began to shift [USEPA 2004].

The first step municipalities and cities took to implement waste water infrastructure was to decide the design of their systems. Two designs were primarily used throughout the U.S.: (1) separate sewer systems (SSSs); and (2) combined sewer systems (CSSs). The SSSs take domestic, commercial, and industrial waste waters to treatment plants, while a separate storm drain system takes in runoff from the street, into the gutter, and enters the system through an opening in the curb called a catch basin. Catch basins serve as the neighborhood entry point to the journey into the assigned waterway. However this system receives no treatment or filtering process [City of Los Angeles 2011]. See Figure 10.2. The CSSs are single-pipe sewer systems that convey sanitary waste waters (domestic, commercial and industrial) and storm water runoff to a publicly owned treatment works facility [USEPA 1999]. See Figure 10.3.

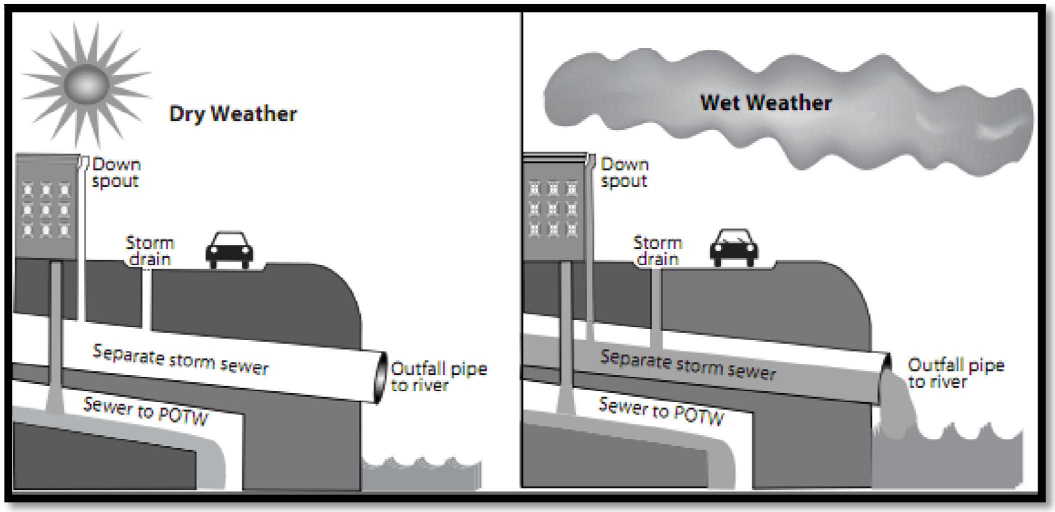

Figure 10.2 Example of separate sewer system [USEPA 2004].

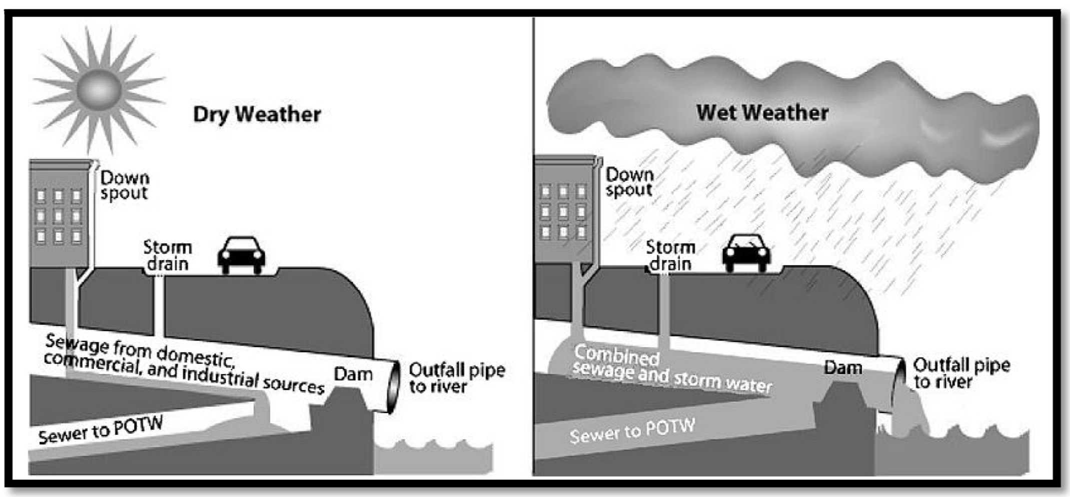

Figure 10.3 Example of a combined sewer system and overflow [USEPA 2004].

10.4.2.1.1 Separate sewer systems (SSSs)

Despite higher costs to develop, sanitary sewer systems are located in all fifty states and is the more popular design-system nationwide than combined systems. Although the higher costs come from creating a dual-pipe system, SSS treatment costs are much less, since storm water is transferred straight to waterways. Despite the separate systems, sanitary sewer outflows (SSOs) still occur and discharge out of manholes and onto city streets, sidewalks, and other terrestrial locations from: blockage, structural/mechanical/electrical failures, collapsed or broken sewer pipes, insufficient conveyance capacity, vandalism, and/or high levels of infiltration and inflow during wet weather [USEPA 1999].

10.4.2.1.2 Combined sewers systems (CSSs)

This type of system provides a much more effective method of accumulating and transferring both waste and storm water together. However, the backup of systems, especially in wet weather, create a dilemma for treatment plants, eventually leading to combined sewer outflows (CSOs). The amount and frequency of outflow differ from city to city and outflow to outflow. Some discharge rarely, while others activate during every heavy rainfall [USEPA 1999]. When constructed, CSSs were normally designed to hold three to five times the average dry weather flow [USEPA 1999]. However, with more open, permeable areas being paved and built over, the amount of runoff builds, creating a much higher volume and flow of water. State and local authorities have not allowed construction of new CSSs since the first half of the century [USEPA 1999]. Most of these systems are located in the Northeast, Midwest, Southeast, and Pacific Northwest region.

10.4.3 Storm and Waste Water Impacts from Earthquakes

Given that the waste water infrastructure in parts of the United States and countries around the Pacific Rim is in terrible conditions, the impacts of an earthquake on a system on could prove to be disastrous, depending on the severity of the earthquake, emergency preparedness, and overall strength and resiliency of the system. With U.S. and world economies in shambles, the necessary funding and ability to undertake retrofits may not be possible in time to handle seismic activity of overwhelming strength.

The following are possible earthquake impacts to waste water infrastructures:

- **Floating sewers -** occurs due to earthquake-induced liquefaction. These instances occur when the sewer is within a liquefiable area (below groundwater) in combination with a change in grade that will impact gravity sewer operation and maintenance. In event of floatation, sewer may fail but continue to function short term. However, replacement of pipe is required for long term stability. Figure 10.4 is an example of a floating sewer from the most recent earthquake in 2011 in Japan.

➢ **Sewer Leaks/Collapsed sewers –** occurs from intense shaking, as well as a possible pipe failure due to age and/or wear-and-tear from corrosiveness. Sewer leaks are difficult to detect and usually require TVing. However, may continue to function in the short term. Figure 10.5 is an example of engineers investigating a crack in the waste water system leading to a potential leak from the 1995 Kobe earthquake. On the other hand, collapsed sewage pipelines require immediate response to avoid public health issues and contamination of ground water by causing sewage backups and/or overflows as well as sinkholes.

➢ **Treatment plants vulnerable to liquefaction and shaking damage** – occurs when plants are located in low-lying liquefiable areas. Effects may stall treatment of water leading to outfalls and contamination of open water ways. Figure 10.6 shows the damage done from liquefaction to the Higashinada waste water treatment plant from the 1995 Kobe earthquake [Ballantyne NA].

Figure 10.4 Example of a floating sewer from 2011 Japan earthquake [Towhata 2011].

Figure 10.5 **Example of sewage leaks from 1995 Kobe earthquake [Ballantyne NA].**

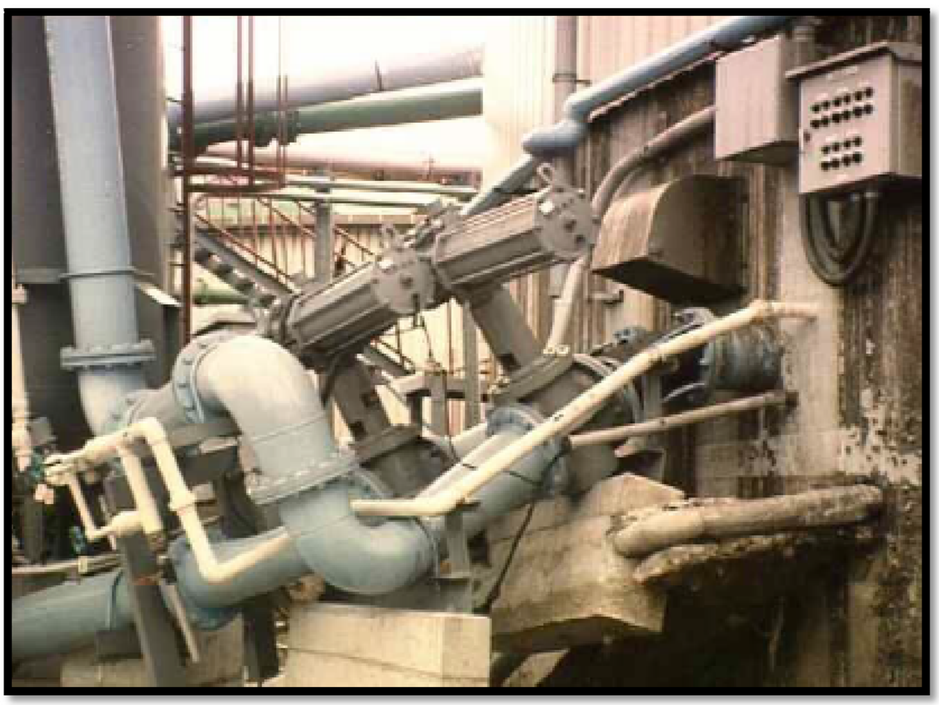

Figure 10.6 **Higashinada treatment plant from 1995 Kobe earthquake [Ballantyne NA].**

10.4.3.1 Consequences of a Non-Functioning System

The functions of a waste water system that both convey sanitary and storm waters to appropriate destination points are among the most important functions a city requires. Depending on the severity of the earthquake effects a city absorbs, failures to the system could lead from mild to disastrous outcomes. The local, federal, and world economies would be affected by possible business and trade interruptions. The environment would be affected as well. Untreated water could infiltrate into ground water used for drinking, as well as backflow or outflow into urban centers and nearby waterways. The population would observe the largest disadvantage. Reliance on waste water infrastructure providing citizens with everyday needs such as flushing a toilet, washing clothes, taking showers, and more would be jeopardized as well as possible property damages not only to the system but to household, business, and industrial units.

10.5 CASE STUDY BACKGROUND: SEATTLE

Established in 1851, Seattle is located in the Pacific Northwestern portion of the United States in the state of Washington and is home to a population of over 602,000 residents (City of Seattle 2005, *see* Seattle's population and demographics). Seattle is surrounded by two water bodies; the salt waters of the Puget Sound to the West and the fresh waters of Lake Washington to the East. The City also lies between two mountain ranges, the Olympics to the West and the Cascade Mountain Range to the East. Figure 10.7 is a map of Seattle and its surrounding geographic elements.

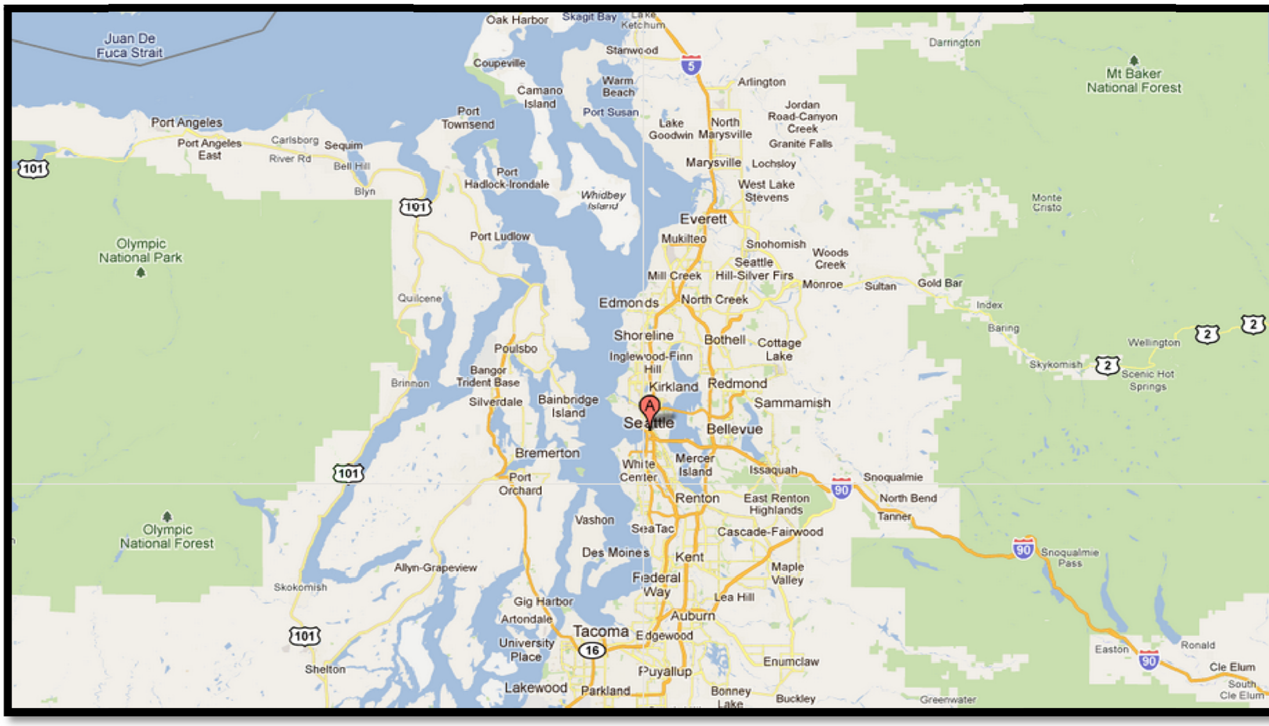

Figure 10.7 Map of Seattle (Google).

The Seattle Fault Zone is a combination of "thrust and reverse" faults that travel through the heart of downtown Seattle. See Figure 10.8. However, experts are not necessarily certain of the amount of earth covering this fault line. Seismic geologists who study and have studied the Seattle Fault all agree that the areas within downtown Seattle as well as the adjacent communities are all at risk from the fault line. This fault runs through to the southwest Washington Cascade foothills.

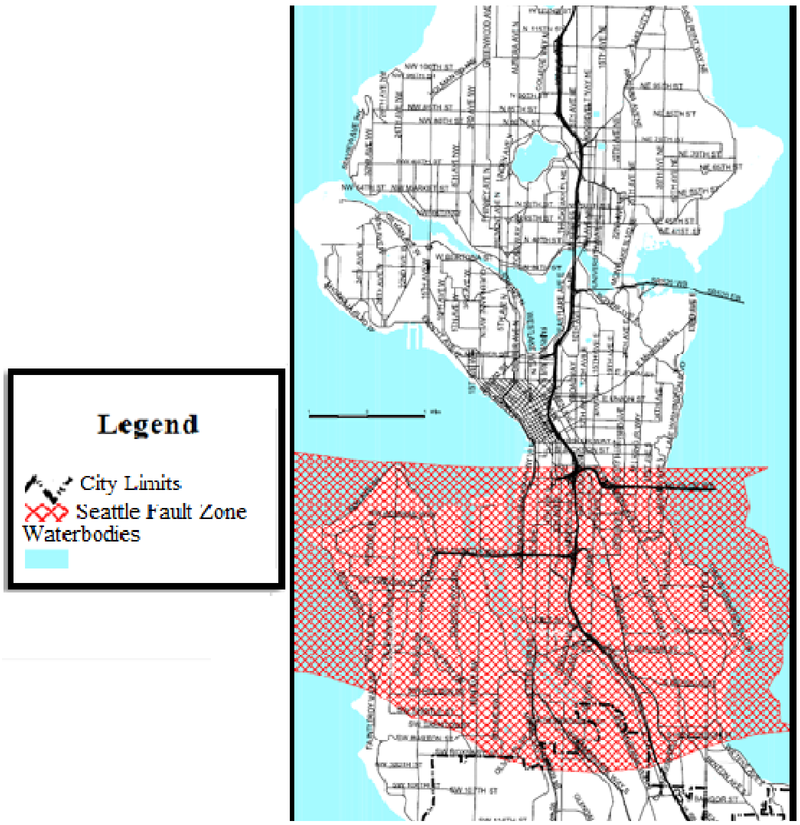

Figure 10.8 Seattle fault zone map [City of Seattle 2004].

10.5.1 Natural Environment

The natural environment of Seattle is fairly active in geologic terms. The process of glaciation has been occurring around Western Washington for the past two million years. Glaciation is a process where large sheets of ice move slowly and then melt back. When the large sheets move towards land, they grind against the Earth's surface, leaving sand, gravel and silt in their wake. The ground layers left by the glaciers are irregular, contributing to slope instability and landslide risk [City of Seattle 2004]. Although natural occurrences such as glaciation, windstorms, earthquakes, and volcanoes all lead to slope instability, constant development and disturbance of the natural environment from human beings have been an increasing motive for ground failures as well. The hilly topography of Seattle, seen in Figure 10.9, can lead to disastrous ground effects if not managed appropriately. Contour lines that are close together indicate a steep slope. Contour lines that have a wide distance between them indicate relatively level terrain.

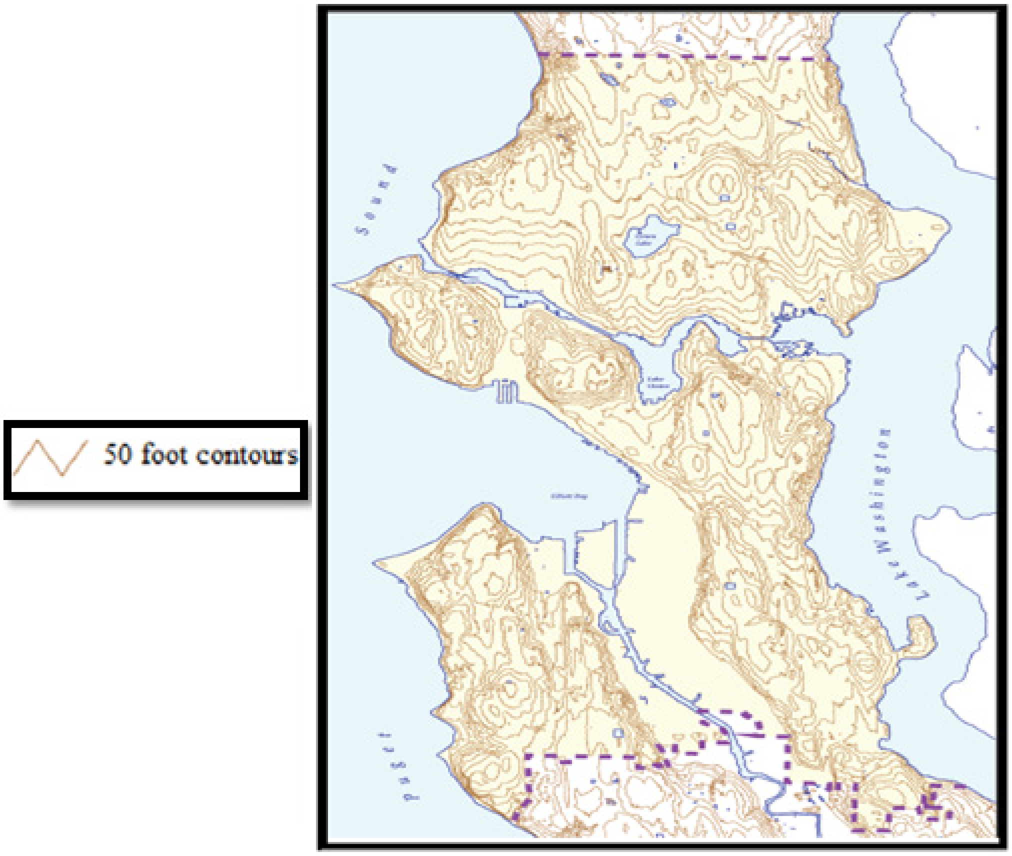

Figure 10.9 Contour map of Seattle [City of Seattle 2004].

The climate of Seattle is controlled by wind patterns from the Pacific Ocean to the West. Dramatic seasonal changes in the city are rare. Rainfall is synonymous to the city of Seattle, however in comparison the city receives much less rainfall than other cities in the eastern portion of the U.S. The most amount of rainfall occurs between mid-October and March, while temperatures remain mild for the summers and winters [City of Seattle 2004]. Snowfall is not a frequent event; however, it is a possibility that should be taken into account.

10.5.2 Built Environment

Despite being established in the mid-nineteenth century, it took the city of Seattle nearly forty years to develop its first public waste water system, triggered by exponential population growth and typhoid outbreaks near the Lake Union vicinity [City of Seattle 2010, see Restore our waters]. However, similar to cities developing waste water systems, the strategy of Seattle was to transport waste and storm water away from the more populous areas and into waterways nearby.

Not until 1947 were studies conducted to study the effects of raw sewage which spurred construction of waste treatment plants to treat locally discarded waters in the 1950s and 1960s [City of Seattle 2010, see Drainage and waste water management].

10.5.2.1 Outflow Issues

During the development stages, the design concept Seattle chose to implement was the combined sewer system (CSS). Although effective at first in the earlier stages of the twentieth century, the ever-growing population and the amount of impervious and built environment expansion began to have effect on the drainage lines, especially during heavy rainstorms; eventually leading to CSOs discharging at record rates and having devastating effects to the water quality and overall environment around Seattle's local waterways and the Puget Sound. Not until the latter half of the 20th century was the issue of CSO-reduction studied, when in 1960, the volume amount of CSOs recorded was over 34 billion gallons [City of Seattle 2010, see Drainage and waste water management].

Since the 1960 recordings of CSOs, Seattle has been on the forefront of reducing the amount of outflows and complying with Federal mandates, most notably the National Pollutant Discharge Elimination System (NPDES) provision of the Clean Water Act of 1972. NPDES controls the amount of a state's water pollution by regulating point sources that convey contaminants into national waterways. Along with the Clean Water Act, NPDES is monitored and regulated by the U.S. Environmental Protection Agency (USEPA), which in turn directs state agencies to enforce and encourage compliance for local jurisdictions. For the state of Washington, the Department of Ecology is responsible for the state's compliance of the federal mandate.

In order to curb the amount of CSOs, new waste water infrastructure, SSSs and partially separated sewer systems were constructed. Figure 10.10 is a current map of Seattle's service area and sewer system type. Table 10.3 represents a more-detailed summary of the map represented in Figure 10.10. Beginning in the 1970s, Seattle began constructing partially separated sewer systems. These systems were designed to take storm water from streets and convey that water to outflows, similar to SSOs. However, the difference between the partially separated systems and the SSSs is the partial systems did not take storm water from the commercial, industrial or residential structures [City of Seattle 2010, see Restore our waters].

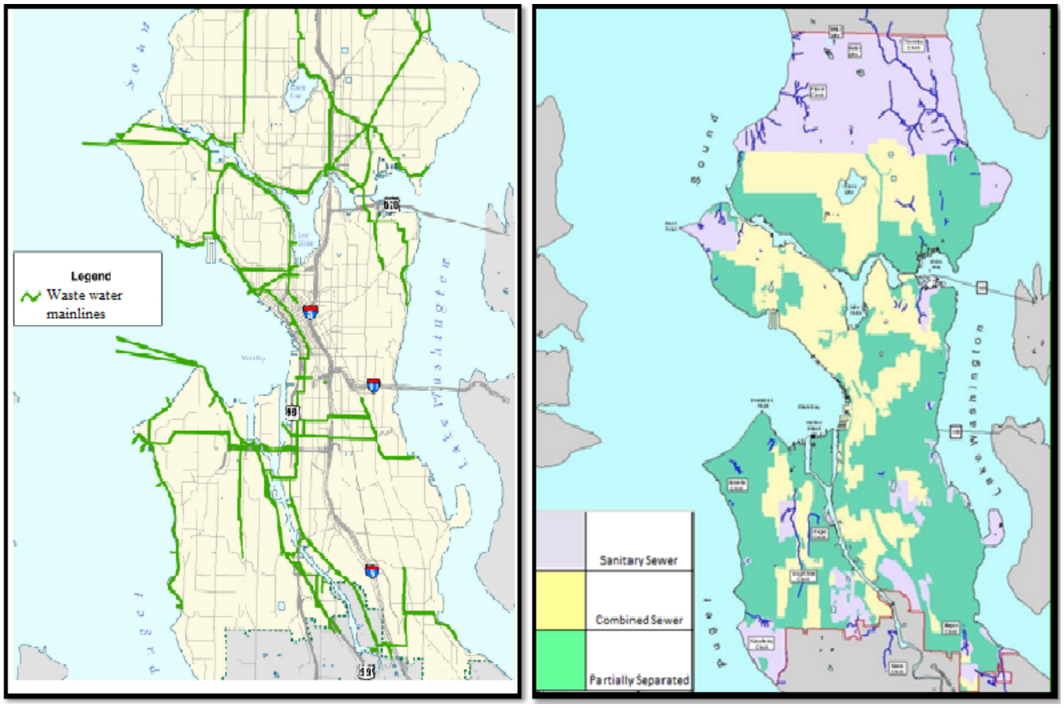

Figure 10.10 **Seattle sewer system service map [City of Seattle 2005, see Comprehensive drainage plan].**

Table 10.3 **Summary of Seattle waste water facts [City of Seattle 2010, see drainage and waste water management].**

Number	Description of Infrastructure
92	Permitted CSO outfalls (90 currently active)
83	Control structures
67	Waste water pump stations
448	Miles of sanitary sewers
968	Miles of combined sewers
460	Miles storm mainlines
5.5	Miles of waste water force mains
38	CSO storage tanks
39,000	Catch basins
220	Mile of ditch and culvert

Though the new infrastructure helped reduce the volume of CSOs, loosening of soils, overflows, and pollution into waterways were and are still occurring. During heavy rains in Seattle, storm water (about 90%) and sewage (about 10%) exceed the capacity of the system causing a CSO into a nearby waterway [City of Seattle 2010, see Restore our waters]. In response, the City began to further their goal of reducing CSOs. Table 7.4 below show the costs spent to improve the storm and waste water infrastructure. Already discussed were the partial separation projects. Other projects the City had invested into were the storage in storm water-basins and storage facilities eventually emptying the basins and facilities and conveying the storm water to treatment centers; and retrofitting the system.

Table 10.4 CSO reduction costs and projects from 1968-2009, [City of Seattle 2010, see Restore our waters].

Amount	Project	% of $524 million spent
$385 Million	Partial Segregation	73%
$134 Million	Storage	26%
$5 Million	Retrofits	1%

The past efforts resulted in a significant decrease in the volume and frequency of CSOs. According to the Seattle Public Utilities (SPU), since 1960, the volume of CSOs was down from over 34 billion gallons discharged per year, to just over 100 million in 2009. The frequency of outflows is down as well, from 2800 events in 1980 to just over 200 in 2009 [City of Seattle 2010, see Restore our waters]. The City's goal is to reduce the frequency amount per year to 90 outflows, equaling one outflow per active CSO.

Although the significant decline of CSOs is a great step towards strengthening the city's storm water system in the event of a catastrophic event, the installation of more grey infrastructure only increases the vulnerability of the city. The city's "fix-it-first" approach to storm and waste water systems, although a good start, is not sustainable; environmentally, economically, or socially. Through local projects, programs, and policies, as well as implementing less traditional infrastructure, the city can reduce the stress on its system and become increasingly resilient before and after earthquakes.

10.6 GREEN INFRASTRUCTURE AND RELATED POLICIES

Green infrastructure and related policies integrate the natural environment into urban settings to create an interconnected network of green space and environmentally-conscious-thinking that aids in conserving the natural ecosystem as well as the way human populations live today. The environmental approach differs from conventional tactics with open space planning as well as looking into conservation values and actions in concert with land development, growth management and built infrastructure planning [Benedict 2001]. With populations growing throughout earthquake-prone cities, the need for land use planning is needed more, providing citizens with not only an aesthetically-pleasing environment, but a sustainable one as well.

10.6.1 Green Storm Water Infrastructure and Low-Impact Development

The terms “green infrastructure” and “low-impact development” (LID) stem from engineering and planning perspective that take an approach to incorporate the natural environment in its design. Green infrastructure has several benefits besides managing storm water as well, which will be discussed later in this report. Conventional infrastructure’s primary use is for conveying residual waters out to open waterways or treatment plants, whether it was cleansed of contaminants or not. However, the main purpose of green infrastructure is to assure that the quality of their rivers, streams, lakes and estuaries is protected from the impacts of development and urbanization, especially with the exponential growth of communities all throughout the United States [USEPA 2010, see Green infrastructure case studies].

The infiltration process into the ground of storm water is important within cities. This process not only reduces stress on storm water systems, but also cleans possible contaminated water before entering into the ground water below as well as reducing floods in nearby streets. The collective force of such rainwater scours streams, loosens soil, erodes stream banks and thereby causes large quantities of sediment and other entrained pollutants to enter water bodies each time it rains, such as sewer outflows, discussed in the past section [USEPA 2010, see Fact sheet].

There are several types of green infrastructure designs that help reduce the negative impacts of storm water, see Table 10.5. Each green storm water infrastructure (GSI) and LID type follow practices that green design hope to accomplish. Those practices are as follow:

- <u>Conservation design</u> – used to minimize the generation of runoff by preserving open space
- <u>Infiltration practices</u> – engineered structures or landscape features designed to capture and infiltrate runoff
- <u>Runoff storage</u> – collection of runoff from impervious surfaces captured for reuse or gradually infiltrated, evaporated, or used to irrigate plants
- <u>Runoff conveyance practices</u> – used to slow flow-velocities, lengthen the runoff time of concentration, and delay peak flows that are discharged off-site
- <u>Filtration practices</u> – used to treat runoff by filtering through media that are designed to capture pollutants through the processes of physical filtration of solids and/or cat ion exchange of dissolved pollutants
- <u>Low-impact landscaping</u> – selecting proper soils and selecting plant species adapted to microclimates of a site greatly increases the successes of plant establishment and growth, thereby stabilizing soils [USEPA 2007].

Table 10.5 Types and functions of green infrastructure design [Rutherford 2007].

Type	Functions
Disconnected roof leaders, grassy swales and rain gardens	Promotes infiltration and groundwater recharge;
Roadside curb cuts	Directs road runoff onto grassy swales and rain gardens
Permeable pavement and green roofs	Reduces runoff
Rock pits and other catch basins and detention ponds	Detains rain water, slow it down and reduce/avoid the impact of peak flows
Water conserving infrastructure such as low-flow fixtures, and metering systems	Water reclamation and redistribution
Energy conserving systems such as district heat distribution, landfill gas recovery, sewer heat recovery and industrial process heat recovery	Reduces costs
Green building features	Privately controlled system, responsible for own system

The GSIs and LIDs promote a smarter approach to growth in expanding communities and cities. With an increase in population, the likelihood of increased pollution is more than likely. By installing these types of infrastructure, cities can approach age-old problems in new ways that are more sustainable for its civilians, such as: flood control, combined sewer overflows, Clean Water Act requirements and basic asset management of publicly owned treatment works [USEPA 2010, see Fact sheet].

10.6.2 Seattle Green Infrastructure and Policies

The beginnings of green storm water infrastructure and low-impact development in Seattle came in the early 1990s. The movement began in response to the Clean Water Act and the Endangered Species Act, both pertaining to the endangerment of the salmon population in the Pacific Northwest. This event along with an effort to reforest urban areas in 1994, in which capital was committed to parkland forest restoration, was a big push for Seattle and the country to see the advantages of utilizing nature within a built environment [Wise 2008]. In comparison to traditional "vault and pipe" storm water infrastructure, GISs and LIDs offer the following benefits:

- Integration into the landscape and beautification, which encourage landowner acceptance and maintenance;
- Failure of one or more small natural drainage system (NDS) sites does not compromise the integrity of the entire system;
- Improved effectiveness over time of vegetation, as opposed to deterioration over time of pipes and vaults;
- Source control of runoff reduces the need for expensive conveyance, detention, and treatment systems, as well as waterway remediation; and
- Reduction of impervious surfaces reduces costs of street and drainage improvements in low to medium density residential areas [City of Seattle 2007].

10.6.2.1 Infrastructure

With the GSIs and LIDs mentioned earlier in this report, the city of Seattle has started and completed several projects that have put different designs of green infrastructure together to enhance local communities' storm water management systems. A notable example that applies different designs of green infrastructure is the Street Edge Alternatives (SEA Streets); Seattle's first (and pilot) NDS. This project was meant to mimic pre-development pasture conditions prior to traditional piped systems. SPU had reduced impervious surfaces to eleven percent (11%) less than a traditional street and provided swales, and added over 100 evergreen trees and shrubs. After monitoring for two years after being built, the SEA Streets had shown to have reduced the total volume of storm water leaving the street by ninety-nine percent (99%) [City of Seattle 2007]. Figure 10.11 is a collage of pictures taken from SEA Streets throughout Seattle.

Figure 10.11 Collage of SEA Streets Natural Drainage Systems [City of Seattle 2007].

Through the environmental, economic, and social successes seen through the SEA Streets, more projects have been completed and are projected to begin in the upcoming years. Seattle has also proposed drainage code that will require green infrastructure in new and redeveloped areas and will give residents credits against utility fees for installing recognized features [City of Seattle 2007].

10.6.2.2 Policies

Not only have Seattle's streets spawned new projects, but has also helped more policies incorporating environmentally-friendly practices gain traction as well. Table 10.6 shows different green-related policies in Seattle that are associated with waste and storm water systems.

Table 10.6 Environmentally-incorporated policies for the City of Seattle.

Policy	Function
Restore Our Waters	Slows the flow of storm water and let the rain soak in, keep water clean and prevent pollution at its source, and replant and restore native trees, plants and in-water habitat
Fats, Oils & Grease Disposal	Prohibits the discharge of waste water containing more than one hundred parts per million by weight of fat, oil or grease, and has also required private pre-treatment facilities to intercept grease to be maintained in a continuously efficient operation at all times.
Street Sweep Project	Removes pollutants from roadways before they wash off into our receiving waters
Saving Water Partnership	Manages water-use more efficiently through education and incentives
Residential RainWise Program	Handles storm water on residential properties through education and incentives
Seattle Green Factor	Landscape requirement designed to increase the quantity and quality of planted areas in Seattle while allowing flexibility for developers and designers to meet development standards

The infrastructures and related policies in this section all aim to reduce the negative effects done to the waste water systems, both storm and sanitary. However, these designs and practices have deeper beneficial attributes when dissected more closely. The next section will examine the unseen benefits of "green" thinking for earthquake and community disaster preparedness.

10.7 RESULTS

Despite being primarily known for controlling storm water in an efficient manner, green infrastructure and environmentally-friendly applications can also affect the way a city handles earthquake-induced vulnerabilities as well as increase community and storm water infrastructure resiliency. My findings investigate GSIs, LIDs, and nature-friendly related policies and their effects on waste water infrastructure and vulnerabilities by reducing the effects of seismic activity and increasing the resiliency of a community before and after seismic activity(s) occur.

10.7.1 Critical Infrastructure Protection

Advanced engineering methods have offered several cities the opportunity to prepare and mitigate their infrastructures for potentially devastating earthquakes and their secondary hazards, albeit local governments have the funds necessary to fund such endeavors. However, in terms of earthquake mitigation, is there a way the natural environment can help increase the resiliency and reduce the amount of vulnerability to an infrastructure?

During urban development, several cities relied on natural elements to build their infrastructures (i.e. bored out trees used as water pipes) due to their availability and relatively low cost. Because technology has advanced extensively throughout the past centuries to produce more reliable and sturdy infrastructure, the need for natural elements was no longer needed. But is there a way today, to combine both techniques to increase resiliency of waste water systems? The benefits of green infrastructure and related policies generated in Seattle, although still in a young phase, have shown feasibility and a promise in the effort for critical infrastructure protection and swifter recovery of these systems within earthquake-prone areas.

10.7.1.1 Corrosion Reduction

One reason for corrosiveness amongst pipes is sanitary water use from homes, businesses, and industrial sites in combination with the contaminants that get conveyed through the system. Theses contaminants include fats, oils, greases, soaps, organic matter, dirt, human waste, etc. These types of waste water are known as black (toilet water) and grey water (clothes washer, bathing, and kitchen use). Just like storm water, black and grey waters form sediments that not only run through open waterways, but also have the capacity to clog drains and pipes through sediment build-up [HRSD 2011]. Other pollutants include heavy metals and possible harmful household contaminants. These come from a number of sources including: medicines, pesticides, herbicides, and paints [HRSD 2011]. The substances can corrode sewer pipes and seriously affect the operation of treatment plants as well as limit the potential of water reuse, therefore should not be disposed with household water [UNEP 2000].

In combination with sediment build-up and contaminants coming from households, sulfur-related compounds (a major element associated with the corrosiveness of sewer pipes) may increase the vulnerability of pipe failures. These compounds are abundant within domestic and commercial sanitary waters. When reaction with hydrogen ions occurs, hydrogen sulfide is created (H_2S), which converts into sulfuric acid. This typically occurs during low-flow dry-weather periods [Fan NA]. The products of corrosion by hydrogen sulfide are characterized ultimately by a complete destruction of the strength of the concrete or steel, which is reduced to a formless mass [Parker 1951]. During the early stages of corrosion, the concrete becomes incrusted by the corrosive products, which will later moisten and finally disintegrate, which can lead to disastrous waste water failures.

In terms of dealing with corroding pipes, cites have the choice to rehabilitate the system by: excavating and replacing pipes, using cured-on place inversion linings, insertion renewal, utilizing liners and use of specialty concrete [USEPA 1991]. Table 10.7 shows the former pipe-rehabilitation methods and more, as well as the applications that go along with them. Although these solutions are necessary to the overall health of waste water infrastructures due to a build-up of sulfide solution, is there an approach that involves incorporating the public with incentives as well as educate them with both waste water systems and environmentally friendly related policies? In order to do this, local governments must take responsibility to make the general public aware of issues and emphasize the importance of managing waste water infrastructure in an efficient way.

Table 10.7 Waste water pipe rehabilitation methods [USEPA 1991].

Method	Application
Insertion Renewal (Sliplining)	Used for cracked or deteriorated sewer pipes
Deformed Pipe Insertion	Similar to sliplining but for smaller circular pipe
Cured-in Place Inversion Lining	Sewer pipe of any geometry; largest current application
Specialty Concrete (Spot repair)	Large sewers or manholes needing structural repair
Coatings	Growing method for pipes and manholes with new application methods being marketed continually
Liners	Used only in structurally sound sewers
Pipe Replacement	Any pipe with major structural defects
Exterior Wrap and Cap	Provides back up corrosion protection and structurally reinforces existing pipeline

The City of Seattle has enacted programs and regulations to reduce the amount of contaminants entering the waste water system. One program, mentioned earlier, is the *Fats, Oils & Grease (FOG) Disposal* municipal code that reduces sewer build-ups (during increased flow periods), costly blockages, and sewer overflows to private properties [City of Seattle 2004]. Penalty fees for discharging FOGs down drains range from $250 to $5000. The following FOG sources are excluded from being emitted into local drainages: cooking oil, butter, lard, shortening, margarine, milk, soup, sauces, oil from cooked meats, sour cream, mayonnaise, cream, and food scraps. By reducing the amount of these FOG materials, which account for one-third of sewer build ups in the city, from commercial and residential drainage systems, sewer pipes can flow more clearly.

Another environmental program Seattle has put in place is the *Saving Water Partnership (SWP)*. This partnership is a group of local utilities within King County (with a majority belonging to the city of Seattle) that seek to reduce the amount of water usage throughout the region by funding water conservation programs. By providing local residential, apartment, and commercial establishments rebates and incentives to become more water-use-conscious, this partnership has helped reduce not only the amount of water used, but the amount of water sent through sewers as well, which may possibly contain hazardous contaminants that promote the conception of sulfuric acid. *The Fred Hutchinson Cancer Research Center* is an excellent example of an incentives and education program supported by SWP. Problems and issues with wasteful water usage were targeted and resolved. Table 10.8 displays the fiscal and water savings figures. By providing business owners, residential, and industrial entities the knowledge of a situation, both financial and environmental, they are more inclined to adapt to more conservative styles. Without learning of the added financial and environmental benefits, the change towards a more sustainable approach would be a more difficult selling point to give to the public.

Table 10.8 Fred Hutchinson Cancer Research Center (Seattle, WA) data [SWP 2002].

Project Cost	**$82,300 (before incentives)**
Rebate	$49,000
Water/Waste water Savings	11.1 million gallons/year = $93,900/year
Payback for Customer	4.25 months

10.7.1.1.1 Effects from urban runoff

As cities expand, waste water management becomes increasingly important to accommodate the growing population. Not only does population growth spur an increase in waste water, but an increase in impervious surfaces. In natural, undeveloped areas, approximately 10% of precipitation becomes runoff, with 50% infiltrating into the ground and 40% returning to the atmosphere through evapo-transpiration [FISRWG 1998]. However, in landscapes with 75-100% of land covered by impenetrable- water surfaces (many urban areas), 55% of that water leads to runoff [Downstream Strategies 2010].

In some areas of Seattle, the combination of both storm and sanitary waste water amalgamate through the same pipes, known as a combined sewer system. During periods of frequent rainfall, residual waste waters could eventually overflow and dump untreated sanitary water into open waterways. Results from a sampling program indicate that concentrations of total and dissolved metals, total suspended solids, nutrients, total petroleum hydrocarbons, pesticides, herbicides, and E. coli and fecal coliform bacteria are present within certain areas of Seattle's waterways [Engstrom 2004]. The presence of these contaminants not only degrades the quality of water to receiving waterways, but can also damage the waste water infrastructure of Seattle as well.

The effect of urban runoff on sewage infrastructure is usually slow over time, yet potentially devastating if not investigated and mitigated immediately after detection. Runoff, just like sanitary waste water, transports sediments and solid pollutants into the system, clogging and negatively affecting the system. For the city of Seattle's combined sewer system, this poses a major problem with backflow and discharges that harmfully affect the environment concurrently. Another issue of urban runoff is the contaminants and their corrosive effects on the infrastructure. Table 10.9 displays the different contaminants conveyed from urban runoff into sewer drainage systems and their sources. Some of these contaminants, described earlier in this section, can stem from household yard such as pesticides and herbicides.

Table 10.9 Sources of contaminants from urban storm water runoff [USEPA 1999].

Contaminant	Contaminant Sources
Sediment and Floatables	Streets, lawns, driveways, roads, construction activities, atmospheric deposition, drainage channel erosion
Pesticides and Herbicides	Residential lawns and gardens, roadsides, utility right-of-ways, commercial and industrial landscaped areas, soil wash-off
Organic Materials	Residential lawns and gardens, commercial landscaping, animal wastes
Metals	Automobiles, bridges, atmospheric deposition, industrial areas, soil erosion, corroding metal, surfaces, combustion processes
Oil and Grease/ Hydrocarbons	Roads, driveways, parking lots, vehicle maintenance areas, gas stations, illicit dumping to storm drains
Bacteria and Viruses	Lawns, roads, leaky sanitary sewer lines, sanitary sewer cross-connections, animal waste, septic systems
Nitrogen and Phosphorus	Lawn fertilizers, atmospheric deposition, automobile exhaust, soil erosion, animal waste, detergents

Several of the contaminants mentioned above have the potential to produce sulfuric acid, a corrosive compound, discussed prior in this section. This occurs when low pH waste waters, usually from industrial sites, in combination with increased temperatures, comes in contact with the concrete sewer structure [Pitt NA]. Research has shown urban storm waters to have both characteristics. The city of Seattle has implemented a program, the Street Sweep Project [Table

8.6], to clean streets before contaminated-filled runoff, whether it is from precipitation or human-caused, is conveyed into the sewer drainage pipes.

Lower pH levels of waste water, when in contact with sewer structures, may spur corrosion rates with an acidic attack. Most pH impacts in urban waters are caused by runoff of rainwater with low pH levels (acid precipitation). In fact, urban areas tend to have more acidic rainfall than less developed areas. Some buffering of low pH rainwater occurs during contact with buildings, parking lots, roads and collection systems, and during overland flow. This is often very site-specific. The alkalinity and capacity of receiving waters to neutralize acidic storm water can also be important, and again is site specific [USEPA 1999].

Water temperature is important to gauge the quality of water. The temperature of water affects some of the important physical properties and characteristics of water, such as specific conductivity and conductance, salinity, and the solubility of dissolved gases (e.g., oxygen and carbon dioxide) [Malina 1996]. Urban runoff has shown to have an increase in temperature when finally carried into drainage system. The temperature of urban waters is often affected directly by urban runoff. Urban runoff can be heated as it flows over rooftops, parking lots and roadways [USEPA 1999]. In fact, several urban areas with older, metal roofing materials often erode harmful contaminants such as zinc and copper, into sewer systems. This not only affects the reactions between water with increased temperatures, but also affects the aquaculture after discharge. Water holds less oxygen as it becomes warmer, resulting in less oxygen being available for respiration by aquatic organisms. Furthermore, elevated temperatures increase the metabolism, respiration, and oxygen demand of fish and other aquatic life [USEPA 1999]. After earthquakes, like what is currently occurring in Christchurch, New Zealand, increased amounts of outfalls took place months after the quakes, negatively affecting water quality and aquatic life.

In order to reduce the effects of urban runoff on the sewer systems, Seattle has developed LID and GSI to reduce the stress and filter out pollutants before entering the system and affecting the infrastructure. Table 7.5 illustrated some of the techniques used throughout the city to reduce potential runoff. One example in Seattle of implementing green infrastructure throughout a community is the High Point Natural Drainage System (NDS), located in the northwestern portion of the city. Figure 10.12 is a map showing the area used for the program. This redevelopment project is currently incorporating storm water LID drainage practices. The High Point area was a low-income housing development that was redeveloped into a mixed-income housing development [Johnson NA]. The High Point area uses NDS swales to first channel runoff through a vegetation/compost amended swale, slowing runoff and allowing for infiltration into the groundwater. Excess runoff is then routed to a conventional storm water conveyance system. The swales have been constructed to provide shallow surface ponding (3 to 10 in.), with 3 to 4 ft of bio-retention soil and an underdrain collection system [Herrera 2008]. This in turn has increased the quality of storm water as well as decreased erosion of downstream waters.

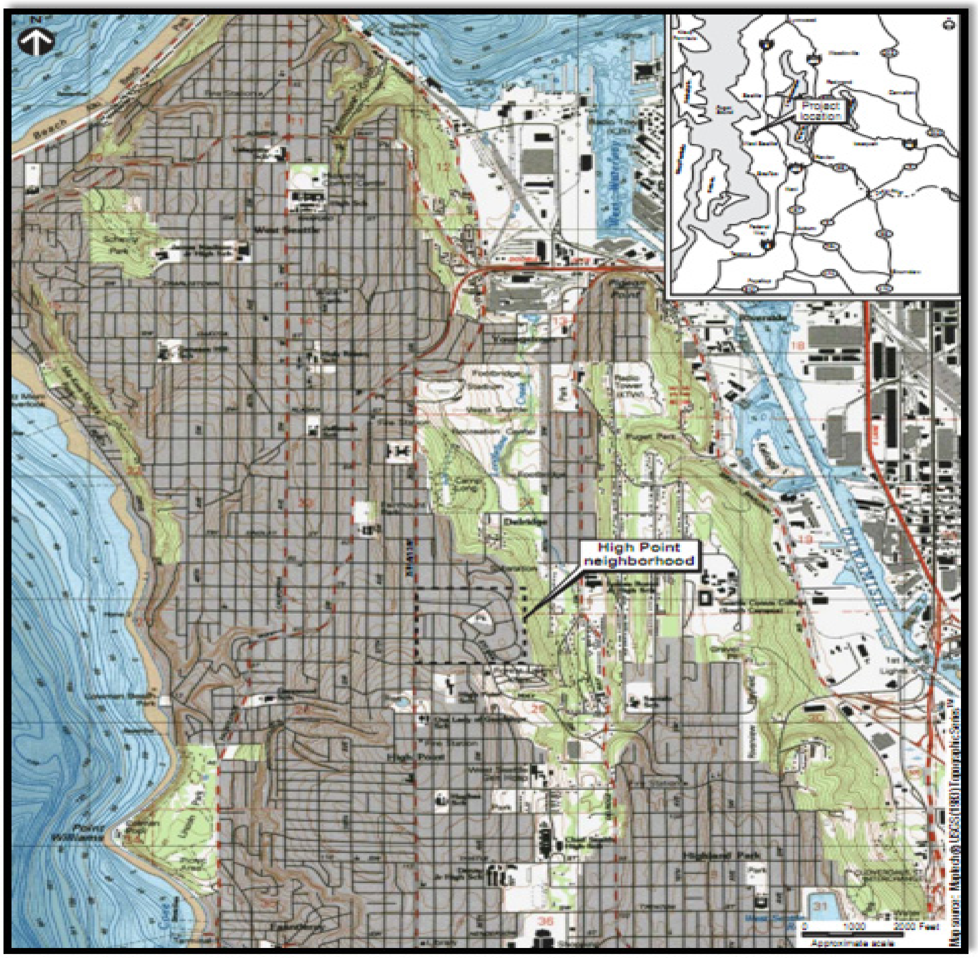

Figure 10.12 Map of High Point redevelopment project site [Herrera 2008].

From the monitoring of the natural drainage systems throughout High Point, conclusions were formulated about the successes of the system. Continuous hydrologic data collected during the monitoring period indicated that the NDS test swale effectively treated all runoff from storm events with precipitation totals below the 6-month, 24-hour and 2-year, 24-hour design storms for water quality treatment and flow control, respectively. In respect to this conclusion, pollutant concentrations in runoff arising from the High Point neighborhood were generally lower than concentrations measured in national studies for the same land use. Additionally, concentrations of metals were at levels that were considered irreducible using conventional storm water controls [Herrera 2008]. By implanting these NDS projects and other low-impact development devices in flood-prone areas throughout the city, Seattle can help strengthen their drainage systems and allow the structures to survive past its designed life durations. Although over time, replacement of grey infrastructure will be necessary, the installation of low-impact development can strengthen the systems until that time and improve the water of quality discharged for future use for aquaculture and for the general population.

10.7.2 Community Resiliency from Green Infrastructure and Policy

Already discussed was the impact green philosophy has on physical waste water infrastructure. However, the influences low-impact development and environmentally-conscious related policies has on community-earthquake-resiliency is substantial and should not be ignored. From economic, environmental, and social perspectives, "greening" prepares cities for the potentially devastating effects associated with earthquakes.

10.7.2.1 Economic Resilience

How local economies react to the earthquake and what methods have been taken before to strengthen the structures, is an important aspect to think about when considering earthquake resiliency. In the case for green infrastructure and low-impact development, what is the cost-benefit for installing these environmentally-conscious devices versus traditional piping? Is it worth it for Seattle to implant green infrastructure and policies for not only short-run economic benefits, but for long-run monetary prosperity for the waste water system as well as the city? Where else could capital go to in times of emergency?

Several cities implanting these devices and policies are looking for short-term cost effectiveness; or the cost of installing green programs versus replacing/repairing old waste water infrastructure. Due to the newness of these devices, cities are taking less risk on LIDs and GSIs, budgeting significantly less for these programs. However, Seattle is not one of those cities. For example, Seattle issued the SPU Drainage and Waste water Fund for FY2007 for $250.0 million.

In order to apportion the Fund appropriately, SPU, with the coordination of the city and other departments, used an asset management approach to prioritize capital budgets. This approach evaluates projects for their economic, environmental, social, and customer service benefits and are weighed against the costs, including ongoing maintenance expenditures. Projects that are not cost-effective are dropped [Civic Federation 2007]. From 2007-2012, SPU and the city of Seattle plan to invest more in green infrastructure, utilizing 13% of the Drainage and Waste water utility budget to finance, as seen in Table 10.10.

Not only will green infrastructure cut installation costs of traditional infrastructure, but will also reduce maintenance and treatment expenditures as well. For low-impact developments, weeding, watering, erosion and sediment control, and replacement of dead plant material for a minimum of three years from installation is needed in order to achieve a minimum eighty percent (80%) survival of all plants [Hinman 2005]. According to Table 10.10, operating costs for low-impact developments (from 2000-2012) will be approximately $434,000. However, for the year of 2011 alone, drainage systems base operating and maintenance costs total over $41 million and $2.6 million in treatment costs [City of Seattle 2010, see Drainage and waste water fund]. The disparity is apparent. Although maintenance is necessary on grey infrastructure, how will installing green infrastructure affect that total cost? Seattle, just like all urban centers, relies on grey infrastructure. And although low-impact development makes sense financially, the combination of both green and grey structures is necessary for the overall well-being of system, structurally as well as economically. More monitoring is necessary to see whether GSIs actually affect and lower operating and maintenance costs for traditional infrastructure.

Table 10.10 2007-2012 Green infrastructure appropriations [Civic Federation 2007].

Project	Timeframe	Expenses through 2005	2006	2007	Total All Years through 2012	Operating Costs
SEA 3rd Ave. NW & NW 107th (Broadview Green Grid)	2000-2007	$ 5,028,000	$ 69,000	$ 94,000	$ 5,191,000	$ 35,000
Best Management Practices Projects	2000-2012	$ 605,000	$ 375,000	$ 595,000	$ 13,437,000	$ -
Bitter Lake/ N 137th Stormwater	2001-2012	$ 14,000	$ -	$ 26,000	$ 1,872,000	$ 10,000
Capital Planning--Low Impact Development	2007-2012	$ -	$ -	$ 321,000	$ 719,000	$ -
Capitol Hill Water Quality Project	2006-2012	$ -	$ -	$ 1,653,000	$ 4,776,000	$ 8,000
Citywide Source Control	2006-2007	$ -	$ 100,000	$ 103,000	$ 203,000	$ -
Creek Flow Control Implementation	2010-2012	$ -	$ -	$ -	$ 6,866,000	$ 45,000
Creeks Vegetation Program	2005-2012	$ 129,000	$ 150,000	$ 185,000	$ 1,131,000	$ -
Demand Management	2007-2012	$ -	$ -	$ 600,000	$ 3,433,000	$ -
Drainage and Wastewater Partnership Program	2007-2012	$ -	$ -	$ 350,000	$ 7,250,000	$ -
High Point Drainage System	2002-2011	$ 2,431,000	$ 1,100,000	$ 1,376,000	$ 5,344,000	$ 294,000
Lakewood Raincatcher Pilot Project	2005-2012	$ 78,000	$ 628,000	$ 851,000	$ 1,825,000	$ -
Lower Densmore Drainage Improvement	2005-2008	$ 152,000	$ 225,000	$ 6,000	$ 388,000	$ -
Natural Drainage System Improvements	2003-2012	$ 82,000	$ 396,000	$ 169,000	$ 3,500,000	$ -
Nbhd.Drainage/Climate Bonus Matching Grant Project	2007-2012	$ -	$ -	$ 150,000	$ 900,000	$ -
Pinehurst Natural Drainage System	2002-2008	$ 3,356,000	$ 1,287,000	$ 30,000	$ 4,687,000	$ 27,000
Raincatcher Creek Pilot Project	2007-2008	$ -	$ -	$ 235,000	$ 447,000	$ -
South Lake Union	2004-2009	$ 131,000	$ 1,130,000	$ 137,000	$ 1,547,000	$ -
Stormwater Mitigation Partnership Program	2005-2010	$ 1,000	$ 50,000	$ 50,000	$ 218,000	$ -
Venema Creek Natural Drainage System	2003-2012	$ 486,000	$ 405,000	$ 309,000	$ 2,619,000	$ 15,000
Water Reuse - Stormwater	2001-2008	$ 50,000	$ 50,000	$ 29,000	$ 153,000	$ -
Water Reuse - Wastewater	2001-2008	$ 392,000	$ 14,000	$ 97,000	$ 540,000	$ -
Watershed Base Creek Flow Control	2005-2011	$ 35,000	$ 150,000	$ 71,000	$ 1,166,000	$ -
TOTAL		$ 12,970,000	$ 6,129,000	$ 7,437,000	$ 68,212,000	$ 434,000
Drainage and Wastewater Fund Total		$ 85,848,000	$ 43,665,000	$ 52,012,000	$ 519,318,000	
Green Infrastructure as % of Total		15.1%	14.0%	14.3%	13.1%	

Lower cost than grey infrastructure expenditures, the risk Seattle is taking on the installation of low-impact development will neither be too costly nor too little, as the amount for green infrastructure versus installation of grey infrastructure is much cheaper. Case studies have shown the installation of green infrastructure has a savings curve of up to 40% cost saving versus conventional "pipe" infrastructure [Kulik 2006]. In Seattle, low-impact developments were compared to traditional or grey infrastructure to illustrate the cost-benefit of each (maintenance and upkeep costs not included). See Table 10.10. It is apparent that up front, green infrastructure may be an acceptable alternative, monetarily-wise. In the project case studies presented in Table 10.11 most projects saved on construction costs, capital that could be used or saved to repair or rehabilitate sewer pipes that pose a threat for failure.

Table 10.11 Cost analysis of natural versus traditional drainage [USEPA 2010, see Fact sheet].

Project	Conventional Development Cost	LID Cost	Cost Difference	Percent Differnce
2nd Avenue SEA Street	$868,803	$651,548	$217,255	25%
Auburn Hills	$2,360,385	$1,598,989	$761,396	32%
Bellingham City Hall	$27,600	$5,600	$22,000	80%
Bellingham Bloedel Donovan Park	$52,800	$12,800	$40,000	76%
Gap Creek	$4,620,600	$3,942,100	$678,500	15%
Garden Valley	$324,400	$260,700	$63,700	20%
Kensington Estates	$765,700	$1,502,900	-$737,200	-96%
Laurel Springs	$1,654,021	$1,149,552	$504,469	30%
Mill Creek[c]	$12,510	$9,099	$3,411	27%
Prairie Glen	$1,004,848	$599,536	$405,312	40%
Somerset	$2,456,843	$1,671,461	$785,382	32%
Tellabs Corporate Campus	$3,162,160	$2,700,650	$461,510	15%

Economically, installing green infrastructure would aid in both mitigation and recovery phases. By saving on traditional drainage systems, excess funds could be put into accounts for pipe replacement and major repairs or emergency funds after disasters. This idea should be investigated more to establish whether a policy may be developed for the addition of more green infrastructure while using more asset management techniques and appropriating funds to projects that need more budget flexibility in case of emergency or immediate rehabilitation.

10.7.2.2 Environmental Resilience

Environmental resiliency refers to the state of the environment both before and after an earthquake. In the event of a destructive earthquake, the original contours and form of the natural terrain and waters (as well as the built environment) will most likely change. After an earthquake, the true temerity and durability of the built environment will be tested. However, that same resilience must be reinforced and improved before time of the disaster strikes. In the case for waste water infrastructure, the city must recognize environmental issues and resolve them speedily in order to avoid serious environmental backlash that affect both the social and economic well-being of the city.

One issue Seattle has taken in order to strengthen their resiliency is to control their CSO, discussed earlier in this report. In a CSS, situated in several areas in the Seattle area, storm water has the potential to intersperse with grey and black water from sanitary sources. Along with pollutants conveyed from storm water runoff, sanitary waste water shares the same path to treatment facilities. During heavy rainstorms, pipes could overflow into open waterways or backflow onto streets and private property, creating a public health issue. During significant seismic events, the city may be inclined to convey raw sewage to nearby waterways. In one of the most recent New Zealand earthquakes, which took place in February of 2011 in Christchurch, the local government did just that. Although waste water overflows were down significantly to 18,788 cubic meters a day (4,963,265 gallons) [recorded on July 16], the peak amount of 67,000 cubic meters a day (17,699,527 gallons) [recorded on June 13] is a good indication of the damage done to the aquatic systems receiving the raw sewage [Christchurch 2011]. Due to contamination, local beaches and areas near waterways were closed to reduce the exposure of hazardous waste water. The aquatic environments were affected as well. Some changes were evident in the marine community as well as geologic changes from predominantly sand/silt to gravel and cobble due to bed uplift following the February quake. Although changes occurred, no major and dramatic changes were observed to cause worry [James 2011]. However, monitoring is still occurring to observe any negative effects from contamination that may have affected aquatic species as well as the aquaculture economy.

The situation in New Zealand was an outcome of several earthquakes. Country emergency recovery units have installed several sanitary waste water devices for citizens to use to reduce the amount of waste water flowing through the combined systems. However, cities along the Pacific Ring of Fire that receives a significant amount of rainfall and/or snowfall, also need to think about naturally occurring water developing events. The city of Seattle has substantially taken steps to consider those events and have undertaken a tough stance on protecting and increasing their environmental waste water infrastructure resiliency. Aside from the green infrastructure talked about heavily already, the local government has developed related policies and programs (Table 10.6) that help reduce the volume of waste water in the system (Saving Water Partnership, Residential RainWise Program, and Seattle Green Factor), but also the quality of the waste water (Restore Our Waters, Fats, Oils & Grease Disposal, and Street Sweep Project). These programs will help increase the environmental resiliency of Seattle by strengthening the aquatic habitats and economy and reducing cleanup costs and recovery expenditures after an earthquake(s) occur.

Another indirect effect environmentally-conscious infrastructure and related policies have on the natural environment is strengthening soils before seismic activity from erosion and landslides that my cause property damage, block roads for emergency responders, and lead to deaths. Despite the possibility of earthquakes, the area's post-glacial geology and the amount of precipitation that falls increases the threat of slope instability within the region. Studies using vegetation to stabilize landslides have been conducted in Seattle to measure the effectiveness of green infrastructure. Dense vegetation were planted along landslide-prone areas, aimed to intercept direct rainfall before raindrops impact the soil surface, thereby reducing or eliminating rainsplash erosion. The overland flow is also reduced in intensity and speed, lessening surface erosion. The root systems of the vegetation can enhance the strength of the soil they penetrate, reducing the likelihood of shallow landslides; and the deeper the roots, the better protection [Kazmierczak 2010]. The effectiveness of implanting strictly vegetation on sloped areas was measured in 2007 with cooperation from USGS. The monitoring results showed the effectiveness of greening infrastructure on slope slides. The review of the Seattle Landslides Project by an independent company has helped to ensure that the process is meeting criteria of scientific rigor [Kazmierczak 2010]. However, the report also stated vegetation is only one of several measures to protect slide-prone areas and the combination of different mitigation methods is the best way to deal with weak slopes.

10.7.2.3 Social Resilience

In order for a city to recover, the general population needs to be prepared to an appropriate degree to assemble and begin the recuperation process. "Social resiliency" is defined as how long it would take for a community to respond to the event, self-organize and incorporate the lessons learned before returning to a [new] normal way of functioning [Sapirstein NA]. The longer it takes a community to recover, the more difficult it becomes to get back to pre-disaster level. If the recovery process shows little or no progress, the city is threatened by people leaving, economic stagnation, and rampant psychological and emotional distress [Sapirstein NA]. With the addition of green infrastructure and related policies, the public is made more aware of their environment, both built and natural, by having: an increase in recreational opportunities and use, improved urban aesthetics and community livability, and overall improved human health and wellness [Downstream Strategies 2010]. The public also gain more confidence within their neighborhoods to participate and protect their community, not only at local and district events, but during times of need and emergency as well. The Seattle local government as well as the Federal government can only do so much. The essence of social resiliency is a grassroots movement, a movement aided and encouraged by installation of green infrastructure and related policies.

10.8 CONCLUSION

Although primarily known for storm and waste water mitigation, green storm water infrastructure (GSIs), low-impact developments (LIDs), and environmentally-conscious related policies have proven to be an excellent tool for Seattle communities to become more earthquake resilient.

- <u>Structurally</u> – in terms of strengthening and protecting actual infrastructure, green infrastructure and related policies have demonstrated their worth. One can argue that by using more green infrastructure and relying less on grey infrastructure, public utilities can focus on more important issues within the water system, both potable and non-potable. In particular, during rainy situations in which earthquakes may occur, the green infrastructures and related policies set in place by a city can reduce the stress put upon the waste water system, thus being able to repair more critical failures. However, with the condition and the amount of reliance the city has on grey waste water infrastructure, the most suitable mitigation and protection for this structure is to rehabilitate and replace aged, corroded, and leaky pipes in combination with green infrastructure. Monitoring after replacement or repair will reveal the true effectiveness and efficiency environmentally-mindful projects have on waste water infrastructure.

Green infrastructure does little to protect and reduce the secondary effects of earthquake hazards (liquefaction, soil compactions, tsunamis, seiches, etc.) than do traditional infrastructure. Although GSIs and LIDs do not reduce secondary earthquake vulnerabilities of cities and infrastructure to a large extent, the presence and installation of these devices increases the resiliency of the city economically, environmentally, and socially:

- <u>Economically</u> – lowers costs for treatment and installation of grey infrastructure. That money can be put into a hazards saving amount in case of emergencies.

➢ Environmentally – the earthquake in Christchurch, New Zealand had created a large mess for the citizens of the city and around that region. By reducing the problem now, although difficult to imagine recurring earthquakes and/or hazards, the city of Seattle is doing itself a favor by reducing the incidents of untreated storm and sanitary waters before heading into open waterways, thus preventing a larger area and volume to clean up and saving money simultaneously.

➢ Socially – by implanting green infrastructures in neighborhoods and small communities as well as educating the public about the dangers of natural hazards and water efficient policies, the city is engaging its public in conversation of hazards. By increasing public participation through these installations and policies, it shows that public education, if done correctly, can create community unity in times of emergency.

10.8.1 Challenges

The combination of both grey and green infrastructure makes the waste water system stronger. The use of both gives public utilities more time, effort and most importantly, money, to service and mitigate areas with sanitary waste water issues, either through repair or replacement of grey infrastructure. However, the reason for including green infrastructure as part of the critical infrastructure protection is difficult to justify. After an earthquake, the importance of asset management is magnified. By implanting green infrastructure around flood-prone communities, Seattle and other cities with similar issues may help strengthen their systems. But, the incentive to protect a waste water system from natural disasters is often very low, due to the federal government. The Federal Emergency Management Agency (FEMA), issues public assistance to local governments in which aid is given to pay part of the costs of rebuilding a community's damaged infrastructure. Generally, public assistance programs pay for 75% of the approved project costs. Public Assistance may include debris removal, emergency protective measures and public services, repair of damaged public property, loans needed by communities for essential government functions and grants for public schools [FEMA 2010]. With this disincentive present, the more important asset management is. With the amount of capital saved by installing green infrastructure, SPU (the drainage and waste water department) and Seattle have an opportunity to become more economically-resilient, which in turn leads to a more environmentally and socially resilient city.

ACKNOWLEDGMENTS

This project was supported by the Pacific Earthquake Engineering Research Center (PEER) and the National Science Foundation (NSF). I would also like to thank my project mentors, Professor May and Ashley Jochim for their guidance, my associate Sarah Welsh-Huggins, my interviewees and contacts for their time and knowledge, and the University of Washington (UW) for allowing me to use their resources.

REFERENCES

Ballantyne, D. (NA). Sewers float and other aspects of sewer performance in earthquakes, *Proc*., Engineering in a Safer World, Nigata, Japan.

Benedict, M, and E McMahon (ed.). (2001). *Green Infrastructure: Smart Conservation for the 21st Century*, Sprawl Watch Clearinghouse, Washington, D.C.

Christchurch Earthquake Journal. (2011). *Sewer Overflows into Waterways*, http://www.chcheqjournal.com/2011/sewer-overflows-waterways-reduce/.

City of Los Angeles. (N.A.). *About the Los Angeles Storm Drain System*, http://www.lastorm water.org/Siteorg/general/lastrmdrn.htm.

City of Seattle (2005). *City of Seattle 2004 Comprehensive Drainage Plan: Vol. 1*, Seattle Public Utilities, Seattle, WA.

City of Seattle (Seattle). Seattle Public Utilities (SPU), (2010). Drainage and waste water fund: 2011-2012 rate study. Seattle, WA: City of Seattle.

City of Seattle (2010). *Drainage and Waste Water Management*, Seattle Public Utilities, Seattle, WA.

City of Seattle (2010). *Restore Our Waters: Combined Sewer Overflow Reduction*, In *CSO Program Overview*, http://www.seattlechannel.org/videos/video.asp?ID=4568.

City of Seattle (2004). *Seattle All-Hazards Mitigation Plan*, Emergency Preparedness Bureau, Seattle Police Department Seattle, WA.

City of Seattle (2007). *Seattle's Natural Drainage Systems*, Seattle Public Utilities Seattle, WA: City of Seattle.

City of Seattle (2005), *Seattle's Population and Demographics*, http://www.seattle.gov/dpd/Research/Population_Demographics/Population_Trends/default.asp, Department of Planning and Development, Seattle, WA.

{The} Civic Federation (ed.). (2007). *Managing Urban Storm Water with Green Infrastructure: Case Studies of Five U.S.. local governments*, the Center for Neighborhood Technology, Chicago, IL.

Downstream Strategies (ed.). (2010). *Plants Not Pipes: Promoting Green Infrastructure and Side Benefits in Region 10,* White Hall, WV: Region VI Planning and Development Council.

Engstrom, A, and D. Booth (2004). Characterizing water quality of urban storm water runoff: interactions of heavy metals and solids in Seattle residential catchments, Unpublished manuscript, Dept. of Civil and Enviro. Engrg., University of Washington, Seattle, WA.

Fan, C, R. Field, W. Pisano, J. Barsanti, and J. Joyce (N.A.). Sewer and tank flushing for corrosion and pollution control (*EPA/600/J-01/120*), Washington D.C.

Federal Emergency Management Agency (2010). The disaster process and disaster aid programs, http://www.fema.gov/hazard/dproc.shtm.

Federal Interagency Stream Restoration Working Group (1998) Stream corridor restoration: principles, processes, and practices, *GPO Item No. 0120-A; SuDocs No. A 57.6/2:EN3/PT.653*.

Google Maps. (2011). [Seattle, Washington] [Aerial Map]. Retrieved from http://maps.google.com/maps?q=seattle%20map&um=1&hl=en&rlz=1C1TSNF_enUS437US437&bav=on.2,or.r_gc.r_pw.r_cp.&biw=1366&bih=667&ie=UTF-8&sa=N&tab=il

Hampton Roads Sanitation District (2011). Basics on corrosion in waste water collection and treatment systems: the corroding environments and materials, *Coatings Manual,* Appendix A (pp. 001-009). Virginia Beach, VA.

Herrera Environmental Consultants, Inc. (2008). *Water Year 2007 Data Report: High Point Phase I Block Scale Monitoring*, City of Seattle, Seattle Public Utilities, Seattle, WA.

Hinman, C. (2005). Low-impact development: technical guidance manual for Puget Sound. Washing State University, Tacoma, WA.

I C Consultants Ltd. (2001). *Pollutants in Urban Waste Water and Sewage Sludge* (L-298), Directorate-General Environment, Luxemburg: Office for Official Publications of the European Communities.

James, A, and S. McMurtrie (ed.) (2011). *Christchurch February Earthquake: Effect on Freshwater Fish of the Upper Avon River*, Environment Canterbury and Christchurch City Council, Christchurch, New Zealand.

Johnson, R, and P. Staeheli (N.A.). Storm water low-impact development practices, City of Seattle, Dept. of Planning and Development, Seattle, WA.

Kazmierczak, A. and J. Carter (2010). Adaptation to climate change using green and blue infrastructure. A database of case studies.

Kulik, J. (2006). Does green infrastructure pay?*,* Proc., Washoe County Commission Chambers: Reno, Nevada*.* Wenk Associates, Inc.

Malina, J.F. (1996). Water quality, Chapter 8, In: *Water Resources Handbook*, L. W. Mays, ed. McGraw-Hill. New York, NY.

Nelson, S. (2011). Slope stability, triggering events, mass movement hazards. Unpublished manuscript, Dept. of Earth and Enviro. Sci., Tulane Univ., New Orleans, Louisiana, http://www.tulane.edu/~sanelson/geol204/slopestability.htm

Parker, C.D. (1951). Mechanics of corrosion of concrete sewers by hydrogen sulfide, *Water Environment Federation*, 23(12):1477.

Pitt, R, & Clark, S. (N.A.). Module 7: sanitary sewer design.

Rutherford, S. (2007). *The Green Infrastructure Guide: Issues, Implementation Strategies and Success Stories,* West Coast Environmental Law Research Foundation, Vancouver, Canada.

Sapirstein, G. (ed.). (N.A.). *Social Resilience: the Forgotten Element in Disaster Reduction*, Organizational Resilience International, Boston, MA.

Saving Water Partnership (2002). *Medical Facility Case Study*, Fred Hutchinson Cancer Research Center, Seattle, WA.

Towhata, I. (2011). Geotechnical damage caused by the recent gigantic earthquake in Japan, *Proc*., 3rd International Conf. on Geotech. Engrg. for Disaster Mitigation and Rehabilitation*,* Tokyo: University of Tokyo.

U.S. Department of Homeland Security, Office of Ground Water and Drinking Water (2007).*Water: critical infrastructure and key resources sector-specific plan as input to the national infrastructure protection plan* (EPA 817-R-07-001). Washington, D.C.

U.S. Environmental Protection Agency, Office of Water (4203) (1991). Combined sewer overflow o&m fact sheet: proper operation and maintenance (*832S91100*). Washington, D.C.

U.S. Environmental Protection Agency (2010). Fact sheet: reducing storm water costs through low-impact development (lid) strategies and practices, http://www.epa.gov/owow/NPS/lid/costs07/factsheet.html.

U.S. Environmental Protection Agency, Office of Wetlands, Oceans and Watersheds (2010). Green infrastructure case studies: municipal policies for managing storm water with green infrastructure (*EPA-841-F-10-004*). Washington, D.C.

U.S. Environmental Protection Agency, Office of Water (4203) (1999). Preliminary data summary of urban storm water best management practices (*EPA 821-R-99-012*), Washington, D.C.

U.S. Environmental Protection Agency, Nonpoint Source Control Branch (2007). Reducing storm water costs through low-impact development (lid) strategies and practices (*EPA 841-F-07-006*), Washington, D.C.

U.S. Environmental Protection Agency, Office of Water (4203) (2004). Report to congress: impacts and control of csos and ssos (*EPA 833-R-04-001*), Washington, D.C.

U.S. Geological Survey (2010). *Lifeline systems*, http://geomaps.wr.usgs.gov/pacnw/lifeline/water.html.

U.S. Geological Survey (1999). *Ring of fire*, http://earthquake.usgs.gov/learn/glossary/?term=Ring%20of%20Fire.

United Nations Environment Programme (UNEP). International Environmental Technology Centre, Division of Technology, Industry and Economics. (2000). Environmentally sound technologies in waste water treatment for the implementation of the UNEP global programme of action (gpa) "guidance on municipal waste water". Osaka, Japan: International Environmental Technology Centre.

Weather.com. Retrieved August 11, 2011, from weather.com

Wise, S. (2008). Green infrastructure rising: best practices in storm water management, Planning, issue and edition unknown.

11 Disaster Resilience of Maritime Ports

SARAH WELSH-HUGGINS

ABSTRACT

The complex networks of global trade depend on ports to provide timely, organized handling of the goods and products that sustain the international economy. The vulnerability of maritime ports to natural disasters threatens to disrupt the normal function of businesses and communities around the world. In the western United States, the fear of damage to ports from a large seismic event is of particular concern. Following a natural disaster, the ability of a port to rebound swiftly and effectively is crucial to minimizing these cascading economic and social disruptions. Evaluations of the disaster preparedness of the two largest container ports in Washington State initiated this discussion of how major earthquakes impact port facilities, why community awareness seismic risk to infrastructure should be increased and what actions are needed to strengthen the interdependencies that determine post-disaster resilience of ports. The limited timeframe of this research prevented a full comprehensive study of these topics; the results presented within are drawn from a qualitative assessment, rather than quantitative analysis. Despite these limitations, the conclusions drawn from this project's findings suggest certain overall trends regarding the disaster resilience of seaports. Many present discussions of disaster resilience emphasize vague ideological aspirations, but the results of this research point to a need for concrete actions and impassioned leadership. As this study concludes, the coordination of the complex interactions among a port's public and private stakeholders is the key to the development of port disaster resilience. Present actions taken by ports to improve their disaster resilience can protect the communities and businesses that they serve from potential post-disaster losses and long-term economic setbacks.

11.1 INTRODUCTION

The economic and social health of the United States and its trading partners depends on the existence of well-functioning networks of transportation and shipping. Disruption to the supply chains through which these networks operate—from either natural or man-made disasters—can have devastating, cascading impacts on the lives of people across the globe. The many operations that rely on the successful operation of US and international trade systems make the protection of such resources essential to the economic vitality of the nation and the world.

In the United States, 95% of international trade moves by waterways [GAO 2007]. Without sufficient security and emergency preparedness at the ports that facilitate this trade, disruptions to transportation and shipping would result in widespread, large-scale loss of services. Risks range from the threat of terrorism to workplace violence to seismic hazards [Holdeman 2011]. Unique governance systems and complex site conditions complicate ports' ability to prepare, react and recover from major hazards. Although terrorism and human attacks are central concerns for ports, regions prone to natural disasters create additional—and perhaps more unwieldy—risks for port facilities.

The destructive potential of natural disasters is a well-documented danger, but one that is challenging to prepare for. Dealing with the unpredictability of natural hazards, and of seismic events in particular, further increases communities' vulnerability to loss of life and property. Following a disaster, the resilience of ports—their ability to return rapidly to near-normal conditions—is crucial to minimize supply chain disruptions and economic losses. Located directly above several large faults in the Western United States, some of the nation's most seismically-vulnerable container port complexes—the ports of Los Angeles and Long Beach in California and the ports of Seattle and Tacoma in Washington—are also key economic drivers of the American trade industry. In 2010, the Port of Los Angeles and the Port of Long Beach had a combined total value of $336,106,323. That same year, the ports of Seattle and Tacoma together equaled $77,121,867 [U.S. Department of Transportation 2011]. These four ports act as thruways for commodities shipped around the globe and the United States. In addition, Seattle and Tacoma act as the main points of entry for almost-all domestic shipping to Alaska.

A key component of resilient systems is the implementation of long-term, pre-disaster mitigation activities. But without clear communication of the importance of these activities, little incentive exists for their development. Academic research to better understand the seismic risks and hazards to a region serves as a catalyst for disaster mitigation. From findings of disaster management and engineering research, it takes interdisciplinary collaboration to educate the public on how best to respond to a disaster. No structure can truly “resist” the force of an earthquake. But knowledge of a hazard and mitigation against it can improve the resilience of infrastructure and communities from disasters [National Research Council 2011]. Disaster resilience for infrastructure exposed to any type of natural hazard is important, but for those communities and structures built in close proximity to fault lines it is vital.

The resilience of businesses and communities in seismically vulnerable areas depends on awareness levels of regional earthquake hazards. In California, risk from earthquakes is well-accepted. The ports of Los Angeles and Long Beach have taken considerable steps to avoid earthquake damage and are considered leaders in the field for their structural mitigation and emergency management plans that address their local seismic hazards [Pearce 2011]. Although the state of Washington also faces the near-future possibility of a serious seismic event, the general public in the Pacific Northwest has a much lower awareness of the threat from a major earthquake than in California. This lack of understanding and the accompanying misconceptions about the dangers of earthquakes to Washington contribute to the enhanced risk of post-earthquake disruptions at the ports of Seattle and Tacoma.

This report presents the findings of an evaluation of the disaster resilience of the two largest seaports—Seattle and Tacoma—in the state of Washington. This project identifies the issues that contribute to the seismic vulnerability of ports and that attempt to make more ports more disaster resilient. Central to this research is the recognition that the interconnections between the public and private sector stakeholders in port operations determine both a port’s profitability and its resiliency.

11.2 BACKGROUND

The vulnerability of a port depends on its regional seismic hazard and on the in-situ conditions at the port facility. This section presents an overview of the seismic hazards and the barriers to disaster resilience for ports and communities in the Pacific Northwest.

11.2.1 Pacific Northwest Seismic Hazards

The West Coast of the United States lies along an area of frequent plate tectonic activity known as the Ring of Fire. The constant movement of the collisions and shifts on the plate boundaries around the Pacific Ocean possess the potential to create powerful earthquakes and tsunamis. In the Pacific Northwest, small-magnitude earthquakes occur daily, but the three main earthquakes zones in this region are also capable of producing seismic events on a much larger scale.

The most common of the Cascadia earthquakes occur at shallow depths—typically less than 20 miles below the ground surface—and are generated within the North American plate as the western Juan de Fuca plate dives beneath it. Shallow earthquakes happen each day in this region yet few are as strong as the 1946 M7.3 earthquake near Vancouver Island, BC [CREW 2009]. Deep earthquakes—which develop at least 25 miles below the surface—also rarely produce shaking above M7.5; historically, a strong deep earthquake strikes in the Pacific Northwest every 10 to 30 years. These earthquakes occur along the Juan de Fuca plate as it descends underneath the North American plate. Although deep earthquakes underneath a plate generally cause less damage than shallow earthquakes, their energy dissipates over a wider area and is capable of affecting a larger geographic region. Cascadia last experienced a strong deep earthquake during the 2001 M6.8 Nisqually earthquake [CREW 2008].

The final type of earthquake, subduction zone earthquakes, are the least common, but have the potential to inflict the most damage. These earthquakes arise from the ruptures in the forceful contact between the Juan de Fuca and North American plates and have the potential to reach M9.0. Such earthquakes could produce strong shaking lasting for several minutes and would cause widespread damage stretching from northern California to British Columbia. Similar seismic events around the world have created massive tsunami waves and aftershocks that reached up to M7.0. Geologic evidence suggests that these subduction zone events occur roughly every 500 years. The last time such an earthquake hit Cascadia was in 1700 and seismologists warn that a high probability exists for a damaging, near-future Cascadia subduction zone earthquake [CREW 2005].

11.2.2 Site Conditions: Port of Seattle and Port of Tacoma

The risk of any large earthquake—whether it develops at shallow or deep depths, or within the subduction zone—poses a threat to all communities and infrastructure in a region of seismic activity. In the Puget Sound region of western Washington, the unconsolidated alluvial soils in the area exacerbate this danger. Alluvial soils come from rivers and streams: 14,000 years ago, glaciers and rivers carrying debris flow from Mt. Rainier deposited nearly 500 feet of loose sediments onto the local topography [Thornsley 2011]. This sedimentary basin affects patterns of ground shaking from earthquakes; the loose layers of differently compacted soils amplify any seismic waves that travel through them.

The vulnerability of infrastructure to earthquake damage resides mainly with the unpredictability of soils' responses to seismic events. The properties of most structures—such as those built of steel, concrete or wood—are well understood. Soil properties, including their seismic responses, however, possess much higher levels of uncertainty. As most ports are typically built on these loose, saturated sands, these structures are highly susceptible to earthquake damage [Na 2008]. In the case of the ports of Seattle and Tacoma, the poorly consolidated Puget Sound sediments provide weak foundation materials for port facilities. Infrastructure damage from a major earthquake would be severe at either of these ports, due to the combination of the in-situ conditions and the threat posed by the fault that passes directly underneath the city of Seattle.

The most common responses of loose, saturated soils subject to earthquake shaking are liquefaction, land subsidence, lateral spreading and landslides. These geotechnical failures typically cause much more of the earthquake damage to port facilities than does the failure of structural components. Around the Puget Sound, the unreliable soils in the sedimentary basin would affect not only the on-site port structures, but also would threaten the regional infrastructure networks that the ports rely on for inland transportation [MacRae 2005]. The wide-reaching effects of supply chain disruptions caused by the collapse of bridges from soil failures and the destruction of local roads from landslides and liquefaction would further halt the normal functions of port operations.

11.2.3 Disaster Resilience of Washington Ports

The unpredictability of earthquakes and the damage that they cause prevents communities from ever truly being ready for a seismic event. But mitigation before a disaster—either from structural engineering codes, community education programs or early earthquake warning systems—may help to reduce some of the widespread social and economic disruptions that follow a major disaster. The resilience of communities, businesses and infrastructure depends on the application of these pre-disaster tools and plans to implement rapid, robust and sustainable disaster response and recovery. Following a disaster, communities need continued access to food and emergency supplies and the disruption of normal supply chains exacerbates post-disaster chaos. Due to the seismic hazards and economic significance of the Pacific Northwest, ports in this region need effective post-disaster resilience of ports to maintain the normal shipping of food and industrial goods. Examples of other ports damaged by earthquakes illustrate this need for resilient shipping networks and port facilities here in the United States.

As an island nation located on the Ring of Fire, Japan experiences frequent, powerful earthquakes. Although much of the country's infrastructure is now built under strict seismic codes, the unpredictability of soils' response to seismic waves continues to complicate the vulnerability of Japan's ports to earthquake damage. The M6.9 1995 Kobe earthquake decimated the Port of Kobe and caused the liquefaction of foundation soils, shifting of the caisson pilings on which docks rested and damage to transportation systems, cranes and natural gas lines. The long delay created by the port's recovery from these damages drove businesses away and ultimately lowered the port's global ranking from 6th to 17th [Chang 2000]. Japanese ports once again suffered earthquake damage when the M9.0 Honshu earthquake in March of 2011 destroyed four ports in northeastern Japan. In the immediate days following the earthquake, all of the nation's ports were briefly closed, which resulted in economic losses of around $3.4 billion in lost seaport trade each day [CNA 2011]. The similar seismic hazard faced by ports in the Pacific Northwest, and in other regions around the world, suggests that communities there would also face large-scale business disruptions in the wake of a major earthquake.

11.3 RESEARCH METHOD

Both port operations and disaster resilience are broad, multi-faceted topics; an analysis of the full spectrum of influences on these was beyond the scope of this project. Due to project time constraints, this research consisted solely of literature reviews and informal interviews. A more comprehensive project would include more rigorous surveys and compilation of data. Reviews of academic journals and government documents on critical infrastructure protection, disaster resilience and Pacific Northwest seismic hazards provided the background for this project. This information narrowed the project's scope and helped to identify potential sources for interviews.

Once these contacts had been located, personal interviews were conducted to gather perspective from the fields of structural and transportation engineering; geo- and earthquake sciences; public affairs and policy; port operations; and emergency and risk management.

The interviews performed for this research drew from expert opinion in three areas: public and private sectors and academic research. Conversations with private port stakeholders and public government officials emphasized the public-private coordination through which ports operate; ports are organized typically as municipal corporations underneath the jurisdiction of state government legislation [Port of Tacoma 2011]. Interviews with university faculty meanwhile provided detailed information on the concept of public-private port interaction, on the disaster resilience of ports in general and on the overall relevance of early warning systems. Table 11.1 lists the public, private and academic affiliations of the individuals with whom interviews were conducted.

Table 11.1 Public, private, and academic contacts.

Public	Private	Public/Private	Academic
Pacific Northwest Economic Region: Center for Regional Disaster Resilience	American Society of Civil Engineers	Port of Seattle	University of California, Berkeley: Seismological Laboratory, Department of Earth and Planetary Science
Washington Military Department: Emergency Management Division	Northland Services	Port of Tacoma	University of Washington: Department of Civil Engineering
	Pearce Global Partners Inc.		University of Washington: Evans School of Public Affairs
	SSA Marine		University of Washington: Institute for Hazard Mitigation Planning and Research, College of Architecture and Urban Planning
	TOTE Shipping		University of Washington: Pacific Northwest Seismograph Network, Department of Earth and Space Sciences

A survey of preliminary questions created the basis for each interview (APPENDIX). Sources were posed a similar series of questions, with modifications based on their areas of expertise. These questions included discussions of:

- Vulnerability of port operations and facilities
- Post-disaster recovery time for ports
- Current level of port disaster preparedness
- Coordination of emergency response with terminal operators and other stakeholders

Many of these interviews—conducted through telephone and in-person conversations and through correspondence via email—led to recommendations for further sources. In total, sixteen interviews were conducted with eighteen different sources (two of the interviews involved discussions with multiple people). Communication with several of these sources provided access to the port emergency management documents and regional disaster resilience plans from which certain key findings were drawn. These documents were received either through hard copy or through PDFs sent via email.

11.4 FINDINGS

The main findings of this project focus on general issues of ports' responses to earthquakes and on the stakeholder interdependencies that dictate ports' pre- and post-disaster actions. The results of this study suggest that most ports share similar vulnerabilities to seismic hazards. The specific concerns and interactions of individual facilities, however, complicate a port's overall disaster resilience. Tables 11.2 and 11.3 compare the potential responses of the Port of Seattle and the Port of Tacoma to seismic hazards and emergency management. Although the results speak directly to the disaster resilience of these two ports, discussion of the findings points to their relevance for maritime container ports in general.

Table 11.2 Summary of findings on seismic hazard.

	Seismic Hazards		
	Port of Seattle	**Shared Vulnerabilities**	**Port of Tacoma**
Geotechnical	-	Poor soil quality	-
Other Natural Disasters	-	Threat of tsunami inundation	Lahars
Structural/Land use	Limited space	Old facilities, outdated seismic codes	-
Supply Chains	Alaskan Way Viaduct	Damage to inland transportation	Bullfrog Junction
	-	Disruption to Alaskan shipping	-

Table 11.3 Summary of findings on emergency preparedness.

	Emergency Preparedness	
	Port of Seattle	**Port of Tacoma**
Level of Hazard Awareness	Varied	Varied
Status of Emergency Management Plans	Limited available information	Comprehensive Emergency Management Plan in place
Stakeholder Interaction	Separation between tenants and landowners	Separation between tenants and landowners
	Expectations of self-sufficiency or government intervention	Coordination with Pierce County

11.4.1 Seismic Hazards—Geotechnical

Due to their waterfront locations, the on-site geotechnical conditions have the most impact on the seismic vulnerability of ports. “If you get a lot of soil movement, it doesn’t matter how good your structure is.” Roeder asserts that the unpredictability of the in-situ material on which ports are built poses greater seismic risks to ports than the collapse of weak infrastructure [Roeder 2011]. As discussed earlier, the saturated, unconsolidated soils found along coasts amplify seismic waves traveling through the ground, which makes fragile ground conditions more susceptible than structural collapse.

The failure of foundation material from any of these seismic side effects weakens the infrastructure on top of it. In turn, structural damage disrupts port operations because the port needs unharmed warehouses, cranes, docks and rail yards to maintain normal business functions. Among these components of port infrastructure, docks and wharves are particularly vulnerable. At most ports, these structures are built on caissons—box-like structures sunk into the weak foundations soils and filled with either water or granular material [Werner 1998]. As demonstrated by the 1995 earthquake damage to the man-made islands of the Port of Kobe, earthquake shaking can easily damage caissons and the surrounding soil. The movement of the ground during an earthquake increases the void spaces in the soil around and within the caissons. These larger gaps between soil particles lower the soil's load-bearing capacity. When the voids in the saturated soils fill with water, the probability of soil failure by liquefaction worsens [Paulsen 2011]. In addition to liquefaction, lateral spreading and land subsidence during an earthquake are also likely to occur.

These types of soil failure can damage port facilities directly, but their impact on the inland intermodal (road, rail, air and water) systems also can induce long term business disruptions for ports and their clients. If a bridge—such as the Magnolia Bridge along the Alaskan Way Viaduct in Seattle—collapses, port operators must find alternative ways to transport commodities. The Magnolia Bridge offers critical access to the POS Terminal 91 and the Smith Cove Cruise Terminal [Port of Seattle 2011]. The loss of that link in the supply chain would limit the ability of these terminals to maintain business continuity.

The 1989 Loma Prieta earthquake in California demonstrated the interrelated damage that both types of failure can produce at intermodal facilities and the on-site port infrastructure. Prior to the 1989 earthquake, the Port of Oakland's waterside and landside rail lines were constructed on separate foundations, with the waterside rail balanced on top of piers. Land subsidence during the 1989 earthquake resulted in uneven changes in elevations of the disparate soil conditions under the tracks. This difference in elevation caused cranes to wrack (or twist) across the two rail lines, preventing the transfer of containers from the waterside to landside rail [Paulsen 2011]. When considering this project's example ports in the state of Washington, the two ports would experience different impacts from soil failure on their facilities.

Seismic hazard maps predict land subsidence at both ports. At the Port of Tacoma, it is unlikely that such an event would produce the severe damage to cranes seen at the Port of

Oakland. Nevertheless, the water and landside sets of rail of POT are both on pilings, meaning the two rail lines would respond similarly to shifts in ground elevation. For this project, the Port of Tacoma shared much of the predicted disaster response of its infrastructure, but similar information from the Port of Seattle was much less accessible. Despite the availability of scientific data on the site's geotechnical characteristics, a fair assessment of the impact of soil failure and ground motions on POS infrastructure cannot be made without a detailed study of the port's structural layout.

11.4.2 Seismic Hazards—Structural/Land Use

Concern over the lack of publicly-available information about some port infrastructure would be less worrisome if all facilities were constructed under modern seismic codes, with appropriate mitigation practices. At many West Coast ports, however, the majority of their structures were built prior to the 1960s or 1970s. The construction of these buildings without inclusion of modern earthquake mitigation techniques increases their vulnerability to seismic hazards. Both the Port of Seattle and the Port of Tacoma sustained little serious structural damage following the 2001 Nisqually earthquake [Asavareungchai 2011; Jacobs-Sverdrup 2001]. This may be accounted perhaps more to the characteristics of the deep Nisqually earthquake than to the particular disaster resilience of either port. Shaking from deep earthquakes affects a wide geographic region but with less severe energy than would be generated by an earthquake generated within the Cascadia subduction zone. Although most of the Puget Sound port infrastructure withstood the 2001 event fairly well, the same response cannot be assumed in the face of future earthquakes. Furthermore, the location of Port of Seattle in downtown Seattle limits its future expansion and improvement of structural resilience. The Port of Tacoma's site contains 6478 acres, while the Port of Seattle's facility has only 1543 [Port of Tacoma 2011; Port of Seattle 2011]. Lack of available new real estate inhibits the port's ability to prepare effectively for future strong earthquakes.

Despite the vulnerability of port infrastructure to the combined effects of soil failure, the age of the structures and the limitations of older building codes, some stakeholders are unaware of—or choose to disregard—the local seismic risks. According to two POS stakeholders (an engineer at the Port of Seattle and an employee at one of the port's main terminal operators), the reasonable performance of infrastructure against the Nisqually earthquake should assuage concerns about risk of future damage [Asavareungchai 2011; McElhoe 2011]. Recent evaluations by the American Society of Civil Engineers, however, suggest that more than 70% of older buildings would not pass the specified seismic life safety standard due to their outdated building codes [National Research Council 2011]. Moreover, the greater the earthquake that strikes a region, the worse the expected performance by structures in the area, regardless of their age. After a major earthquake, a resilient structure "must be capable of withstanding at least a repetition of the event that caused the initial damage without collapse and without additional risk from falling (or other) hazards" [Jacobs-Sverdrup 2001]. Due to the limited information about the status of POS infrastructure, it is difficult to determine how well the port's facilities might meet this goal. Earthquakes and the response of in-situ material to seismic waves are already unpredictable. Lack of certainty about the seismic response of the Port of Seattle's structures further limits its resilience.

The false confidence expressed by some of the Port of Seattle stakeholders in their structures' resilience increases the port's seismic vulnerability. Successful disaster resilience results from recognition of the risk to existing buildings and of the cost-effective need to implement mitigation practices [National Research Council 2011]. Because it is not possible to predict the strength of the next earthquake to occur in a region, assumptions of structural performance based on responses to past earthquakes ignore the current understanding of effective means of disaster resilience.

11.4.3 Seismic Hazards—Other Natural Disasters

Disaster resilience of communities, businesses and infrastructure systems includes the ability to rebound and recovery swiftly not just from earthquakes, but also from tsunamis, lahars and other seismic hazards. Although earthquakes pose the greatest threat to most West Coast ports in the United States, the worry of inundation from tsunamis also exists. Tsunamis result typically from subduction zone earthquakes. After a sub-marine earthquake, the shock from vertical shifts in the sea floor sends out a series of waves across the ocean. As these waves move across the ocean they remain relatively small in height. They grow greater in height as they near land and the depth of the ocean floor decreases. The number and height of tsunami waves depends on the local conditions of where the earthquake strikes and the direction toward which the waves travel. The long travel time of tsunamis across the ocean provides more warning than inland earthquakes, but the massive waves of tsunamis flood everything in their path [CREW 2005]. The National Tsunami Early Warning System operated by the National Oceanic and Atmospheric Administration could help ports to evacuate personnel and initiate some pre-disaster preparations for on-site commodities. Although an early warning could reduce loss of life, the unavoidable flooding expected from a tsunami would result in serious damage to property. Within the first 12 minutes of the arrival of a tsunami, the Port of Tacoma predicts an inundation of two and a half meters to its facilities [Paulsen 2011]. In the immediate hours after a tsunami, business at the port would halt during post-disaster emergency management and assessment. The clean-up from such deep inundation would likely disrupt operations for several days to follow. Although less likely than tsunami flooding, lahars—debris flows initiated by volcanic eruption—could also weaken port structures and harm cargo left exposed to the open. A lahar would swamp a port with debris and likely require extensive clean-up to restore the port facilities to normal. The damage from a man-made or natural disaster may not always be avoided because not every region possesses the same level of risk from seismically-induced hazards. The impact to the local, regional and global supply chains depends, however, on level of a port's resilience in the hours, days and years following a disaster.

11.4.4 Seismic Hazards—Supply Chains

After an earthquake or other disaster, successful recovery efforts begin with reliable community services and functional transportation routes. Damaged roadways or blocked waterways inhibit the ability of first responders to provide needed emergency aid and of businesses to provide the regular services on which communities rely. Soil failure often compromises road networks and railroads during the immediate hours and days following an earthquake. In the event of destruction to inland transportation, waterways and airways provide alternative means of mobility. But faced with a major disaster, these modes are also vulnerable. The collapse of channels, filling of rivers with debris or the liquefaction of airport runways could delay post-disaster response and recovery [Wood and Good 2004]. Moreover, the loss of key transportation links derails regional economic productivity. Physical losses in one area can cripple an entire community, even in regions far removed from the initial disaster.

One example of the potential for cascading impact from earthquake damage is the supply chain to Alaska. Four shipping lines run between the continental United States and Alaska, and these provide Alaska with almost all of its food and manufactured products. All four of these shipping lines originate in the Puget Sound area of Northwest Washington. The two steamship lines—Northland Services Shipping and Alaska Marine Lines—operate out of the Port of Seattle. The two barge lines that service Alaska—Totem Ocean Trailer Express and Horizon Lines—sail from the Port of Tacoma [McElhoe 2011]. Disruptions to the ports through which these companies operate could decimate Alaska's main supply chain. The voyage between Alaska and Tacoma lasts three days; the extent of the impact to Alaska would depend on the location of ships en-route when the disaster strikes [McFarlane 2011]. Continued functionality of these shipping lines equals the resilience of both the companies that manage them and the Alaskan communities that they serve. Resilience of these organizations requires coordinated pre-disaster mitigation and swift post-disaster repair to waterway and inland transportation infrastructure [Stewart 2005]. The existence of reliable networks of transportation supports the tangled, interdependent web of the trade and shipping world.

Ports organize the collection and distribution of cargo to cities across the country and around the world. Waterways, roadways, railways and airways facilitate the movement of this cargo in and out of the ports. In many regions, inland ground modes provide the best means of transportation. In the Pacific Northwest, "ports are useless without access to a road." According to Goodchild, the Ports of Seattle and Tacoma possess some access to waterways, but roads and rail offer the primary means of intermodal transportation [Goodchild 2011]. Nationally, no geographic region is served by only one road or one line of rail, but many ports depend heavily on a single line of transportation to coordinate their inland shipping. Moreover, the existence of alternative routes for ground transportation does not always guarantee their viability. The downtime needed for disaster recovery already produces large economic losses for businesses. The shift of a supply chain to a new route may be expensive or time-consuming. In order to minimize further economic losses and businesses delays, stakeholders should choose a low-cost option that optimizes delivery times.

Prudent disaster management planning involves the identification of these cost and time-effective alternatives. Even though ports typically connect to multiple intermodal routes, many facilities rely heavily on one line of transportation over others. The Alaskan Way Viaduct, part of Washington State Route 99, is the main conduit for inland transportation to and from the Port of Seattle. Serious damage to the viaduct would result from a large earthquake, such as the one predicted soon from the Cascadian subduction zone. After a major earthquake, the liquefaction of weak alluvial would have the greatest impact on the viaduct and surrounding infrastructure. The liquefaction action would produce cascading levels of devastation on this downtown Seattle highway. Liquefied soil would push against the sea wall that supports the viaduct which could lead to the collapse of the sea wall and sections of nearby piers. Utility pipes and electric transmission lines would also break as the soil flows toward the waterfront. Sections of the viaduct would fall, and heavy damage would be expected along much of the roadway [Washington State Department of Transportation 2009]. Such devastation would make the viaduct and its arterial roads impassable until the completion of significant clean-up and repair efforts. The absence of the viaduct from the Port of Seattle's transportation network would obstruct the movement of goods from ships in the port yard to manufacturer and consumers across the continental United States.

Similarly, the reliance of the Port of Tacoma on Bullfrog Rail Junction for the distribution of all railroad shipping poses a serious risk to port business continuity. Around 55% of the cargo transported inland from POT moves via rail [Paulsen 2011]. With only one railroad hub for the port, seismic damage to rail lines miles far away from Tacoma could clog the supply chains that operate through POT. Although the Washington State Department of Transportation carries out some seismic retrofits to highway bridges each year, little research exists on the specific mitigation of railroads against earthquakes [Goodchild 2011]. The involvement of multiple stakeholder groups in both rail shipping and disaster mitigation complicates the study of this issue. Lack of communication between the rail industry and the government agencies, ports and other intermodal shippers that use railroads further lowers the disaster resilience of these networks. Due to the unpredictability of earthquakes and their side effects, failure of stakeholders to coordinate pre-disaster planning and post-disaster collaboration exacerbates the structural damage and economic losses from seismic events. Ports act as throughways, not destinations for cargo: Disruptions to a port or any piece of its supply chain create long-term, cascading impact on communities across the globe. Ultimately, the disaster resilience of the transportation networks through which ports operate may determine the resilience of ports themselves.

11.4.5 Emergency Preparedness—Hazard Awareness and Stakeholder Interaction

Understanding of the risk posed to a region by natural disasters is the first step toward disaster resilience. Without awareness of the hazard level faced, port stakeholders will not undertake mitigation activities nor will they establish effective networks of communication. When stakeholders lack appropriate information about their vulnerability to a disaster, they often defer natural disaster mitigation efforts in favor of what they see as more pressing concerns, such as revenue or unemployment [Wood and Good 2004]. Disregard of the need for pre-disaster mitigation leaves communities ill-prepared for the catastrophic impact of a natural disaster. Resilient businesses and communities are aware of the nature of the hazard they face and undertake effective mitigation prior to an earthquake.

In some countries, unlike in the United States, disaster prevention and community earthquake education are national priorities. During the March 2011 Tohoku earthquake, the Japanese government provided constant, high-quality information to the public about the unfolding disaster. The Japan Meteorological Agency also operates an early warning system that provides the public with a small window of warning in advance of an approaching earthquake. This system disseminates information from the JMA through public and private communication outlets in an attempt to control post-earthquake losses. Although room for improvement to the system exists, the early warning gives time to slow speeding trains, save important data on computers and alert citizens to take cover before the earthquake strikes (Japan Meteorological Agency 2011). The success of this program comes from Japan's national emphasis on earthquake awareness.

In the United States, lower levels of hazard awareness inhibit the implementation of a similar early warning system. Communities that experience more frequent earthquakes possess a better understanding of their vulnerability than regions that do not. The recent M5.8 earthquake that struck Virginia and the Mid-Atlantic region exemplifies this lack of awareness. Few Virginia residents know that their state sits atop an active seismic zone, because the rare earthquakes that hit this area range normally from magnitude 2 to 3 [Mufson andVastag 2011]. Fortunately, the quake caused no major damage. But the unexpected shock it gave to citizens across the country hints at the chaos a larger earthquake could evoke. If the public does not expect such an event, then it can be difficult for entities cognizant of the risk to initiate mitigation measures.

Mid-Atlantic and East Coast earthquakes are uncommon, low magnitude events. Areas such as the Pacific Northwest possess a much higher seismic vulnerability. Tiny earthquakes shake Washington State daily, most too small to be noticed by the general public. But large earthquakes do occur on a regular basis. Seismologists predict that the next major earthquake to hit the region will be much more powerful than even the M6.8 Nisqually event. Regardless of this impending threat, the infrequency of larger-scale events—compared with the seismology of nearby California—gives citizens a false sense of security. At ports this results in a wide range of seismic risk awareness. Many stakeholders maintain an “out of sight, out of mind” mentality that impairs their judgment of a port’s vulnerability.

The small amount of damage after the 2001 Nisqually earthquake encourages a belief among some individuals at POS that future earthquakes pose a similar, limited threat. “We are not going to make changes to prepare for a seismic event: historically, earthquakes have not had much impact,” to the Seattle facilities of Northland Shipping Services, said operations manager Scott McElhoe [2011]. As at most ports, POS shipping operators lease land from the port authority. The port performs general on-site maintenance of its structures, but overall responsibility for the upkeep of property resides with the tenant. According to one Port of Seattle engineer, POS owners are aware of the existing seismic hazard, as well as the need to protect life safety and continue regular shipment of containers. At the same time, the port balances its professed desire for seismic mitigation with a perceived obligation not to misuse the taxpayer dollars that fund its operations [Asavareungchai 2011]. The negative connotations of natural disasters promote disinterest at some ports to prepare for them. For businesses and stakeholders not accustomed to advanced disaster planning, mitigation against hypothetical damage from an earthquake distracts from day-to-day activities. This nonchalant attitude suggests a naiveté about the potential for structural and economic losses after an earthquake.

Preference for reactive measures, rather than decisive pre-disaster planning, prevails among port owners and operators, but it is not universal. “Emergency preparedness for (port) terminals is every man for himself,” said Eric Holdemann, Director of Security at the Port of Tacoma [2011]. This loose governance allows companies with a heightened understanding of seismic vulnerability to implement more effective natural disaster management plans. Earthquake mitigation efforts at ports typically develop on the initiative of a single individual or a small group that recognizes the importance of post-disaster resilience. In comparison with the

Port of Seattle, the overall organization at POT appears more knowledgeable about the future impacts of the next major earthquake. This level of awareness has evolved over the last half a decade, primarily from the motivation of key leaders at the port. Better education of port stakeholders and the general public on the issues of disaster prevention and recovery will further improve the resilience of the port and its supply chains [Pearce 2011]. Without the backing of informed community members, even the most impassioned leaders will find it difficult to implement needed mitigation programs.

11.4.6 Emergency Preparedness—Status of Emergency Management Plans

Even when appropriate levels of hazard awareness exist, ports need structured Emergency Management Plans to organize pre-disaster preparations and to coordinate post-disaster response and recovery. After a disaster—in addition to repairs to physical damage—ports must resolve the many economic, political and social issues that interrupt business operations. Post-disaster resilience requires strategic planning to reduce disaster-related costs, infrastructure damage and economic losses [National Research Council 2011]. An Emergency Management Plan cannot reduce the uncertainty from an earthquake, nor can it improve poor soil conditions along a waterfront. But the identification of key personnel, resources and information prior to a disaster may improve a port's resilience after an actual event.

Central to an organization's emergency management plan should be discussions of mitigation and preparedness, response and recovery. The most effective emergency management plans would arise from coordinated efforts between shipping operators, port owners, government authorities and neighboring ports. Despite the interdependence of these entities, the reality of their uncommunicative relationships means that each organization often develops its own plan with little input from the others. Emergency management plans of shipping companies tend to focus on emergency response supplies for employees and post-disaster containment of cargo [MacFarlane 2011]. Unlike terminal operators who focus solely on their individual company, the broader supply chain that operates through a port requires owners to take more holistic approaches. The "Comprehensive Emergency Management Plan" recently put in place by the Port of Tacoma defines the pre- and post-disaster roles of each office in the port authority [Port of Tacoma 2011]. This ranges from the risk management office to the legal team to real estate and asset management. In addition to the interaction among different branches of the port authority, some pre-disaster coordination exists between the Pierce County Office of Emergency Management and POT.

The POT's overall plan lacks some specificity in its description of certain emergency management activities. But its completion demonstrates the concentrated efforts of POT to improve hazard awareness and resilience. By contrast, repeated assurances of the Port of Seattle's preparedness for an earthquake failed to produce physical documents that verify these claims. This absence of available information suggests a skewed prioritization of emergency management concerns at POS. Furthermore, some terminal operators at POS listed an expectation of rapid government assistance in the event of a major earthquake [McElhoe 2011]. Past disasters such as Hurricane Katrina demonstrated, however, this type of federal aid is not always forthcoming. Ports and other businesses therefore need concrete, self-sustaining plans and focused leadership to organize mitigation and resilience programs. Disorganization and limited hazard awareness are just as dangerous to post-disaster business continuity as are lateral spreading and liquefaction underneath physical structures.

11.5 CONCLUSIONS

Earthquakes are volatile and unpredictable. But humans need not fall back on passive disaster response measures, just because it is difficult to forecast a seismic event. Earthquakes may damage infrastructure and disrupt supply chains, but educated, proactive solutions can minimize long-term impact. These solutions must begin with increased awareness of seismic vulnerability and more effective coordination between stakeholders. The findings of this study suggest four main issues that shape the disaster resilience of ports:

- High seismic vulnerability of infrastructure
- Wide range of levels of hazards awareness and risk perception
- Improvement of disaster preparedness through objective plans and organized leadership
- Governance of disaster resilience by socio-economic interdependencies

These conclusions emphasize a need to increase community hazard awareness and to strengthen the interdependencies that maintain a port. The economic vitality and normal social functions of communities around the world hinge on the resilience of ports' physical infrastructure and business supply chains. Figure 11.1 outlines the suggested progression of disaster resilience.

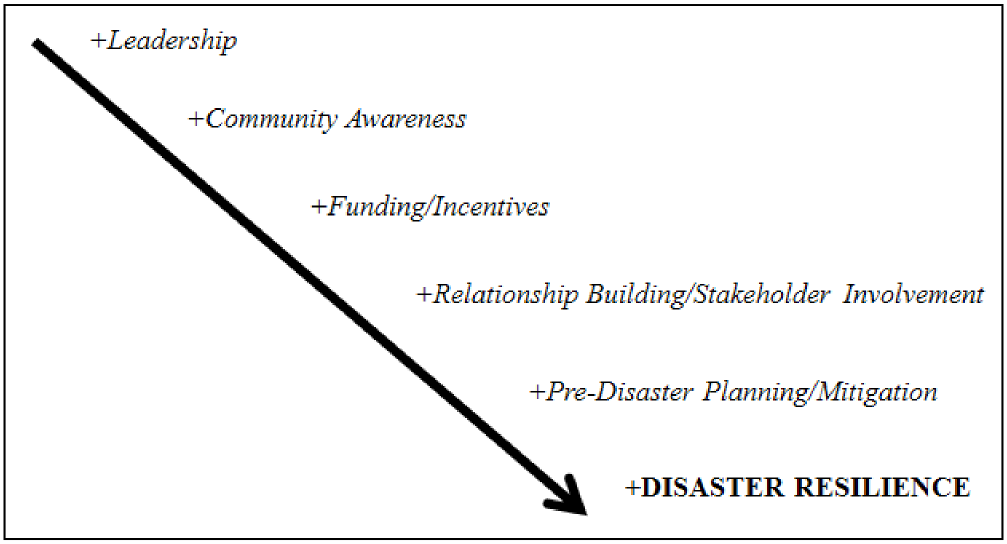

Figure 11.1 Disaster Resilience Chain.

This process begins with emboldened leadership. Leaders who recognize the seismic vulnerability of a region can implement business and community education programs to expand awareness of earthquake hazards and possible mitigation techniques. With a better understanding of the risk to their investments and lifestyles, community stakeholders are more likely to urge governments and ports to implement funding that supports disaster preparedness. Economic competiveness among stakeholders often inhibits coordination, but the introduction of financial incentives would encourage relationship building. Increased interactions and direct funding would help ports and their tenants create concrete disaster mitigation plans. Limited information about the status of emergency management at some ports contributes to the wide range of earthquake preparedness.

Stronger interdependencies and objective emergency management programs will ultimately produce more resilient ports, supply chains and communities. The nature of earthquake hazards prevents an organization from ever achieving complete disaster preparedness. But stakeholder communication and measurable mitigation programs offer meaningful action against post-disaster economic and structural losses. Seismic vulnerabilities and low public awareness necessitate discussions about disaster resilience. Decisive actions by educated leaders and coordinated stakeholders can begin to make these discussions reality.

ACKNOWLEDGMENTS

This project was supported by the Pacific Earthquake Engineering Research Center as part of its 2011 summer research opportunity for undergraduate students. Peter May and Ashley Jochim at the University of Washington's Center for American Politics and Public Policy acted as mentors for this undertaking. This project would have been impossible without their guidance and knowledge. Thanks to Ann Bostrom and Tim Scharks (Evans School for Public Affairs) and Bill Steele (Pacific Northwest Seismograph Network) all at the University of Washington for their support early on. Charles Roeder and Anne Goodchild in the Civil and Environmental Engineering department at University of Washington and Peggy Hellweg (University of Berkeley Seismology Lab) also were of great help.

Eric Holdeman, Lou Paulsen and Trevor Thornsley were generous in the time and information that they shared about the operations and plans of the Port of Tacoma. At the Port of Seattle, Sam Asavareungchai offered helpful perspective on the port's engineering and disaster preparedness programs. Interviews with shipping operators at both ports gave insight into the concerns of other port stakeholders. Thanks to Scott McElhoe (Northland Shipping Services), Curt Campbell (SSA Marine Inc.) and Shannon MacFarlane (TOTE Shipping). Conversations with members of the emergency management community were much appreciated. In particular, Bob Freitag at the University of Washington's Institute for Hazard Mitigation Research, Paula Scalinigi at the Pacific Northwest Economic Regions' Center for Regional Disaster Resilience and Ines Pearce with Pearce Global Partners Inc., provided relevant and informative background information. Interviews with the Washington State Emergency Management Division's Jim Mullen, John Schelling and Wendy Freitag made possible the discussions of the multi-faceted issue of disaster preparedness.

Much gratitude goes to PEER's Outreach Director and coordinator of the PEER REU program, Heidi Faison. Without her backing, this research would not exist. Finally, the encouragement of fellow PEER intern Jason Naanos and the suggestions to drafts of this report from Pam and Andrew Welsh-Huggins were invaluable. Many thanks to all those who supported this project.

REFERENCES

Asavareungchai, S. (2011). Engineer, Port of Seattle. Personal interview, 4 Aug. 2011.

Cascadia Region Earthquake Workgroup (2005). *Cascadia Subduction Zone Earthquakes: A magnitude 9.0 earthquake scenario*, Cascadia Region Earthquake Workgroup, Seattle, WA.

Cascadia Region Earthquake Workgroup (2008). *Cascadia Deep Earthquakes, 2008*, Cascadia Region Earthquake Workgroup, Seattle, WA.

Cascadia Region Earthquake Workgroup (2009). *Cascadia Shallow Earthquakes, 2009*, Cascadia Region Earthquake Workgroup and the King County Office of Emergency Management, Seattle, WA.

Chang, S. E. (2000). Disasters and transport systems: loss, recovery and competition at the Port of Kobe after the 1995 earthquake, *J. Transport Geography*. 8(1):53-65.

CNA's Institute for Public Research (2011). Altered landscapes of catastrophes: Insights from the great east Japan earthquake, *The Expert's Roundtable on Catastrophes*. 26 Apr. 2011. Arlington, VA: CNA's Institute for Public Research, Web, 1 Jul. 2011.

Goodchild, A. (2011). Personal communication, Dept. of Civil and Enviro. Engrg., University of Washington, Seattle, WA.

Government Accounting Office (2007). *Port risk management: Additional Federal Guidance Would Aid Ports in Disaster Planning and Recovery* (GAO-07-412), Washington, D.C.

Hellweg, P. (2011). Personal communication, Seismology Lab., Univ. of Calif., Berkeley, CA.

Holdemann, E. (2011). Personal communication, Port of Tacoma.

Jacobs-Sverdrup (2001). Detailed visual evaluation, Post-Nisqually earthquake facilities evaluation phase II, Prepared for Port of Tacoma Facilities Development. *Port of Tacoma Project No.: E2062*, *Sverdrup Project No.: W3X36700*. Bellevue, WA.

Japan Meteorological Agency (2011). *What Is an Earthquake Early Warning*?, Japan Meteorological Agency. Accessed at http://www.jma.go.jp/jma/en/Activities/eew1.html.

MacFarlane, S. (2011). Personal communication, Totem Ocean Trailer Express.

MacRae, G. (2005). Transportation, *Seattle Fault Earthquake Scenario*, Seattle, WA.

McElhoe, S. (2011). Personal communication, Northland Services Shipping.

Mufson, S., and B. Vastag (2011). For central Virginia's seismic zone, quake is an event of rare magnitude, *Washington Post*.

Na, U.J., et al. (2008). Probabilistic assessment for seismic performance of port structures, *Soil Dyn. Earthq. Engrg.* 28:147–158.

National Research Council (2011). *National Earthquake Resilience: Research, Implementation and Outreach*. Committee on National Earthquake Resilience—Research, Implementation, and Outreach Committee on Seismology and Geodynamics Board on Earth Sciences and Resources Division on Earth and Life Studies. Washington, D.C. National Academies Press.

Paulsen, L. (2011). *Comprehensive Management Plan*, *V.1*, Port of Tacoma. v.1, Tacoma, WA.

Paulsen, L. (2011). Personal communication, Port of Tacoma, Tacoma, WA.

Pearce, I. (2011). Personal communication, Pearce Global Partners, Inc.

Pittman, E. (2010). *Earthquake Early Warning System Coming to California*, Emergency Management. http://www.emergencymgmt.com/disaster/Earthquake-Early-Warning-System-California.html.

Port of Seattle (2011). *Community: Regional Transportation*, Port of Seattle. http://www.portseattle.org/community/development/regionaltransport.shtml.

Port of Tacoma (2011). *About the Port: Organization and Leadership*, *Port of Tacoma,* http://www.portoftacoma.com/organization.

Roeder, C. (2011). Personal communication, Dept of Civil and Enviro. Engrg., Univ. of Washington, Seattle, WA.

Stewart, M. (2005). Community impacts, response and recovery, *Seattle Fault Earthquake Scenario*, Seattle, WA.

Thornsley, T. (2011). Port of Tacoma. “RE: Student Researching Disaster Resilience of Port of Tacoma.” Message to Sarah Welsh-Huggins. 11 Jul. 2011. Email.

U.S. Department of Transportation. (2011). *U.S. Waterborne Foreign Trade by Custom District*. Washington, D.C., http://www.marad.dot.gov/library_landing_page/data_and_statistics/Data_and_Statistics.htm.

Washington State Department of Transportation (2009). *Alaskan Way Viaduct: Earthquake Simulation*, Online posting. Youtube. 23 Oct. 2009. 25 Aug. 2011.

Werner, S.D., ed. (1998). *Seismic Guidelines for Ports*, ASCE, Technical Council on Lifeline Earthquake Engineering 12: 6–50. Reston, VA.

Wood, N.J., and J.W. Good. (2004). Vulnerability of port and harbor communities to earthquake and tsunami hazards: The use of GIS in community hazard planning, *Coastal Management*. 32:243-269.

APPENDIX

Sample interview questions:

Vulnerability:

What are the most vulnerable facilities/operations at the port?

What disruptions would most affect the ability to recover from a seismic event? How long would recovery take for a major earthquake – days, weeks, months or more?

What studies has the port undertaken of the economic costs of potential earthquake disruptions? Where can I obtain this information?

Emergency, Response, and Recovery Planning

In what ways is the port prepared for an earthquake? In what ways is it lacking?

Following a disaster, which facilities are most critical in terms of the port's ability to resume normal functions as quickly as possible?

How does the port coordinate its emergency response and recovery with terminal operators and other clients?

PEER REPORTS

PEER reports are available individually or by yearly subscription. PEER reports can be ordered at http://peer.berkeley.edu/publications/peer_reports.html or by contacting the Pacific Earthquake Engineering Research Center, 325 Davis Hall mail code 1792, Berkeley, CA 94720. Tel.: (510) 642-3437; Fax: (510) 665-1655; Email: peer_editor@berkeley.edu

PEER 2011/10 *Earthquake Engineering for Resilient Communities: 2011 PEER Internship Program Research Report Collection.* Eds. Heidi Faison and Stephen A. Mahin. December 2011.

PEER 2011/09 *Calibration of Semi-Stochastic Procedure for Simulating High-Frequency Ground Motions.* Jonathan P. Stewart, Emel Seyhan, and Robert W. Graves. December 2011.

PEER 2011/08 *Water Supply in regard to Fire Following Earthquake.* Charles Scawthorn. November 2011.

PEER 2011/07 *Seismic Risk Management in Urban Areas. Proceedings of a U.S.-Iran-Turkey Seismic Workshop.* September 2011.

PEER 2011/06 *The Use of Base Isolation Systems to Achieve Complex Seismic Performance Objectives.* Troy A. Morgan and Stephen A. Mahin. July 2011.

PEER 2011/05 *Case Studies of the Seismic Performance of Tall Buildings Designed by Alternative Means.* Task 12 Report for the Tall Buildings Initiative. Jack Moehle, Yousef Bozorgnia, Nirmal Jayaram, Pierson Jones, Mohsen Rahnama, Nilesh Shome, Zeynep Tuna, John Wallace, Tony Yang, and Farzin Zareian. July 2011.

PEER 2011/04 *Recommended Design Practice for Pile Foundations in Laterally Spreading Ground.* Scott A. Ashford, Ross W. Boulanger, and Scott J. Brandenberg. June 2011.

PEER 2011/03 *New Ground Motion Selection Procedures and Selected Motions for the PEER Transportation Research Program.* Jack W. Baker, Ting Lin, Shrey K. Shahi, and Nirmal Jayaram. March 2011.

PEER 2011/02 *A Bayesian Network Methodology for Infrastructure Seismic Risk Assessment and Decision Support.* Michelle T. Bensi, Armen Der Kiureghian, and Daniel Straub. March 2011.

PEER 2011/01 *Demand Fragility Surfaces for Bridges in Liquefied and Laterally Spreading Ground.* Scott J. Brandenberg, Jian Zhang, Pirooz Kashighandi, Yili Huo, and Minxing Zhao. March 2011.

PEER 2010/05 *Guidelines for Performance-Based Seismic Design of Tall Buildings.* Developed by the Tall Buildings Initiative. November 2010.

PEER 2010/04 *Application Guide for the Design of Flexible and Rigid Bus Connections between Substation Equipment Subjected to Earthquakes.* Jean-Bernard Dastous and Armen Der Kiureghian. September 2010.

PEER 2010/03 *Shear Wave Velocity as a Statistical Function of Standard Penetration Test Resistance and Vertical Effective Stress at Caltrans Bridge Sites.* Scott J. Brandenberg, Naresh Bellana, and Thomas Shantz. June 2010.

PEER 2010/02 *Stochastic Modeling and Simulation of Ground Motions for Performance-Based Earthquake Engineering.* Sanaz Rezaeian and Armen Der Kiureghian. June 2010.

PEER 2010/01 *Structural Response and Cost Characterization of Bridge Construction Using Seismic Performance Enhancement Strategies.* Ady Aviram, Božidar Stojadinović, Gustavo J. Parra-Montesinos, and Kevin R. Mackie. March 2010.

PEER 2009/03 *The Integration of Experimental and Simulation Data in the Study of Reinforced Concrete Bridge Systems Including Soil-Foundation-Structure Interaction.* Matthew Dryden and Gregory L. Fenves. November 2009.

PEER 2009/02 *Improving Earthquake Mitigation through Innovations and Applications in Seismic Science, Engineering, Communication, and Response. Proceedings of a U.S.-Iran Seismic Workshop.* October 2009.

PEER 2009/01 *Evaluation of Ground Motion Selection and Modification Methods: Predicting Median Interstory Drift Response of Buildings.* Curt B. Haselton, Ed. June 2009.

PEER 2008/10 *Technical Manual for Strata.* Albert R. Kottke and Ellen M. Rathje. February 2009.

PEER 2008/09 *NGA Model for Average Horizontal Component of Peak Ground Motion and Response Spectra.* Brian S.-J. Chiou and Robert R. Youngs. November 2008.

PEER 2008/08 *Toward Earthquake-Resistant Design of Concentrically Braced Steel Structures.* Patxi Uriz and Stephen A. Mahin. November 2008.

PEER 2008/07 *Using OpenSees for Performance-Based Evaluation of Bridges on Liquefiable Soils.* Stephen L. Kramer, Pedro Arduino, and HyungSuk Shin. November 2008.

PEER 2008/06 *Shaking Table Tests and Numerical Investigation of Self-Centering Reinforced Concrete Bridge Columns.* Hyung IL Jeong, Junichi Sakai, and Stephen A. Mahin. September 2008.

PEER 2008/05 *Performance-Based Earthquake Engineering Design Evaluation Procedure for Bridge Foundations Undergoing Liquefaction-Induced Lateral Ground Displacement.* Christian A. Ledezma and Jonathan D. Bray. August 2008.

PEER 2008/04 *Benchmarking of Nonlinear Geotechnical Ground Response Analysis Procedures.* Jonathan P. Stewart, Annie On-Lei Kwok, Yousseff M. A. Hashash, Neven Matasovic, Robert Pyke, Zhiliang Wang, and Zhaohui Yang. August 2008.

PEER 2008/03 *Guidelines for Nonlinear Analysis of Bridge Structures in California.* Ady Aviram, Kevin R. Mackie, and Božidar Stojadinović. August 2008.

PEER 2008/02 *Treatment of Uncertainties in Seismic-Risk Analysis of Transportation Systems.* Evangelos Stergiou and Anne S. Kiremidjian. July 2008.

PEER 2008/01 *Seismic Performance Objectives for Tall Buildings.* William T. Holmes, Charles Kircher, William Petak, and Nabih Youssef. August 2008.

PEER 2007/12 *An Assessment to Benchmark the Seismic Performance of a Code-Conforming Reinforced Concrete Moment-Frame Building.* Curt Haselton, Christine A. Goulet, Judith Mitrani-Reiser, James L. Beck, Gregory G. Deierlein, Keith A. Porter, Jonathan P. Stewart, and Ertugrul Taciroglu. August 2008.

PEER 2007/11 *Bar Buckling in Reinforced Concrete Bridge Columns.* Wayne A. Brown, Dawn E. Lehman, and John F. Stanton. February 2008.

PEER 2007/10 *Computational Modeling of Progressive Collapse in Reinforced Concrete Frame Structures.* Mohamed M. Talaat and Khalid M. Mosalam. May 2008.

PEER 2007/09 *Integrated Probabilistic Performance-Based Evaluation of Benchmark Reinforced Concrete Bridges.* Kevin R. Mackie, John-Michael Wong, and Božidar Stojadinović. January 2008.

PEER 2007/08 *Assessing Seismic Collapse Safety of Modern Reinforced Concrete Moment-Frame Buildings.* Curt B. Haselton and Gregory G. Deierlein. February 2008.

PEER 2007/07 *Performance Modeling Strategies for Modern Reinforced Concrete Bridge Columns.* Michael P. Berry and Marc O. Eberhard. April 2008.

PEER 2007/06 *Development of Improved Procedures for Seismic Design of Buried and Partially Buried Structures.* Linda Al Atik and Nicholas Sitar. June 2007.

PEER 2007/05 *Uncertainty and Correlation in Seismic Risk Assessment of Transportation Systems.* Renee G. Lee and Anne S. Kiremidjian. July 2007.

PEER 2007/04 *Numerical Models for Analysis and Performance-Based Design of Shallow Foundations Subjected to Seismic Loading.* Sivapalan Gajan, Tara C. Hutchinson, Bruce L. Kutter, Prishati Raychowdhury, José A. Ugalde, and Jonathan P. Stewart. May 2008.

PEER 2007/03 *Beam-Column Element Model Calibrated for Predicting Flexural Response Leading to Global Collapse of RC Frame Buildings.* Curt B. Haselton, Abbie B. Liel, Sarah Taylor Lange, and Gregory G. Deierlein. May 2008.

PEER 2007/02 *Campbell-Bozorgnia NGA Ground Motion Relations for the Geometric Mean Horizontal Component of Peak and Spectral Ground Motion Parameters.* Kenneth W. Campbell and Yousef Bozorgnia. May 2007.

PEER 2007/01 *Boore-Atkinson NGA Ground Motion Relations for the Geometric Mean Horizontal Component of Peak and Spectral Ground Motion Parameters.* David M. Boore and Gail M. Atkinson. May. May 2007.

PEER 2006/12 *Societal Implications of Performance-Based Earthquake Engineering.* Peter J. May. May 2007.

PEER 2006/11 *Probabilistic Seismic Demand Analysis Using Advanced Ground Motion Intensity Measures, Attenuation Relationships, and Near-Fault Effects.* Polsak Tothong and C. Allin Cornell. March 2007.

PEER 2006/10 *Application of the PEER PBEE Methodology to the I-880 Viaduct.* Sashi Kunnath. February 2007.

PEER 2006/09 *Quantifying Economic Losses from Travel Forgone Following a Large Metropolitan Earthquake.* James Moore, Sungbin Cho, Yue Yue Fan, and Stuart Werner. November 2006.

PEER 2006/08 *Vector-Valued Ground Motion Intensity Measures for Probabilistic Seismic Demand Analysis*. Jack W. Baker and C. Allin Cornell. October 2006.

PEER 2006/07 *Analytical Modeling of Reinforced Concrete Walls for Predicting Flexural and Coupled–Shear-Flexural Responses*. Kutay Orakcal, Leonardo M. Massone, and John W. Wallace. October 2006.

PEER 2006/06 *Nonlinear Analysis of a Soil-Drilled Pier System under Static and Dynamic Axial Loading.* Gang Wang and Nicholas Sitar. November 2006.

PEER 2006/05 *Advanced Seismic Assessment Guidelines.* Paolo Bazzurro, C. Allin Cornell, Charles Menun, Maziar Motahari, and Nicolas Luco. September 2006.

PEER 2006/04 *Probabilistic Seismic Evaluation of Reinforced Concrete Structural Components and Systems.* Tae Hyung Lee and Khalid M. Mosalam. August 2006.

PEER 2006/03 *Performance of Lifelines Subjected to Lateral Spreading.* Scott A. Ashford and Teerawut Juirnarongrit. July 2006.

PEER 2006/02 *Pacific Earthquake Engineering Research Center Highway Demonstration Project.* Anne Kiremidjian, James Moore, Yue Yue Fan, Nesrin Basoz, Ozgur Yazali, and Meredith Williams. April 2006.

PEER 2006/01 *Bracing Berkeley. A Guide to Seismic Safety on the UC Berkeley Campus.* Mary C. Comerio, Stephen Tobriner, and Ariane Fehrenkamp. January 2006.

PEER 2005/16 *Seismic Response and Reliability of Electrical Substation Equipment and Systems.* Junho Song, Armen Der Kiureghian, and Jerome L. Sackman. April 2006.

PEER 2005/15 *CPT-Based Probabilistic Assessment of Seismic Soil Liquefaction Initiation.* R. E. S. Moss, R. B. Seed, R. E. Kayen, J. P. Stewart, and A. Der Kiureghian. April 2006.

PEER 2005/14 *Workshop on Modeling of Nonlinear Cyclic Load-Deformation Behavior of Shallow Foundations.* Bruce L. Kutter, Geoffrey Martin, Tara Hutchinson, Chad Harden, Sivapalan Gajan, and Justin Phalen. March 2006.

PEER 2005/13 *Stochastic Characterization and Decision Bases under Time-Dependent Aftershock Risk in Performance-Based Earthquake Engineering.* Gee Liek Yeo and C. Allin Cornell. July 2005.

PEER 2005/12 *PEER Testbed Study on a Laboratory Building: Exercising Seismic Performance Assessment.* Mary C. Comerio, editor. November 2005.

PEER 2005/11 *Van Nuys Hotel Building Testbed Report: Exercising Seismic Performance Assessment.* Helmut Krawinkler, editor. October 2005.

PEER 2005/10 *First NEES/E-Defense Workshop on Collapse Simulation of Reinforced Concrete Building Structures.* September 2005.

PEER 2005/09 *Test Applications of Advanced Seismic Assessment Guidelines.* Joe Maffei, Karl Telleen, Danya Mohr, William Holmes, and Yuki Nakayama. August 2006.

PEER 2005/08 *Damage Accumulation in Lightly Confined Reinforced Concrete Bridge Columns.* R. Tyler Ranf, Jared M. Nelson, Zach Price, Marc O. Eberhard, and John F. Stanton. April 2006.

PEER 2005/07 *Experimental and Analytical Studies on the Seismic Response of Freestanding and Anchored Laboratory Equipment.* Dimitrios Konstantinidis and Nicos Makris. January 2005.

PEER 2005/06 *Global Collapse of Frame Structures under Seismic Excitations*. Luis F. Ibarra and Helmut Krawinkler. September 2005.

PEER 2005//05 *Performance Characterization of Bench- and Shelf-Mounted Equipment.* Samit Ray Chaudhuri and Tara C. Hutchinson. May 2006.

PEER 2005/04 *Numerical Modeling of the Nonlinear Cyclic Response of Shallow Foundations.* Chad Harden, Tara Hutchinson, Geoffrey R. Martin, and Bruce L. Kutter. August 2005.

PEER 2005/03 *A Taxonomy of Building Components for Performance-Based Earthquake Engineering.* Keith A. Porter. September 2005.

PEER 2005/02 *Fragility Basis for California Highway Overpass Bridge Seismic Decision Making.* Kevin R. Mackie and Božidar Stojadinović. June 2005.

PEER 2005/01 *Empirical Characterization of Site Conditions on Strong Ground Motion.* Jonathan P. Stewart, Yoojoong Choi, and Robert W. Graves. June 2005.

PEER 2004/09 *Electrical Substation Equipment Interaction: Experimental Rigid Conductor Studies.* Christopher Stearns and André Filiatrault. February 2005.

PEER 2004/08 *Seismic Qualification and Fragility Testing of Line Break 550-kV Disconnect Switches.* Shakhzod M. Takhirov, Gregory L. Fenves, and Eric Fujisaki. January 2005.

PEER 2004/07 *Ground Motions for Earthquake Simulator Qualification of Electrical Substation Equipment.* Shakhzod M. Takhirov, Gregory L. Fenves, Eric Fujisaki, and Don Clyde. January 2005.

PEER 2004/06 *Performance-Based Regulation and Regulatory Regimes.* Peter J. May and Chris Koski. September 2004.

PEER 2004/05 *Performance-Based Seismic Design Concepts and Implementation: Proceedings of an International Workshop.* Peter Fajfar and Helmut Krawinkler, editors. September 2004.

PEER 2004/04 *Seismic Performance of an Instrumented Tilt-up Wall Building.* James C. Anderson and Vitelmo V. Bertero. July 2004.

PEER 2004/03 *Evaluation and Application of Concrete Tilt-up Assessment Methodologies.* Timothy Graf and James O. Malley. October 2004.

PEER 2004/02 *Analytical Investigations of New Methods for Reducing Residual Displacements of Reinforced Concrete Bridge Columns.* Junichi Sakai and Stephen A. Mahin. August 2004.

PEER 2004/01 *Seismic Performance of Masonry Buildings and Design Implications.* Kerri Anne Taeko Tokoro, James C. Anderson, and Vitelmo V. Bertero. February 2004.

PEER 2003/18 *Performance Models for Flexural Damage in Reinforced Concrete Columns.* Michael Berry and Marc Eberhard. August 2003.

PEER 2003/17 *Predicting Earthquake Damage in Older Reinforced Concrete Beam-Column Joints.* Catherine Pagni and Laura Lowes. October 2004.

PEER 2003/16 *Seismic Demands for Performance-Based Design of Bridges.* Kevin Mackie and Božidar Stojadinović. August 2003.

PEER 2003/15 *Seismic Demands for Nondeteriorating Frame Structures and Their Dependence on Ground Motions.* Ricardo Antonio Medina and Helmut Krawinkler. May 2004.

PEER 2003/14 *Finite Element Reliability and Sensitivity Methods for Performance-Based Earthquake Engineering.* Terje Haukaas and Armen Der Kiureghian. April 2004.

PEER 2003/13 *Effects of Connection Hysteretic Degradation on the Seismic Behavior of Steel Moment-Resisting Frames.* Janise E. Rodgers and Stephen A. Mahin. March 2004.

PEER 2003/12 *Implementation Manual for the Seismic Protection of Laboratory Contents: Format and Case Studies.* William T. Holmes and Mary C. Comerio. October 2003.

PEER 2003/11 *Fifth U.S.-Japan Workshop on Performance-Based Earthquake Engineering Methodology for Reinforced Concrete Building Structures.* February 2004.

PEER 2003/10 *A Beam-Column Joint Model for Simulating the Earthquake Response of Reinforced Concrete Frames.* Laura N. Lowes, Nilanjan Mitra, and Arash Altoontash. February 2004.

PEER 2003/09 *Sequencing Repairs after an Earthquake: An Economic Approach.* Marco Casari and Simon J. Wilkie. April 2004.

PEER 2003/08 *A Technical Framework for Probability-Based Demand and Capacity Factor Design (DCFD) Seismic Formats.* Fatemeh Jalayer and C. Allin Cornell. November 2003.

PEER 2003/07 *Uncertainty Specification and Propagation for Loss Estimation Using FOSM Methods.* Jack W. Baker and C. Allin Cornell. September 2003.

PEER 2003/06 *Performance of Circular Reinforced Concrete Bridge Columns under Bidirectional Earthquake Loading.* Mahmoud M. Hachem, Stephen A. Mahin, and Jack P. Moehle. February 2003.

PEER 2003/05 *Response Assessment for Building-Specific Loss Estimation.* Eduardo Miranda and Shahram Taghavi. September 2003.

PEER 2003/04 *Experimental Assessment of Columns with Short Lap Splices Subjected to Cyclic Loads.* Murat Melek, John W. Wallace, and Joel Conte. April 2003.

PEER 2003/03 *Probabilistic Response Assessment for Building-Specific Loss Estimation.* Eduardo Miranda and Hesameddin Aslani. September 2003.

PEER 2003/02 *Software Framework for Collaborative Development of Nonlinear Dynamic Analysis Program.* Jun Peng and Kincho H. Law. September 2003.

PEER 2003/01 *Shake Table Tests and Analytical Studies on the Gravity Load Collapse of Reinforced Concrete Frames.* Kenneth John Elwood and Jack P. Moehle. November 2003.

PEER 2002/24 *Performance of Beam to Column Bridge Joints Subjected to a Large Velocity Pulse.* Natalie Gibson, André Filiatrault, and Scott A. Ashford. April 2002.

PEER 2002/23 *Effects of Large Velocity Pulses on Reinforced Concrete Bridge Columns.* Greg L. Orozco and Scott A. Ashford. April 2002.

PEER 2002/22 *Characterization of Large Velocity Pulses for Laboratory Testing.* Kenneth E. Cox and Scott A. Ashford. April 2002.

PEER 2002/21 *Fourth U.S.-Japan Workshop on Performance-Based Earthquake Engineering Methodology for Reinforced Concrete Building Structures.* December 2002.

PEER 2002/20 *Barriers to Adoption and Implementation of PBEE Innovations.* Peter J. May. August 2002.

PEER 2002/19 *Economic-Engineered Integrated Models for Earthquakes: Socioeconomic Impacts.* Peter Gordon, James E. Moore II, and Harry W. Richardson. July 2002.

PEER 2002/18 *Assessment of Reinforced Concrete Building Exterior Joints with Substandard Details.* Chris P. Pantelides, Jon Hansen, Justin Nadauld, and Lawrence D. Reaveley. May 2002.

PEER 2002/17 *Structural Characterization and Seismic Response Analysis of a Highway Overcrossing Equipped with Elastomeric Bearings and Fluid Dampers: A Case Study*. Nicos Makris and Jian Zhang. November 2002.

PEER 2002/16 *Estimation of Uncertainty in Geotechnical Properties for Performance-Based Earthquake Engineering.* Allen L. Jones, Steven L. Kramer, and Pedro Arduino. December 2002.

PEER 2002/15 *Seismic Behavior of Bridge Columns Subjected to Various Loading Patterns.* Asadollah Esmaeily-Gh. and Yan Xiao. December 2002.

PEER 2002/14 *Inelastic Seismic Response of Extended Pile Shaft Supported Bridge Structures.* T.C. Hutchinson, R.W. Boulanger, Y.H. Chai, and I.M. Idriss. December 2002.

PEER 2002/13 *Probabilistic Models and Fragility Estimates for Bridge Components and Systems.* Paolo Gardoni, Armen Der Kiureghian, and Khalid M. Mosalam. June 2002.

PEER 2002/12 *Effects of Fault Dip and Slip Rake on Near-Source Ground Motions: Why Chi-Chi Was a Relatively Mild M7.6 Earthquake.* Brad T. Aagaard, John F. Hall, and Thomas H. Heaton. December 2002.

PEER 2002/11 *Analytical and Experimental Study of Fiber-Reinforced Strip Isolators*. James M. Kelly and Shakhzod M. Takhirov. September 2002.

PEER 2002/10 *Centrifuge Modeling of Settlement and Lateral Spreading with Comparisons to Numerical Analyses***.** Sivapalan Gajan and Bruce L. Kutter. January 2003.

PEER 2002/09 *Documentation and Analysis of Field Case Histories of Seismic Compression during the 1994 Northridge, California, Earthquake.* Jonathan P. Stewart, Patrick M. Smith, Daniel H. Whang, and Jonathan D. Bray. October 2002.

PEER 2002/08 *Component Testing, Stability Analysis and Characterization of Buckling-Restrained Unbonded Braces™.* Cameron Black, Nicos Makris, and Ian Aiken. September 2002.

PEER 2002/07 *Seismic Performance of Pile-Wharf Connections.* Charles W. Roeder, Robert Graff, Jennifer Soderstrom, and Jun Han Yoo. December 2001.

PEER 2002/06 *The Use of Benefit-Cost Analysis for Evaluation of Performance-Based Earthquake Engineering Decisions*. Richard O. Zerbe and Anthony Falit-Baiamonte. September 2001.

PEER 2002/05 *Guidelines, Specifications, and Seismic Performance Characterization of Nonstructural Building Components and Equipment*. André Filiatrault, Constantin Christopoulos, and Christopher Stearns. September 2001.

PEER 2002/04 *Consortium of Organizations for Strong-Motion Observation Systems and the Pacific Earthquake Engineering Research Center Lifelines Program: Invited Workshop on Archiving and Web Dissemination of Geotechnical Data, 4–5 October 2001.* September 2002.

PEER 2002/03 *Investigation of Sensitivity of Building Loss Estimates to Major Uncertain Variables for the Van Nuys Testbed.* Keith A. Porter, James L. Beck, and Rustem V. Shaikhutdinov. August 2002.

PEER 2002/02 *The Third U.S.-Japan Workshop on Performance-Based Earthquake Engineering Methodology for Reinforced Concrete Building Structures*. July 2002.

PEER 2002/01 *Nonstructural Loss Estimation: The UC Berkeley Case Study.* Mary C. Comerio and John C. Stallmeyer. December 2001.

PEER 2001/16 *Statistics of SDF-System Estimate of Roof Displacement for Pushover Analysis of Buildings.* Anil K. Chopra, Rakesh K. Goel, and Chatpan Chintanapakdee. December 2001.

PEER 2001/15 *Damage to Bridges during the 2001 Nisqually Earthquake.* R. Tyler Ranf, Marc O. Eberhard, and Michael P. Berry. November 2001.

PEER 2001/14 *Rocking Response of Equipment Anchored to a Base Foundation.* Nicos Makris and Cameron J. Black. September 2001.

PEER 2001/13 *Modeling Soil Liquefaction Hazards for Performance-Based Earthquake Engineering.* Steven L. Kramer and Ahmed-W. Elgamal. February 2001.

PEER 2001/12 *Development of Geotechnical Capabilities in OpenSees.* Boris Jeremić. September 2001.

PEER 2001/11 *Analytical and Experimental Study of Fiber-Reinforced Elastomeric Isolators*. James M. Kelly and Shakhzod M. Takhirov. September 2001.

PEER 2001/10 *Amplification Factors for Spectral Acceleration in Active Regions.* Jonathan P. Stewart, Andrew H. Liu, Yoojoong Choi, and Mehmet B. Baturay. December 2001.

PEER 2001/09 *Ground Motion Evaluation Procedures for Performance-Based Design.* Jonathan P. Stewart, Shyh-Jeng Chiou, Jonathan D. Bray, Robert W. Graves, Paul G. Somerville, and Norman A. Abrahamson. September 2001.

PEER 2001/08 *Experimental and Computational Evaluation of Reinforced Concrete Bridge Beam-Column Connections for Seismic Performance.* Clay J. Naito, Jack P. Moehle, and Khalid M. Mosalam. November 2001.

PEER 2001/07 *The Rocking Spectrum and the Shortcomings of Design Guidelines.* Nicos Makris and Dimitrios Konstantinidis. August 2001.

PEER 2001/06 *Development of an Electrical Substation Equipment Performance Database for Evaluation of Equipment Fragilities*. Thalia Agnanos. April 1999.

PEER 2001/05 *Stiffness Analysis of Fiber-Reinforced Elastomeric Isolators.* Hsiang-Chuan Tsai and James M. Kelly. May 2001.

PEER 2001/04 *Organizational and Societal Considerations for Performance-Based Earthquake Engineering.* Peter J. May. April 2001.

PEER 2001/03 *A Modal Pushover Analysis Procedure to Estimate Seismic Demands for Buildings: Theory and Preliminary Evaluation.* Anil K. Chopra and Rakesh K. Goel. January 2001.

PEER 2001/02 *Seismic Response Analysis of Highway Overcrossings Including Soil-Structure Interaction.* Jian Zhang and Nicos Makris. March 2001.

PEER 2001/01 *Experimental Study of Large Seismic Steel Beam-to-Column Connections.* Egor P. Popov and Shakhzod M. Takhirov. November 2000.

PEER 2000/10 *The Second U.S.-Japan Workshop on Performance-Based Earthquake Engineering Methodology for Reinforced Concrete Building Structures.* March 2000.

PEER 2000/09 *Structural Engineering Reconnaissance of the August 17, 1999 Earthquake: Kocaeli (Izmit), Turkey.* Halil Sezen, Kenneth J. Elwood, Andrew S. Whittaker, Khalid Mosalam, John J. Wallace, and John F. Stanton. December 2000.

PEER 2000/08 *Behavior of Reinforced Concrete Bridge Columns Having Varying Aspect Ratios and Varying Lengths of Confinement.* Anthony J. Calderone, Dawn E. Lehman, and Jack P. Moehle. January 2001.

PEER 2000/07 *Cover-Plate and Flange-Plate Reinforced Steel Moment-Resisting Connections.* Taejin Kim, Andrew S. Whittaker, Amir S. Gilani, Vitelmo V. Bertero, and Shakhzod M. Takhirov. September 2000.

PEER 2000/06 *Seismic Evaluation and Analysis of 230-kV Disconnect Switches.* Amir S. J. Gilani, Andrew S. Whittaker, Gregory L. Fenves, Chun-Hao Chen, Henry Ho, and Eric Fujisaki. July 2000.

PEER 2000/05 *Performance-Based Evaluation of Exterior Reinforced Concrete Building Joints for Seismic Excitation.* Chandra Clyde, Chris P. Pantelides, and Lawrence D. Reaveley. July 2000.

PEER 2000/04 *An Evaluation of Seismic Energy Demand: An Attenuation Approach.* Chung-Che Chou and Chia-Ming Uang. July 1999.

PEER 2000/03 *Framing Earthquake Retrofitting Decisions: The Case of Hillside Homes in Los Angeles.* Detlof von Winterfeldt, Nels Roselund, and Alicia Kitsuse. March 2000.

PEER 2000/02 *U.S.-Japan Workshop on the Effects of Near-Field Earthquake Shaking.* Andrew Whittaker, ed. July 2000.

PEER 2000/01 *Further Studies on Seismic Interaction in Interconnected Electrical Substation Equipment.* Armen Der Kiureghian, Kee-Jeung Hong, and Jerome L. Sackman. November 1999.

PEER 1999/14 *Seismic Evaluation and Retrofit of 230-kV Porcelain Transformer Bushings*. Amir S. Gilani, Andrew S. Whittaker, Gregory L. Fenves, and Eric Fujisaki. December 1999.

PEER 1999/13 *Building Vulnerability Studies: Modeling and Evaluation of Tilt-up and Steel Reinforced Concrete Buildings.* John W. Wallace, Jonathan P. Stewart, and Andrew S. Whittaker, editors. December 1999.

PEER 1999/12 *Rehabilitation of Nonductile RC Frame Building Using Encasement Plates and Energy-Dissipating Devices.* Mehrdad Sasani, Vitelmo V. Bertero, James C. Anderson. December 1999.

PEER 1999/11 *Performance Evaluation Database for Concrete Bridge Components and Systems under Simulated Seismic Loads.* Yael D. Hose and Frieder Seible. November 1999.

PEER 1999/10 *U.S.-Japan Workshop on Performance-Based Earthquake Engineering Methodology for Reinforced Concrete Building Structures.* December 1999.

PEER 1999/09 *Performance Improvement of Long Period Building Structures Subjected to Severe Pulse-Type Ground Motions*. James C. Anderson, Vitelmo V. Bertero, and Raul Bertero. October 1999.

PEER 1999/08 *Envelopes for Seismic Response Vectors.* Charles Menun and Armen Der Kiureghian. July 1999.

PEER 1999/07 *Documentation of Strengths and Weaknesses of Current Computer Analysis Methods for Seismic Performance of Reinforced Concrete Members.* William F. Cofer. November 1999.

PEER 1999/06 *Rocking Response and Overturning of Anchored Equipment under Seismic Excitations.* Nicos Makris and Jian Zhang. November 1999.

PEER 1999/05 *Seismic Evaluation of 550 kV Porcelain Transformer Bushings.* Amir S. Gilani, Andrew S. Whittaker, Gregory L. Fenves, and Eric Fujisaki. October 1999.

PEER 1999/04 *Adoption and Enforcement of Earthquake Risk-Reduction Measures.* Peter J. May, Raymond J. Burby, T. Jens Feeley, and Robert Wood.

PEER 1999/03 *Task 3 Characterization of Site Response General Site Categories*. Adrian Rodriguez-Marek, Jonathan D. Bray, and Norman Abrahamson. February 1999.

PEER 1999/02 *Capacity-Demand-Diagram Methods for Estimating Seismic Deformation of Inelastic Structures: SDF Systems*. Anil K. Chopra and Rakesh Goel. April 1999.

PEER 1999/01 *Interaction in Interconnected Electrical Substation Equipment Subjected to Earthquake Ground Motions.* Armen Der Kiureghian, Jerome L. Sackman, and Kee-Jeung Hong. February 1999.

PEER 1998/08 *Behavior and Failure Analysis of a Multiple-Frame Highway Bridge in the 1994 Northridge Earthquake.* Gregory L. Fenves and Michael Ellery. December 1998.

PEER 1998/07 *Empirical Evaluation of Inertial Soil-Structure Interaction Effects.* Jonathan P. Stewart, Raymond B. Seed, and Gregory L. Fenves. November 1998.

PEER 1998/06 *Effect of Damping Mechanisms on the Response of Seismic Isolated Structures.* Nicos Makris and Shih-Po Chang. November 1998.

PEER 1998/05 *Rocking Response and Overturning of Equipment under Horizontal Pulse-Type Motions.* Nicos Makris and Yiannis Roussos. October 1998.

PEER 1998/04 *Pacific Earthquake Engineering Research Invitational Workshop Proceedings, May 14–15, 1998: Defining the Links between Planning, Policy Analysis, Economics and Earthquake Engineering.* Mary Comerio and Peter Gordon. September 1998.

PEER 1998/03 *Repair/Upgrade Procedures for Welded Beam to Column Connections.* James C. Anderson and Xiaojing Duan. May 1998.

PEER 1998/02 *Seismic Evaluation of 196 kV Porcelain Transformer Bushings.* Amir S. Gilani, Juan W. Chavez, Gregory L. Fenves, and Andrew S. Whittaker. May 1998.

PEER 1998/01 *Seismic Performance of Well-Confined Concrete Bridge Columns.* Dawn E. Lehman and Jack P. Moehle. December 2000.

ONLINE REPORTS

The following PEER reports are available by Internet only at http://peer.berkeley.edu/publications/peer_reports.html

PEER 2011/107 *Nonlinear Site Response and Seismic Compression at Vertical Array Strongly Shaken by 2007 Niigata-ken Chuetsu-oki Earthquake.* Eric Yee, Jonathan P. Stewart, and Kohji Tokimatsu. December 2011.

PEER 2011/106 *Self Compacting Hybrid Fiber Reinforced Concrete Composites for Bridge Columns.* Pardeep Kumar, Gabriel Jen, William Trono, Marios Panagiotou, and Claudia Ostertag. September 2011.

PEER 2011/105 *Stochastic Dynamic Analysis of Bridges Subjected to Spacially Varying Ground Motions.* Katerina Konakli and Armen Der Kiureghian. August 2011.

PEER 2011/104 *Design and Instrumentation of the 2010 E-Defense Four-Story Reinforced Concrete and Post-Tensioned Concrete Buildings.* Takuya Nagae, Kenichi Tahara, Taizo Matsumori, Hitoshi Shiohara, Toshimi Kabeyasawa, Susumu Kono, Minehiro Nishiyama (Japanese Research Team) and John Wallace, Wassim Ghannoum, Jack Moehle, Richard Sause, Wesley Keller, Zeynep Tuna (U.S. Research Team). June 2011.

PEER 2011/103 *In-Situ Monitoring of the Force Output of Fluid Dampers: Experimental Investigation.* Dimitrios Konstantinidis, James M. Kelly, and Nicos Makris. April 2011.

PEER 2011/102 *Ground-motion prediction equations 1964 - 2010.* John Douglas. April 2011.

PEER 2011/101 *Report of the Eighth Planning Meeting of NEES/E-Defense Collaborative Research on Earthquake Engineering.* Convened by the Hyogo Earthquake Engineering Research Center (NIED), NEES Consortium, Inc. February 2011.

PEER 2010/111 *Modeling and Acceptance Criteria for Seismic Design and Analysis of Tall Buildings.* Task 7 Report for the Tall Buildings Initiative - Published jointly by the Applied Technology Council. October 2010.

PEER 2010/110 *Seismic Performance Assessment and Probabilistic Repair Cost Analysis of Precast Concrete Cladding Systems for Multistory Buildlings.* Jeffrey P. Hunt and Božidar Stojadinovic. November 2010.

PEER 2010/109 *Report of the Seventh Joint Planning Meeting of NEES/E-Defense Collaboration on Earthquake Engineering. Held at the E-Defense, Miki, and Shin-Kobe, Japan, September 18–19, 2009.* August 2010.

PEER 2010/108 *Probabilistic Tsunami Hazard in California.* Hong Kie Thio, Paul Somerville, and Jascha Polet, preparers. October 2010.

PEER 2010/107 *Performance and Reliability of Exposed Column Base Plate Connections for Steel Moment-Resisting Frames.* Ady Aviram, Božidar Stojadinovic, and Armen Der Kiureghian. August 2010.

PEER 2010/106 *Verification of Probabilistic Seismic Hazard Analysis Computer Programs.* Patricia Thomas, Ivan Wong, and Norman Abrahamson. May 2010.

PEER 2010/105 *Structural Engineering Reconnaissance of the April 6, 2009, Abruzzo, Italy, Earthquake, and Lessons Learned.* M. Selim Günay and Khalid M. Mosalam. April 2010.

PEER 2010/104 *Simulating the Inelastic Seismic Behavior of Steel Braced Frames, Including the Effects of Low-Cycle Fatigue.* Yuli Huang and Stephen A. Mahin. April 2010.

PEER 2010/103 *Post-Earthquake Traffic Capacity of Modern Bridges in California.* Vesna Terzic and Božidar Stojadinović. March 2010.

PEER 2010/102 *Analysis of Cumulative Absolute Velocity (CAV) and JMA Instrumental Seismic Intensity (I_{JMA}) Using the PEER–NGA Strong Motion Database.* Kenneth W. Campbell and Yousef Bozorgnia. February 2010.

PEER 2010/101 *Rocking Response of Bridges on Shallow Foundations.* Jose A. Ugalde, Bruce L. Kutter, and Boris Jeremic. April 2010.

PEER 2009/109 *Simulation and Performance-Based Earthquake Engineering Assessment of Self-Centering Post-Tensioned Concrete Bridge Systems.* Won K. Lee and Sarah L. Billington. December 2009.

PEER 2009/108 *PEER Lifelines Geotechnical Virtual Data Center.* J. Carl Stepp, Daniel J. Ponti, Loren L. Turner, Jennifer N. Swift, Sean Devlin, Yang Zhu, Jean Benoit, and John Bobbitt. September 2009.

PEER 2009/107 *Experimental and Computational Evaluation of Current and Innovative In-Span Hinge Details in Reinforced Concrete Box-Girder Bridges: Part 2: Post-Test Analysis and Design Recommendations.* Matias A. Hube and Khalid M. Mosalam. December 2009.

PEER 2009/106 *Shear Strength Models of Exterior Beam-Column Joints without Transverse Reinforcement.* Sangjoon Park and Khalid M. Mosalam. November 2009.

PEER 2009/105 *Reduced Uncertainty of Ground Motion Prediction Equations through Bayesian Variance Analysis.* Robb Eric S. Moss. November 2009.

PEER 2009/104 *Advanced Implementation of Hybrid Simulation.* Andreas H. Schellenberg, Stephen A. Mahin, Gregory L. Fenves. November 2009.

PEER 2009/103 *Performance Evaluation of Innovative Steel Braced Frames.* T. Y. Yang, Jack P. Moehle, and Božidar Stojadinovic. August 2009.

PEER 2009/102 *Reinvestigation of Liquefaction and Nonliquefaction Case Histories from the 1976 Tangshan Earthquake.* Robb Eric Moss, Robert E. Kayen, Liyuan Tong, Songyu Liu, Guojun Cai, and Jiaer Wu. August 2009.

PEER 2009/101 *Report of the First Joint Planning Meeting for the Second Phase of NEES/E-Defense Collaborative Research on Earthquake Engineering.* Stephen A. Mahin et al. July 2009.

PEER 2008/104 *Experimental and Analytical Study of the Seismic Performance of Retaining Structures.* Linda Al Atik and Nicholas Sitar. January 2009.

PEER 2008/103 *Experimental and Computational Evaluation of Current and Innovative In-Span Hinge Details in Reinforced Concrete Box-Girder Bridges. Part 1: Experimental Findings and Pre-Test Analysis.* Matias A. Hube and Khalid M. Mosalam. January 2009.

PEER 2008/102 *Modeling of Unreinforced Masonry Infill Walls Considering In-Plane and Out-of-Plane Interaction.* Stephen Kadysiewski and Khalid M. Mosalam. January 2009.

PEER 2008/101 *Seismic Performance Objectives for Tall Buildings.* William T. Holmes, Charles Kircher, William Petak, and Nabih Youssef. August 2008.

PEER 2007/101 *Generalized Hybrid Simulation Framework for Structural Systems Subjected to Seismic Loading.* Tarek Elkhoraibi and Khalid M. Mosalam. July 2007.

PEER 2007/100 *Seismic Evaluation of Reinforced Concrete Buildings Including Effects of Masonry Infill Walls.* Alidad Hashemi and Khalid M. Mosalam. July 2007.

The Pacific Earthquake Engineering Research Center (PEER) is a multi-institutional research and education center with headquarters at the University of California, Berkeley. Investigators from over 20 universities, several consulting companies, and researchers at various state and federal government agencies contribute to research programs focused on performance-based earthquake engineering.

These research programs aim to identify and reduce the risks from major earthquakes to life safety and to the economy by including research in a wide variety of disciplines including structural and geotechnical engineering, geology/seismology, lifelines, transportation, architecture, economics, risk management, and public policy.

PEER is supported by federal, state, local, and regional agencies, together with industry partners.

PEER reports can be ordered at http://peer.berkeley.edu/publications/peer_reports.html or by contacting

Pacific Earthquake Engineering Research Center
University of California, Berkeley
325 Davis Hall, mail code 1792
Berkeley, CA 94720-1792
Tel: 510-642-3437
Fax: 510-642-1655
Email: peer_editor@berkeley.edu

ISSN 1547-0587X